TUM School of Engineering and Design
Technische Universität München

Modeling, planning, and optimizing public transport systems with automated, electric, and mixed-sized bus fleets

Mohammad Sadrani

Vollständiger Abdruck der von der TUM School of Engineering and Design der Technischen Universität München zur Erlangung eines

Doktors der Ingenieurwissenschaften (Dr.-Ing.)

genehmigten Dissertation.

Vorsitz:

Prof. Dr. Maximilian Schiffer

Prüfende der Dissertation:

1. Prof. Dr. Constantinos Antoniou
2. Prof. Dr. Alejandro Tirachini
3. Prof. Silvio Nocera, Ph.D.

Die Dissertation wurde am 02.11.2023 bei der Technischen Universität München eingereicht und durch die TUM School of Engineering and Design am 30.04.2024 angenommen.

Acknowledgments

I would like to express my deepest gratitude to my supervisor, Prof. Constantinos Antoniou, and my co-supervisor, Prof. Alejandro Tirachini. Their unwavering support, guidance, and insightful feedback have been invaluable throughout this wonderful journey. Their expertise and dedication have significantly contributed to my growth as a researcher.

I am deeply grateful to my beloved wife, my parents, and my brother. Their immense support, sacrifices, and encouragement have been the cornerstone of my academic pursuits.

Thank you all for making this journey a truly enriching and unforgettable experience.

Abstract

The advent of automated and electric buses, with their unique characteristics (such as human driving cost savings, charging needs, and driving range limitations related to energy consumption), introduces new aspects to the planning and operation of public transportation services. Therefore, this dissertation aims to develop novel mathematical optimization models and solution algorithms for the optimal planning of urban bus systems with automated, electric, and mixed-sized vehicles. It focuses on the development of (i) automated bus planning models, (ii) Electric Bus (EB) planning models equipped with a detailed (microscopic) energy estimation framework, (iii) multi-dimensional decision-making models for the selection of optimal charging strategies for EB systems, and (iv) mixed-fleet bus planning models.

In our formulation of automated bus systems, we develop a novel Mixed-Integer Nonlinear Programming (MINLP) model to optimize service frequency and bus size, considering time-dependent demand, stochastic travel times, and users' discomfort from crowding for sitting and standing passengers. The model is tested on real-world bus routes in Regensburg (Germany) and Santiago (Chile). We also formulate an EB planning problem as an Integer Nonlinear Programming (INLP) model, integrating a detailed energy consumption model (based on longitudinal vehicle dynamics) into the planning process. The model optimizes the selection of vehicle types and service frequencies to minimize total costs. The model applicability is investigated on a real bus corridor in Santiago, Chile. Besides, we propose a Multi-Criteria Decision-Making (MCDM) approach for selecting the best EB charging strategy, considering economic, environmental, social, operational, and quality-of-service criteria. A Fuzzy Best-Worst Method (FBWM) is developed to determine the weight of criteria, and a Fuzzy Ranking of Alternatives through Functional mapping of criterion subintervals into a Single Interval (FRAFSI) method is designed to rank available charging options. Finally, to address a Mixed-Fleet Bus Scheduling (MFBS) problem, a novel MINLP model is developed to optimize vehicle assignment and dispatching plans, considering user and operator costs and passenger comfort. To enhance the optimization process, we develop two hybrid metaheuristics, Genetic Algorithm combined with Simulated Annealing (GA-SA) and Grey Wolf Optimizer combined with Simulated Annealing (GWO-SA), with a Taguchi approach to calibrate their parameters. We test the developed model and metaheuristics on a real bus corridor in Santiago, Chile.

This dissertation presents several novel findings. We find that although the operator benefits of automation are greater in high-income (developed) countries, the level of public transport

demand plays a significant role, as substantial user cost savings from automation are attainable in crowded routes, even in lower-income (developing) countries. Additionally, a fixed energy rate in EB planning, rather than a detailed model, reduces planning accuracy as demand rises. In optimizing mixed-fleet operations, more advanced algorithms enhance service quality and fleet size optimization in crowded scenarios, whereas simpler algorithms suffice for lower-demand situations.

Zusammenfassung

Das Aufkommen automatisierter und elektrischer Busse mit ihren einzigartigen Merkmalen (z. B. Kosteneinsparungen durch menschliches Fahren, Ladebedarf und Reichweitenbeschränkungen im Zusammenhang mit dem Energieverbrauch) bringt neue Aspekte für die Planung öffentlicher Verkehrsdienste mit sich. Ziel dieser Dissertation ist es daher, neuartige mathematische Optimierungsmodelle und Lösungsalgorithmen für die optimale Planung von Stadtbussystemen mit automatisierten, elektrischen und gemischten Fahrzeugen zu entwickeln. Sie konzentriert sich auf die Entwicklung von (i) Modellen für die Planung von automatisierten Bussen, (ii) Modellen für die Planung von Elektrobussen (EB), die mit einem detaillierten (mikroskopischen) Rahmen für die Energieschätzung ausgestattet sind, (iii) mehrdimensionalen Entscheidungsmodellen für die Auswahl optimaler Ladestrategien für EB-Systeme und (iv) Modellen für die Planung von gemischten Busflotten.

In unserem automatisierten Busplanungsmodell entwickeln wir eine neuartige Formulierung der gemischt-ganzzahligen nichtlinearen Programmierung (MINLP) zur Optimierung der Bedienungshäufigkeit und der Busgröße unter Berücksichtigung der zeitabhängigen Nachfrage, der stochastischen Reisezeiten und des Unbehagens der sitzenden und stehenden Fahrgäste durch Überfüllung. Das Modell wird auf realen Buslinien in Regensburg (Deutschland) und Santiago (Chile) getestet. Wir formulieren auch ein EB-Planungsproblem als ein Modell der ganzzahligen nichtlinearen Programmierung (INLP) und integrieren ein detailliertes Energieverbrauchsmodell (basierend auf der Längsdynamik der Fahrzeuge) in den Planungsprozess. Das Modell optimiert die Auswahl von Fahrzeugtypen und Bedienungshäufigkeiten zur Minimierung der Gesamtkosten. Die Anwendbarkeit des Modells wird auf einem realen Buskorridor in Santiago, Chile, untersucht. Außerdem schlagen wir einen multikriteriellen Entscheidungsfindungsansatz (MCDM) zur Auswahl der besten EB-Ladestrategie vor, der ökonomische, ökologische, soziale, betriebliche und Servicequalitätskriterien berücksichtigt. Es wird eine Fuzzy Best-Worst-Methode (FBWM) entwickelt, um die Gewichtung der Kriterien zu bestimmen, und eine Fuzzy Ranking of Alternatives through Functional mapping of criterion subintervals into a Single Interval (FRAFSI) Methode wird entwickelt, um eine Rangfolge der verfügbaren Gebührenoptionen zu erstellen. Schließlich wird ein neuartiges MINLP-Modell zur Optimierung der Fahrzeugzuweisung und des Fahrplans unter Berücksichtigung der Kosten für Benutzer und Betreiber sowie des Fahrgastkomforts entwickelt, um ein Problem der gemischten Busflotte (MFBS) zu lösen. Um den Optimierungsprozess zu verbessern, entwickeln wir zwei hybride

Metaheuristiken, den Genetischen Algorithmus kombiniert mit Simulated Annealing (GA-SA) und den Grey Wolf Optimizer kombiniert mit SA (GWO-SA), mit einem Taguchi-Ansatz zur Kalibrierung ihrer Parameter. Wir testen das entwickelte Modell und die Metaheuristik auf einem realen Buskorridor in Santiago, Chile.

Diese Dissertation präsentiert mehrere neue Erkenntnisse. Wir stellen fest, dass der Nutzen der Automatisierung für den Betreiber zwar in Ländern mit hohem Einkommen (Industrieländern) größer ist, dass aber das Niveau der Nachfrage nach öffentlichen Verkehrsmitteln eine wichtige Rolle spielt, da selbst in Ländern mit niedrigem Einkommen (Entwicklungsländern) auf überfüllten Strecken beträchtliche Einsparungen bei den Nutzerkosten durch Automatisierung erzielt werden können. Außerdem verringert ein fester Energietarif in der EB-Planung anstelle eines detaillierten Modells die Planungsgenauigkeit bei steigender Nachfrage. Bei der Optimierung des Betriebs mit gemischten Flotten verbessern fortschrittlichere Algorithmen die Servicequalität und die Optimierung der Flottengröße in überfüllten Szenarien, während einfachere Algorithmen für Situationen mit geringerer Nachfrage ausreichen.

Contents

List of Figures

List of Tables

1 Introduction

1.1 Research motivation

The emergence of automated and electric buses, distinguished by their unique attributes (such as human driving cost savings and driving range constraints related to energy consumption), presents new dimensions in the planning and operation of public transportation services. The design and mathematical modeling of these emerging fleets require a deep understanding of the factors that distinguish them from traditional fleets. This dissertation attempts to explore the evolving landscape of urban bus systems, with a primary focus on the development of state-of-the-art mathematical optimization models and solution algorithms to address the challenges and opportunities associated with the planning of automated, electric, and mixed-sized bus fleets.

The rise of automated vehicles, offering automated driving capabilities, holds the potential to revolutionize the transportation landscape (Nair and Bhat, 2021). Particularly, public transport is considered as one of the most suitable candidates to benefit from automated driving capabilities. In urban bus operations, human driving costs (drivers' salaries) can account for a significant share of the total operating costs, e.g., between 30% and 70% of total bus operator costs in countries such as Japan, Australia, Chile and Germany (Abe, 2019; Tirachini and Antoniou, 2020). The adoption of automated bus operations with autonomous driving technologies can significantly reduce human-related driving costs by eliminating (at least a part of) drivers' wages.

Based on the levels of driving automation defined by the Society of Automotive Engineers (SAE), future vehicles can operate with no need for human driving under certain conditions at Level 4, and under all conditions at Level 5 (SAE, 2018). Hence, it is expected that automation capabilities will significantly impact the public transport industry and services in the coming years, at least for operations in segregated environments such as busways. Furthermore, as this technology matures, it is predicted that the prices of connected and autonomous vehicle technologies will progressively reduce at certain annual rates within lower and upper bounds of 5% and 10% (Mosquet et al., 2015; Bansal and Kockelman, 2017), thereby providing a greater opportunity for public transportation agencies to accelerate the deployment of fully automated transport systems on their routes with lower capital costs in the next decades.

Concurrently, the transition to Electric Buses (EBs) has gained momentum in urban public transport agencies. EBs offer energy-efficient and environmentally friendly alternatives

to traditional diesel buses, with benefits such as higher energy efficiency and reduced levels of noise, local pollution, and greenhouse gas (GHG) emissions when powered by clean energy sources (Adheesh et al., 2016; Logan et al., 2020). However, EBs come with specific characteristics, including range limitations and the need for robust charging infrastructure. To make informed decisions during the planning phase of electric public transport systems, a comprehensive understanding of the factors influencing energy consumption is crucial. This understanding ensures that energy demands are neither underestimated nor overestimated, which can lead to more reliable choices regarding vehicle types, battery capacities, charging strategies, charging point locations, and service frequencies.

Furthermore, transitioning to EB fleets requires significant investments in charging infrastructure, as well as supportive policy and regulatory measures. The choice of the optimal charging strategy emerges as a central decision, with options encompassing overnight (slow) charging and opportunity (fast) charging systems. As the demand for eco-friendly transportation continues to grow and the adoption of EBs in public transport systems rises, this decision becomes increasingly pivotal. However, selecting the best strategy is a multifaceted challenge, as each option brings its own set of advantages and disadvantages.

In some urban settings, public transportation agencies are confronted with the need to operate mixed fleets encompassing vehicles of various types and capacities. This situation arises due to various reasons, such as specific supply-and-demand patterns, transitional phases (during which operators need to incorporate different vehicle types or technologies, combining traditional vehicles and newly acquired ones), historical considerations (when different sizes of buses are purchased at different times through different contracts), and resource limitations. The challenge of managing mixed fleets is particularly relevant, given that operating heterogeneous fleets is common in public transport systems, especially within large and complex cities. For instance, the bus network in Santiago, Chile, is composed of 317 routes, out of which 116 routes (37%) are operated with heterogeneous fleets during the morning peak period, either combining small (8-meter long) with standard (12-meter long) buses, or standard with articulated (18-meter long) buses in one single route (Sadrani et el., 2022a). Hence, establishing a methodological foundation to address the planning challenges and solution complexities associated with fleet heterogeneity in mixed-fleet bus operations is essential for the efficient optimization of dispatching programs, considering the utilization of services with different features within a mixed operating environment.

1.2 Research objectives and framework

1.2.1 Automated bus planning

As for the first objective of this dissertation, we aim to explore and analyze the concurrent effects of crowding-related externalities (on-board crowding discomfort and denied boarding situations) and travel time stochasticity on the optimal deployment of automated bus fleets, when determining the optimal service frequency and vehicle size as tactical planning decisions. For this purpose, we develop a novel Mixed-Integer Nonlinear Programming (MINLP) optimization model, considering stochastic travel times, time-varying passenger flows, crowding discomfort factors for both sitting and standing passengers, and the possibility of denied boarding due to capacity constraints. Notably, the model is able to estimate in-vehicle crowding discomfort at a microscopic level, bus by bus, depending on the number of sitting and standing passengers traveling inside each bus at each route segment. Taking both passengers' and operators' costs into account, the objective of the model is to find the optimal service frequency and vehicle size with minimal total costs of a public transport service.

To evaluate the applicability of the proposed model, several deployment scenarios are simulated through the combination of different cases: (i) vehicle technology (human-driven or automated vehicles), (ii) travel time between stops (deterministic or stochastic travel times), and (iii) crowding discomfort externalities (considering or ignoring in-vehicle crowding costs). Our experiments are executed for two real-world case studies in Regensburg, Germany, and Santiago, Chile.

To further assess the possible effects of automation on the social costs of a public transportation service, an extensive range of sensitivity analysis tests are carried out on human driving cost savings with different automation levels, travel time uncertainty, dwell time regularity, the time lost to open and close doors with automation, crowding multipliers, denied boarding saving values, and user- and operator-oriented design solutions. Moreover, to handle travel time stochasticity in the solution process, we incorporate a Monte Carlo Simulation (MCS) program into the evaluation phase of our solution algorithm, enabling us to conduct enough evaluation runs to determine the objective function value of each solution, as opposed to a single run that is suitable for deterministic cases. The mathematical model developed in this research, along with its results, has been published in Sadrani et al. (2022b), forming part of the methodological framework that amalgamates vehicle automation capabilities, crowding externalities, and travel time stochasticity within the automated bus planning problem.

1.2.2 Electric bus planning

For the second objective of this dissertation, our focus is directed towards exploring the role of integrating a detailed (variable) energy consumption model into the tactical planning of EB fleets. This exploration seeks to uncover the impacts of route topography and vehicle dynamics (e.g., slope- and load-sensitive effects) on the critical decisions regarding the optimal type and number of vehicles to be acquired in the early stages of EB projects. To achieve this objective, we propose an EB fleet planning problem in the form of an Integer Nonlinear Programming (INLP) model, which integrates a variable energy consumption model (based on longitudinal vehicle dynamics) into the planning phase of EB fleets. The proposed model considers both passenger and bus operator costs to optimize vehicle type and service frequency needed to achieve a proper supply level.

The model applicability is investigated on a real bus corridor in Santiago de Chile, which crosses the city from west to east and is subject to an increasing slope when running east. Several scenarios of operations are simulated under different demand levels (low vs. high demand levels), energy estimation methods (variable vs. simplified fixed energy demand), and route conditions (with vs. without slope). Specifically, by integrating energy-related variables into the planning process, we identify several novel findings, making a significant contribution to the scientific understanding of this field. The optimization model, solution algorithms, and outcomes of this study have been compiled in a manuscript, Sadrani et al. (2023b), which is under review.

Moreover, while our EB planning model encompasses an overnight charging strategy within its planning framework, another pivotal issue in the electrification of bus networks pertains to selecting the optimal charging strategy from a variety of options, such as overnight (slow) charging and opportunity (fast) charging systems. This critical aspect lays the groundwork for our third dissertation objective. Hence, we attempt to continue our investigations to provide a comprehensive understanding of the factors affecting policymakers' decisions in selecting the best charging strategy for EB systems. Overall, choosing the best charging option is a challenging task since each option has advantages and disadvantages. To tackle this issue effectively, policymakers need to consider multiple factors (with different dimensions) concurrently, calling for the management of a Multi-Criteria Decision-Making (MCDM) problem. This dissertation thus aims to address the selection of charging strategies for EB systems as a MCDM framework, assisting policymakers in making informed decisions using a reliable decision-making tool for the comparison and assessment of possible charging

alternatives based on a wide range of criteria that are relevant in practice. The decision-making models and findings of this research have been published in Sadrani et al. (2023c).

It should be noted that, in the above-mentioned models, although we address the selection of optimal vehicle size among multiple vehicle sizes (e.g., among 8, 12, 15, and 18-m long buses), we focus on the modeling and operation of uniform (homogeneous) fleets, composed of vehicles of the same size, e.g., if a vehicle size of 12-m is selected as the optimal size, a fleet of 12-m buses is operated at an optimal frequency level obtained in the frequency setting phase.

1.2.3 Mixed-fleet bus planning

Finally, as the last objectives of this dissertation, we explore the planning aspects and solution complexities associated with fleet heterogeneity within mixed operating environments, where buses of different types and capacities can be utilized to meet passenger flows. For this purpose, we develop two versions of the Mixed-Fleet Bus Scheduling (MFBS) problem: an initial simplified version and an advanced model.

We commence with the simpler version of the MFBS problem, which serves as the foundation for comprehending and addressing the modeling and computational complexities of mixed-fleet operations. In this context, we formulate a novel MINLP model that optimizes dispatching schemes, encompassing dispatching sequence and timing, in scenarios where a fixed number of buses with different sizes are available to meet route demand. The primary objective is to minimize average passenger waiting times, with stochastic travel times between stops and vehicle capacity constraints (i.e., introducing extra waiting time due to denied boarding). Given the discrete set of feasible dispatching sequences, this problem presents itself as a complex permutation-based combinatorial optimization problem, proved to be strongly NP-Hard. To tackle this complexity, we develop an exact decomposition-based method, as well as a Simulated Annealing (SA) metaheuristic, coupled with a Monte Carlo Simulation (MCS) framework, to solve it. We test the model and solution algorithm through numerous numerical experiments, employing real data from an actual bus corridor in Sydney, Australia. Furthermore, to highlight the value of having fine-grained demand information (every 15 minutes instead of every 60 minutes) when designing a dispatching scheme, the experiments are also tested with low-resolution demand volumes (one-hour-dependent demand volumes). The mathematical model and solution algorithms developed in this version have been published in Sadrani et al. (2022a).

We then progress to the development of a more comprehensive MFBS model, significantly expanding upon the previous MINLP formulation. This advanced version contains a broader spectrum of real-world operational constraints (encompassing elements such as resource availability constraints, sitting and standing space constraints), and a wider array of objective functions (including operator costs (which were not considered in the simpler MFBS model) and user costs, taking into account in-vehicle trip times and trip comfort). Furthermore, this advanced version introduces new integer decision variables regarding vehicle assignment programs. Hence, our advanced problem goes beyond optimizing vehicle dispatching plans (dispatching sequence and time), and also addresses the optimization of vehicle assignment programs (the optimal determination of the number and type of vehicles needed for mixed-fleet deployments).

The inclusion of these realistic elements increases the complexity of solving the MFBS problem significantly. Thus, the development of reliable and advanced solution algorithms to effectively address these challenges becomes paramount. We develop two hybrid metaheuristic algorithms, Genetic Algorithm combined with Simulated Annealing (GA-SA) and Grey Wolf Optimizer combined with Simulated Annealing (GWO-SA), with a Taguchi approach to calibrate the metaheuristics' parameters.

The performance of the metaheuristics is extensively evaluated on small, medium, and large-scale test samples, considering solution quality and CPU time. Results show that the GWO-SA outperforms the other metaheuristics. We also compare the metaheuristics' outcomes with the optimal solutions acquired by GAMS software in small and medium-sized samples. The developed model and metaheuristics are applied to a real-world bus corridor in Santiago, Chile, characterized by high passenger crowding levels during the morning peak period. We conduct sensitivity analyses to evaluate the sensitivity of mixed-fleet deployment programs to factors such as demand levels, solution techniques, crowding inconvenience valuations, and uncertain driving times. The mathematical model and metaheuristics developed in this version have been presented in a manuscript, Sadrani et al. (2023a), which is under review.

1.2.4 Research questions

In summary, to achieve the research objectives, the main research questions addressed in this dissertation are listed as follows:

1. **Crowding and stochastic travel times in automated bus systems:**

- How do considerations of crowding-related aspects, specifically crowding discomfort, and the uncertainty of travel times impact the planning of automated bus systems across various levels of human driving cost savings?
- Do frequencies and bus sizes increase at comparable rates for both human-driven and automated bus fleets when accounting for in-vehicle crowding as a factor of travel disutility for passengers?
- Can the deployment of automated bus systems contribute to mitigating or eliminating denied boardings in crowded bus corridors?

2. **Detailed energy consumption models in EB fleet planning:**

- How does incorporating a variable (detailed) energy consumption model into the tactical planning of EB fleets influence decisions regarding the optimal type and number of vehicles to acquire for early-stage EB projects?

3. **Multi-criteria decision-making for charging strategies:**

- How can a multi-dimensional decision-making framework be developed to tackle the selection of optimal charging strategies for EB systems, thereby aiding policymakers in making well-informed decisions regarding the electrification of bus networks?

4. **Optimizing mixed-fleet bus operations:**

- To what extent can optimizing vehicle assignment and dispatching plans for mixed-fleet bus operations, encompassing fleet size, fleet composition, dispatching sequences, and dispatching times, lead to reduced total costs (user and operator costs)?

5. **Advanced computational intelligence algorithms in mixed-fleet scheduling:**

- To what extent can the development and implementation of more advanced computational intelligence algorithms, such as hybrid metaheuristics, enhance the quality of service and operator costs in MFBS problems?

1.3 Contribution statement

This dissertation endeavors to advance the modeling, planning, and optimization capabilities of public transport services with automated, electric, and mixed-sized bus fleets. It contributes to the field of public transport planning by introducing novel mathematical modeling frameworks and solution algorithms. Furthermore, the research identifies several novel findings and insights, significantly enhancing our scientific understanding of the differences associated with planning emerging bus fleets compared to traditional ones. The key research components of this dissertation are illustrated in Fig. 1-1.

1.3.1 Automated bus planning

The main contributions in our comprehensive formulation of an automated bus planning problem are summarized in three aspects. First, for the first time in the literature, we model the effects of in-vehicle crowding discomfort when determining the optimal service frequency and vehicle size for automated bus fleets, considering the perceptions of both standing and sitting passengers from crowding disutility. Additionally, we conduct a comparative analysis between the planning of automated and conventional human-driven bus fleets, in the presence of crowding discomfort impacts. This analysis is conducted within different country contexts, such as Germany and Chile, representing examples of both developing and developed countries. While it is expected that frequencies and bus sizes are going to increase for both fleets of human-driven and automated buses if in-vehicle crowding is considered as a source of travel disutility for users, the crucial question arising here is whether these items are increased at a similar rate for both fleets or not. This issue has implications for the optimal design of future public transport systems, for the comfort level that will be delivered to users (in terms of occupancy rates inside vehicles), and for the cost-benefit analysis of public transport investments in crowding-sensitive frameworks.

Second, we investigate if implementing an automated bus system can decrease the number of left-behind travelers (denied boarding situations) in busy bus routes, due to providing more frequent services at lower operating costs with automation.

Third, the effects of travel time stochasticity on the optimal deployment of an automated bus system vs. a human-driven bus system are closely examined, given that the potential provision of more certain travel times is an added benefit of automation in public transport.

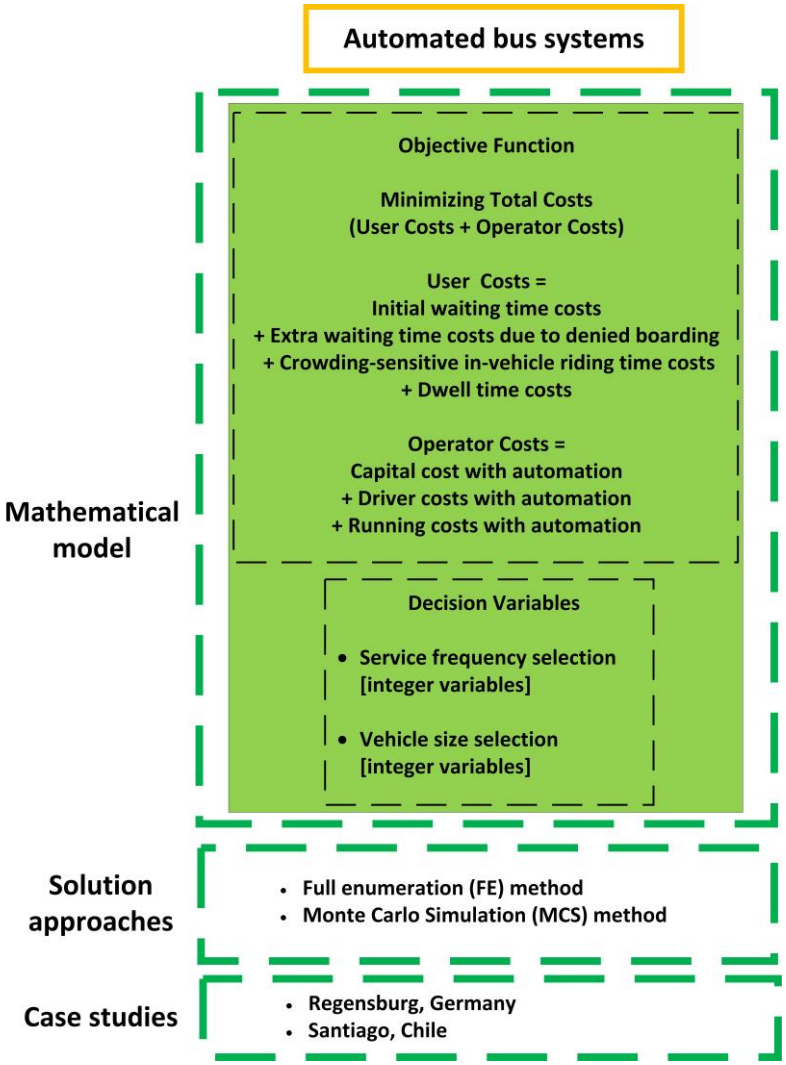

(a) Automated bus planning.

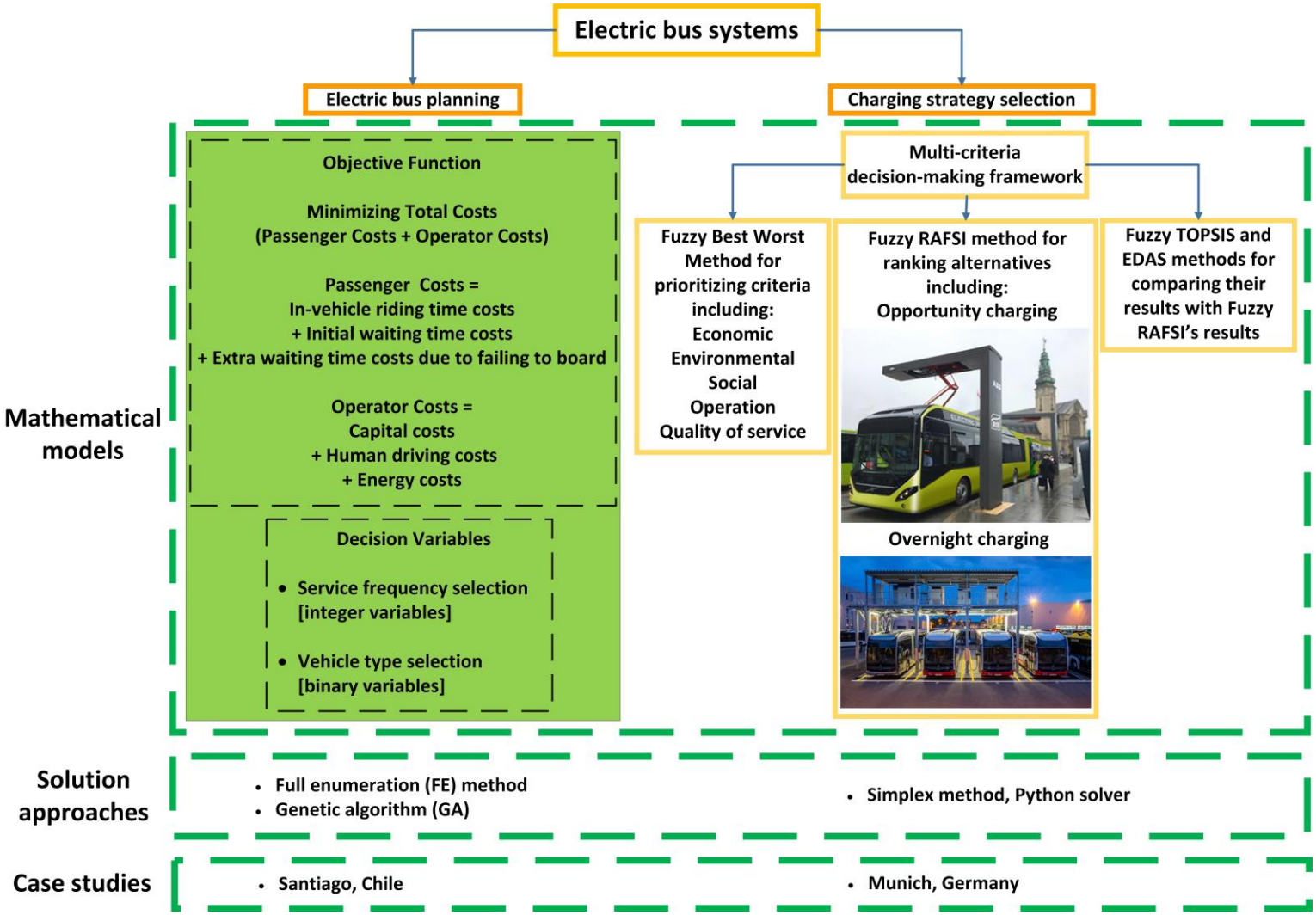

(b) Electric bus planning.

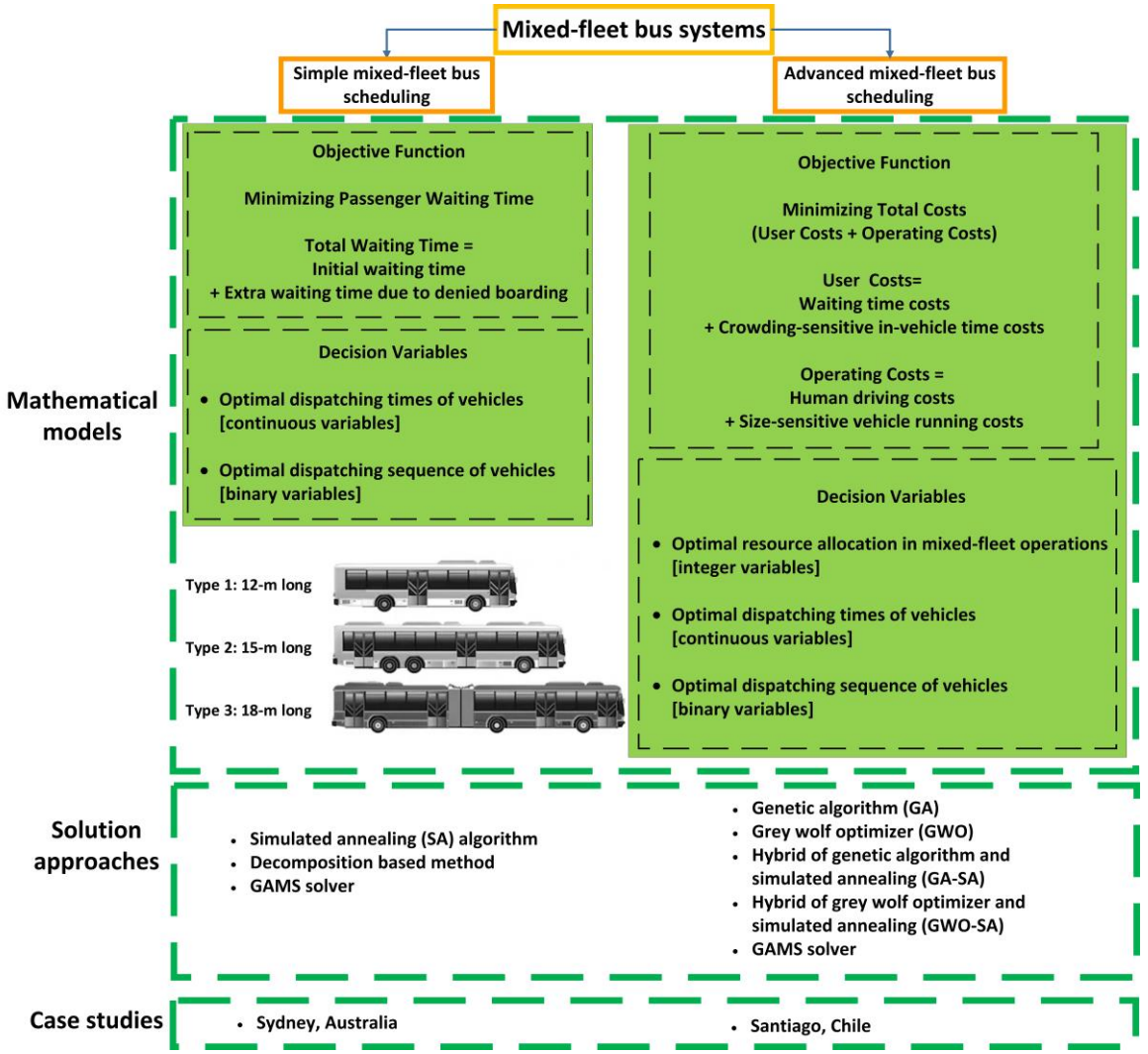

(c) Mixed-fleet bus planning.

Figure 1-1 Overview of research components in the present dissertation.

1.3.2 Electric bus planning

The contributions of this dissertation to the EB literature include (i) the development of an EB tactical planning optimization model, by combining contributions from energy consumption dynamics, transport economics, passenger flow behavior, and operations research to optimize public transport supply with EB fleets, and (ii) the introduction of a decision-making framework for selecting EB charging strategies.

In the context of EB planning, this dissertation develops a novel mathematical optimization framework in the form of an INLP model, which integrates a variable (detailed) energy consumption model into the tactical planning phase of EB fleets, when determining the optimal supply levels for public transport services with EBs, as it can provide valuable insights into the sensitivity of vehicle type selection and frequency plans to different assumptions regarding energy consumption modeling. Our contributions include optimizing vehicle type selection and service frequencies with EBs, developing a comprehensive cost model, considering size-varying factors affecting the economic aspects of EB operations, time-dependent passenger demand modeling, and formulating the EB planning problem as a combinatorial optimization model. From a policy point of view, this model would be helpful, especially in the early stages of an EB project, assisting in informed decisions about the type and number of vehicles that should be acquired. We apply our model to a bus route in Santiago de Chile and conducted several sensitivity tests to analyze the results.

Secondly, this dissertation addresses a gap in the literature by introducing a novel decision-making methodology for selecting charging strategies for urban EB systems. To address this issue, we create a MCDM framework that offers a comprehensive, multi-dimensional approach for comparing and evaluating potential EB charging strategies based on (i) economic, (ii) environmental, (iii) social, (iv) operational, and (v) quality-of-service implications. We conduct a systematic effort, involving a comprehensive literature review and interviews with EB experts, to identify, refine, and establish a comprehensive and evidence-based list of criteria relevant to policymakers when selecting charging strategies for EB systems. To determine the weight of the criteria, we develop a Fuzzy Best-Worst Method (FBWM). We then introduce a Fuzzy Ranking of Alternatives through Functional mapping of criterion subintervals into a Single Interval (FRAFSI) approach for the assessment and ranking of available charging strategies for EB systems, including overnight (slow) and opportunity (fast) charging strategies. We extend our evaluations by testing

alternative ranking methods, including fuzzy TOPSIS and fuzzy EDAS, allowing us to compare the outcomes of various methods for addressing our problem.

1.3.3 Mixed-fleet bus planning

Finally, this dissertation makes substantial contributions to the realm of MFBS problems, including the creation of novel optimization models (in two versions, simple and advanced) for the MFBS issue and the development of solution algorithms to address the combinatorial complexity of such problems.

First, regarding the formulation, we mathematically model the planning aspects of mixed-bus fleets using a novel MINLP model, allowing for the optimization of vehicle dispatching solutions (determining the dispatching order and time of vehicles), and vehicle assignment solutions (determining the optimal number and type of vehicles assigned for operations) in mixed-fleet operations.

Second, we propose an exact decomposition-based method and a SA algorithm, paired with a MCS method, for solving simple versions of the MFBS. In particular, the SA's search operators are exclusively designed to take advantage of producing only feasible neighboring solutions.

Third, we develop two new hybrid metaheuristics, GA-SA and GWO-SA, to efficiently address the complexities of the advanced versions of MFBS for large-scale scenarios. We also perform a comparative analysis of the metaheuristics' results against the optimal solutions obtained by GAMS solver in small and medium-sized samples. Notably, our real-world application shows that the choice of metaheuristic for the MFBS is not innocuous, as the most sophisticated algorithms perform better in terms of improving trip comfort precisely when crowding levels are high, whereas when the demand density is low, the choice of solution algorithm is less relevant. This empirical application provides invaluable managerial insights for optimizing the operational planning of mixed bus fleets, thereby enhancing operational efficiency and passenger comfort.

1.4 Dissertation structure

The dissertation's structure, as summarized in Fig. 1-2, outlines the organization of the remaining chapters:

Chapter 2 (Literature Review): This chapter provides a review of existing literature related to the planning and operations of automated, electric, and mixed-fleet bus systems. It also highlights the research gaps identified in the field.

Chapter 3 (Model Formulation): This chapter presents the mathematical models developed within this dissertation. It encompasses a MINLP model for automated bus planning, an INLP model for EB planning, MCDM models for selecting charging strategies, and two MINLP models designed to address MFBS problems in simple and advanced versions.

Chapter 4 (Solution Algorithms): This chapter describes the solution algorithms introduced to address the computational complexities of the formulated models, including various exact and metaheuristic algorithms.

Chapter 5 (Results and Discussion): This chapter presents the outcomes derived from applying the proposed models and solution algorithms in real-life case studies. It offers an in-depth assessment of their practical applicability and discusses the implications of these findings.

Chapter 6 (Sensitivity Analysis): This chapter focuses on sensitivity analysis, exploring how variations in model parameters affect the outcomes. It provides insights into the robustness and sensitivity of the models to different factors.

Chapter 7 (Conclusions): This chapter summarizes the primary models and algorithms presented in the dissertation. It highlights the key findings and managerial insights derived from the research. Additionally, it discusses the limitations of the work and suggests potential directions for future research.

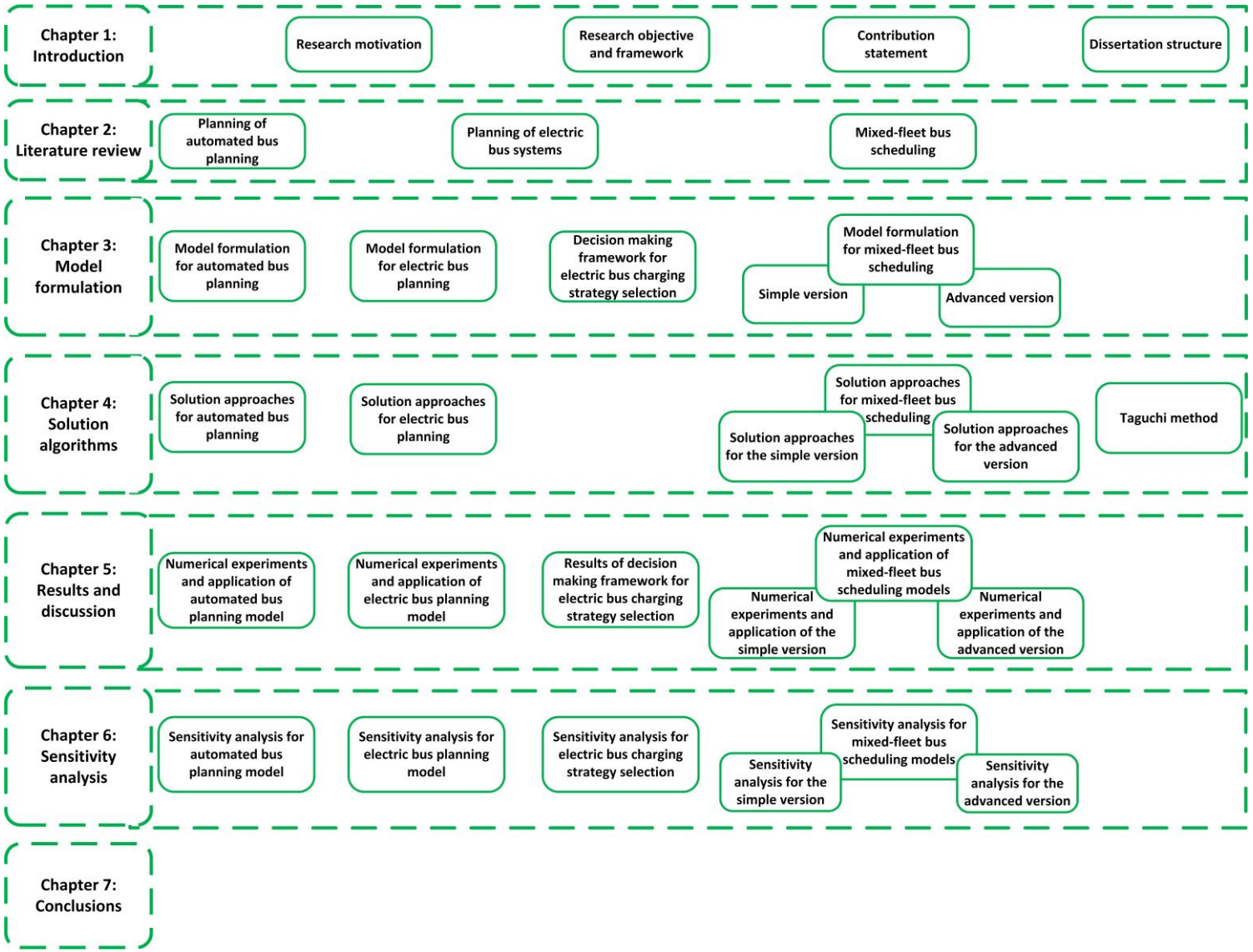

Figure 1-2 Dissertation structure.

2 Literature review

This chapter reviews the existing literature on the planning and operations of automated, electric, and mixed-fleet bus fleets. It also identifies gaps in the literature, setting the stage for the contributions presented in this dissertation.

2.1 Planning of automated bus systems

2.1.1 Vehicle automation

The deployment of automated public transport systems for improving the level of service and reducing the social costs of a public transportation service has emerged as a research topic in the past decade. Generally, people appear to be positive about the deployment of (future) automated bus systems (Alessandrini et al., 2011; Ceder, 2021; Distler et al., 2018; Eden et al., 2017). Thus far, a broad spectrum of connected and autonomous driving technologies have been evolved and introduced to automated public transport systems for providing more robust autonomous mobility services, such as bus platooning, lane-keeping, collision avoidance, bus precision docking (i.e., providing a stable distance between vehicles and platforms at stations), automated emergency braking, Cooperative Adaptive Cruise Control (CACC), Vehicle-to-Vehicle (V2V) and Vehicle-to-Infrastructure (V2I) communications (Lazarus et al., 2018; Lutin, 2018). Hence, beyond human driving cost savings with automation, it is expected that the deployment of automated vehicles can positively affect public transport systems in various aspects via leveraging full automation capabilities (Tirachini and Antoniou, 2020).

2.1.2 Related studies on automated bus planning

In recent years, a growing number of studies have focused on the optimal design and deployment of automated bus services to minimize the social costs of public transport services. W. Zhang et al. (2019) proposed a total cost minimization model to find the optimal bus frequency and size for fleets of conventional, semi-automated, and fully-automated buses on a generic hub-and-branch network. Given the reduction or elimination of in-vehicle crew costs with automation, results showed that automated vehicle solutions optimally suggest a higher service frequency and a smaller vehicle size. This result has been also replicated by, Fielbaum (2020) and Tirachini and Antoniou (2020). Overall, despite the increase of capital

costs due to the inclusion of automation technologies inside buses, fully-automated buses exhibit great potential through the reduction of operating and waiting costs. Fielbaum (2020) proposed a feeder–trunk automated vehicle public transport model, taking advantage of vehicle automation and mixing on-demand systems for local trips (feeder) with a more traditional system for longer trips (trunk). It was found that the technology of automation pushes the system toward providing larger fleets of smaller vehicles. Tirachini and Antoniou (2020) presented an optimization model to assess the impacts of vehicle automation on optimal vehicle size, service frequency, fare, subsidy, and degree of economies of scale. The model was tested using data from Chile and Germany, taken as illustrative examples of developing and developed countries. Results showed that automated services benefit users, through a reduction of waiting times and optimal fares, operators, through a reduction of operating cost, and the public sector, through a reduction of the first-best optimal subsidy per bus trip. Moreover, it was found that the benefits of automation are more prominent in countries where drivers' wages are higher (such as Germany relative to Chile), due to larger savings of human-related driving costs with automation.

Hatzenbühler et al. (2020) proposed an analytical model to optimize frequency and vehicle capacity for human-driven and automated bus fleets, while considering the sum of passenger and operator costs on a weighted normalized basis, where weighting factors allow for the analysis of passenger- and operator-oriented solutions. The model was applied to a real-life case study in Kista (Stockholm, Sweden), and the results showed that automated bus services have the potential to attract passengers through improved service provision. Badia and Jenelius (2021) assessed the possible effects of vehicle automation and electrification on the design and optimization of feeder transit services in suburban areas. For this purpose, an analytical model was proposed based on continuum approximations, while considering and comparing the applicability of two different operating strategies of feeder transit systems: parallel fixed lines and door-to-door trips. The authors modeled user costs and operator costs, while considering the economic effects of new vehicle technologies on system cost structures. The findings showed that the effect of automation on the applicability between the two feeder options is clearly more significant than the effect of electrification.

To determine the optimal frequencies of autonomous minibuses when serving several sublines, Gkiotsalitis et al. (2021) developed a stochastic optimization model as a Mixed-Integer Linear Programming (MILP) formulation, while accounting for the stochasticity of passenger demand. The problem objective was to minimize the sum of operational and

passenger waiting time costs. The model performance was tested under deterministic and stochastic demand scenarios, showing 10-40% operational cost savings when assigning optimal frequency solutions to sublines. Besides, to improve the level of service and reduce running costs at operational planning levels, some scholars have attempted to create new mathematical formulations for the optimization of skip-stop tactics and other operational strategies (such as holding and speed changing), while accounting for automated driving capabilities in public transport services (Cao and Ceder, 2019; Cao et al., 2019).

As for the operation with mixed fleets, Dai et al. (2020) developed an INLP model to optimize vehicle types and dispatch times for a mixed fleet of human-driven and automated buses. The authors assumed that the capacity of automated buses can be dynamically changed at terminals through assembling/dissembling minibus modules. The model objective was to minimize passenger and bus operating costs. Results showed that passenger costs can be reduced significantly using dynamic dispatching solutions. Tian et al. (2021) proposed a stochastic programming model to optimize the fleet size required for mixed fleet operations with conventional and automated vehicles in a bus network, while aiming to minimize passenger waiting times and operator costs under stochastic demand conditions. Results confirmed the benefits of automated buses that can be allocated to different bus lines in a more flexible manner.

2.1.3 Crowding in public transport systems: effects and modeling approaches

Public transport systems in several cities across the globe are experiencing increasing congestion and crowding with the rapid growth of public transportation ridership (Jenelius, 2018). Indeed, public transport crowding can negatively affect users' trip experience and service performance (Drabicki et al., 2021). For instance, crowding phenomena can significantly escalate the discomfort of public transport users inside vehicles (i.e., in-vehicle crowding discomfort), as well as the possibility of denied boardings (Cats et al., 2016; Hörcher and Tirachini, 2021; Tirachini et al., 2013). To simulate realistic operating conditions, only few studies in the literature of automated bus services (Dai et al., 2020; Hatzenbühler et al., 2020) have considered the possibility of denied boardings. Nonetheless, to the best of our knowledge, an explicit modeling of in-vehicle crowding discomfort (at a microscopic resolution for both sitting and standing travelers) has not yet been included in the optimal design and deployment of automated bus systems. Besides, covering this issue would

be more notable in a state-of-the-art model that also contains other aspects of operations explicitly, enabling us to capture crowding discomfort effects together with the concurrent effects of travel time stochasticity and driving cost saving levels with automation on the planning of automated buses.

It has been found that on-board comfort has a profound effect on the satisfaction and loyalty of public transport users (Soza-Parra et al., 2019; Van Lierop et al., 2018). In-vehicle crowding discomfort leads to an increase in the value of in-vehicle time savings (Hörcher et al., 2017). Indeed, the effect of in-vehicle crowding on travel time disutility is typically expressed using an additional in-vehicle travel time multiplier, called crowding multiplier, which increases with the occupancy of vehicles and is larger for standing passengers than for sitting passengers (Jenelius, 2020; Tirachini et al., 2013; Tirachini et al., 2017; Wardman and Whelan, 2011; Whelan and Crockett, 2009; Yap et al., 2020).

To optimize public transport frequency and vehicle size in the presence of crowding externalities, the crowding phenomenon is usually included in service supply optimization models through forming a total cost function, in which the user cost is sensitive to in-vehicle crowding levels (An et al., 2020; Jara-Díaz and Gschwender, 2003; Tirachini et al., 2014). For instance, for the determination of optimal frequency and vehicle size, Jara-Díaz and Gschwender (2003) and Tirachini et al. (2014) have highlighted the importance of considering in-vehicle crowding discomfort as a source of disutility for travelers, leading to an increase in frequency and vehicle size compared to the cases in which the user cost is assumed to be insensitive to in-vehicle crowding levels. Likewise, many other studies have so far focused on determining public transport planning decisions while accounting for in-vehicle crowding discomfort, e.g., in frequency and vehicle size determination problems (Batarce et al., 2016; Cats and Glück, 2019; Hörcher and Graham, 2018; Klumpenhouwer and Wirasinghe, 2016; Zhang et al., 2020); frequency determination problems (Agrawal et al., 2020; Hörcher et al., 2020; Hörcher et al., 2018; Jiang et al., 2014; Pathak et al., 2020; Qin, 2014; Suman and Bolia, 2019); timetabling design methods (Shang et al., 2019); seat provision in public transport (De Palma et al., 2015; Hamdouch et al., 2011; Hörcher et al., 2018).

Besides, for further discussion in this regard, the interested readers are referred to the review paper of Hörcher and Tirachini (2021) who have identified crowding discomfort as an important ingredient in the determination of vehicle size and frequency. An in-depth discussion of in-vehicle discomfort matters is also given in the Transit Cooperative Research Program

(TCRP)-165 Report (2013), where the quality of service thresholds are also presented and categorized from an on-board comfort perspective. Overall, the most common way to deal with in-vehicle crowding discomfort is to increase service frequency (Batarce et al., 2016; Tirachini et al., 2013; Tirachini et al., 2014; Van Lierop et al., 2018).

Regarding implications for cost-benefit analysis, Cats et al. (2016) developed a novel modeling framework considering the dynamics of public transport congestion in the appraisal of large public transport investments. A case study of a metro extension in Stockholm indicated that the benefits gained by the inclusion of dynamic congestion and crowding effects into a cost-benefit analysis can constitute more than a third of the total passenger benefits, and such effects are remarkably underestimated by a static model. Along the same lines, Tirachini et al. (2016) estimated that not accounting for standing externalities in Singapore's East-West MRT line underestimates the disutility of travel time by 28% in the morning peak period. All these findings clearly point to the relevance of crowding externalities for system design and estimation of benefits in public transport project appraisal. Crowding costs are considered in the cost-benefit analysis of transport investments in the United Kingdom, France, Sweden, Australia, New Zealand, and Japan (ITF/OECD, 2014).

As for the value of waiting time savings, several studies have revealed that the value of waiting time is higher than that of in-vehicle time, as passengers feel more dissatisfied with their waiting times at stops (e.g., Wardman, 2004; Xumei et al., 2011; Cats et al., 2016). Hence, waiting time is considered as one of the most striking travel time components for evaluating the level of service from a passenger's point of view (Niu et al., 2015). Particularly, in high-demand public transport corridors during peak periods, waiting times can be too long for passengers who are unable to board a service due to a lack of capacity, thereby reducing the attractiveness and reliability of a public transport system substantially. With the rapid growth of public transportation ridership, left behind passengers due to overcrowding is becoming a main concern for many transit agencies (Sun and Xu, 2012; Zhu et al., 2017). This challenging problem is particularly prevalent on some crowded public transport systems across the globe (e.g., Beijing, Moscow, Sao Paulo, Santiago, Hong Kong), in which it is not unusual to operate vehicles at (or near) crush capacity[1] during the peak hours (Tirachini et al., 2014).

[1] Vehicles are operated with (near) full capacity, e.g., a high density of standees is observed inside vehicles.

2.1.4 Stochastic nature of public transport operations: effects of travel time stochasticity

One of the main sources of instability in urban bus operations is the variations of vehicle travel times between stops, caused by a wide range of external factors, such as traffic congestion, traffic lights, weather, and human driving behavior (Muñoz et al., 2020). In this context, several scholars have employed log-normal distribution to model stochastic running times of buses (Cats et al., 2011; Dai et al., 2020; Dai et al., 2019; Delgado et al., 2012; Hickman, 2001; Jiamin et al., 2003; Sánchez-Martínez et al., 2016).

The explicit inclusion of travel time stochasticity into the frequency setting problem of automated buses is another incremental contribution to the automated bus literature. As the closest relevant study in relation to this subject, accounting for stochastic travel times, we refer to Dai et al. (2020). Nonetheless, compared to our research, a different scheduling problem with a mixed bus operating environment has been addressed in Dai et al. (2020), focusing on real-time dispatching of automated buses with varying capacities among human-driven buses to provide a more flexible capacity solution to passenger demand fluctuations. Besides, fleet size determination, vehicle capital costs, human driving cost savings with automation, and crowding discomfort effects have not been considered in their study.

Unreliable travel times have a negative impact on passenger waiting time at stops (Durán-Hormazábal and Tirachini, 2016). In addition, although waiting time affects overall user satisfaction (Dell'Olio et al., 2011; Tyrinopoulos and Antoniou, 2008), waiting time due to unreliability (e.g., travel time uncertainty) has deeper negative consequences on users' satisfaction (Rietveld et al., 2001; Van Lierop et al., 2018). Hence, unexpected waiting delays associated with unreliable services can substantially degrade the attractiveness of a public transport system. On the other hand, the differences in human driving functions, which can introduce considerable uncertainty in travel time during real-world operations (Wang and Sun, 2020), can be much less pronounced in the operation with automated vehicles due to the elimination of distracted driving and bad driving behavior (Azad et al., 2019). Moreover, Dai et al. (2020) assume that automated buses can dynamically and accurately adjust their running times given the forward and backward headways thanks to automation capabilities, thus making automated bus systems more robust to random disruptions. Nonetheless, it is worth noting that the public acceptance of driverless bus systems can be affected by users' perceptions about the security and safety of such systems in real-world operations. For example, the findings of the current stage of automated bus programs show that there is still a propensity for the use of human-driven buses for trips longer than few minutes,

as there are still some concerns about the operational safety of automated buses among users, especially in mixed traffic environments (Dong et al., 2019; Horschutz Nemoto et al., 2021; Salonen, 2018).

Driving time volatility between stops can also lead to a further growth of irregularity in dwell times of vehicles at stops due to poor service reliability, early or late services (van Oort, 2014), i.e., travel time variations have adverse effects on dwell time regularity at stops. Nonetheless, this aspect has still not been studied in the deployment of a fleet of automated vehicles that might be operated with different travel time variation levels. The possible influences of automation on travel time volatility, and dwell time regularity are extensively examined in this research.

2.1.5 Research gap analysis

The extant literature on public transport design and optimization with automated vehicles still has several relevant research questions open for inquiry. We can first mention the impacts of in-vehicle crowding externalities on determining the optimal frequency and vehicle size for an automated bus system. Two effects of passenger crowding deserve particular attention in the comparison of human-driven vs. automated vehicles: the crowding discomfort as increasing the value of travel time savings, and the possibility of passengers not being able to board vehicles due to capacity constraints. Second, despite the stochastic nature of public transport operations, the possible effects of automation on travel time variability and dwell time regularity have not yet been studied in the literature of automated bus operations.

2.2 Planning of electric bus systems

2.2.1 Electric bus planning

Global Carbon Dioxide (CO_2) emissions have risen by 90% since 1970, with 78% attributed to fossil fuel combustion (Boden et al., 2017). With the growth of worldwide environmental concerns and climate change crisis, Electric Vehicles (EVs) (including electric bicycles, cars, and buses) are being promoted as an alternative to conventional diesel vehicles, with many governments offering incentive policies to accelerate their adoption (Shen et al., 2019).

In recent years, there has been growing interest among urban public transport agencies in the adoption of EBs, which offer several benefits over diesel buses, such as higher energy efficiency and lower levels of noise, local pollution and GHG emissions when powered with clean energy (Adheesh et al., 2016; Logan et al., 2020). However, due to the unique characteristics of EBs, such as range anxiety and charging infrastructure constraints, it is crucial to have a comprehensive understanding of the factors that influence their energy consumption for effective implementation of electric public transport systems. Accurate planning and decision-making should take into account real-world driving conditions, fluctuations in passenger loads, and route topologies (see Fig. 2-1) to avoid unrealistic energy demand estimations, which can undermine the quality and applicability of decisions made by policymakers during the planning stage of EB systems, e.g., when selecting vehicle type, battery capacities, charging strategies, location of charging points, and service frequency (related to the fleet size) (Basma et al., 2020; Hjelkrem et al., 2021).

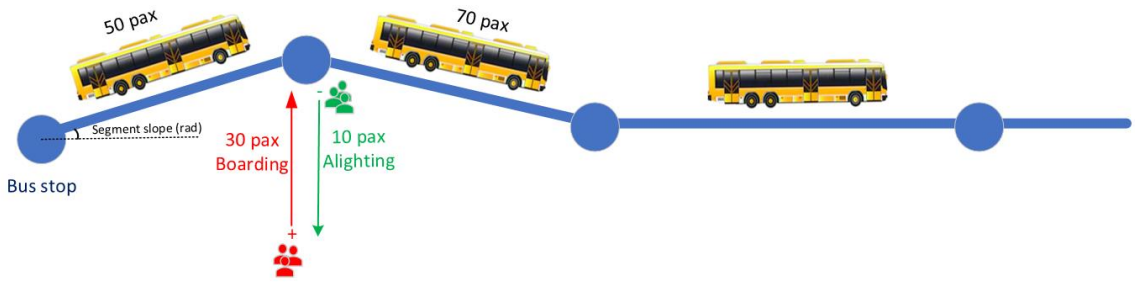

Figure 2-1 An illustrative example of changes in passenger load, vehicle speed, and road slope when traveling at different sections.

Numerous studies have explored the key factors that influence the energy demand of EBs (Gao et al., 2017; Gallet et al., 2018; Göhlich et al., 2018; Al-Ogaili et al., 2020; Hjelkrem et al., 2021; Ma et al., 2021; Abdelaty et al., 2021; Chen et al., 2021; Fiori et al., 2021). These studies employ a common longitudinal dynamics model to estimate the energy consumed by EBs, which considers various resistance forces that act on the vehicle when it is in motion (rolling resistance, aerodynamic drag resistance, grade resistance, and inertial force). The impact of factors such as vehicle weight, passenger load, vehicle speed, route gradients, and auxiliary devices (e.g., air conditioning, heating, in-vehicle displays, and headlights) on the energy consumption of EBs has been widely investigated.

One notable factor that has received significant attention is passenger load (vehicle occupancy rates), which can fluctuate considerably as passengers board and alight at each stop. For example, Gallet et al. (2018) applied a comprehensive energy demand model to the bus network in Singapore and found that the energy consumed by EBs increased during morning and evening peak periods due to higher passenger loads and reduced vehicle speeds resulting from increased traffic congestion. Similarly, Al-Ogaili et al. (2020) used a longitudinal dynamics model to examine the energy demand of EBs in Malaysia and identified road slope and load as the most influential variables.

Hjelkrem et al. (2021) estimated EB energy consumption levels using a longitudinal vehicle dynamics model validated using real datasets from Norway and China. They found that passenger occupancy rates (vehicle load) can significantly influence energy demand requirements for EBs. However, the authors considered constant occupancy rates throughout the entire operation and acknowledged that a more realistic modeling framework is necessary to capture actual occupancy rates under time-dependent demand flows (i.e., stop-level interactions between passengers and vehicles should be modeled to estimate alighting and boarding numbers at each stop).

Overall, it is widely acknowledged that passenger load plays a significant role in the energy consumption of EBs, as evidenced by numerous studies (Zhou et al., 2016; Kivekäs et al., 2018; Basma et al., 2020; Harris et al., 2020; Franca, 2018; Luo et al., 2020; Vepsäläinen et al., 2019; Abdelaty and Mohamed, 2022; among others). Specifically, the total weight of an EB (which includes both the empty bus weight and the passenger load) directly influences rolling resistance (frictional resistance between surfaces and wheels), grade force (force required to travel uphill/downhill), and inertia force (changes in the kinetic energy of a vehicle when accelerating/decelerating).

In some studies on Electric Vehicle Routing Problems (EVRPs), researchers have assumed the energy demand of a vehicle to be linearly proportional to the trip distance for the sake of simplicity (Schneider et al., 2014; Keskin and Çatay, 2016; Hiermann et al., 2016). However, to make accurate estimations of energy demand based on the longitudinal dynamics of vehicles, several recent studies have attempted to consider more realistic factors such as vehicle speed, weight, payload, and route gradients (Goeke and Schneider, 2015; Lin et al., 2016; Zhang et al., 2018; Li et al., 2020; Basso et al., 2019; Pelletier et al., 2019a).

Weight-related factors are particularly important for heavy-duty vehicles such as trucks and buses used in freight and public transport services (Basma et al., 2020). Service providers need to estimate the demand carried by vehicles when planning transport activities. For instance, an articulated 18-m long bus with a capacity of 140 passengers and an average passenger weight of 75 kg can reach a total load of 10,500 kg when running at full capacity, which is around 50% of the curb weight of the vehicle (17-22 tons). Operating vehicles with near-full capacity is a common issue in crowded bus systems that serve large numbers of passengers during peak hours (see Tirachini et al., 2013 and Sadrani et al., 2022a for more information on the crowding phenomenon in public transport systems). Thus, neglecting the effects of passenger load on energy consumption can result in inaccurate adjustments to supply schemes, such as service frequency and vehicle type, in the planning phase of EB systems, leading to increased social costs of public transportation services. In this context, increasing the service frequency of a bus service can reduce crowding costs, waiting times, and energy consumption per vehicle due to a reduction in passenger load. However, this approach requires more vehicles for operations.

2.2.2 Charging strategy selection

One critical consideration in the electrification of bus networks is the choice of the optimal charging strategy from a range of options, such as overnight (slow) and opportunity (fast) charging systems. In this section, we perform a thorough analysis of the literature to find and extract criteria that can affect the charging strategy selection for EB systems. The articles that have undergone review can be divided into two categories. The first category includes articles on EBs, and their text and tables are carefully reviewed to extract the pertinent criteria. The second group includes MCDM papers, giving us a more organized viewpoint for the discovery and classification of new criteria based on the opinions of experts. Finally, the criteria derived from the literature and experts' judgments and their descriptions are listed in Tables 2-1 and 2-2, respectively.

Table 2-1 Related criteria for choosing the best charging method for EBs.

Category	Criteria	Sub-criteria	Reference
Economic	Battery cost		Benoliel et al. (2021), Lajunen and Lipman (2016), Campos et al. (2021), Mahmoud et al. (2016), Basma et al. (2022a), Vilppo and Markkula (2015), Ecer (2021), Saadon Al-Ogaili et al. (2020), Gallet et al. (2018)
	Infrastructure cost		
		• Charging equipment cost	Benoliel et al. (2021), Lajunen and Lipman (2016), Campos et al. (2021), Mahmoud et al. (2016), Basma et al. (2022a), Pelletier et al. (2019b), Vilppo and Markkula (2015), Guo and Zhao (2015), Gallet et al. (2018)
		• Land acquisition cost	Benoliel et al. (2021), Lajunen and Lipman (2016), Campos et al. (2021), Mahmoud et al. (2016), Basma et al. (2022a), Pelletier et al. (2019b), Vilppo and Markkula (2015), Koirala et al. (2022), Guo and Zhao (2015)
	Operational cost		
		• Labor cost	Basma et al. (2022a), Vilppo and Markkula (2015), Guo and Zhao (2015)
		• Electricity tariff	Benoliel et al. (2021), Rupp et al. (2020), Basma et al. (2022a), Vilppo and Markkula (2015), Guo and Zhao (2015)
		• Battery replacement cost	Lajunen and Lipman (2016), Basma et al. (2022a), Vilppo and Markkula (2015), Jaguemont et al. (2016), Guo and Zhao (2015)
		• Maintenance cost	Mahmoud et al. (2016), Basma et al. (2022a), Pelletier et al. (2019b), Vilppo and Markkula (2015), Koirala et al. (2022), Guo and Zhao (2015)
Environmental	GHG emission		Lajunen and Lipman (2016), Rupp et al. (2020), Mahmoud et al. (2016)
	Energy consumption		Benoliel et al. (2021), Rupp et al. (2020), Mahmoud et al. (2016), Basma et al. (2022a), Vilppo and Markkula (2015), Loganathan et al. (2021), Ecer (2021), Basma et al. (2022a), Saadon Al-Ogaili et al. (2020), Gallet et al. (2018)
	Environmental pollution after demolition		Lai et al. (2022), Guo and Zhao (2015)
	GHG emissions for battery production		Lai et al. (2022)
	Water consumption in battery production		Kelly et al. (2021), Wu et al. (2021)
	Ecological environment impacts		Sang et al. (2022), Guo and Zhao (2015)
Social	Job opportunity		Basma et al. (2022a), Sadrani et al. (2023b)
	Fire risk		D. Yu et al. (2019), P. Sun et al. (2020)

Category	Criteria	Sub-criteria	Reference
Operation	Charging infrastructures' impacts on surrounding residential areas		Sang et al. (2022), Guo and Zhao (2015)
	City landscape		Experts
	Vehicle capacity		Ecer (2021), Basma et al. (2022a)
	Energy monitoring		Li et al. (2013), Loganathan et al. (2021)
	Driving range		Mahmoud et al. (2016), Basma et al. (2022a), Ecer (2021), Saadon Al-Ogaili et al. (2020), Gallet et al. (2018)
	Charging duration		Rupp et al. (2020), Mahmoud et al. (2016), Basma et al. (2022a), Jaguemont et al. (2016), Ecer (2021)
	Scheduling complexity		Experts
Quality of service	Crowding		Sadrani et al. (2022a), Sadrani et al. (2022b)
	Travel time		Lajunen and Lipman (2016), Rupp et al. (2020), Longo et al. (2021)
	Reliability		Basma et al. (2022a), Sadrani et al. (2022b)

Table 2-2 Description of each criterion.

Row	Criteria	Short description
1	Battery cost	This relates to the Battery pack price.
2	Charging equipment cost	This relates to the costs of purchasing and installing the chargers, including charging equipment and charging stations.
3	Land acquisition cost	This relates to the cost of purchasing the required land for charging stations.
4	Labor cost	This relates to the required drivers' and staff's salary who work at the charging stations, taking into account the wages on the night shift.
5	Electricity tariff	This relates to electricity tariff costs during the charging process.
6	Battery replacement cost	This relates to various aging processes brought on by battery charging rates and frequency, and the need to replace batteries after a certain number of working hours or lifetime.
7	Maintenance cost	This relates to the costs of regular checks, repairing, or replacing components for vehicles, and charging equipment.
8	GHG emission	This relates to the GHG emissions in two stages: during the production and distribution of electricity, and during its usage.
9	Energy consumption	This relates to different factors that influence the energy consumption of vehicles (factors such as battery weight and passenger load).
10	Environmental pollution after demolition	This relates to the amount of pollution emitted to the environment at the end of the battery lifecycle for demolition or recycling.
11	GHG emissions for battery production	This relates to the pollutants produced in the battery production process.
12	Water consumption in battery production	This relates to the amount of water to produce each tone of the battery.
13	Ecological environment impacts	This relates to the various effects such as soil erosion, construction waste, vegetation destruction, and construction sewage caused by producing batteries and building charging stations.
14	Job opportunity	This relates to the created job opportunities (part-time and full-time) including drivers and charging stations staffs.
15	Fire risk	This relates to the possibility and risk of a fire in the batteries and depot/charging stations.
16	Charging infrastructures' impacts on surrounding residential areas	This relates to the impacts of the EB charging process on residents' living, such as noise pollution, wastewater generation, electromagnetic field interference, solid waste production, and emission of toxic gases.
17	City landscape	This relates to the charging stations' effects on the perspective of the city.
18	Vehicle capacity	This relates to the passenger-carrying capacity which depends on the internal design of vehicles.
19	Energy monitoring	This relates to the monitoring of energy levels (remaining energy) during operations to avoid energy lacking problems.

Row	Criteria	Short description
20	Driving range	This relates to the distance that can be traveled with one battery charge (km).
21	Charging duration	This relates to the required time for charging batteries.
22	Scheduling complexity	This relates to the computational complexity in planning efforts.
23	Crowding	This relates to the level of crowding inside vehicles, affecting users' trip comfort.
24	Travel time	This relates to the round-trip time considering charging events during operations.
25	Reliability	This relates to the service regularity from the users' point of view.

2.2.2.1 Electric bus studies: criteria analysis and extraction

As presented in Table 2-1, the implementation of charging strategies for EB systems in practice can be impacted by several factors, such as economic, environmental, social, operational, and quality-of-service factors, described below.

- **Economic**

Due to the considerable financial outlay required to electrify urban bus networks, economic aspects, among others, can significantly influence operators' strategic and tactical decisions, e.g., when selecting the best type of charging infrastructure for EBs. Several studies in the literature have investigated the economic aspects of EBs. Basma et al. (2022a) developed a method that evaluates the technical and financial performance of EB fleets by taking into account costs associated with purchasing, operating, maintaining, and building infrastructure. The results show that EB fleet ownership costs can be significantly reduced by optimizing the charging infrastructure and battery size based on operational limitations. Vilppo and Markkula (2015) assessed the economic aspects of EBs in a mid-sized city. After a comprehensive background analysis, the difference in the lifetime cost of EBs and diesel buses was calculated based on the selected parameters. Two types of Li-ion batteries and different opportunity charging strategies were assessed: charging at the depot, charging at the end stop(s), and charging at the line stops. Lajunen and Lipman (2016) analyzed the carbon dioxide emissions and lifecycle costs of various city bus technologies, including natural gas, diesel, hybrid electric, electric transit buses, and fuel cell hybrid.

To develop bus replacement plans for electrifying bus systems, an integer linear programming that modeled the EB fleet transition problem is presented by Pelletier et al. (2019b). The proposed model considers acquisition and operating costs, salvage revenues, demand charges, and charging infrastructure investments. Benoliel et al. (2021) provided a framework for the optimal deployment of depot and opportunity charging strategies. This study shows EB transit network design is susceptible to the energy consumption of buses. Overall, Table 2-1 presents the main economic criteria and sub-criteria identified to be relevant to the EB charging strategy selection problem, supported by pertinent references. For instance, the infrastructure cost includes two basic components, including charging equipment costs and land acquisition costs.

It is worth noting that there are various energy storage systems available for EBs, such as battery-powered (e.g., lithium-ion, nickel-manganese-cobalt, and nickel-cadmium batteries), super-capacitors, fuel cells, and flywheels (Kraft et al., 2020; J. Manzolli et al., 2022; Rahman et al., 2020). However, we focus on lithium-ion batteries as they are currently the most popular energy storage system[2] for EBs due to their high energy density, long lifespan, relatively low cost, and technology maturity (Kraft et al., 2020; Lai et al., 2022; Loganathan et al., 2021; J. Manzolli et al., 2022).

- **Environmental**

The environmental effects of batteries used in EBs have been investigated from different aspects, such as GHG emissions from the power generation, emissions, and water consumption in the battery production and recycling phases. Kelly et al. (2021) analyzed the life cycle of battery-grade lithium carbonate and lithium hydroxide monohydrate produced from brine and spodumene ores. In a survey Wu et al. (2021), they presented a life cycle assessment framework to assess the environmental costs associated with battery packs for EVs. In addition, some models are presented to estimate the energy consumption of EBs such as a model that integrates

[2] It should be noted that we do not consider battery technology as a separate criterion in our dissertation, where focusing on one type of battery (lithium-ion batteries) would make the decision-making process more accurate for experts to evaluate alternatives (fast and slow) based on various criteria, without introducing increased complexity and inconsistency to the decision-making process and lessening the decision makers' discriminatory power. Besides, including other battery technologies in our problem could have made the comparisons infeasible in some parts, as it introduces a dependency on the battery technology in addition to the charging strategy. For instance, experts cannot provide fair judgments in the presence of more than one battery technology when evaluating alternatives (slow and fast charging) regarding criteria such as battery cost, battery replacement cost, fire risk, GHG emissions in battery production and recycling phases, water consumption in battery production, and more.

longitudinal dynamics models and digital elevation to plan the installation of EBs (Basma et al., 2020; Gallet et al., 2018; Longo et al., 2021; Saadon Al-Ogaili et al., 2020).

Regarding the environmental emissions of various charging methods, it has been reported that overnight charging, which uses renewable energy sources during off-peak hours, can decrease emissions and enhance the environmental performance of EB systems (X. Chen et al., 2018). Nevertheless, overnight charging can also raise the need for infrastructure for power distribution and storage. Besides, fast charging can result in greater emissions from power generation owing to the increased demand on the grid. A review of the literature also shows that the availability of renewable energy sources plays a critical role in the selection of a charging strategy. For example, it has been found that in regions with a high penetration of renewable energy sources, overnight charging can be a more sustainable option compared to fast charging (Lopez de Briñas et al., 2022).

- **Social**

The third category of extracted criteria examines the social aspect of alternatives. The literature and our interviews with experts on the selection of charging strategy show that social factors, such as fire risk, the impact on the quality of life for residents, and the public perception, are important considerations. It has been pointed out that overnight charging can reduce noise pollution and improve the quality of life for residents living near bus depots, however, fast charging can lead to increased noise pollution and visual impacts due to the installation of charging infrastructure in public spaces (Guo and Zhao, 2015; Sang et al., 2022; Vilppo and Markkula, 2015). Another factor in this category is fire risk. The increased use of EVs has brought attention to safety concerns due to potential fire risks posed by high-energy batteries. P. Sun et al. (2020) conducted a review of the recent fire safety concerns regarding EVs and the thermal runaway and fire incidents in Li-ion batteries. Moreover, in a survey by D. Yu et al. (2019), a fire test model using hard case prismatic LiFePO4 cells is built to investigate the fire characteristics and methods for extinguishing fires in the lithium-ion batteries utilized in EBs.

- **Operation**

Next, we discuss the operational set of criteria. Particularly, due to the unique characteristics of EBs (such as range anxiety and battery charging restrictions), a fundamental

understanding of the factors influencing EB operations is of practical importance for the electrification of public transportation systems. In this regard, Campos et al. (2021) investigated how the limited driving range of EBs affects bus operations under a depot charging strategy. They created a model that evaluates the performance of the routes according to the type of charging strategy and calculates the total costs of bus services while taking range and energy limits into account. They found that the charging strategy at the depot even without being the most profitable option, is adequate when the design and operation parameters of the bus route fall below specific values. Since the driving range and charging duration of EBs are influenced by the properties of their on-board battery packs (such as type, capacity, voltage, price, and lifespan), the assessment of battery performance for vehicles has been the subject of several studies, while offering explicit insights on this problem. Loganathan et al. (2021) presented a methodology for selecting the best Li-Ion battery for EVs while using the weighted sum model which is a MCDM method. It has been shown that the evaluation of the state of charge is one of the most crucial challenges in EV battery management systems. The effects of cold weather on Li-ion batteries, which result in capacity/power fading of Li-ion battery technology, are discussed by Jaguemont et al. (2016). They also discussed the ideal approach for low-temperature operations. Lai et al. (2022) reviewed the life cycle assessment of Lithium-ion batteries over their entire life cycle, while describing the framework, types, standards, methods, and technological difficulties involved in conducting a life cycle evaluation. They also looked at the steps of lithium-ion battery manufacturing, use, repurposing, and material recycling.

Furthermore, Ecer (2021) applied MCDM methods for selecting the best battery type for EVs. In this study, ten battery types are chosen as alternatives and different multi-criteria techniques such as SECA, MARCOS, MAIRCA, COCOSO, ARAS, and COPRAS are used for ranking alternatives. Mahmoud et al. (2016) provided a review of different features of hybrid, fuel-cells, and EBs using simulation models, while assessing the operational characteristics of each technology. The study by Li et al. (2013) employed three algorithms (Luenberger Observer, Extended Kalman Filter (EKF), and Sigma Point Kalman Filter (SPKF)) to measure lithium-ion batteries' state of charge. The results showed that the SPKF provided better numerical stability for determining the battery's state of charge.

Whilst some factors, such as charging duration and driving range, are more frequently observed in the EB literature (supported by several references), the planning complexity of EB systems, depending on charging infrastructure types, is a novel criterion brought up in our

interview by some experts from academia and industry. The significance of this factor, ranked 13 out of 25 criteria, will be shown by our findings.

- **Quality of service**

The last category of criteria is dedicated to quality-of-service (including crowding, travel time, and reliability), measuring the performance of alternatives from users' viewpoints. Depending on the type of charging facilities, the amount of time needed for charging events influences the travel time and regularity of EB operations. For example, it has been stated that overnight charging systems have the potential to lessen the risk of operational delays caused by charging idle times (Basma et al., 2022a). Also, Rupp et al. (2020) presented a new methodology to balance the economic and ecological aspects of using EBs to achieve both the protection of the environment and the economical operation of the buses. They optimized EBs' charging times as a function of CO_2 emissions and electricity tariffs considering different charging scenarios affecting the time required for EBs' charging during service and thus travel time.

Besides, varying views are found in the literature and among experts regarding the reliability of charging strategies. It has been pointed out that overnight charging can also increase the reliability of EB systems for riders by reducing the need for backup energy generators and increasing the availability of buses during peak hours (Glotz-Richter and Koch, 2016). Another study found that fast charging can increase the reliability and convenience of EB systems for riders by reducing the need for long layovers and increasing the flexibility of bus routes (Nichoals and Hall, 2018).

Specifically, we consider various criteria related to battery performance and size for both fast and slow charging methods, enabling our charging-strategy-selection MCDM problem to assess cost- and technical-related aspects of batteries directly or indirectly. Indeed, our problem can properly account for size-sensitive technical aspects of batteries when evaluating charging alternatives (slow and fast charging) against relevant criteria, such as battery cost (considering larger vs. smaller battery packs in slow and fast charging, respectively), battery replacement cost (considering battery lifespan and operating conditions such as temperature), maintenance cost, charging equipment cost (considering low- and high-powered chargers in slow and fast charging), charging duration (considering long vs. short charging times for slow and fast charging), energy consumption (considering battery weight and its impacts on energy

consumption), energy monitoring, vehicle capacity (considering battery size and its impacts on vehicle internal space/layout), driving range, GHG emissions in battery production phase (considering battery size), GHG emissions in battery recycling phase, water consumption in battery production phase, and fire risk.

2.2.2.2 Multi-criteria decision-making studies

MCDM methods are the tools used to select the best option from a range of alternatives, while evaluating the performance of each alternative concerning a number of different criteria. To evaluate and determine the weight of the criteria in this dissertation, we utilize a FBWM, which is essentially the fuzzy version of the Best Worst Method (BWM) originally introduced by Rezaei (2015), and is now a well-liked MCDM method that has drawn increasing interest from researchers in various fields (Behzad et al., 2020; Muhammet Deveci et al., 2021; Torkayesh et al., 2021a; Torkayesh et al., 2021b; Torkayesh et al., 2022; S. Zolfani et al., 2019; S. H. Zolfani and Chatterjee, 2019).

Guo and Zhao (2017) expanded the BWM in a fuzzy way for the first time, allowing for better management of uncertainties and ambiguities of decision makers' viewpoints in comparisons. Based on this method, fuzzy pairwise comparisons of the criteria are performed using decision makers' linguistic terms, which are then transformed into fuzzy ratings. The FBWM has been utilized in several areas, including the assessment of the environmental impacts of ship recycling (Soner et al., 2022), the selection of sustainable suppliers (Ecer and Pamucar, 2020), the effectiveness of destination management in small islands (Yamagishi et al., 2022), detecting obstacles for solar energy development (Mostafaeipour et al., 2021), evaluating banking industry performance (Seyfi-Shishavan et al., 2021), and determining the ideal mix of alternative power plants (Omrani et al., 2018).

We also use FRAFSI for evaluating and ranking alternative EB charging strategies, including overnight and opportunity charging. First introduced by Žižović et al. (2020), the RAFSI approach has gained popularity in recent years and has been used to address a diverse range of issues, such as floating photovoltaic power plant site selection (Muhammet Deveci et al. 2022a), autonomous vehicle selection for implementation in the metaverse (Muhammet Deveci et al., 2022b), e-scooter parking location determination (Muhammet Deveci et al., 2023), flight base selection for flight academies (x et al., 2021), and

incinerator location selection (Boré et al., 2022). Our use of FRAFSI accommodates uncertainty and imprecision in decision maker's opinions, resulting in a more robust and accurate ranking of alternatives.

In addition to the FRAFSI, we also test two other ranking methods, namely fuzzy TOPSIS and fuzzy EDAS. C.-T. Chen (2000) extended the TOPSIS method to the fuzzy environment, making it suitable for decision-making problems involving uncertainty. Fuzzy TOPSIS has been applied in diverse areas, such as robot selection (Chu and Lin, 2003), evaluation of shopping websites (C.-C. Sun and Lin, 2009), facility location selection (Ertuğrul and Karakaşoğlu, 2008), supplier selection (Junior et al., 2014), project selection for oil-fields development (Amiri, 2010), ranking renewable energy supply systems (Şengül et al., 2015), and software requirements selection (Nazim et al., 2022).

The fuzzy EDAS method, introduced by Keshavarz-Ghorabaee et al. (2016), is another efficient tool for handling uncertain decision-making problems. Unlike fuzzy TOPSIS (which selects the optimal solution based on the maximum distance from the negative solution and the minimum distance from the positive ideal solution), fuzzy EDAS chooses the best alternative based on its distance from the average solution (Kahraman et al., 2017). Fuzzy EDAS has been used extensively in different application fields, such as selecting carpenter manufacturers (Stević et al., 2018), solid waste disposal site selection (Kahraman et al., 2017), hospital selection (Kutlu Gündoğdu et al., 2018), green supplier selection (S. Zhang et al., 2019), and renewable energy selection (Demirtas et al., 2021).

Next, a number of studies that used MCDM methods in the EB context are discussed. A crucial study related to our research is that of M. Deveci and Torkayesh (2021), who addressed the problem of selecting an appropriate charging strategy for EBs as a MCDM problem. The authors proposed a novel approach based on Interval-Valued Neutrosophic Sets (IVNS) to evaluate and rank four charging options, including opportunity charging, depot charging, inductive charging, and no shift. They used Shannon's entropy under the IVNS to determine the weight of the criteria and MACONT to rank the charging options. The results from a case study in Turkey demonstrated that depot charging is the most appropriate solution for Istanbul's bus systems. Wołek et al. (2021) applied different multi-criteria analysis methods to select bus routes for electrification in Gdynia. They consider a variety of criteria, such as economic, social, technological, and environmental factors. They highlighted the value of multi-criteria analysis methodologies at a crucial yet early stage of the operational level decision-making process for electrifying public transportation.

Sang et al. (2022) utilized a combined framework of three methods (DEMATEL, PROMETHEE, and Prospect Theory) to evaluate EB charging stations. The findings demonstrate that EBs require more consideration when deployed due to their higher purchasing costs compared to diesel buses. Türk et al. (2021) employed an interval type-2 fuzzy-based MCDM technique combined with a SA algorithm to determine the ideal place for EB charging stations for the municipal bus company in Istanbul.

2.2.3 Research gap analysis

To the best of our knowledge, no research has explored the effects of passenger load volatility on energy consumption in the tactical planning of EB systems, such as to influence frequency (that relates to fleet size) and vehicle size decisions before the actual operation of an electric bus line, for instance, when deciding to replace diesel buses by electric buses in an existing service. Previous studies on EB scheduling problems have primarily relied on a fixed energy demand rate (in kWh/km) across all driving cycles and routes, while neglecting the dynamic changes in driving and route conditions (Paul and Yamada, 2014; Xylia et al., 2017; Bi et al., 2017; Wang et al., 2017; Ke et al., 2016; Jefferies and Göhlich, 2018; Tirachini and Antoniou, 2020; among others). Thus, this approach fails to account for differences in energy consumption resulting from changes in traffic congestion and passenger load during operations.

Another research gap in the deployment of EB systems is the need to determine the optimal fleet size and vehicle type (e.g., 12-m or 18-m electric bus) while taking into account both user and operator costs. The preferences of service providers (on the supply side) can differ from those of public transport users (on the demand side), and therefore designers must consider the desires and interests of both parties to determine the optimal supply levels for public transport services (Ibarra-Rojas et al., 2015; Hörcher and Tirachini, 2021; Sadrani et al., 2022b). For instance, while deploying smaller EBs with lower frequency (lower fleet size) can save capital and operational costs for bus agencies, it can increase passengers' waiting times and reduce the desirability of bus services, particularly if some passengers are confronted with capacity restrictions in boarding the first coming service (fail-to-board situations). In this context, Li et al. (2019) developed a novel EB scheduling model that integrated bus operating characteristics and passenger flow behavior into one model, aiming to minimize total costs (passenger plus operator costs). The optimal fleet size for EB fleets was

determined at a level that is satisfactory for both operating costs and user costs (e.g., passengers' waiting time cost). However, existing optimization models for determining the optimal vehicle type and fleet size in EB operations, whether utilizing fast-charging or overnight charging at depots, have primarily focused on reducing operator costs, while neglecting passengers' perceptions of the quality of service, such as waiting times and inconvenience caused by overcrowding (failing to board) (Chao and Xiaohong, 2013; Wang et al., 2017; Rogge et al., 2018; He et al., 2019; Yao et al., 2020; Zhou et al., 2022). Thus, a more comprehensive framework that considers the costs of both users and transport operators is necessary to achieve solutions that balance the profits of both sides.

Besides, despite the critical nature of charging strategy selection in shaping the electrification of bus networks, there is a paucity of research that specifically addresses this issue. In this research, we aim to address the gap in the literature on the selection of charging strategies for urban EB systems as a MCDM problem. As reviewed earlier, to the best of our knowledge, the only previous work that tackled this issue as a MCDM problem was by M. Deveci and Torkayesh (2021), where they considered operational, economic, infrastructure, and environmental criteria in their evaluation (a total of 14 criteria), while lacking several crucial criteria (such as battery cost, travel time, land acquisition cost, charging equipment cost, energy consumption, scheduling complexity, energy monitoring, charging infrastructures' impacts on surrounding residential areas, GHG emission and water consumption for battery production, vehicle capacity, labor cost, city landscape, and fire risk). However, our work extends their study by considering a more comprehensive spectrum of criteria, including economic, environmental, social, operational, and quality-of-service criteria (a total of 25 criteria). This broadening of the criteria provides a more comprehensive understanding of the factors affecting policymakers' decisions in selecting charging strategies for EBs. Additionally, M. Deveci and Torkayesh (2021) relied on the perspectives of only 4 experts from the transportation sector. However, our dissertation incorporates the perspectives of 11 experts from both academia and industry, resulting in a broader and more reliable range of viewpoints in our assessments. Besides, while M. Deveci and Torkayesh (2021) do not provide a systematic analysis of the criteria affecting charging strategy selection (using relevant sources from the extant EB literature), our work provides a thorough and evidence-based set of criteria through a comprehensive literature review and expert survey (as presented in Table 2-1). This not only adds credibility to our findings, but also offers a valuable reference for policymakers and future research in this field. We also provide a more detailed discussion of the results along

with an in-depth evaluation of practical implications and trade-offs involved in each option for stakeholders. For example, our analysis examines the relative importance of each category and each factor within each category, as well as the global weight of factors.

2.3 Mixed-fleet bus scheduling

2.3.1 Dispatching scheduling of homogeneous bus fleets

The optimization of dispatching plans for homogeneous fleets has been the subject of several studies in the public transport literature (Berrebi et al., 2015; Gkiotsalitis, 2020a; Luo et al., 2019; Gkiotsalitis and Alesiani, 2019; Zhang and Liu, 2019; Gkiotsalitis and Liu, 2022). The major objective of these efforts is to enhance the quality of service offered to passengers by optimizing the dispatching times of vehicles in response to temporal fluctuations in passenger demand. For instance, Gkiotsalitis and Alesiani (2019) proposed a bus dispatching problem considering uncertain passenger demand and driving times, to create an optimal timetable with reliable dispatching times. They developed a Genetic Algorithm (GA) to address the problem and achieved a 5% improvement in service regularity during operations based on an application to a bus line in Singapore. Similarly, Luo et al. (2019) addressed a dynamic bus dispatching problem to minimize users' waiting times, while accounting for dynamic changes in passenger demand and road congestion. In these studies, the quality of service is merely evaluated based on users' travel times (e.g., waiting times), while ignoring users' perceptions (experience) of trip comfort inside services, for instance, regarding passenger crowding. Moreover, it is obvious that in the operation with buses of one size, the setting of bus dispatching order has no meaning to bus operators.

To date, there are a large number of published studies in the field of timetabling and vehicle scheduling that have endeavored to improve the quality of services provided to users by minimizing passenger waiting time at stops (e.g., Newell, 1971; Nachtigall and Voget, 1997; Niu and Zhou, 2013; Barrena et al., 2014a,b; Niu et al., 2015; Sánchez-Martínez et al., 2016; Hassannayebi and Zegordi, 2017; Luo et al., 2019; Abdolmaleki et al., 2020; Altazin et al., 2020; among many others). Passenger waiting time can be strongly influenced by bus dispatching headways (Ceder and Marguier, 1985). Up to now, the problem of setting dispatching headways has attracted considerable scholarly attention. Szeto and Wu (2011) proposed a joint optimization model for the route design and frequency setting problems. The main objective of the model was to minimize the number of transfers and the total travel time.

An integrated solution method made up of a GA and a neighborhood search heuristic was developed to solve the problem. Hadas and Shnaiderman (2012) proposed a new method for determining the dispatching headways and vehicle sizes based on the stochastic characteristics of Automatic Passenger Counting (APC) and Automatic Vehicle Location (AVL) data within a supply chain optimization model. The objective of the model was to minimize the total cost due to empty seats and unserved demand. Li et al. (2013) developed a stochastic optimization model involving random passenger demand, boarding/alighting times and bus travel times, to find the optimal frequency with the aim of minimizing the waiting time for users and maximizing the expected bus company profits. The model was compared to the traditional frequency setting models of Newell (1971) and Ceder (1984). Martínez et al. (2014) proposed a MILP formulation for a transit frequency optimization problem. Since the model was intractable for large instances on a real transit network in Uruguay, a Tabu Search approach was adopted to solve the problem.

Berrebi et al. (2015) proposed a real-time bus dispatching policy to minimize passenger waiting time on a high-frequency bus route. For a general railway network, Meng et al. (2016) developed a cumulative flow variables-based integer programming model for dispatching trains under a stochastic environment, including stochastic capacity breakdown durations, segment running times and station dwell times. Gkiotsalitis and Cats (2018) developed a mathematical model for setting the dispatching headways of bus lines in a city network. The model explicitly included bus capacity and fleet size constraints. Moreover, demand, headway and travel time variations at different time periods were taken into account. The results showed that the dispatching headways are particularly susceptible to changes in some factors, such as demand volumes and bus running costs.

Furthermore, in a more recent strand of literature dealing with bus dispatching problems, Zhang and Liu (2019) formulated a time-dependent bus dispatching problem in a multi-modal context. In lieu of explicitly optimizing the size of dispatched bus fleet, the authors developed an adaptive fleet size adjustment approach with a target level of bus loading factor. Gkiotsalitis (2020a) extended a mathematical model for a periodic bus dispatching control of high-frequency services. An iterative gradient approximation solution method was also designed to reduce the computing burden of the proposed periodic dispatching control. Moreover, Gkiotsalitis and Van Berkum (2020a) introduced a novel rolling-horizon optimization model for adjusting the dispatching times of buses in rolling horizons. The proposed strategy outperforms myopic methods that determine the dispatching time of each

bus trip in isolation. In the above-mentioned studies, vehicle dispatching schemes are designed for the operation with uniform fleets of buses (uniform-fleet operation), i.e., public transport providers do not need to deal with a heterogeneous fleet dispatching problem, in which vehicles of different sizes are concurrently used to meet the passenger demand.

2.3.2 Dispatching scheduling of heterogeneous (mixed) bus fleets

In some cities, urban public transportation agencies have to operate combining vehicles of different sizes on their routes, due to specific demand patterns, historical reasons or resource limitations, e.g., when different sizes of buses are purchased at different times through different contracts. Such a situation takes place for example in peak periods if the total fleet size required is larger than the number of articulated buses at disposal; therefore, the agency uses standard and articulated buses at the same time. However, compared to research on homogeneous fleets (reviewed in the previous section), there is limited literature addressing the planning issue for heterogeneous bus fleets (dell'Olio et al., 2012; Ceder et al., 2013; Dai et al., 2020; Duran-Micco et al., 2020; Sadrani et al., 2022a). For instance, dell'Olio et al. (2012) constructed an optimization model with constraints on bus capacity to optimize bus size and headway. A series of numerical experiments were conducted using different fleet configurations, including homogenous fleets made up of buses of the same size, and heterogeneous fleets composed of different bus sizes. The findings demonstrated that a better service can be provided by the use of heterogeneous fleets. In another study which set out to create a bus scheduling timetable based on multiple bus sizes, Ceder et al. (2013) formulated a bi-objective mathematical model, in which the first objective was to minimize the deviation of the headways from a desired even headway, and the second one was to minimize the deviation of the observed passenger loads from a desired even-load level of the vehicles at the maximum-load point. Duran-Micco et al. (2020) addressed the determination of frequencies for mixed fleets in a bus network using a heuristic memetic algorithm based on the NSGA-II concept. The results demonstrated that mixed fleet deployments contribute to reduced GHG emissions and users' trip times. Dai et al. (2020) developed a real-time dispatching framework using an INLP formulation to assess the benefits of incorporating modular automated vehicle pods alongside human-driven buses. They employed a dynamic programming algorithm but highlighted the need for more effective solution techniques, particularly in handling performance degradation with an increasing rolling horizon.

However, these studies did not address the optimization of dispatching patterns in mixed fleets, while dispatching solutions for such fleets are influenced not only by dispatching intervals but also by the sequence in which vehicles are deployed, considering the utilization of services with different capacities within the operating environment (see Fig. 2-2). To effectively manage the dynamic changes in passenger flows over time and space, it is crucial to tackle the planning challenges associated with fleet heterogeneity and enhance the management of vehicle capacity. Furthermore, these studies do not consider users' discomfort from crowding and its implications for the scheduling of heterogeneous bus fleets.

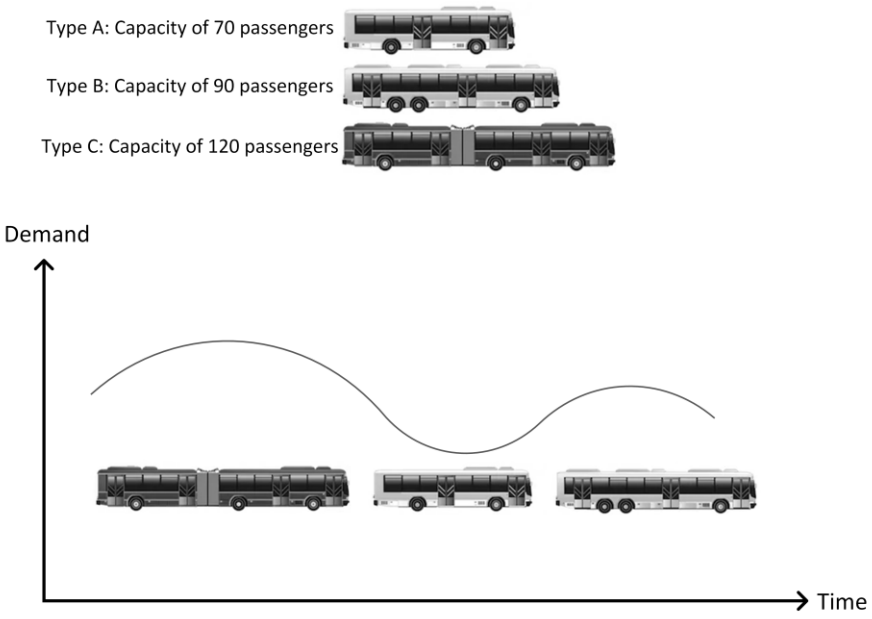

Figure 2-2 Optimization concept of vehicle dispatching sequence in mixed-fleet deployments (allowing for better management of vehicle capacity in response to dynamic changes in passenger demand).

2.3.3 Designing timetables with dynamic passenger demand

In the literature of public transport services, there has been a growing number of publications focusing on the topic of designing timetables with dynamic passenger demand (e.g., Canca et al., 2014; Robenek et al., 2018; Zhang et al., 2018; Meng and Zhou, 2019). For instance, to achieve an efficient train timetable that can fully utilize the limited infrastructure and rolling stock resources, Meng and Zhou (2019) developed an integrated train service plan optimization model with variable passenger demand. The authors introduced a team-based scheduling approach to coordinate demand assignment, routing, and timetabling tasks. The

proposed method could efficiently increase operators' profits and passenger travel demand satisfaction. Nowadays, with the rapid development of monitoring technologies, there are several tools to obtain detailed demand information through on-vehicle equipment, such as APC and AVL devices and smartcard payment systems. For example, Munizaga and Palma (2012) proposed a new method to estimate a public transport Origin–Destination matrix at a high level of accuracy from smartcard data in Santiago, Chile. In another work undertaken by Aguiléra et al. (2014) in Paris, the authors developed a new method to measure passenger flows in an underground transit system using Cell-phone data. They showed that the measures are consistent with those inferred from automated fare collection data. The knowledge of precise demand information is assumed by Niu et al. (2015) to develop a nonlinear integer programming model that finds the optimal skip-stop pattern on a rail transit corridor. The objective of the model was to minimize the total passenger waiting time under both high and medium-resolution time-varying demand data.

2.3.4 Public transport planning levels: strategic, tactical, and operational decisions

Public transport planning decisions are typically categorized into three levels, namely strategic, tactical, and operational decisions. For example, at the strategic planning level (related to long-term decisions), the set of routes and stops are determined. At the tactical planning level (related to medium-term decisions), fleet size requirement is determined, including the number and type of vehicles purchased to operate. Finally, at the operational planning level, short-term decisions (e.g., vehicle scheduling, driver scheduling, and driver rostering) are made. We refer the interested readers to Desaulniers and Hickman (2007) and Farahani et al. (2013) for a comprehensive review of these aspects. For example, Desaulniers and Hickman (2007) stated that the common way is to consider strategic and tactical planning decisions as input, and then determine a better way of using the agencies' resources in order to improve the level of service provided to users in operational planning decisions. Moreover, public transport operators may be able to perform interlining between different bus routes (i.e., the allocation of one vehicle to a different line at the end of one round), and interlining decisions could be adopted in real-time cases, for instance, to deal with sudden changes on demand conditions. In such a case, even though the total bus fleet is fixed, the fleet per route does not need to be fixed.

The operational planning stage enables transport operators to improve the level of service offered to travelers through more effective resource allocation. These operational planning problems, associated with short-term plans, should be solved periodically during operations, on a weekly basis, daily basis or multiple times per day at various planning intervals. This periodicity ensures that the most up-to-date operating conditions, such as changes in passenger flows over time and space and weather conditions, are taken into account. Therefore, in addition to planning quality and accuracy, the processing time required to solve these problems is of practical significance for policymakers. However, the complexity of operational bus scheduling problems, often classified as NP-hard problems (see Gkiotsalitis and Cats, 2021 for a comprehensive review), poses challenges for exact solution methods in addressing these problems efficiently within reasonable time frames. This underlines a need for the design and selection of more efficient solution algorithms for problems of this nature, such as metaheuristic algorithms, which offer the advantage of discovering practically good (not necessarily exact) solutions within rational computational (CPU) times (Ge et al., 2022; Tang et al., 2022). Besides, this computational difficulty will increase even more when planners aim to incorporate more practical elements into the operational scheduling of bus services, such as mixed fleet configurations, users' trip comfort, and driving time uncertainty.

Several studies have employed metaheuristics to address various public transport operational planning problems, including vehicle dispatching setting problems (Zhang et al., 2018; Sadrani et al., 2022a), delay and disruption management problems (Wang et al., 2019; Xu et al., 2018), and stopping pattern determination problems (Chen et al., 2015; Mou et al., 2020). However, most existing research focuses on homogeneous fleets, in which the operation of vehicles of the same size and type is optimized.

2.3.5 Research gap analysis

While a considerable amount of literature has been published on the problem of setting bus dispatching headways, there have been no attempts to examine how bus dispatching policies can affect passenger and operator costs in a mixed-fleet operation (i.e., in the operation with buses of different sizes), considering the fact that a mixed fleet of vehicles can provide services with different passenger-carrying capacities during real-world operations. Moreover, to the best of our knowledge, no prior research has addressed the optimization of vehicle assignment programs for mixed-fleet operations, which determine the number and type of

vehicles assigned for operations considering real-life resource constraints and vehicle operating costs. Additionally, no study in the literature incorporates users' trip comfort (users' perceptions of crowding inconvenience) in the optimal deployment of mixed fleets. Accounting for these realistic elements in a more comprehensive model adds complexity to the solution phase of the MFBS problem. Thus, there is also a crucial need for the development of more reliable/advanced solution algorithms to effectively address these challenges.

3 Model formulation

This chapter includes the mathematical models developed in this dissertation. It encompasses a MINLP model for automated bus planning, an INLP model for EB planning, an MCDM model for charging strategy selection, and two MINLP models designed to address MFBS problems in simple and advanced versions. Table 3-1 includes the notations employed in our problem formulations within this dissertation.

3.1 Model formulation for automated bus planning

We develop a mathematical modeling framework for solving the problem of setting service frequency and vehicle size for fleets of human-driven or automated buses. To this end, we formulate a comprehensive objective function, which calculates both user and operator costs, to minimize the total costs of a public transport service in the presence of crowding externalities, time-dependent demand flows, and stochastic travel times. Besides, several constraints are modeled to represent real-world operating conditions, such as vehicle movement, passenger flow, and vehicle capacity restrictions in line with the remaining on-board capacity of vehicles during operations (see Fig. 3-1).

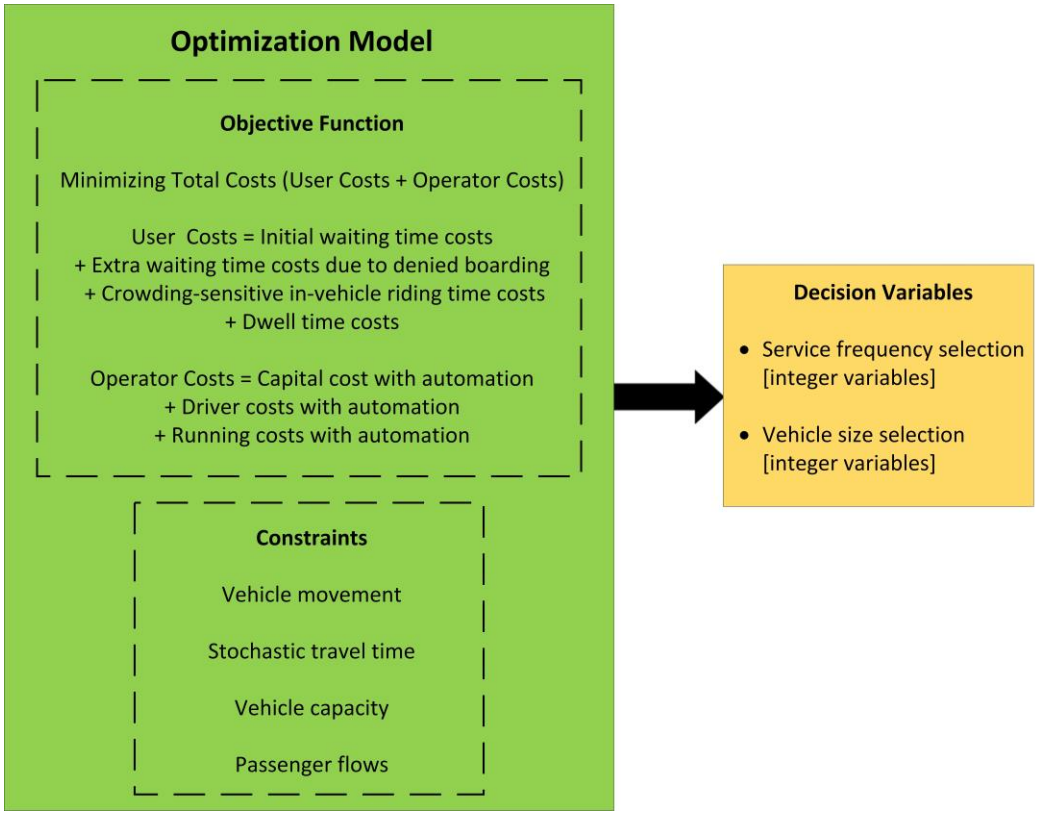

Figure 3-1 Overview of the optimization model framework in the proposed automated bus system problem.

Table 3-1 List of notation.

Symbol	Description	Unit
V	Set of buses, V= $\{1, 2, \dots, N_v\}$	
S	Set of stops, $S = \{1, 2, \dots, N_s\}$	
M	Set of vehicle types, $M = \{1, 2, \dots, m\}$	
i	Index of buses	
m	Index of vehicle types	
j, k	Index of stops (from origin j to destination k)	
N_s	Number of stops on the route	
R	Route length	km
$\lambda_j[t]$	Passenger arrival rate at stop j at time t	pax/min

Symbol	Description	Unit
U_m	Maximum resource availability on vehicles of type m	veh
$OD_{j,k}[t]$	Destination distribution matrix (the percentage of passengers at stop j, who aim to travel from stop j to stop k, $k > j$) at time t	%
P	Total demand (the total number of waiting passengers who arrived at stops), which is a constant value during the entire study period	pax
$f_{\min}$	Minimum frequency	veh/h
$f_{\max}$	Maximum frequency	veh/h
T	Start of the study period	min
δ_a	Acceleration time	s
δ_d	Deceleration time	s
r_j	Mean running times between stops $j-1$ and j	min
σ_j	Standard deviation of running times between stops $j-1$ and j	min
τ	Time required for opening and closing bus doors	s
T_c	Cycle time	min
α_a	Average alighting time per passenger	s/pax
α_b	Average boarding time per passenger	s/pax
P_i^a	Proportion of passengers alighting through the busiest door of bus i	%
P_i^b	Proportion of passengers boarding through the busiest door of bus i	%
T_1	First dispatching time (beginning of the planning horizon)	min
T_2	Last dispatching time (end of the planning horizon)	min
$h_{\min}$	Minimum dispatching headway	min
$h_{\max}$	Maximum dispatching headway	min
G	Starting point of the planning period	
P_a	Proportion of passengers alighting through the busiest door of a bus	%
P_b	Proportion of passengers boarding through the busiest door of a bus	%

Symbol	Description	Unit
h	Dispatching headway from the first stop	min
φ^{w1}	Monetary value of initial waiting time	€/h
φ^{w2}	Monetary value of extra waiting time due to denied boarding	€/h
φ^{v}	Monetary value of in-vehicle travel time	€/h
φ^{d}	Hourly driving cost	€/veh-h
φ_m^u	Running cost of a vehicle of type m	€/veh-h
φ^{run}	Running cost of a vehicle per kilometer	€/veh-km
φ^{cap}	Capital cost of a vehicle per hour, i.e., cost of owning or renting a vehicle per hour	€/veh-h
φ^{e}	Unit cost of energy	€/kWh
φ_m^c	Capital cost of a type-m vehicle per hour	€/veh-h
c_m	Passenger-carrying capacity of a vehicle from type-m	pax/veh
a_m	Standing floor area inside a vehicle of type m	m^2
b_m	Fully battery capacity of a vehicle from type-m	kWh
ξ	Maximum allowable level of battery capacity usage	%
m_{pax}	Average weight of one passenger	kg
C	Vehicle passenger-carrying capacity	pax/veh
B	Vehicle battery capacity	kWh
ω	Driving cost coefficient for reflecting the level of reduction in human driving costs due to automation	
β	Capital cost coefficient for reflecting the level of increase in vehicle capital costs due to automation	
θ	Running cost coefficient for reflecting the level of reduction in vehicle running costs due to automation	
α^{sit}	Seated in-vehicle time multiplier	
α^{stand}	Standing in-vehicle time multiplier	
$C(v_s)$	Total capacity of a vehicle, which is a function of the vehicle size	pax/veh

Symbol	Description	Unit
$G^{\text{sit}}(v_s)$	Number of seats inside a vehicle, which is a function of the vehicle size	
N_v	Fleet size	veh
C_i	Total capacity of bus i	pax/veh
$\mathrm{A}_{\mathrm{i}}^{\text{stand}}$	Standing floor area inside bus service i	m^2
φ_i^u	Running cost of bus service i	€/veh-h
$\pi_{i,j}^{sit}$	Crowding multiplier for sitting passengers inside bus service i when traveling between station $j-1$ and station j	
$\pi_{i,j}^{\text{stand}}$	Crowding multiplier for standing passengers inside bus service i when traveling between station $j-1$ and station j	
$T_{i,j}^a$	Arrival time of bus i at stop j	min
$T_{i,j}^d$	Departure time of bus i from stop j	min
$T_{i,j}^s$	Dwell time of bus i at stop j	min
$T_{i,j}^r$	Running time of bus i between stops $j-1$ and j	min
T_i^c	Cycle time of service i to complete one round trip	min
$H_{i,j}$	Headway between buses $i-1$ and i at stop j	min
$TE_{i,j}$	Energy consumed by service i to travel between stations $j-1$ and j	kWh
$N_{i,j,k}^c$	Number of passengers with trip $j \to k$ arriving at stop j during the headway between buses $i-1$ and i	pax
$N_{i,j,k}^f$	Number of passengers with trip $j \to k$ failing to board bus i at stop j	pax
$N_{i,j,k}^w$	Number of passengers with trip $j \to k$ waiting for bus i at stop j	pax
$N_{i,j}^c$	Total number of passengers arriving at stop j during the headway between buses $i-1$ and i	pax
$N_{i,j}^f$	Total number of passengers failing to board bus i at stop j	pax
$N_{i,j}^w$	Total number of passengers waiting for bus i at stop j	pax
$N_{i,j}^{on}$	Number of passengers inside bus i between stops $j-1$ and j	pax
$N_{i,j}^{\text{sit}}$	Number of seated passengers inside bus i between stops $j-1$ and j	pax
$N_{i,j}^{\text{stand}}$	Number of standing passengers inside bus i between stops $j-1$ and j	pax

Symbol	Description	Unit
$N_{i,j}^{\mathrm{v}}$	Remaining active capacity inside bus i at station j after the alighting phase	pax
$D_{i,j}^{\mathrm{stand}}$	Density of standing passengers inside bus i between stops $j-1$ and j	pax/m^2
$F_{i,j}$	Load factor of bus i between stops $j-1$ and j	pax/seat
$N_{i,j}^{b}$	Number of passengers boarding bus i at stop j	pax
$N_{i,j}^{a}$	Number of passengers alighting bus i at stop j	pax
$N_{i,j,k}^{s}$	Number of passengers with trip $j \to k$, who can successfully board bus i at stop j	pax
$L_{i,j}$	Passenger load carried by service i between stations $j-1$ and j	kg
E_i^c	Energy consumed by service i to travel from the depot to the original station	kWh
E_i^r	Energy consumed by service i to return from the original station to the depot	kWh
f	Service frequency (Allowed frequency values: $f \in \underbrace{\{f_{\min}, f_{\min}+1, \ldots, f_{\max}-1, f_{\max}\}}_{\text{discrete set with } (f_{\max}-f_{\min})+1 \text{ elements}}$)	veh/h
x_m	Binary variable that is 1 if a fleet of buses of type m is operated; otherwise 0	
v_s	Vehicle size (four bus sizes used as candidates: $v_s \in \{8, 12, 15, 18\}$ meters)	m
x_{mi}	Binary variable which is 1 if a type m vehicle is dispatched as i-th service; otherwise 0	
B_m	Number of type m vehicles assigned for operations	veh
$T_{i,1}^d$	Dispatching time of bus i from the first stop	min

3.1.1 Model assumptions for automated bus planning

The main assumptions employed in our problem formulation are listed as follows:

- We consider high-frequency bus systems, where the arrivals of passengers at stations are assumed to be random.
- We consider 15-minute-dependent demand volumes, remaining fixed during each 15-minute interval (every 15 minutes).
- We consider a general bi-directional bus corridor with even dispatching headways from the first stop.

- We model varying dwell times (flow-dependent dwell times), which can vary for a vehicle at each stop as a function of the number of passengers getting off and on at that stop.
- We assume a log-normal distribution for stochastic running times between stops.
- We consider vehicle capacity restrictions, and hence:
  - ✓ (a) boarding numbers will never exceed the residual capacity inside vehicles;
  - ✓ (b) extra waiting times are considered for denied boarding situations;
  - ✓ (c) when boarding demand is larger than the residual capacity inside a bus, the chance of boarding is assumed to be the same for all the travelers waiting for that bus, independent of their trip destinations[1].
- We assume that overtaking is not permitted during bus operations.
- For user cost calculations, we distinguish between the monetary values of in-vehicle travel time, initial waiting time, and extra waiting time due to denied boarding.
- We estimate passenger occupancy rates, the number of seated and standing passengers inside vehicles, and crowding discomfort at a microscopic level, bus by bus.
- We assume that the user cost is sensitive to on-board crowding levels, i.e., the impacts of on-board crowding on the disutility of in-vehicle travel time for both seated and standing passengers are modeled.
- We assume that the technology of automation can:
  - ✓ (a) increase vehicle capital costs due to including automation technologies inside vehicles;
  - ✓ (b) reduce human driving costs;
  - ✓ (c) reduce vehicle running costs through a reduction in fuel/energy consumption due to providing a more balanced driving style.

3.1.2 Optimization model for automated bus planning

The proposed automated bus system problem is formulated as follows:

[1] This is a common assumption that has been employed by several studies in the literature (e.g., Wang et al., 2015; Gao et al., 2016; Sánchez-Martínez et al., 2016; Dai et al., 2020).

$$Z = \underbrace{Z_{\text{w}} + Z_{v}}_{Z_p} + \underbrace{Z_{\text{cap}} + Z_{\text{driver}} + Z_{\text{run}}}_{Z_o} \tag{3-1}$$

$$\text{Master Problem} \begin{cases} \underset{f\ ,v_s}{\text{Min}}\ Z \\ \text{Subject to constraints (3-12)-(3-32)} \end{cases} \tag{3-2}$$

$$Z_w = Z_w^{(i)} + Z_w^{(ii)} \tag{3-3}$$

$$Z_w^{(i)} = \varphi^{w1} \sum_{i \in V} \sum_{j \in S} N_{i,j}^{c} \ . \ \frac{H_{i,j}}{2} \tag{3-4}$$

$$Z_w^{(ii)} = \varphi^{w2} \sum_{i \in V, i \geq 2} \sum_{j \in S} N_{i-1,j}^{f} \ . H_{i,j} \tag{3-5}$$

$$Z_v = Z_v^{\text{ride}} + Z_v^{\text{dwell}} \tag{3-6}$$

$$Z_v^{\text{ride}} = \varphi^{v} \sum_{i \in V} \sum_{j \in S, j \geq 2} \left(T_{i,j}^{r} + \delta_{\text{a}} + \delta_{d} \right) . \left(\alpha^{\text{sit}} \ N_{i,j}^{\text{sit}} \ + \ \alpha^{\text{stand}} \ N_{i,j}^{\text{stand}} \right) \tag{3-7}$$

$$Z_v^{\text{dwell}} = \varphi^{v} \sum_{i \in V} \sum_{j \in S, j \geq 2} \left(N_{i,j}^{on} - N_{i,j}^{a} \right) . \ T_{i,j}^{s} \tag{3-8}$$

$$Z_{\text{cap}} = \beta \ \varphi^{\text{cap}} \sum_{i \in V} \sum_{j \in S, j \geq 2} \left(T_{i,j}^{s} + T_{i,j}^{r} + \delta_{\text{a}} + \delta_{d} \right) \tag{3-9}$$

$$Z_{\text{driver}} = \omega \ \ \varphi^{d} \sum_{i \in V} \sum_{j \in S, j \geq 2} \left(T_{i,j}^{s} + T_{i,j}^{r} + \delta_{\text{a}} + \delta_{d} \right) \tag{3-10}$$

$$Z_{\text{run}} = \theta \ . \ \varphi^{run} . \ R \ . \ N_{v} \tag{3-11}$$

Subject to:

$$f \in \left\{ f_{\min}, f_{\min} + 1, \ ..., f_{\max} - 1, f_{\max} \right\} \tag{3-12}$$

$$N_{v} = \left\lceil f . T_{c} \right\rceil \tag{3-13}$$

$$H_{i,j} = T_{i,j}^{d} - T_{i-1,j}^{d} \quad \forall i \in V - \left\{ 1 \right\}, \forall j \in S \tag{3-14}$$

$$T_{i,j}^{a} = T_{i,j-1}^{d} + \delta_{\mathrm{a}} + T_{i,j}^{r} + \delta_{d} \quad \forall i \in V, \forall j \in S - \{1\} \tag{3-15}$$

$$T_{i,j}^{r} \sim \text{lognormal}\,(r_j,\ \sigma_j) \quad \forall i \in V, \forall j \in S - \{1\} \tag{3-16}$$

$$T_{i,1}^{d} = T + (i-1)h \quad \forall i \in V \tag{3-17}$$

$$T_{i,j}^{d} = T_{i,j}^{a} + T_{i,j}^{s} \quad \forall i \in V, \forall j \in S - \{1\} \tag{3-18}$$

$$T_{i,j}^{s} = \tau + P_a \alpha_a N_{i,j}^{a} + P_b \alpha_b N_{i,j}^{b} \quad \forall i \in V, \forall j \in S \tag{3-19}$$

$$N_{i,j,k}^{c} = \int_{T_{i-1,j}^{d}}^{T_{i,j}^{d}} \lambda_j[t].\, OD_{j,k}[t].\, dt \quad \forall i \in V, \forall j,k \in S, k > j \tag{3-20}$$

$$N_{i,j,k}^{w} = N_{i,j,k}^{c} + N_{i-1,j,k}^{f} \quad \forall i \in V, \forall j,k \in S, k > j \tag{3-21}$$

$$N_{i,j}^{c} = \sum_{k \in S, k > j} N_{i,j,k}^{c} \quad \forall i \in V, \forall j \in S \tag{3-22}$$

$$N_{i,j}^{f} = \sum_{k \in S, k > j} N_{i,j,k}^{f} \quad \forall i \in V, \forall j \in S \tag{3-23}$$

$$N_{i,j}^{w} = \sum_{k \in S, k > j} N_{i,j,k}^{w} \quad \forall i \in V, \forall j \in S \tag{3-24}$$

$$N_{i,j}^{on} = N_{i,j-1}^{on} - N_{i,j-1}^{a} + N_{i,j-1}^{b} \quad \forall i \in V, \forall j \in S - \{1\} \tag{3-25}$$

$$N_{i,j}^{\text{sit}} = \min\left\{G^{\text{sit}}(v_s),\ N_{i,j}^{on}\right\} \quad \forall i \in V, \forall j \in S \tag{3-26}$$

$$N_{i,j}^{\text{stand}} = \max\left\{0,\ N_{i,j}^{on} - G^{\text{sit}}(v_s)\right\} \quad \forall i \in V, \forall j \in S \tag{3-27}$$

$$F_{i,j} = \frac{N_{i,j}^{on}}{G^{\text{sit}}(v_s)} \quad \forall i \in V, \forall j \in S \tag{3-28}$$

$$N_{i,j}^{b} = \min\left\{N_{i,j}^{w},\ C(v_s) - N_{i,j}^{on} + N_{i,j}^{a}\right\} \quad \forall i \in V, \forall j \in S \tag{3-29}$$

$$N_{i,j}^{a} = \sum_{j' \in S, j' < j} N_{i,j',j}^{s} \quad \forall i \in V, \forall j \in S - \{1\} \tag{3-30}$$

$$N^{s}_{i,j,k} = \frac{N^{b}_{i,j}}{N^{w}_{i,j}} N^{w}_{i,j,k} \quad \forall i \in V, \forall j,k \in S, k > j \tag{3-31}$$

$$N^{f}_{i,j,k} = N^{w}_{i,j,k} - N^{s}_{i,j,k} \quad \forall i \in V, \forall j,k \in S, k > j \tag{3-32}$$

The objective function (3-1) minimizes the total cost of a public transport service, defined as the sum of user and operator costs. User cost (Z_p) is composed of two components: waiting and in-vehicle time costs. Operator cost (Z_o) is comprised of three components: capital, driver, and running costs. A single-objective optimization model allows for establishing a trade-off between user and operator costs simultaneously, thus finding the optimal solution that leads to the minimum total cost (social cost) of a public transportation service. In this model, we employ various monetary valuations[2] to translate all travel time/distance elements which are relevant to passengers and operators into their equivalent cost values. Further details are provided on each monetary term in the following.

It has been shown that the value of waiting time at stops is larger than the value of in-vehicle time (Cats et al., 2016; Lu et al., 2018; Wardman, 2004). Moreover, the value of extra waiting time due to denied boarding (for passengers left behind due to capacity constraints) is larger than the value of initial waiting time experienced in normal cases (Cats and Jenelius, 2018; Cats et al., 2016). For instance, Cats et al. (2016) assumed that one minute waiting time after being denied boarding is perceived 3.5 times as onerous as one minute initial waiting time. Accordingly, using three different monetary valuations, namely φ^{w1}, φ^{w2}, and φ^{v} [€/h], we distinguish between the monetary values of initial waiting time, extra waiting time caused by denied boarding, and in-vehicle time.

For operator cost estimations, vehicle capital costs and driver costs are commonly defined on a temporal basis [€/veh-h or €/veh-day], whereas running costs are defined on a spatial basis [€/veh-km] (Tirachini and Antoniou, 2020). Hence, in our setting, φ^{d} and φ^{cap} [€/veh-h] are used to convert vehicle operating hours into driver and vehicle capital costs respectively, whereas φ^{run} [€/veh-km] is used to translate the distance traveled by vehicles into their running costs.

[2] φ^{w1} [€/h], φ^{w2} [€/h], and φ^{v} [€/h] are used for user cost calculations. Moreover, φ^{cap} [€/veh-h], φ^{d} [€/veh-h], and φ^{run} [€/veh-km] are used for operator cost calculations.

Considering the objective function (3-1) and the problem constraints, the master problem for the joint optimization of service frequency (f) and vehicle size (v_s) is presented in Eq. (3-2).

As indicated in expression (3-3), the total waiting time cost accounts for: (i) initial waiting time costs for new passengers entering stops during the headway, plus (ii) extra waiting time costs due to denied boarding considered for left-behind passengers, who could not board the earlier bus due to crowding.

Buses run frequently enough in high-frequency bus systems, and thus passengers do not need to coordinate their arrivals with the arrival times of vehicles, i.e., we assume random arrivals at stations. Accordingly, the average waiting time is estimated as half of the headway ($H_{i,j}/2$) for travelers in group (i) [see Eq. (3-4)], in line with a common assumption in this field (e.g., Furth and Wilson, 1981; Wu et al., 2017; Gkiotsalitis and Cats, 2018; Dai et al., 2020; Sadrani et al., 2022a). However, the extra waiting time is the entire headway ($H_{i,j}$) for travelers in group (ii), who must wait for the next vehicle [see Eq. (3-5)]. Given the higher value of extra waiting time (φ^{w2}) than that of initial waiting time (φ^{w1}), denied boardings can lead to a remarkable increase in passengers' waiting time costs.

The cost of passengers' in-vehicle time has two components: the cost of riding time between stops, i.e., $Z_{\mathrm{v}}^{\mathrm{ride}}$, as well as the cost of dwell time at stops, i.e., $Z_{\mathrm{v}}^{\mathrm{dwell}}$ [see Eq. (3-6)].

As presented in expression (3-7), the cost of riding time between stops is obtained through multiplying the total number of on-board passengers (including both seated and standing passengers) by the total time required for traveling between each two successive stops. Besides, the user cost is sensitive to in-vehicle crowding levels in this formulation, which enables us to estimate in-vehicle discomfort costs for passengers depending on occupancy levels inside each vehicle at each segment of the route. Indeed, in-vehicle crowding has been found as a significant source of travel disutility for both seated and standing passengers, thereby increasing perceived in-vehicle times for both groups of travelers. Following Wardman and Whelan (2011), we draw a distinction between the value of in-vehicle time for seated and standing passengers through employing crowding multipliers of α^{sit} and α^{stand} respectively. As indicated in Table 3-2[3], crowding multipliers increase with the growth of the load factor and are larger for standing passengers than for seated passengers. For instance, to estimate the user cost of crowding, when the passenger load factor is 110%, the perceived

[3] The values presented in Table 3-2 have been taken from the meta-study of Wardman and Whelan (2011).

in-vehicle time is increased to [1.05 × (actual in-vehicle time)] for seated passengers, whereas it is increased to [1.62 × (actual in-vehicle time)] for standees. In our numerical experiments, we will widely examine the influences of on-board crowding and standing on determining the optimal service frequency and vehicle size for a fleet of automated buses vs. human-driven buses.

As can be seen in (3-8), $Z_{\mathrm{v}}^{\mathrm{dwell}}$ is related to those passengers, $N_{i,j}^{on} - N_{i,j}^{a}$, inside bus i whose destination is not bus stop j (i.e., they do not need to alight at stop j), so they have to stay inside bus i during alighting and boarding times (dwell time) at that stop.

Table 3-2 Crowding multipliers (Source: Wardman and Whelan, 2011).

Load factor[4] $F_{i,j}$ (%)	$\boldsymbol{\alpha^{\mathrm{sit}}}$	$\boldsymbol{\alpha^{\mathrm{stand}}}$
0–75	0.86	—
75–100	0.95	—
100–125	1.05	1.62
125–150	1.16	1.79
150–175	1.27	1.99
175–200	1.40	2.20
200–	1.55	2.44

Operator cost elements, incorporated into the objective function (3-1), are described here. Vehicle automation can potentially affect operator costs in three aspects: a rise in capital cost, and reduction in driver and running costs. Following Tirachini and Antoniou (2020), we formulate operator costs in a general manner for human-driven bus operations, and the effects of vehicle automation on operator costs (including capital, driver, and running costs) are separately described by additional factors, namely β ($\beta \geq 1$), ω ($0 \leq \omega \leq 1$), and θ ($0 \leq \theta \leq 1$). Obviously, for human-driven bus operations in our framework, such factors would be equivalent to one.

The total vehicle capital cost (fleet acquisition cost) is estimated by Eq. (3-9). For automated bus fleets, coefficient β ($\beta \geq 1$) represents the level of increase in vehicle capital costs due to including automation technologies in vehicles, e.g., $\beta = 1.5$ indicates an increase

[4] Load factor inside a vehicle is defined as the ratio between the actual number of passengers inside the vehicle and the seating capacity of the vehicle [see Eq. (3-28)].

of 50% in vehicle capital costs with automation. This parameter value has been estimated by Tirachini and Antoniou (2020) for different vehicle sizes.

The total driving cost is estimated by Eq. (3-10). It is not expected that the technology of automation can totally eliminate human-related driven costs, as some employees are still retained to control or monitor the operation of bus routes with automated driving technologies, provide information to users, and safeguard the security of operations and passengers, among other new needs of personnel that may arise in an automated public transport system (Abe, 2019; Tirachini and Antoniou, 2020). Hence, for automated fleets, coefficient ω $(0 \leq \omega \leq 1)$ reflects the level of current human driving costs being needed after automation. For example, $\omega = 0$ shows the case of full driving cost savings with automation, whereas $\omega = 0.6$ shows that 40% of salaries are saved with automation.

Eq. (3-11) accounts for the total running cost (e.g., energy consumption, tires, maintenance) based on the total distance traveled by vehicles.

Coefficient θ $(0 \leq \theta \leq 1)$ represents the level of reduction in running costs with automated vehicles, which can reduce fuel/energy consumption per veh-km due to providing more balanced driving functions thanks to, e.g., V2V and V2I communications (Wadud, 2017; Bösch et al., 2018; Tirachini and Antoniou, 2020). For example, $\theta = 0.9$ means that 10% of vehicle running costs per kilometer can be saved with automation.

We model vehicle motion constraints, as well as passenger flow constraints acting in accordance with the available capacity of vehicles during operations (i.e., the possibility of denied boarding due to a shortage of capacity). Overall, a bus movement model includes the calculations of five key elements: arrival times at stops, departure times from stops, headways between consecutive vehicles, dwell times at stops, and running times between successive stops. Furthermore, our passenger flow constraints include the calculations of six components: the number of passengers waiting at stops, the number of seated/standing passengers inside vehicles, the number of passengers who can/cannot successfully board vehicles, and the number of passengers alighting at stops.

The service frequency is regarded as a decision variable, which can be chosen from a discrete set of values subject to predefined lower and upper bounds of $f_{\min}$, and $f_{\max}$ [veh/h] [see Eq. (3-12)].

In general, $f_{\min}$ is often given by a minimum capacity (or maximum waiting time) that is exogenously defined in public transport systems. As mentioned in the model assumptions, we

focus on high-frequency bus services, where buses run frequently enough so that passengers do not need to coordinate their arrivals with bus arrivals. In this regard, some studies in the literature have considered high-frequency service as services operating with a frequency of at least 5 [veh/h] or more (e.g., Bartholdi and Eisenstein, 2012; Chiraphadhanakul and Barnhart, 2013; Gkiotsalitis and Van Berkum, 2020a). On the other hand, $f_{\max}$ is given by the capacity of bus stops (Tirachini, 2014).

The fleet size requirement is obtained by the expression in Eq. (3-13). T_c represents the total travel time during one cycle or round-trip (Tirachini et al., 2014).

Headway between vehicles $i-1$ and i at stop j is obtained according to Eq. (3-14).

As can be seen in (3-15), the arrival time of bus i at stop j is obtained through the sum of: (1) the departure time of bus i from stop $j-1$, (2) acceleration time for leaving stop $j-1$, (3) the running time between stops $j-1$ and j, and (4) deceleration time for entering stop j.

Running times are stochastic, drawn from a log-normal distribution in Eq. (3-16). In our numerical experiments, we perform a sensitivity analysis on travel time variability for automated vehicle fleet operations with changes in the standard deviation of travel times.

It is assumed that vehicles are dispatched at even dispatching headways from the first stop. As indicated in Eq. (3-17), an even interval of h minutes ($h = 60/f$) is considered between the dispatching of vehicles, e.g., for a frequency of 20 (veh/h), buses are dispatched every 3 minutes from the first stop. Besides, we assume that the first bus is dispatched at a certain time which is the beginning of the study period (T) (i.e., the departure time of the first bus from the first stop is set to the first time point).

At other bus stops, the departure time of bus i at stop j is obtained by adding its dwell time to its arrival time at stop j, as presented in Eq. (3-18). We model flow-dependent dwell times. Regarding the alighting and boarding policy, we assume that passengers use the same doors for alighting and boarding, and that the boarding process will always begin after finishing the alighting process (i.e., sequential alighting and boarding, in which the alighting process has priority over the boarding process). Hence, the total dwell time at a stop depends on the sum of the passengers' alighting and boarding times (Tirachini et al., 2014). As presented in Eq. (3-19), the dwell time of bus i at stop j depends on the number of passengers getting off and on through the busiest bus door, plus a fixed "dead" time spent opening and closing bus doors.

Parameters P_a and P_b represent respectively the proportions of passengers alighting and boarding through the busiest door of a bus, and are dependent on the number of bus doors (note that the values of such size-dependent parameters are given in Tables A2 and A3 in Appendix A) (Tirachini et al., 2014). Parameters α_a and α_b represent the average alighting and boarding times per passenger respectively, and depend on fare payment methods, bus floor height, platform configuration, and so on. Another relevant aspect to explain here is the effects of active vehicle capacity constraints on dwell times. Indeed, since we explicitly account for vehicle capacity constraints, the dwell times of vehicles (in terms of boarding time) can depend on the remaining capacity of vehicles at each stop (the boarding numbers, $N_{i,j}^{b}$ in Eq. (3-29), cannot exceed the remaining capacity). Moreover, in our numerical studies, we carry out a sensitivity analysis on the dead time (τ) to evaluate the possible effects of vehicle automation on the process of opening and closing bus doors.

Given time-dependent demand volumes, Eq. (3-20) calculates the number of passengers arriving at origin stop j over the headway, who wait for the arrival of bus i to travel from stop j to stop k (trip $j \rightarrow k$).

Following Gao et al. (2016) and Sadrani et al. (2022a), we use 15-minute-dependent demand data, remaining fixed during each 15-minute interval. For an in-depth discussion of fine-grained demand information and demand aggregation intervals under different degrees of demand availability for public transport planning, we refer to Sadrani et al. (2022a). In this regard, the authors have examined and compared the effects of demand data resolution on the accuracy of waiting time estimations. Hence, 15-minute-dependent demand data are introduced as fine-grained demand information that can suitably capture passenger demand variations for planning purposes.

Considering passengers left behind by the earlier bus (i.e., bus $i-1$) at stop j, the total number of passengers with trip $j \rightarrow k$ waiting for bus i at stop j includes two groups of passengers [see Eq. (3-21)]: (i) the new passengers arriving at stops during the headway, modeled in Eq. (3-20), and (ii) those passengers previously left behind.

According to the above-mentioned definitions, it is evident that Eqs. (3-22)-(3-24) will always hold. For instance, passengers waiting for bus i at stop j can have various trip destinations. Hence, given the definitions of $N_{i,j,k}^{w}$ and $N_{i,j}^{w}$, to calculate the total number of passengers waiting for bus i at stop j, all the waiting passengers at that stop with any trip destinations (trip $j \rightarrow k, k > j$) are summed together using Eq. (3-24).

As shown in Eq. (3-25), the number of on-board passengers of bus i between stops $j-1$ and j, $N_{i,j}^{on}$, includes those passengers who have remained on bus i from the earlier segment $(j-2 \rightarrow j-1)$ as they do not need to alight at stop $j-1$, i.e., $(N_{i,j-1}^{on} - N_{i,j-1}^{a})$, plus passengers getting on bus i at stop $j-1$, denoted by $N_{i,j-1}^{b}$. Note that vehicles are empty when reaching the first stop (i.e., $N_{i,1}^{on} = 0,\ \forall i \epsilon V$).

The number of seated passengers on bus i between stops $j-1$ and j is equal to the minimum value between the number of seats and the number of passengers inside bus i [see Eq. (3-26)].

The number of standees inside bus i between stops $j-1$ and j is obtained through (3-27). Load factor $F_{i,j}$, defined as the ratio between the number of on-board passengers and the total number of bus seats, reflects the degree of occupancy inside bus i when traveling between stops $j-1$ and j. High load factors are related to crowding externalities inside vehicles [see Eq. (3-28)] (Wardman and Whelan, 2011; Tirachini et al., 2013).

The number of passengers who are able to board bus i at stop j will never exceed the residual capacity of bus i at that stop [see Eq. (3-29)]. As can be seen in (3-30), the alighting demand for bus i at stop j will include those passengers boarding bus i at the previous stops, aiming to reach stop j. Note that the alighting demand is zero at the first stop (i.e., $N_{i,1}^{a} = 0, \forall i \epsilon V$).

As explained before, when capacity is not sufficient to meet the whole boarding demand, we consider the same chance of boarding for all passengers, as modeled in Eq. (3-31). Finally, in Eq. (3-32), we calculate the number of passengers with trip $j \rightarrow k$, who are unable to board bus i at stop j due to crowding.

3.2 Model formulation for electric bus planning

In this section, we develop a novel mathematical optimization framework in the form of an INLP model, which integrates a detailed (variable) energy consumption model based on longitudinal vehicle dynamics into the planning phase of EB fleets. For this purpose, we combine contributions from energy consumption dynamics, transport economics, passenger flow behavior, and operations research to optimize public transport supply with EB fleets (see Fig. 3-2). Moreover, in our numerical experiments, we test the applicability of our approach by applying it to a real bus corridor in Santiago de Chile and simulating several scenarios of

operations under different demand levels (low vs. high demand levels), energy estimation methods (variable vs. simplified fixed energy demand), and route conditions (with vs. without slope).

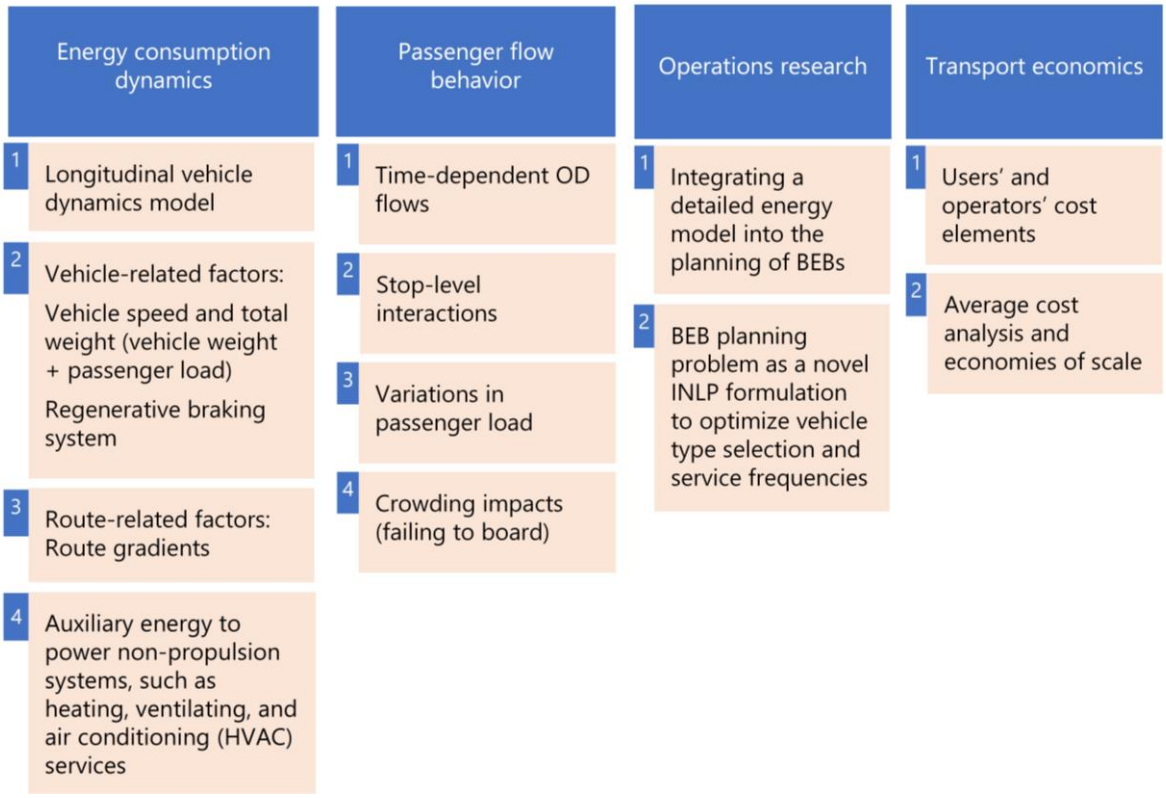

Figure 3-2 An overview of key research components for our proposed EB fleet planning model.

3.2.1 Energy estimation modeling

This section outlines a comprehensive EB energy consumption model, adopted from the integration of various research efforts in the existing EB literature. The model accounts for microscopic-level tractive mechanical energy, auxiliary energy, and regenerative braking system abilities, and is based on a longitudinal vehicle dynamics model. We draw on multiple sources (e.g., Shekhar et al., 2016; Gallet et al., 2018; Tang et al., 2019; Göhlich et al., 2018; Al-Ogaili et al., 2020; Alwesabi et al., 2020; Ma et al., 2021; Abdelaty et al., 2021; Chen et al., 2021; Fiori et al., 2021) to achieve this model.

Overall, the total amount of energy (TE) required for EB operations is derived from two parts [see Eq. (3-33)]:

(i) Auxiliary energy needed to run auxiliary facilities, e.g., air conditioners, activating bus doors, heating, in-vehicle displays, and so on.

(ii) Mechanical energy related to the tractive force at the wheels, leading to the movement of a vehicle against forces opposed to it.

$$TE = E_{aux} + E_{tr} \tag{3-33}$$

To determine the auxiliary energy (E_{aux}), we assume a constant auxiliary power P_{aux} throughout the entire operating hours (see Eq. (3-34) where t is the total trip time, containing running and dwell times), which is commonly assumed in previous EB energy consumption models (e.g., Gallet et al., 2018; Tang et al., 2019; Al-Ogaili et al., 2020; Ma et al., 2021). However, it is worth noting that the occupancy levels inside vehicles can affect the amount of energy needed for Heating, Ventilating, and Air Conditioning (HVAC) services, despite our assumption of fixed auxiliary energy consumption during operations.

$$E_{aux} = P_{aux} t \tag{3-34}$$

The tractive force required for the movement of EBs can vary at different segments of a route, due to changes in driving conditions (e.g., driving speed and passenger load) and route characteristics (e.g., road slope), resulting in variations in energy consumption. Four different resistance forces opposing the movement of a vehicle are included in the tractive force equation, as shown in Eq. (3-35) (Gallet et al., 2018; Al-Ogaili et al., 2020):

$$F_t = F_d + F_r + F_g + F_a \tag{3-35}$$

- **Aerodynamic drag force (**$F_d = 0.5 p A C_d v^2$**)**: This force stems from the resistance of air when a vehicle is moving. p (kg/m^3), A (m^2), C_d, and v (m/s) reflect the air density, vehicle frontal area, drag coefficient, and vehicle travel speed respectively.
- **Rolling resistance (**$F_r = M g C_r \cos\phi$**)**: This force stems from the frictional resistance created between road surface and vehicle wheels. M ($M = W + L$) reflects the total vehicle weight (kg) [including the weight of an empty (unloaded) vehicle (W), plus passenger load (L)]. Also, parameters g (9.81 m/s^2), C_r, and ϕ (rad) reflect the gravitational constant, rolling resistance coefficient, and route slope respectively.

- **Grade force ($F_g = Mg\sin\phi$)**: This force stems from the road slope (i.e., the force needed to go uphill/downhill).
- **Inertia force ($F_a = \delta Ma$)**: This force stems from the variation of a vehicle's kinetic energy, which occurs when the vehicle accelerates or decelerates. $a = dv/dt$ represents the acceleration rate (m/s2) (a is negative in the deceleration phase), and δ is the mass factor taking the inertia of rotating parts (such as wheels, motor shaft and rotor) into account.

Let E_{tr} denote the energy consumption needed to provide the tractive force of a vehicle over a journey between two successive bus stations:

$$E_{tr} = \eta\left(0.5pAC_d v^2 + MgC_r\cos\phi + Mg\sin\phi + \delta Ma\right)d \tag{3-36}$$

where d is the traveled distance, and η is an efficiency factor that accounts for energy losses occurring in the phase of transferring energy from a battery to wheels. Besides, it is worth noting that EBs with regenerative braking technologies can take advantage of recuperating a part of kinetic energy when the tractive force is negative, e.g., such a situation occurs when driving over downhill road sections ($sin\phi < 0$) or in the braking phase ($a < 0$). Accordingly, considering both energy consumption phase (positive tractive force) and energy regeneration phase (negative tractive force), two possible cases are presented for the calculation of η in Eq. (3-37):

$$\eta = \begin{cases} \dfrac{1}{\eta_t \eta_r \eta_m} & \text{for } F_t \geq 0 \\ r_{\text{reg}} \eta_t \eta_r \eta_m & \text{for } F_t < 0 \end{cases} \tag{3-37}$$

where the efficiency of the drivetrain, inverter, as well as the motor are expressed using η_t, η_r, and η_m respectively. Besides, r_{reg} (regeneration factor) reflects the level of kinetic energy that can be recuperated by means of a regenerative braking system, considering the fact that the whole energy cannot be ideally recuperated, owing to battery restrictions and energy losses in the recharging phase (Gallet et al., 2018).

Once a desired speed is reached, urban bus services are often steered by a constant speed at a given segment (called "cruise speed"), and the needs for acceleration or deceleration activities will reappear in two main situations: at intersections and bus stops, resulting in a

typical trapezoidal velocity profile. The cruise speed may be conditioned by external issues, such as speed limits, traffic condition, weather, road closures and so on. Obviously, on bus lanes and dedicated bus corridors (e.g., BRT systems), public transport providers can take advantage of running buses at a higher level of speed with more predictable/stable driving functions, as shown with real-world data (Durán-Hormazábal and Tirachini, 2016).

In our setting for urban EB services, the amount of energy consumption is estimated for each bus at each segment of the route (i.e., for bus i between each two successive stops $j-1$ and j). Passenger load, road slope and vehicle travel speed can vary from one segment to another according to realistic conditions. The total mass of bus i is updated at a microscopic level:

$$M_{i,j} = W + L_{i,j} \tag{3-38}$$

where W represents the constant bus curb (unloaded) weight, as well as $L_{i,j}$ is the passenger load of bus i between each pair of adjacent stops ($j-1$ and j), obtained through multiplying the average weight of one passenger (m_{pax}) by the number of passengers being carried by bus i between stations $j-1$ and j ($N_{i,j}^{\text{on}}$) (i.e., $L_{i,j} = N_{i,j}^{\text{on}} \times m_{\text{pax}}$).

Beyond vehicle loads, neglecting road gradients could considerably reduce the accuracy of energy estimation for EBs (Gallet et al., 2018; Al-Ogaili et al., 2020). According to Gallet et al. (2018) in this regard, route gradients are obtained through the calculation of elevation change and route length between each two consecutive stations. There exist various data sources to extract elevation information, such as Digital Elevation Map (DEM) data for roads (Liu et al., 2017).

Table 3-3 presents typical parameter values employed in the energy estimation model for EBs, as suggested in Gallet et al. (2018). It should be noted that our work considers EB operations under overnight charging concepts, where the weight of the battery pack can be significant and is included in W. For instance, Al-Ogaili et al. (2020) reported that a standard 12-meter EB designed for overnight charging requires a large battery size (with "three parallel strings of three packs in series") to achieve a storage capacity of 270 kWh, resulting in a battery weight of about 3700 kg.

Table 3-3 Parameters for EB energy consumption model.

Parameter	Unit	Value
Empty vehicle weight with its battery pack (W)	kg	14800 (SB[5]), 23600 (AB[6])
Auxiliary power (P_{aux})	kW	10 (SB), 15 (AB)
Drag coefficient (C_d)	–	0.6
Rolling resistance (C_r)	–	0.01
Air density (ρ)	kg/m^3	1.2
Vehicle frontal area (A)	m^2	8.3
Inertia factor (δ)	–	1.1
Drivetrain and gearbox efficiency (η_t)	–	0.97
Inverter efficiency (η_r)	–	0.95
Motor efficiency (η_m)	–	0.91
Regeneration factor (r_{reg})	–	0.60

Generally, in contrast to fast charging strategies at stops or on routes, EBs are characterized by a large enough battery pack under overnight (depot) charging strategies to maintain the operations of half or even one full day (Shekhar et al., 2016; Göhlich et al., 2018; Teichert et al., 2019; Häll et al., 2019; Rupp et al., 2020; Sadrani et al., 2023c). For instance, Häll et al. (2019) estimated that a fully charged battery under an overnight charging strategy can enable buses to operate for an entire day, with an energy consumption rate of 0.9 (kWh/km). Based on real-world operations of EBs in Aachen, Germany, Rupp et al. (2020) reported that a 300-kWh battery capacity is sufficient for an articulated bus to operate all day with overnight charging.

Besides, for the current operational programs of EBs engaged only with depot charging at night in Singapore, Gallet et al. (2018) found that the driving range of EBs can vary depending on local traffic conditions (directly affecting the operating speeds of EBs, and the number of acceleration/deceleration activities), with heavy traffic conditions resulting in a range of 250 km and light traffic conditions resulting in a range of 350 km. The current EB range record (for a 12-m bus) seems to be held by the Iveco e-Way EB[7], which operated for 12 hours at an average velocity of 46 km/h, covering about 530 km on a single charge with a battery pack of 350 kWh under an overnight charging strategy. However, this test program was conducted without HVAC use in Germany at a temperature of 10-15 °C. Thus, given the cost

[5] Standard Bus (SB) with a length of 12 m.
[6] Articulated Bus (AB) with a length of 18 m.
[7] "https://www.sustainable-bus.com/news/527-km-on-one-charge-for-the-iveco-e-way-by-heuliez/."

and weight implications of large battery packs for overnight charging, we explicitly consider such aspects when assessing vehicle capital costs and load-dependent energy consumption.

The advantages and disadvantages of various charging programs, such as fast charging at stations versus overnight charging at depots during idle times, have been extensively researched in multiple studies that primarily focus on optimizing charging strategies, infrastructure, charging station locations, and battery sizing (e.g., Kunith et al., 2017; He et al., 2019; Rogge et al., 2018; Houbbadi et al., 2019; Teichert et al., 2019; Liu et al., 2021; Uslu and Kaya, 2021; Basma et al., 2022a; Sadrani et al., 2023c). Overall, it has been found that while a fast-charging system allows operators to deploy EBs with smaller on-board batteries and save battery costs, it can result in significantly higher charging infrastructure costs for operators due to expensive on-route fast-charging stops. On the other hand, the implementation of an overnight charging strategy can allow for the use of cheaper depot chargers and off-peak electricity tariffs, but it may lead to increased vehicle battery costs. Additionally, overnight charging can mitigate the risk of schedule delays caused by idle charging times during operations. Hence, buses with tight schedules tend to prefer overnight charging, while buses with low frequencies can benefit from multiple charging events throughout the day (Kunith et al., 2017). Overall, in such studies aimed at determining the most suitable charging strategy, a trade-off analysis between the costs associated with purchasing the vehicle (including its battery) and installing the charging infrastructure is needed. It should be noted that the optimization of charging strategy is not the focus of our planning model that has been already confined to a typical overnight charging concept.

3.2.2 Model assumptions for electric bus planning

We make the following assumptions on passenger flows, fleet composition, and cost calculations:

- We examine high-frequency routes, in which the operation of bus services is frequent enough that travelers do not have to arrange plan (in advance) for arrivals at stations (i.e., the assumption of random arrivals will hold).
- We simulate a situation for planning a single bus line on a bi-directional route, such as BRT systems.
- We consider a uniform (homogeneous) bus fleet, composed of buses of identical size.

- If travelers are confronted with capacity limitations when getting on a vehicle, we assume that the boarding opportunity would be analogous for all travelers, with no dependency on their trip destinations. This is a common assumption used by several studies (Sánchez-Martínez et al., 2016; Dai et al., 2020; Sadrani et al., 2022b).
- We simulate operations for a certain analysis period.
- For calculating user costs, we differentiate between the time valuations for in-vehicle riding, initial waiting, and additional waiting because of failing to board.

3.2.3 Optimization model for electric bus planning

We introduce an INLP formulation for the EB fleet scheduling problem. Our model optimizes the selection of vehicle types and frequency plans to achieve a desired supply level, while minimizing total costs, including user and operator costs, and accounting for time-dependent passenger flows and load-dependent energy consumption. Besides, several constraints are formulated to consider real-life conditions in urban bus operations (see Fig. 3-3). Table 3-1 presents the notation used in our formulation.

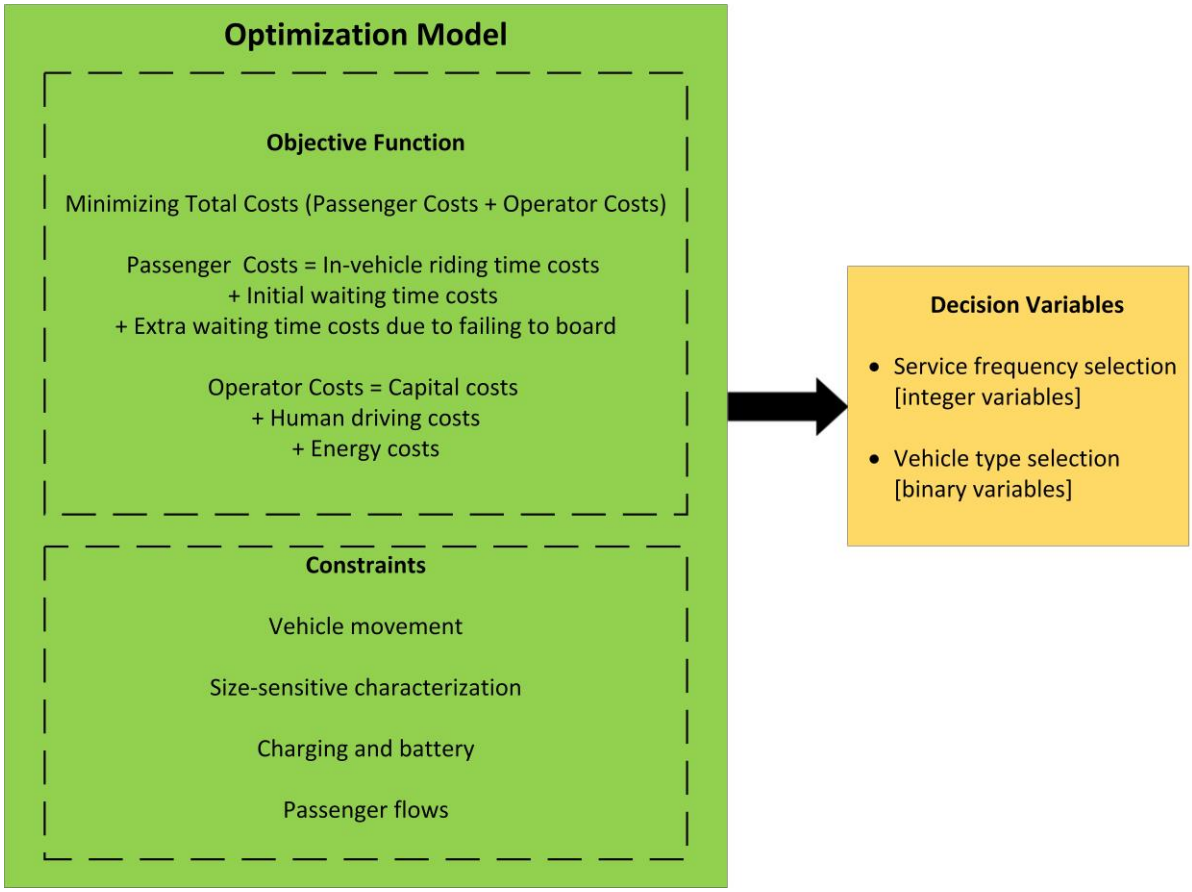

Figure 3-3 Overview of the optimization model framework in the proposed EB planning problem.

The proposed EB fleet scheduling problem is formulated as follows:

$$\min_{f,x_m} \quad Z_{\text{Total}} = \underbrace{Z_{\text{inv}} + Z_{\text{wait}}}_{Z_p} + \underbrace{Z_{\text{cap}} + Z_{\text{driver}} + Z_{\text{energy}}}_{Z_o} \tag{3-39}$$

$$Z_{\text{inv}} = \varphi^{v} \sum_{i \in V} \sum_{j \in S} N_{i,j}^{on} T_{i,j}^{r} \tag{3-40}$$

$$Z_{\text{wait}} = \varphi^{w1} \sum_{i \in V} \sum_{j \in S} N_{i,j}^{c} \frac{H_{i,j}}{2} + \varphi^{w2} \sum_{i \in V, i \geq 2} \sum_{j \in S} N_{i-1,j}^{f} H_{i,j} \tag{3-41}$$

$$Z_{\text{cap}} = \sum_{m \in M} \sum_{i \in V} \sum_{j \in S} x_m \varphi_m^{c} \left(T_{i,j}^{r} + T_{i,j}^{s} \right) \tag{3-42}$$

$$Z_{\text{driver}} = \varphi^{\text{d}} \sum_{i \in V} \sum_{j \in S} \left(T_{i,j}^{r} + T_{i,j}^{s} \right) \tag{3-43}$$

$$Z_{\text{energy}} = \varphi^{\text{e}} \sum_{i \in V} \sum_{j \in S} TE_{i,j} \; + \; \varphi^{\text{e}} \sum_{i \in V} \left(E_i^c + E_i^r \right) \tag{3-44}$$

Subject to:

$$H_{i,j} = T_{i,j}^d - T_{i-1,j}^d \qquad \forall i \in V, \forall j \in S - \{1\} \tag{3-45}$$

$$T_{i,j}^a = T_{i,j-1}^d + T_{i,j}^r \qquad \forall i \in V, \forall j \in S \tag{3-46}$$

$$T_{i,1}^d = G + (i-1)\frac{60}{f} \qquad \forall i \in V \tag{3-47}$$

$$T_{i,j}^d = T_{i,j}^a + T_{i,j}^s \qquad \forall i \in V, \forall j \in S - \{1\} \tag{3-48}$$

$$T_{i,j}^s = \tau + \alpha_a N_{i,j}^a + \alpha_b N_{i,j}^b \qquad \forall i \in V, \forall j \in S \tag{3-49}$$

$$T_i^c = \sum_{j \in S} \left(T_{i,j}^r + T_{i,j}^s \right) \qquad \forall i \in V \tag{3-50}$$

$$N_v = \left\lceil f \,.\, T_{90th}^{\,c} \right\rceil \tag{3-51}$$

$$\sum_{m \in M} x_m = 1 \tag{3-52}$$

$$C = \sum_{m \in M} c_m x_m \tag{3-53}$$

$$B = \sum_{m \in M} b_m x_m \tag{3-54}$$

$$E_i^c + E_i^r + \sum_{j \in S} TE_{i,j} \le \xi B \qquad \forall i \in V \tag{3-55}$$

$$N_{i,j,k}^c = \int_{T_{i-1,j}^d}^{T_{i,j}^d} \lambda_j [t] . OD_{j,k} [t] . dt \qquad \forall i \in V, \forall j,k \in S, k > j \tag{3-56}$$

$$N_{i,j,k}^w = N_{i,j,k}^c + N_{i-1,j,k}^f \qquad \forall i \in V, \forall j,k \in S, k > j \tag{3-57}$$

$$N^{c}_{i,j} = \sum_{k \in S, k > j} N^{c}_{i,j,k} \qquad \forall i \in V, \forall j \in S \tag{3-58}$$

$$N^{f}_{i,j} = \sum_{k \in S, k > j} N^{f}_{i,j,k} \qquad \forall i \in V, \forall j \in S \tag{3-59}$$

$$N^{w}_{i,j} = \sum_{k \in S, k > j} N^{w}_{i,j,k} \qquad \forall i \in V, \forall j \in S \tag{3-60}$$

$$N^{on}_{i,j} = N^{on}_{i,j-1} - N^{a}_{i,j-1} + N^{b}_{i,j-1} \qquad \forall i \in V, \forall j \in S \tag{3-61}$$

$$L_{i,j} = N^{on}_{i,j} . m_{\text{pax}} \qquad \forall i \in V, \forall j \in S \tag{3-62}$$

$$N^{b}_{i,j} = \min\left\{N^{w}_{i,j}, C - N^{on}_{i,j} + N^{a}_{i,j}\right\} \qquad \forall i \in V, \forall j \in S \tag{3-63}$$

$$N^{a}_{i,j} = \sum_{j' \in S, j' < j} N^{s}_{i,j',j} \qquad \forall i \in V, \forall j \in S \tag{3-64}$$

$$N^{s}_{i,j,k} = N^{w}_{i,j,k} \frac{N^{b}_{i,j}}{N^{w}_{i,j}} \qquad \forall i \in V, \forall j, k \in S, k > j \tag{3-65}$$

$$N^{f}_{i,j,k} = N^{w}_{i,j,k} - N^{s}_{i,j,k} \qquad \forall i \in V, \forall j, k \in S, k > j \tag{3-66}$$

$$f \in \left\{f_{\min}, f_{\min} + 1, \ldots, f_{\max} - 1, f_{\max}\right\} \tag{3-67}$$

$$x_m \in \{0,1\} \qquad \forall m \in M \tag{3-68}$$

In Eq. (3-39), the objective function is presented for minimizing the total costs, containing both passenger and operator costs. Passenger cost (Z_p) has two elements: in-vehicle riding and waiting time costs. Operator cost (Z_o) has three elements: capital, human driving, and energy costs. In the following, each cost element is described in detail.

In-vehicle riding time cost (Z_{inv}): As presented in Eq. (3-40), the in-vehicle time cost is calculated for on-board passengers based on riding times spent traveling between stops. Parameter φ^{v} [€/h] represents the value of in-vehicle time, used to convert passengers' in-vehicle times into equivalent cost values.

Waiting time cost (Z_{wait}): In Eq. (3-41), we calculate the total waiting time costs considering two possible cases that might be perceived by passengers: (a) for new coming passengers, $N_{i,j}^{c}$ (experiencing an initial waiting time), and (b) for fail-to-board passengers, $N_{i-1,j}^{f}$ (experiencing an excess waiting time).

For case (a): Given that we study high-frequency routes (where the assumption of random arrivals of travelers at stations will hold), the waiting time is estimated to be half of the headway.

For case (b): If capacity restrictions prevent travelers from boarding a particular service, they are required to wait for the subsequent service, which results in an additional waiting time equal to the entire headway ($H_{i,j}$) [see the second part of Eq. (3-41)].

The waiting time value perceived by travelers at stations is greater than the value of travel time spent inside public transport vehicles, as the waiting process is more burdensome from passengers' viewpoint (Wardman, 2004; Cats et al., 2016; Lu et al., 2018; Sadrani et al., 2022c). Besides, the financial impact of failing to board and experiencing prolonged waiting is even more pronounced than the cost of initial waiting time under normal circumstances (Cats et al., 2016; Yap and Cats, 2021). For example, as reported by Cats et al. (2016), an extra waiting time is 3.5 times more unpleasant than the initial expected waiting time, because it is perceived in the form of an unexpected delay that has a more negative impact on public transport users. Hence, to provide a comprehensive framework for passenger cost computations, we differentiate between the financial valuations of on-board riding time (φ^{v}), initial waiting time (φ^{w1}), as well as the additional waiting time for left-behind travelers (φ^{w2}).

Capital cost (Z_{cap}): The acquisition costs of EB fleets for operators depend on the vehicle type with its battery pack properties (e.g., the use of either 12-meter buses or 18-meter articulated buses) and the total fleet size (the total number of vehicles needed). For example, in order to provide a higher level of frequency (more frequent services) by means of a higher number of buses, service providers need to acquire more vehicles, increasing the capital costs.

In operator cost calculations, a temporal basis [€/veh-h] is usually used to represent capital costs, i.e., the capital cost in Eq. (3-42) is estimated based on the operating hours of available vehicles when serving demand on a route (Zhang et al., 2019; Tirachini and Antoniou, 2020; Hatzenbühler et al., 2021). Size-dependent cost parameter φ^{c} [€/veh-h] is the capital (acquiring) cost of a vehicle per hour, which depends on the size of

the EB with its battery pack size and properties (Tirachini and Antoniu, 2020). It is worth noting that to estimate vehicle capital cost parameter φ^{c} [€/veh-h], the initial purchase price of a vehicle is prorated based on equivalent hours of operation[8] during the whole lifetime of a typical urban bus while taking various economic factors into account (e.g., asset life, operating hours per year, discount rate, etc.) (Tirachini and Antoniu, 2020; Badia and Jenelius, 2021).

Driver cost (Z_{driver}): As presented in (3-43), the human driving cost is estimated considering the total amount of time spent driving along the route. The cost parameter φ^{d} [€/veh-h], named hourly driving cost, reflects the gross salary paid to each driver for one-hour driving, and is assumed to be independent of the vehicle type (e.g., 12-m or 18-m bus) steered by drivers (Tirachini and Antoniu, 2020).

Energy cost (Z_{energy}): As described in Section 3.2.1, we estimate the vehicle energy consumption using a detailed model, accounting for the amount of energy consumed by each service i between each two consecutive stations $j-1$ and j while considering the actual driving and route conditions [see Eq. (3-44)]. Besides, the second term accounts for the energy consumption of vehicles in the depot trips.

As shown in Eq. (3-45), the headway is the time duration between the departing of two consecutive vehicles from the same station. It should be noted that the headway in Eq. (3-45) can vary between different services at different stations, as the departure times of services can be affected by alighting and boarding demands (dwelling time) at each station [the dwell time modeling is further explained in Eq. (3-49)].

According to Eq. (3-46), the arriving time of service i at station j is derived from the summation of its departure time from the former station (station $j-1$) and its riding time between two adjacent stations $j-1$ and j. As shown in Eq. (3-47), a regular headway (every $60/f$ min) is considered for dispatching buses from the first station. Besides, this formulation reflects that the dispatching time of the first bus will occur at the beginning point of the planning period (denoted by G).

The departure time of service i from station j is derived from the addition of its dwell time to the arrival time of the service at that station [see Eq. (3-48)]. In Eq. (3-49), we model

[8] As for the idea behind this strategy (calculating vehicle capital costs based on operating hours), we commonly follow the approach of assuming the useful life span of a bus as a function of the total number of kilometers that a bus could run, which is then translated into operating hours, while not considering the idle time (e.g., in depots) due to a usual simplification. Under this approach, what matters is the total number of hours that a bus can be in operation. Based on empirical data, we assumed 12 years as the lifetime of buses, and 3700 hours per year to then annualize the capital cost and relate it to hours of operation (for more details, we refer to Tirachini and Antoniu, 2020).

flow-dependent dwell times. Accordingly, the bus dwell time is calculated based on alighting and boarding numbers at each station, and the time associated with opening and closing doors. In this formulation, it is assumed that the boarding phase will occur after the alighting phase. Hence, the dwell time contains the sum of both getting off and on times (Tirachini et al., 2014; Sadrani et al., 2022b). As defined in Eq. (3-50), the cycle time of a bus, which is the time that a bus takes to complete one round trip, contains cruising times (between stops) and dwell times at bus stops. The cycle time is a variable as vehicles' dwell times will depend on boarding and alighting demands, affected by the frequency level obtained for operations. The fleet size requirement is obtained through Eq. (3-51), where we use the 90th percentile of cycle time for the fleet size calculation, which is a common aspect in the literature (Gkiotsalitis and Cats, 2018; Sadrani et al., 2022b).

Eq. (3-52) indicates that a uniform fleet of vehicles is operated (i.e., the fleet contains buses of the same type). As shown in Eqs. (3-53) and (3-54), the passenger-carrying capacity and battery capacity of vehicles are dependent on the vehicle type operated. Eq. (3-55) ensures that the usable battery capacity would be sufficient to meet the assigned trips to vehicles.

In the presence of time-dependent passenger arrival flows, Eq. (3-56) calculates passenger volumes (aiming to travel from j to k) who reach station j over the headway interval between services $i-1$ and i. Considering travelers left behind by the former service (service $i-1$) at station j, the total number of travelers (with journey $j \rightarrow k$) waiting for service i at station j [see Eq. (3-57)] is obtained from the summation of: (a) new travelers reaching stations over the headway interval, modeled in Eq. (3-56), and (b) fail-to-board travelers, if any, who were confronted with capacity deficiency in boarding the former service (service $i-1$), needing to wait for arriving the subsequent service.

It is clear that Eqs. (3-58)-(3-60) will always hold in view of our modeling definitions. For example, travelers waiting for service i at station j can have various journey destinations. Thus, in view of the definitions of $N_{i,j,k}^{w}$ and $N_{i,j}^{w}$, the summation of those travelers (with journey $j \rightarrow k$, $k > j$) leads to the whole population waiting for service i at station j [see Eq. (3-60)].

As indicated in Eq. (3-61), the number of passengers carried by service i between stations $j-1$ and j ($N_{i,j}^{on}$) will include: (a) those passengers staying inside service i from the preceding stop-to-stop trip (i.e., from the sector $j-2 \rightarrow j-1$) because they did not need to get off at station $j-1$, i.e., ($N_{i,j-1}^{on} - N_{i,j-1}^{a}$), and (b) passengers who have recently boarded service i at

station $j-1$, i.e., $N_{i,j-1}^{b}$. Subsequently, the total passenger load carried by service i between stations $j-1$ and j is estimated in Eq. (3-62), where m_{pax} (kg) represents the average weight of one passenger.

Eq. (3-63) shows that the demand for boarding vehicles cannot be larger than the active capacity of vehicles at each station. Eq. (3-64) calculates the alighting demand for service i at station j, containing travelers getting on service i at the earlier stations, who intend to reach destination station j. According to Eq. (3-65), all the passengers have the chance to board in the case of a capacity shortage. In Eq. (3-66), we calculate the number of travelers (aiming to travel from j to k) left behind by service i at station j, owing to capacity restrictions. Eventually, the domains of decision variables are expressed as constraints (3-67) and (3-68) in our combinatorial optimization problem. For instance, the service frequency (f) is an integer variable selected from a discrete set: $\{f_{\min}, f_{\min}+1, \dots, f_{\max}-1, f_{\max}\}$ (this set contains $(f_{\max}-f_{\min})+1$ elements). It is worth noting that $f_{\min}$ and $f_{\max}$ represent the minimum and maximum allowable frequencies for operations, respectively, and are exogenously determined by policymakers based on route operational conditions.

3.3 Decision making framework for electric bus charging strategy selection

The adoption of EBs in urban areas is a promising solution to reducing GHG emissions in the transportation sector and mitigating the effects of climate change (Logan et al., 2020; Perumal et al., 2022). EBs produce zero tailpipe emissions and can be powered by renewable energy sources, making them a sustainable and environmentally friendly alternative to traditional diesel or gasoline-powered buses. In addition, EBs have lower operating costs, improve air quality, and reduce the health risks associated with air pollution (J. A. Manzolli et al., 2022). However, transitioning to EB fleets requires significant investments in charging infrastructure, as well as supportive policy and regulatory measures. One crucial step in the electrification of bus networks is selecting the best type of charging strategy from a variety of options, such as overnight (slow) charging and opportunity (fast) charging systems. With the increasing demand for environmentally friendly transportation and the growing adoption of EBs in public transport systems, this step is becoming increasingly important for public transport agencies. However, choosing the best strategy is a challenging task since each option has advantages and disadvantages. To tackle this issue effectively, policymakers need to consider multiple factors (with different dimensions) concurrently,

calling for the management of a MCDM problem. This research thus attempts to address the selection of charging strategies for EB systems as a MCDM problem, assisting policymakers in making informed decisions using a reliable decision-making tool for the comparison and assessment of possible charging options/alternatives based on a wide range of criteria that are relevant in practice.

In urban EB operations, two common charging strategies[9] are overnight (slow) charging at depots and opportunity (fast) charging at stations (see Fig. 3-4) (Xylia and Silveira, 2018; Zaneti et al., 2022):

1) **Overnight (slow) charging:** EBs are charged while they are not in service, typically during the night, at a depot[10].
2) **Opportunity (fast) charging:** EBs are charged at various points, such as bus stops, throughout their operations whenever an opportunity arises[11].

[9] It is worth noting that, as stated in (Zaneti et al., 2022), various terminology (vocabulary combinations) can be found in the literature for naming charging strategies, such as fast (opportunity, on-street, at-station) and slow (overnight, depot) charging (other than the names of fast and slow charging). However, beyond the issue of nomenclature, power and time are what differentiate them. Following the most common terminology and considering the power, we adopt the terms opportunity (fast) charging and overnight (slow) charging strategies, referring to short and long charging periods respectively (Xylia and Silveira, 2018; Zaneti et al., 2022). Opportunity charging involves connecting the EB for a few minutes, followed by circulating and reconnecting for several repetitions. In contrast, overnight charging requires continuous charging for a long duration, such as six hours, with the connector being plugged in.

[10] In overnight charging, low-powered (slow) chargers are used to recharge EBs over a longer period of time.

[11] In opportunity charging, high-powered (fast) chargers are used to recharge EBs quickly.

(a) Overnight charging[12]

(b) Opportunity charging [13]

Figure 3-4 Overnight (depot) charging vs. opportunity (fast) charging.

In the following, we provide a brief comparison of the pros and cons of each option (overnight charging vs. opportunity charging) (Basma et al., 2022b; Kunith et al., 2017; Perumal et al., 2022; Teichert et al., 2019; Xylia and Silveira, 2018):

- **Battery costs:** Opportunity charging systems require smaller on-board batteries, reducing battery costs.
- **Planning efforts:** Opportunity charging systems require more intricate planning with multiple charging stations along bus routes.

[12] Mercedes-Benz eCitaro Plant Gets 1.2 MW Charging Station (insideevs.com).

[13] https://insideevs.com/news/337013/abb-hints-at-big-ev-bus-project-35-vehicles-8-450-kw-chargers/.

- **Charging infrastructure costs:** Opportunity charging systems require higher infrastructure costs, related to the installation of high-powered (fast) chargers and the procurement of land in multiple locations throughout the city.
- **Battery weight impacts:** Overnight charging systems require heavier battery packs, increasing the energy consumption of EBs.
- **Electricity tariff:** Overnight charging systems can take advantage of cheaper off-peak electricity tariffs at night.
- **Service delays:** Overnight charging systems allow EBs to be charged while off-duty, reducing the risk of operational delays caused by charging idle times during daily operations.

As the above comparison shows, such advantages and disadvantages put operators in a challenging trade-off situation, highlighting the importance of having a robust decision-making tool to handle the charging strategy selection for EB systems.

3.3.1 Decision making structure

In this research, the criteria are assessed and weighted using a FBWM. A FRAFSI approach is also used to rank the options. In addition, two further methods, including fuzzy TOPSIS (C.-T. Chen, 2000) and fuzzy EDAS (Keshavarz-Ghorabaee et al., 2016), are applied, and their results are compared with those of the FRAFSI. As shown in Fig. 3-5, the research method used in this dissertation contains four key stages:

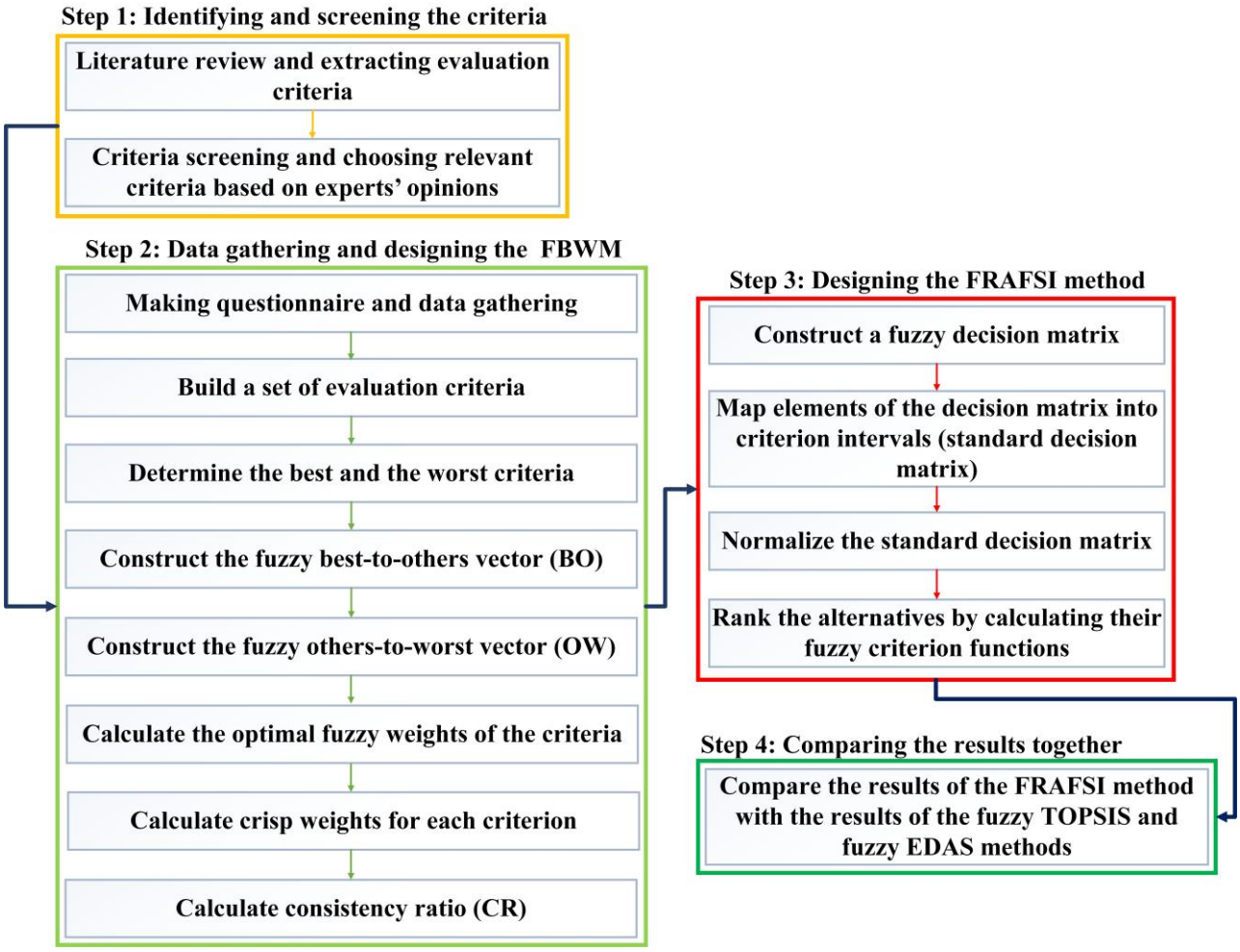

Figure 3-5 Decision-making structure.

Step 1: The evaluation criteria for choosing the best charging method for EBs are identified and extracted in a hybrid effort composed of a literature review and interviews with EB experts. The initial list of criteria was also inspected and revised by seven experts to extract the most important factors, while taking several aspects into account, such as having the ideal number of criteria and sub-criteria (Pfeffer, 2003), optimizing the reliability of comparisons between criteria (Rezaei, 2015), and improving the decision makers' discriminatory power (Wanke et al., 2016). The final criteria are classified into five dimensions: economic, environmental, social, operation, and quality-of-service (see Fig. 3-6).

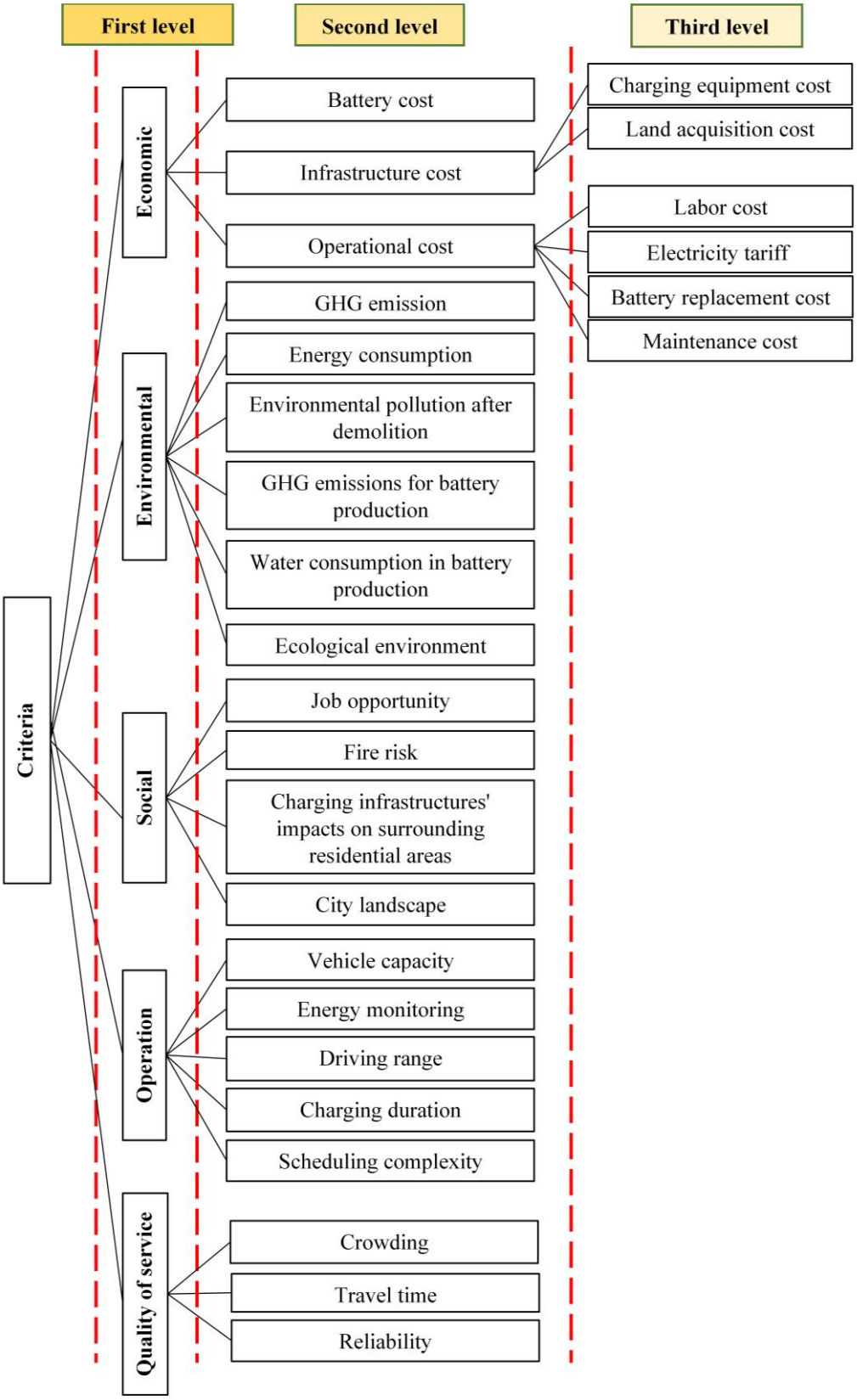

Figure 3-6 Related criteria for the selection of charging strategies for EBs.

Step 2: For collecting the required data, a FBWM questionnaire is designed and provided to the experts. We consulted 11 experts from both academia and industry via an online questionnaire. The demographics of experts are given in Table 3-4. The criteria's weights are then computed through the FBWM.

Table 3-4 Demographics of experts.

Expert No.	Background	Country	Education level
1	Academia (Associate professor)	Germany	PhD
2	Industry	Germany	Master
3	Academia (Associate professor)	Chile	PhD
4	Academia (Associate professor)	Austria	PhD
5	Academia (Associate professor)	Greece	PhD
6	Academia (Assistant professor)	Netherlands	PhD
7	Industry	Germany	PhD
8	Academia (Assistant professor)	Singapore	PhD
9	Industry	Germany	PhD
10	Industry	India	Master
11	Industry	Germany	Master

Step 3: The alternatives are ranked using the FRAFSI technique.

Step 4: Finally, two further methods including the fuzzy TOPSIS and fuzzy EDAS are used for ranking alternatives, and their results are compared with the FRAFSI's results.

In the following, the FBWM, FRAFSI, TOPSIS and EDAS methods are described.

3.3.2 Fuzzy best worst method

Rezaei (2015) proposed the Best Worst Method (BWM) which is a vector-based Multi-Criteria Decision-Making (MCDM) approach to estimate the criteria's weights $(w_1, w_2 \ldots, w_n)$ through pairwise comparisons. BWM has several features that make it interesting to use (Rezaei, 2015):

- It needs fewer pairwise comparisons relative to other MCDM methods which are matrix-based. For instance, AHP, which has been extensively used for MCDM problems, needs $n(n-1)/2$ pairwise comparisons, while BWM employs only $2n-3$ pairwise comparisons. It can save a significant amount of time for experts.
- Compared to AHP, it employs more consistent comparisons, which can increase the reliability of the results.

Guo and Zhao (2017) developed the fuzzy version of the BWM (FBWM)to better handle ambiguities and uncertainties of decision makers' opinions in comparisons. With this approach, fuzzy pairwise comparisons of the criteria are carried out using the decision makers' linguistic expressions, converted into fuzzy ratings.

The process of weighing the criteria by the FBWM involves the implementation of seven stages as follows (Guo and Zhao, 2017):

Stage 1: Establish a group of criteria for evaluation, denoted as $\{c_1, c_2, \ldots, c_n\}$.

Stage 2: Identify the best (most important) and worst (least important) criteria.

Stage 3: Create the fuzzy best-to-others vector (BO) reflecting the preference of the most important (best) criterion against all other criteria. This vector is represented as:

$$\tilde{A}_B = (\tilde{a}_{B1}, \tilde{a}_{B2}, \ldots, \tilde{a}_{Bn}) \quad (3\text{-}69)$$

where the value of $\tilde{a}_{Bj}$ reflects the preference of the best criterion against criterion j, with $\tilde{a}_{BB}$ that is equal to (1,1,1).

According to Table 3-5, the linguistic expressions are converted to fuzzy numbers.

Stage 4: Create the fuzzy others-to-worst vector (OW) reflecting the preference of all criteria against the least important (worst) criterion. This vector is represented:

$$\tilde{A}_W = (\tilde{a}_{1W}, \tilde{a}_{2W}, \ldots, \tilde{a}_{nW}) \quad (3\text{-}70)$$

where the value of $\tilde{a}_{jW}$ reflects the preference of criterion j against the worst criterion, with $\tilde{a}_{WW}$ that is equal to (1,1,1).

Table 3-5 Linguistic phrases and equivalent fuzzy numerical function (Torkayesh et al., 2021b).

Linguistic terms	**Membership function**
Equally important	(1,1,1)
Weakly important	(2/3,1,3/2)
Fairly important	(3/2,2,5/2)
Very important	(5/2,3,7/2)
Absolutely important	(7/2,4,9/2)

Stage 5: Compute the optimal fuzzy values for the criteria's weights. Fuzzy weights $(\widetilde{W}_1^*, \widetilde{W}_2^*, \dots, \widetilde{W}_n^*)$ are calculated by solving a non-linear optimization model that consists of a min-max objective function, as presented in Eq. (3-71). This objective function aims to minimize the maximum absolute difference between fuzzy weights obtained from fully consistent comparisons and the weights obtained from the present comparisons for all criteria.

$$\min \ max_j \left\{ \left| \frac{\widetilde{W}_B}{\widetilde{W}_j} - \tilde{a}_{Bj} \right|, \left| \frac{\widetilde{W}_j}{\widetilde{W}_W} - \tilde{a}_{jW} \right| \right\}$$

$$s.t. \begin{cases} \sum_{j=1}^{n} R(\widetilde{W}_j) = 1 \\ l_j^w \le m_j^w \le u_j^w \\ l_j^w \ge 0 \\ \mathrm{j} = 1, 2, \dots, \mathrm{n} \end{cases} \tag{3-71}$$

where $\widetilde{W}_B = (l_B^w, m_B^w, u_B^w)$, $\widetilde{W}_j = (l_j^w, m_j^w, u_j^w)$, $\widetilde{W}_W = (l_W^w, m_W^w, u_W^w)$, $\tilde{a}_{Bj} = (l_{Bj}, m_{Bj}, u_{Bj})$, $\tilde{a}_{jW} = (l_{jW}, m_{jW}, u_{jW})$.

The optimization problem can be expressed as follows:

$$\min \tilde{\xi}$$

$$s.t. \begin{cases} \left|\frac{\widetilde{W}_B}{\widetilde{W}_j} - \tilde{a}_{Bj}\right| \leq \tilde{\xi} \\ \left|\frac{\widetilde{W}_j}{\widetilde{W}_W} - \tilde{a}_{jW}\right| \leq \tilde{\xi} \\ \sum_{j=1}^{n} R(\widetilde{W}_j) = 1 \\ l_j^w \leq m_j^w \leq u_j^w \\ l_j^w \geq 0 \\ \mathrm{j} = 1, 2, \ldots, \mathrm{n} \end{cases} \tag{3-72}$$

where $\tilde{\xi} = (l^{\xi}, m^{\xi}, u^{\xi})$.

Considering $l^{\xi} \leq m^{\xi} \leq u^{\xi}$, and $\tilde{\xi}^* = (k^*, k^*, k^*)$, $k^* \leq l^{\xi}$, Eq. (3-72) is expressed as follows:

$$\min \tilde{\xi}^*$$

$$s.t. \begin{cases} \left|\frac{(l_B^w, m_B^w, u_B^w)}{(l_j^w, m_j^w, u_j^w)} - (l_{Bj}, m_{Bj}, u_{Bj})\right| \leq (k^*, k^*, k^*) \\ \left|\frac{(l_j^w, m_j^w, u_j^w)}{(l_W^w, m_W^w, u_W^w)} - (l_{jW}, m_{jW}, u_{jW})\right| \leq (k^*, k^*, k^*) \\ \sum_{j=1}^{n} R(\widetilde{W}_j) = 1 \\ l_j^w \leq m_j^w \leq u_j^w \\ l_j^w \geq 0 \\ \mathrm{j} = 1, 2, \ldots, \mathrm{n} \end{cases} \tag{3-73}$$

The optimal fuzzy values for the criteria's weights are obtained by solving Eq. (3-73).

Stage 6: Crisp weights for each criterion are obtained using Eq. (3-74):

$$crisp\left(\widetilde{N}\right) = \frac{l_i + 4m_i + u_i}{6} \tag{3-74}$$

Stage 7: The Consistency Ratio (CR) is used to assess the consistency and accuracy of the calculated weights. A fuzzy comparison is considered completely consistent when $\tilde{a}_{Bj} \times \tilde{a}_{jW} = \tilde{a}_{BW}$, where $\tilde{a}_{BW}$ refers to the preference of the best criterion against the worst criterion (Rezaei, 2015). When $\tilde{a}_{Bj} \times \tilde{a}_{jW} \neq \tilde{a}_{BW}$, inconsistency rate will increase. The

highest inconsistency rate occurs when $\tilde{a}_{jW}$ and $\tilde{a}_{Bj}$ are both equal to $\tilde{a}_{BW}$. Since $\frac{\tilde{W}_B}{\tilde{W}_j} \times \frac{\tilde{W}_j}{\tilde{W}_W} = \frac{\tilde{W}_B}{\tilde{W}_W}$, it can be converted to:

$$(\tilde{a}_{Bj} - \tilde{\xi}) \times (\tilde{a}_{jW} - \tilde{\xi}) = (\tilde{a}_{BW} + \tilde{\xi}) \tag{3-75}$$

For the maximum fuzzy inconsistency, Eq. (3-75) is stated as follows:

$$(\tilde{a}_{BW} - \tilde{\xi}) \times (\tilde{a}_{BW} - \tilde{\xi}) = (\tilde{a}_{BW} + \tilde{\xi}) \tag{3-76}$$

which turns into:

$$\tilde{\xi}^2 - (1 + 2\tilde{a}_{BW})\tilde{\xi} + (\tilde{a}_{BW}{}^2 - \tilde{a}_{BW}) = 0 \tag{3-77}$$

where $\tilde{\xi} = (l^{\xi}, m^{\xi}, u^{\xi})$, $\tilde{a}_{BW} = (l_{BW}, m_{BW}, u_{BW})$.

The largest possible fuzzy value for $\tilde{a}_{BW}$ is (7/2, 4, 9/2) (see Table 3-5), meaning that the maximum value of l_{BW}, m_{BW}, and u_{BW} cannot be greater than 9/2. Eq. (3-77) can be thus converted to the following form:

$$\xi^2 - (1 + 2u_{BW})\xi + (u_{BW}{}^2 - u_{BW}) = 0 \tag{3-78}$$

where u_{BW} would be 1, 3/2, 5/2, 7/2, and 9/2 successively. The largest possible ξ is obtained by solving Eq. (3-78) with various u_{BW}. Table 3-6 lists the Consistency Index (CI) for FBWM with regard to different linguistic terms.

Table 3-6 Consistency index for FBWM (Torkayesh et al., 2021b).

Linguistic terms	Equally important (EI)	Weakly important (WI)	Fairly important (FI)	Very important (VI)	Absolutely important (AI)
$\tilde{a}_{BW}$	(1, 1, 1)	(2/3, 1, 3/2)	(3/2, 2, 5/2)	(5/2, 3, 7/2)	(7/2, 4, 9/2)
CI	3.00	3.80	5.29	6.69	8.04

Therefore, CR can be calculated as follows:

$$CR = \frac{\tilde{\xi}^*}{CI} \tag{3-79}$$

3.3.3 Fuzzy ranking of alternatives through functional mapping of criterion subintervals into a single interval method

Žižović et al. (2020) developed a novel technique for the Ranking of Alternatives through Functional mapping of criterion subintervals into a Single Interval (RAFSI). This technique has three key benefits: (i) a simple algorithm, (ii) the use of a novel approach to normalize data that is appropriate for making reasonable decisions, and (iii) the elimination of the rank reversal problem, which is a significant drawback of available multiple attribute decision-making techniques. In this work, we use the fuzzy version of the RAFSI method (FRAFSI), which can allow for handling uncertainties and imprecisions in decision maker's opinions, thus producing a more robust and accurate evaluation of alternatives. The process is described as follows:

Stage 1: Create an aggregated fuzzy decision matrix. Suppose we consulted k experts to evaluate m alternatives $\{A_1, A_2, \ldots, A_m\}$ concerning a set of criteria $\{c_1, c_2, \ldots, c_n\}$ using a fuzzy linguistic scale. The evaluation provided by each expert is represented in the form of a matrix:

$$X^{(e)} = \begin{bmatrix} \theta_{11}^{(e)} & \theta_{12}^{(e)} & \cdots & \theta_{1n}^{(e)} \\ \theta_{21}^{(e)} & \theta_{22}^{(e)} & \cdots & \theta_{2n}^{(e)} \\ \vdots & \vdots & \ddots & \vdots \\ \theta_{m1}^{(e)} & \theta_{m2}^{(e)} & \ldots & \theta_{mn}^{(e)} \end{bmatrix}; 1 \le i \le m;\ 1 \le j \le n;\ 1 \le e \le k \tag{3-80}$$

where $\theta_{ij}^{(e)} = \left(\theta_{ij}^{l(e)}, \theta_{ij}^{s(e)}, \theta_{ij}^{u(e)}\right)$ indicates the fuzzy value calculated using a fuzzy linguistic scale. Eq. (3-81), the fuzzy Heronian operator (Dejian Yu, 2013), is used to aggregate k fuzzy decision matrices into the matrix $X = [\tilde{\theta}_{ij}]_{m\times n}$:

$$\tilde{\theta}_{ij} = \left(\tilde{\theta}_{ij}^{l}, \tilde{\theta}_{ij}^{s}, \tilde{\theta}_{ij}^{u}\right) = \begin{cases} \tilde{\theta}_{ij}^{l} = \left(\dfrac{2}{k(k+1)} \displaystyle\sum_{i=1}^{n}\sum_{j=i}^{n} \tilde{\theta}_{i}^{lp}\tilde{\theta}_{j}^{lq}\right)^{\frac{1}{p+q}} \\ \tilde{\theta}_{ij}^{s} = \left(\dfrac{2}{k(k+1)} \displaystyle\sum_{i=1}^{n}\sum_{j=i}^{n} \tilde{\theta}_{i}^{sp}\tilde{\theta}_{j}^{sq}\right)^{\frac{1}{p+q}} \\ \tilde{\theta}_{ij}^{u} = \left(\dfrac{2}{k(k+1)} \displaystyle\sum_{i=1}^{n}\sum_{j=i}^{n} \tilde{\theta}_{i}^{up}\tilde{\theta}_{j}^{uq}\right)^{\frac{1}{p+q}} \end{cases} \tag{3-81}$$

where $\tilde{\theta}_{ij} = \left(\tilde{\theta}_{ij}^{l}, \tilde{\theta}_{ij}^{s}, \tilde{\theta}_{ij}^{u}\right)$ indicates the averaged fuzzy number, and $p, q \ge 0$ represent sets of non-negative numbers.

Stage 2: The elements of the aggregated decision matrix are transformed into criterion intervals. The decision maker sets the ideal and anti-ideal values for each criterion, represented

by $\tilde{\theta}I_j$ and $\tilde{\theta}N_j$. A function is then defined for each alternative, as presented in Eq. (3-82), mapping the intervals in the aggregated decision matrix to a new interval $[n_1, n_b]$:

$$f_i\left(C_j\right) = \frac{n_b - n_1}{\tilde{\theta}I_j - \tilde{\theta}N_j}\tilde{\theta}_{ij} + \frac{\tilde{\theta}I_j \,.n_1 - \tilde{\theta}N_j \,.n_b}{\tilde{\theta}I_j - \tilde{\theta}N_j} \tag{3-82}$$

where n_b and n_1 are the ratios of the ideal and anti-ideal values, as well as $\tilde{\theta}_{ij}$ represents the fuzzy value of the alternative i for criterion j from the aggregated decision matrix. The result is the standard decision matrix, $T = \left[\widetilde{\emptyset}_{ij}\right]_{m\times n}$. It is recommended that the ideal value should be significantly better than the anti-ideal value, with a ratio of at least 6:1 (Kaya et al., 2022).

Stage 3: Normalize the elements in the standard decision matrix (T) using Eq. (3-83):

$$\widehat{\emptyset}_{ij} = \begin{matrix} \frac{\widetilde{\emptyset}_{ij}}{2A}, & for \max criteria \\ \frac{H}{2\widetilde{\emptyset}_{ij}}, & for \min criteria \end{matrix} \tag{3-83}$$

where A represents the arithmetic mean of n_1 and n_b, and H represents their harmonic mean.

Stage 4: Rank the alternatives by calculating their fuzzy criterion functions. Using Eq. (3-84), the fuzzy criterion function is calculated for each alternative. The alternative that has the highest value in the fuzzy criterion function is considered the best one.

$$\tilde{Q}_i = \sum_{j=1}^{n} \widetilde{w}_j \widehat{\emptyset}_{ij} \tag{3-84}$$

3.3.4 Fuzzy technique for order preference by similarity to ideal solution

Stage 1: Calculate the criteria's weights.

Stage 2: Create the fuzzy matrix.

$$\begin{aligned} &\widetilde{D} = [\tilde{x}_{ij}]_{m\times n}, i = 1, 2, \dots, m; j = 1, 2, \dots, n \\ &\tilde{x}_{ij} = \frac{1}{k}\sum_{p=1}^{k} \tilde{x}_{ij}^{p}, p = 1, 2, \dots, k \end{aligned} \tag{3-85}$$

where $\tilde{x}_{ij}^{p} = (a_{ij}^{p}, b_{ij}^{p}, c_{ij}^{p})$ represents the evaluation made by expert p for alternative A_i concerning criterion C_j.

Stage 3: Normalize the fuzzy decision matrix.

$$\tilde{R} = [\tilde{r}_{ij}]_{m\times n}, i = 1, 2, \dots, m; j = 1, 2, \dots, n \tag{3-86}$$

where $\tilde{r}_{ij} = \left(\frac{a_{ij}}{c_j^+}, \frac{b_{ij}}{c_j^+}, \frac{c_{ij}}{c_j^+}\right), c_j^+ = max_i\, c_{ij}$.

Stage 4: Construct a weighted normalized fuzzy decision matrix.

$$\tilde{V} = [\tilde{v}_{ij}]_{m\times n}, i = 1, 2, \dots, m; j = 1, 2, \dots, n \tag{3-87}$$

where $\tilde{v}_{ij} = \tilde{r}_{ij} \otimes \tilde{w}_j$, and $\tilde{w}_j$ refers to the weight assigned to criterion j.

Stage 5: Calculate fuzzy ideal solutions, including the fuzzy positive-ideal solution (FPIS) and fuzzy negative-ideal solution (FNIS).

The positive triangular fuzzy numbers fall within the range of [0,1]. Hence, the fuzzy positive ideal reference point (FPIS, A^+) and the fuzzy negative ideal reference point (FNIS, A^-) can be described as:

$$A^+ = (\tilde{v}_1^+, \tilde{v}_2^+, \dots, \tilde{v}_n^+) \tag{3-88}$$

$$A^- = (\tilde{v}_1^-, \tilde{v}_2^-, \dots, \tilde{v}_n^-) \tag{3-89}$$

where $\tilde{v}_1^+ = (1, 1, 1)$ and $\tilde{v}_1^- = (0, 0, 0), j = 1, 2, \dots, n$.

Stage 6: Determine the distance between each alternative and the FPIS and FNIS.

$$d_i^+ = \sum_{j=1}^{n} d(\tilde{v}_{ij}, \tilde{v}_j^+), i = 1, 2, \dots, m; j = 1, 2, \dots, n \tag{3-90}$$

$$d_i^- = \sum_{j=1}^{n} d(\tilde{v}_{ij}, \tilde{v}_j^-), i = 1, 2, \dots, m; j = 1, 2, \dots, n \tag{3-91}$$

where d_i^+ and d_i^- indicate the distance between alternative i and FPIS and FNIS, respectively.

Stage 7: Obtain the closeness coefficient and sort the order of alternatives.

$$CC_i = \frac{d_i^-}{d_i^+ + d_i^-}, i = 1, 2, \dots, m \tag{3-92}$$

The alternative with the greatest closeness coefficient is considered the best one.

3.3.5 Fuzzy evaluation based on distance from average solution method

Stage 1: Calculate the criteria's weights.

Stage 2: Create the fuzzy matrix.

$$\begin{aligned} &\widetilde{D} = [\tilde{x}_{ij}]_{m\times n}, i = 1, 2, \dots, m; j = 1, 2, \dots, n \\ &\tilde{x}_{ij} = \frac{1}{k}\sum_{p=1}^{k} \tilde{x}_{ij}^p, p = 1, 2, \dots, k \end{aligned} \tag{3-93}$$

where $\tilde{x}_{ij}^p$ represents the evaluation made by expert p for alternative A_i concerning criterion C_j.

Stage 3: Construct the fuzzy matrix of average solutions.

$$AV = [\widetilde{av}_j]_{1\times n}, i = 1, 2, \dots, m; j = 1, 2, \dots, n \tag{3-94}$$

$$\widetilde{av}_j = \frac{1}{m}\sum_{i=1}^{m} \tilde{x}_{ij} \tag{3-95}$$

Stage 4: B and N are the sets of beneficial and non-beneficial criteria, respectively. The matrices of positive (PDA) and negative (NDA) distances from average solutions are computed as follows:

$$PDA = [p\check{d}a_{ij}]_{m\times n} \tag{3-96}$$

$$NDA = [n\check{d}a_{ij}]_{m\times n} \tag{3-97}$$

$$p\check{d}a_{ij} = \begin{cases} \dfrac{\psi(\tilde{x}_{ij}\theta\widetilde{av}_j)}{k(\widetilde{av}_j)} & if \quad j\epsilon B \\ \dfrac{\psi(\widetilde{av}_j\theta\tilde{x}_{ij})}{k(\widetilde{av}_j)} & if \quad j\epsilon N \end{cases} \tag{3-98}$$

$$n\check{d}a_{ij} = \begin{cases} \dfrac{\psi(\widetilde{av}_j\theta\tilde{x}_{ij})}{k(\widetilde{av}_j)} & if \quad j\epsilon B \\ \dfrac{\psi(\tilde{x}_{ij}\theta\widetilde{av}_j)}{k(\widetilde{av}_j)} & if \quad j\epsilon N \end{cases} \tag{3-99}$$

where $\tilde{pda}_{ij}$ and $\tilde{nda}_{ij}$ indicate the distances between the performance value of alternative i and the average solution, in a positive or negative sense respectively, concerning criterion j.

Stage 5: Determine the total of positive and negative weighted distances for each alternative.

$$\tilde{sp}_i = \sum_{j=1}^{n} (\tilde{w}_j \otimes \tilde{pda}_{ij}) \tag{3-100}$$

$$\tilde{sn}_i = \sum_{j=1}^{n} (\tilde{w}_j \otimes \tilde{nda}_{ij}) \tag{3-101}$$

where $\tilde{w}_j$ refers to the weight assigned to criterion j.

Stage 6: Normalize the values of $\tilde{sp}_i$ and $\tilde{sn}_i$ for all alternatives.

$$\tilde{nsp}_i = \frac{\tilde{sp}_i}{max_i\,(k(\tilde{sp}_i))} \tag{3-102}$$

$$\tilde{nsn}_i = 1 - \frac{\tilde{sn}_i}{max_i\,(k(\tilde{sn}_i))} \tag{3-103}$$

Stage 7: Compute the appraisal score $\tilde{as}_i$ for all alternatives and rank them.

$$\tilde{as}_i = \frac{1}{2}\,(\tilde{nsp}_i \oplus \tilde{nsn}_i) \tag{3-104}$$

The alternative with the greatest appraisal score is considered the best one.

3.4 Model formulation for mixed-fleet bus scheduling

In this section, we focus on the formulation and examination of two versions of the MFBS problem: a simpler version for initial analysis and a more advanced model.

- **Simple MFBS version:**

We begin with the formulation of a simpler MFBS problem (see Fig. 3-7), serving as a foundation to comprehend and address the inherent complexities of this combinatorial problem, even in its basic form—a problem known to be strongly NP-Hard. In this version (which has been published in Sadrani et al., 2022a), we formulate a MINLP model to optimize dispatching schemes (dispatching orders and times) when a fixed number of buses of different sizes are available to serve demand along a route. We focus on minimizing the average passenger waiting time, with stochastic travel times between stops and vehicle capacity constraints (i.e., introducing extra waiting time due to denied boarding). We also develop an exact decomposition-based method and a SA metaheuristic algorithm to solve it.

- **Advanced MFBS version:**

Then, to take a step further to achieve a more comprehensive MFBS model, we consider a broader set of real-world operational elements and decision variables in the MFBS formulation (including in-vehicle trip times, users' trip comfort, resource constraints, and operator costs). Hence, our advanced version of the MFBS problem goes beyond optimizing vehicle dispatching plans and also addresses the optimization of vehicle assignment programs, enabling efficient resource utilization (the optimal determination of the number and type of vehicles needed for mixed-fleet deployments) (see Figs. 3-7 and 3-8, where the additional components introduced in the advanced MFBS model, compared to the simple version, are highlighted in red for clarity).

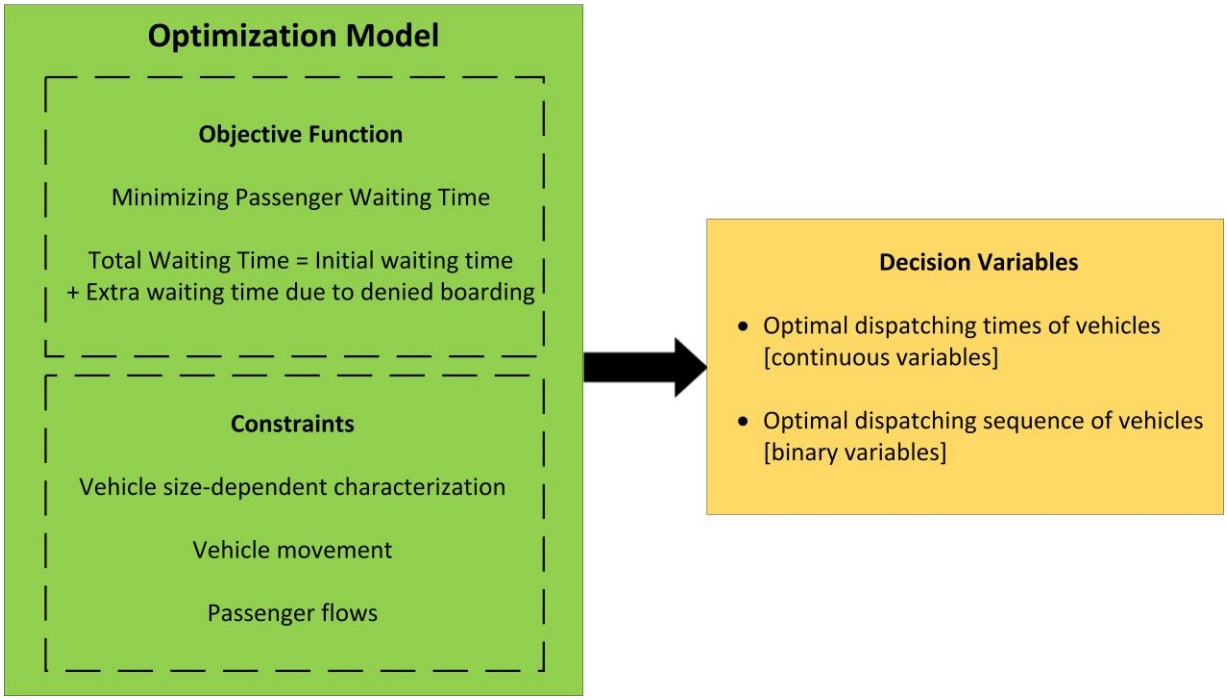

Figure 3-7 Overview of the simple optimization model framework in the proposed MFBS problem.

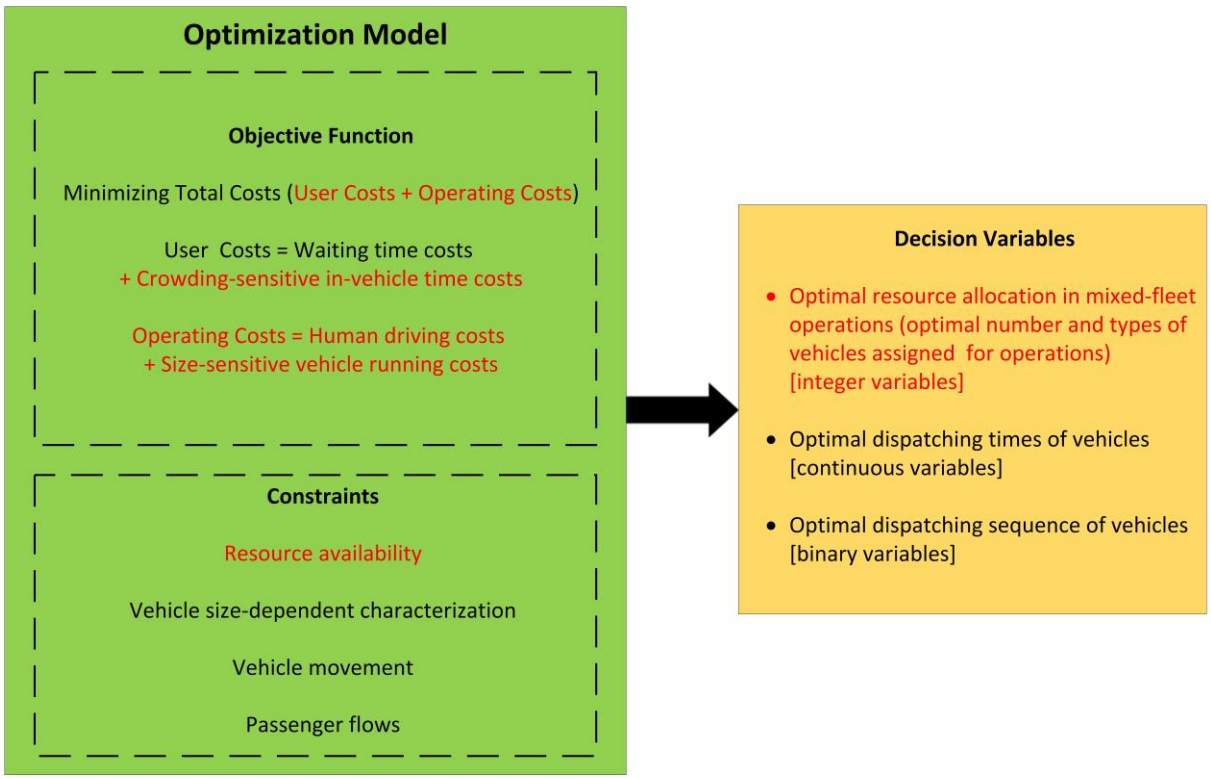

Figure 3-8 Overview of the advanced optimization model framework in the proposed MFBS problem.

3.4.1 Model formulation for the simple version of the mixed-fleet bus scheduling problem

In this section, we formulate a detailed objective function that is accurately able to compute passenger waiting times even in the case of failing to board due to a lack of capacity (extra waiting time due to denied boarding). Moreover, several different constraints that need to be considered in real-world urban bus operations are formulated, such as passenger flow constraints, vehicle movement constraints, resource availability constraints, and vehicle capacity constraints in the presence of different sizes of buses which can provide services with different capacities during a mixed-fleet operation (see Fig. 3-7). The notation used in the model formulation is listed in Table 3-1.

3.4.1.1 Model assumptions for the simple version of the mixed-fleet bus scheduling problem

Before presenting the model, the main assumptions and aspects considered in the mathematical formulation of a mixed-fleet operation are summarized as follows:

- We focus on high-frequency bus services, and thus headways are so short that passengers do not need to plan for arriving at stops.
- There exists a given mixed fleet composed of three different bus sizes: 12-meter (standard) bus with a capacity of 70 passengers and 2 doors, 15-meter (rigid) bus with a capacity of 90 passengers and 3 doors, and 18-meter (articulated) bus with a capacity of 120 passengers and 4 doors (see Fig. 3-9).
- We focus on the operational planning level, and we assume that the fleet size (the number and type of vehicles) is already determined at the tactical planning level.
- The number of buses of each size is given, i.e., for a certain bus size, the number of associated available vehicles is already given. As an illustrative example, suppose a given mixed fleet: {12, 12, 12, 12, 12, 15, 15, 15, 18, 18}, in which the resource limitations on buses of each size are known, which are at 5, 3, and 2 for 12-, 15-, and 18-m long buses respectively.
- We consider bus operations during a predefined planning horizon on a general bi-directional bus corridor.
- We assume that the first and last buses are dispatched at certain times, which are the beginning and end of the planning horizon for the sake of simplicity.
- We model varying dwell times, which can vary depending on the bus type (i.e., the number of bus doors, see Fig. 3-9) and on the number of passengers alighting and boarding at each stop.

- We assume that vehicles are not permitted to overtake each other.
- We assume that travel times of vehicles between stops are stochastic, drawn from a log-normal distribution.
- We explicitly model vehicle capacity constraints, and therefore:
  - ✓ (a) the number of passengers who can successfully board a vehicle at a stop cannot exceed the remaining capacity inside the vehicle at that stop;
  - ✓ (b) in the case of failing to board due to capacity constraints for any number of times, the model is able to continue computing the actual waiting time of passengers (even if some passengers are being left behind by two or more successive services due to an oversaturated condition) until they successfully board a bus service with enough room, i.e., introducing extra waiting times for passengers left behind due to a lack of capacity, who have to wait for the next coming vehicle(s);
  - ✓ (c) if there is not enough capacity inside a bus to carry all the passengers waiting for it at a stop, we assume that all the waiting passengers, irrespective of their destinations, have the same chance to board.

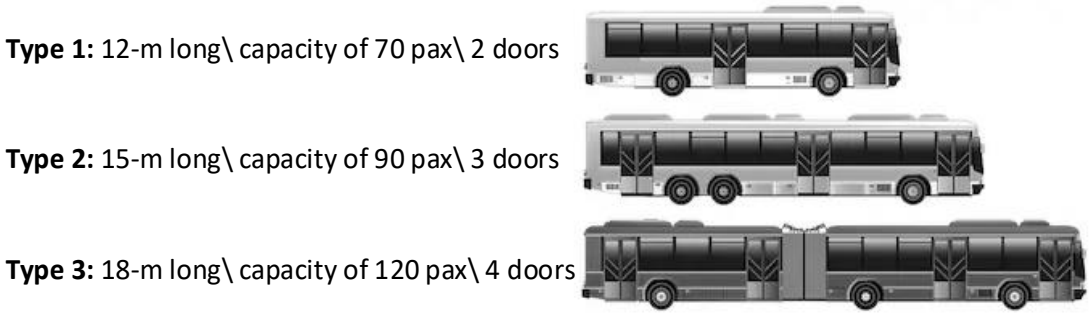

Figure 3-9 Three different available bus types used for mixed-fleet operations in this work.

3.4.1.2 Optimization model for the simple version of the mixed-fleet bus scheduling problem

The mixed-fleet vehicle dispatching problem is formulated as follows:

$$\underset{x_{mi},T^d_{i,1}}{Min} \quad \text{AWT}=\frac{1}{P}\cdot\sum_{i\in V,i\geq 2}\sum_{j\in S}\sum_{k\in S,k>j}\left(\underbrace{\lambda_j\left[T^d_{i-1,j}\right].OD_{j,k}\left[T^d_{i-1,j}\right].H_{i,j}\cdot\frac{H_{i,j}}{2}}_{\text{(i)}}+\underbrace{N^f_{i-1,j,k}\cdot H_{i,j}}_{\text{(ii)}}\right) \tag{3-105}$$

Subject to:

$$\sum_{m\in M}x_{mi}=1 \qquad \forall i\in V \tag{3-106}$$

$$C_i=\sum_{m\in M}x_{mi}c_m \qquad \forall i\in V \tag{3-107}$$

$$\sum_{i\in V}x_{mi}=B_m \qquad \forall m\in M \tag{3-108}$$

$$H_{i,j}=T^d_{i,j}-T^d_{i-1,j} \qquad \forall i\in V-\{1\},\forall j\in S \tag{3-109}$$

$$T^a_{i,j}=T^d_{i,j-1}+\delta_a+T^r_{i,j}+\delta_d \qquad \forall i\in V,\forall j\in S-\{1\} \tag{3-110}$$

$$T^r_{i,j}\sim \text{lognormal}\,(r_j,\sigma_j) \qquad \forall i\in V,\forall j\in S-\{1\} \tag{3-111}$$

$$T^d_{i,j}=T^a_{i,j}+T^s_{i,j} \qquad \forall i\in V,\forall j\in S-\{1\} \tag{3-112}$$

$$h_{\min}\leq T^d_{i,1}-T^d_{i-1,1}\leq h_{\max} \qquad \forall i\in V-\{1\} \tag{3-113}$$

$$T^s_{i,j}=\tau+P^a_i\alpha_a N^a_{i,j}+P^b_i\alpha_b N^b_{i,j} \qquad \forall i\in V,\forall j\in S \tag{3-114}$$

$$N^w_{i,j,k}=\lambda_j\left[T^d_{i-1,j}\right].OD_{j,k}\left[T^d_{i-1,j}\right].(\overbrace{T^d_{i,j}-T^d_{i-1,j}}^{H_{i,j}})+N^f_{i-1,j,k} \qquad \forall i\in V-\{1\},\forall j,k\in S,j<k \tag{3-115}$$

$$N^w_{i,j}=\sum_{k\in S,k>j}N^w_{i,j,k} \qquad \forall i\in V,\forall j\in S \tag{3-116}$$

$$N^{on}_{i,j}=N^{on}_{i,j-1}-N^a_{i,j-1}+N^b_{i,j-1} \qquad \forall i\in V,\forall j\in S-\{1\} \tag{3-117}$$

$$N_{i,j}^{b} = \min\left\{N_{i,j}^{w}, C_i - N_{i,j}^{on} + N_{i,j}^{a}\right\} \qquad \forall i \in V, \forall j \in S \tag{3-118}$$

$$N_{i,j}^{a} = \sum_{j' \in S, j' < j} N_{i,j',j}^{s} \qquad \forall i \in V, \forall j \in S - \{1\} \tag{3-119}$$

$$N_{i,j,k}^{s} = \frac{N_{i,j}^{b}}{N_{i,j}^{w}} N_{i,j,k}^{w} \qquad \forall i \in V, \forall j,k \in S, j < k \tag{3-120}$$

$$N_{i,j,k}^{f} = N_{i,j,k}^{w} - N_{i,j,k}^{s} \qquad \forall i \in V, \forall j,k \in S, j < k \tag{3-121}$$

$$T_{i,1}^{d} \geq 0 \qquad \forall i \in V \tag{3-122}$$

$$x_{mi} \in \{0,1\} \qquad \forall m \in M, \forall i \in V \tag{3-123}$$

As can be seen in expression (3-105), the objective of the problem is to minimize the Average Waiting Time (AWT), obtained through dividing the total waiting time by the total demand P (P is a fixed value during the entire analysis period). The total waiting time is composed of two parts: (i) waiting time for new passengers arriving at stops over the headway, and (ii) extra waiting time for passengers who were unable to board the preceding vehicle due to a lack of capacity, who have to wait for the next vehicle(s). Indeed, the total waiting time is derived from expression (3-115), in which the number of waiting passengers in both groups is computed (i.e., (i) the group of new arriving passengers, and (ii) the group of left-behind passengers). In high-frequency bus systems, headways are so short that passengers do not need to plan their arrival at stops, i.e., they arrive randomly at stops over the headway. Hence, for passengers in the group (i), the waiting time is averagely estimated as half of the headway ($H_{i,j}/2$), which is a well-known estimation in the literature of high-frequency bus services due to the random and unplanned arrival of passengers at stops (e.g., Furth and Wilson, 1981; Wu et al., 2017; Gkiotsalitis and Cats, 2018; Dai et al., 2020). On the other hand, for passengers in the group (ii) who were unable to board the previous service due to overcrowding, the extra waiting time is equal to the whole headway ($H_{i,j}$) because they have to wait for the next bus service. As a result, if a considerable number of passengers are left behind due to capacity constraints, passengers' total waiting time can climb dramatically, thereby declining the

attractiveness of a public transport system substantially. Note that the formulation of $N_{i,j,k}^{f}$ in Eq. (3-121) enables us to compute the actual number of passengers being left behind by each vehicle. Accordingly, even if some passengers are left behind by two or more consecutive services due to an oversaturated condition (denied boarding for several cycles), the model is able to count them among the group of left-behind passengers ($N_{i,j,k}^{f}$). Hence, we can still correctly calculate their waiting times until they successfully board a service.

As can be seen in expression (3-105), dispatching headways of vehicles can directly affect the waiting times of passengers in both groups (i) and (ii). Moreover, we attempt to investigate how a proper decision on vehicle dispatching order with the consideration of time-dependent demand volumes can lead to a better utilization of vehicles' capacity, thereby reducing the number of passengers being left behind in group (ii) who need to wait for next arriving vehicle(s) (i.e., preventing denied boarding problems from further exacerbation). Hence, regarding the decision variables considered in the proposed mixed-fleet dispatching problem, we seek to find the optimal dispatching schemes, including the optimal dispatching order of vehicles[14] (x_{mi}) and also the optimal dispatching times of vehicles from the original stop ($T_{i,1}^{d}$).

In light of the fact that bus operators can provide services with different capacities during a mixed-fleet operation depending on the dispatching order of each vehicle, expression (3-106) represents the size of vehicle allocated to i-th bus service. As can be seen in expression (3-107), the passenger-carrying capacity of bus service i depends on its size, e.g., the maximum number of passengers accommodated by a 12-m long bus is $c_1 = 70$ (pax). As explained in the model assumptions, we assume that there exists a given mixed fleet with buses of different sizes and the number of buses of each size is already given. Constraint (3-108) expresses resource limitations on the number of buses of each size for the three different bus sizes involved in our mixed-fleet operations. This constraint can make the problem more complicated, due to the combinatorial nature of the problem in terms of dispatching sequences. In essence, given the existence of a discrete set of dispatching sequences, which can be practically prescribed for buses in our mixed-fleet operation, constraint (3-108) turns the

[14] Three different bus types are available in our mixed-fleet operations (see Fig. 3-9): type 1 is a 12-m long bus; type 2 is a 15-m long bus, and type 3 is an 18-m long bus, hence:
Binary variable x_{1i} would be 1 if a 12-m vehicle is allocated to i^{th} bus service, otherwise 0;
Binary variable x_{2i} would be 1 if a 15-m vehicle is allocated to i^{th} bus service, otherwise 0;
Binary variable x_{3i} would be 1 if an 18-m vehicle is allocated to i^{th} bus service, otherwise 0.

proposed problem into a permutation-based combinatorial optimization problem (permutations with repetition due to the presence of several analogous buses in the given fleet).

Vehicle movement constraints that need to be considered in real-world urban bus operations are given in (3-109)-(3-114). Headway between two consecutive buses $i-1$ and i at stop j is calculated by (3-109). As can be seen in expression (3-110), the arrival time of bus i at stop j depends on four different time components: (1) the departure time of bus i from stop $j-1$, (2) the time required to accelerate from zero to cruise speed when bus i leaves stop $j-1$, (3) the running time between two adjacent bus stops $j-1$ and j, and (4) the time required to decelerate from cruise speed to zero when bus i wants to enter stop j.

In real-world operations, a broad range of external factors can affect bus running times, such as traffic conditions, traffic signals, bus drivers' behavior, weather, and so on (Wang and Haghani, 2020). Hence, buses might experience different running times between two adjacent stops $j-1$ and j. As can be seen in expression (3-111), to reflect realistic operating conditions, we assume that running times between stops are stochastic, drawn from a log-normal distribution with mean and standard deviation of r_j and σ_j respectively. As it is clear from (3-112), bus i leaves stop j after the completion of alighting and boarding processes (i.e., dwell time) at that stop.

The departure times of buses from the first stop ($T_{i,1}^{d}$) are considered as decision variables in this dissertation. Indeed, buses can leave the first stop with varying dispatching headways during a predefined planning horizon denoted as $[T_1, T_2]$. Nevertheless, the dispatching headways are confined to the range of $[h_{\min}, h_{\max}]$ defined by policies [see constraint (3-113)]. Since this research focuses on high-frequency bus services, the upper bound is considered to be 12 minutes. The lower bound is also set to be 2 minutes in order to mitigate the bus bunching[15] phenomenon. Moreover, for the sake of problem simplicity, it is assumed that the first and last buses are dispatched at the beginning and end of the planning horizon respectively (i.e., $T_{1,1}^{d} = T_1$ and $T_{N_v,1}^{d} = T_2$).

As can be seen in expression (3-114), the dwell time of bus i at stop j depends on the number of passengers alighting and boarding at that stop through the busiest bus door, plus the fixed time spent opening and closing bus doors. With regard to the boarding and alighting policy, we assume that passengers use the same doors for alighting and boarding, however, the

[15] Bus bunching phenomenon will happen when two or more buses on the same route arrive simultaneously at the same stop.

alighting process has priority over the boarding process (i.e., sequential boarding and alighting, in which boarding process is started after finishing the alighting process). Accordingly, the total dwell time at a stop will depend on the sum of the passengers' boarding and alighting times (Tirachini et al., 2014). Parameters α_a and α_b are the average alighting and boarding times per passenger respectively and depend on fare collection technology, bus floor height, platform layout, and so on. Moreover, parameters P_i^a and P_i^b represent respectively the proportions of passengers alighting and boarding through the busiest door of bus i and are dependent on the number of bus doors. For example, in the case of sequential boarding and alighting at all doors, the more doors a bus has the faster boarding and alighting is (Tirachini et al., 2014). In this research, we consider a heterogeneous bus fleet composed of three different bus sizes: 12-m long bus with 2 doors, 15-m long bus with 3 doors, and 18-m long bus with 4 doors (see Fig. 3-9).

In the following, passenger flow constraints given by (3-115)-(3-121) are described. Under time-dependent passenger demand, the actual number of passengers with trip $j \rightarrow k$ waiting for bus i at stop j ($N_{i,j,k}^w$) is essentially derived from the sum of two different groups of passengers (i.e., $N_{i,j,k}^w = \underbrace{\int_{T_{i-1,j}^d}^{T_{i,j}^d} \lambda_j[t].OD_{j,k}[t].dt}_{\text{(i)}} + \underbrace{N_{i-1,j,k}^f}_{\text{(ii)}}$). The first group includes new passengers reaching their origin stops during the headway, whereas the second group includes those passengers who were unable to board the previous bus due to a dearth of capacity.

Since we are working with high-frequency bus systems, the headway (the time interval between the departures of two successive buses from one station, $H_{i,j} = T_{i,j}^d - T_{i-1,j}^d$) is a short enough time interval, during which the destination distribution vector and the passenger arrival rate $\lambda_j[t]$ do not fluctuate notably (Gao et al., 2016). Accordingly, following Gao et al. 2016, we assume that these parameters remain constant during the headway (from the departure time of vehicle $i-1$ to the departure time of vehicle i), and are equal to $OD_{j,k}[T_{i-1,j}^d]$ and $\lambda_j[T_{i-1,j}^d]$. Therefore, the proposed integral form in the case of group (i) can be approximately rewritten, as presented in Eq. (3-115).

According to the definitions of $N_{i,j,k}^w$ and $N_{i,j}^w$, expression (3-116) always holds. Indeed, the total number of passengers waiting for bus i at stop j is obtained through summing up across all the waiting passengers at origin stop j with different destinations ($k > j$). As can be seen in expression (3-117), the number of passengers traveling inside bus i between

stops $j-1$ and j, $N_{i,j}^{on}$, is composed of those passengers remaining on bus i from the former segment ($j-2 \rightarrow j-1$) as their destination was not stop $j-1$, i.e., ($N_{i,j-1}^{on} - N_{i,j-1}^{a}$), plus passengers boarding bus i at stop $j-1$, i.e., $N_{i,j-1}^{b}$. Note that buses are empty when they arrive at the first stop (i.e., $N_{i,1}^{on} = 0,\ \forall i \epsilon V$). Expression (3-118) indicates that the number of passengers who can successfully get on bus i at stop j cannot be larger than the remaining capacity inside bus i at that stop.

As indicated in (3-119), the number of passengers who alight bus i at stop j will include the passengers who boarded bus i at the prior stops with the intention of traveling to stop j. Note that there is no demand for alighting at the first stop (i.e., $N_{i,1}^{a} = 0, \forall i \epsilon V$). As discussed in the model assumptions, if there is not enough room on bus i to carry all the passengers waiting for it at stop j, we assume that all the passengers, regardless of their destinations, have the same chance to get on [see expression (3-120)]. The number of passengers with trip $j \rightarrow k$, who are unable to board bus i at stop j due to a lack of capacity is obtained by (3-121). Indeed, Eq. (3-121) can account for the actual number of passengers left behind by each vehicle at any stop. Accordingly, even if denied boarding occurs for several cycles for some passengers due to an overcrowded situation, the model is able to count them among the left-behind passengers and to calculate their extra waiting time until they successfully board an available service. Constraints (3-122) and (3-123) define the domain of decision variables.

3.4.2 Model formulation for the advanced version of the mixed-fleet bus scheduling problem

In this section, we design and present an advanced mathematical model for the MFBS problem. The simpler model in Sadrani et al. (2022a) has some limitations that need to be addressed for a more comprehensive understanding of mixed-fleet bus dispatching. First, Sadrani et al. (2022a) focused solely on minimizing passengers' waiting times, overlooking other important factors such as users' in-vehicle time, trip comfort, and operator costs. Second, their model assumed a fixed number of vehicles, disregarding the optimization of resource allocation programs that determine the optimal number and type of vehicles required for mixed-fleet operations[16]. This limitation hampers the ability to optimize fleet size and composition, limiting the adaptability of the dispatching system to varying resource constraints and demand conditions. Third, their study only utilized the SA algorithm as a solution approach, without exploring if other advanced algorithms find better dispatching plans in terms of quality of service and/or operator costs. Given the combinatorial complexity of the MFBS problem, it is crucial to evaluate the performance of various algorithms to ensure robustness and effectiveness. Particularly, our research findings highlight the significance of utilizing more advanced algorithms to tackle the challenges of vehicle assignment in crowded scenarios requiring larger fleet sizes.

To bridge these gaps, a novel MFBS problem is proposed that considers more realistic components, including in-vehicle trip times, users' trip comfort, resource constraints, and operator costs (see Fig. 3-8). This programming model goes beyond optimizing vehicle dispatching plans and also addresses the optimization of vehicle assignment programs, enabling efficient resource utilization (the optimal determination of the number and type of vehicles needed for mixed-fleet deployments). To tackle the complexity of the MFBS problem (as a combinatorial optimization problem) and ensure practical viability, we employed two well-established metaheuristics: Genetic Algorithm (GA) and Grey Wolf Optimizer (GWO). We also developed two hybrid metaheuristic algorithms, GA-SA (a combination of GA and SA) and GWO-SA (a combination of GWO and SA), demonstrating promising performance in

[16] In essence, the absence of operator cost modeling and resource constraints in the study of Sadrani et al. (2022a) prevented the optimization of fleet size, fleet composition, and quantities for efficient operations. Specifically, in a mixed operating system, the running costs of vehicles are influenced by their size, with larger buses (e.g., 18-m long) incurring higher costs compared to smaller ones (e.g., 12-m long). However, larger buses offer the benefit of reducing passenger inconvenience caused by crowding. Thus, achieving the optimal fleet size and composition requires a comprehensive cost analysis encompassing both user (demand) and operator (supply) aspects.

improving solution quality and optimization capabilities. A Taguchi approach was utilized to calibrate the parameters of these metaheuristics, ensuring their robustness in solving the MFBS problem.

3.4.2.1 Model assumptions for the advanced version of the mixed-fleet bus scheduling problem

Here, we outline the main assumptions and modeling attributes used to formulate the advanced MFBS problem:

- The entrance of commuters at stations is assumed as random.
- There is sufficient capacity available to cover the total passenger demand, which is a pervasive assumption in the stage of operational planning (Vuchic, 2017; Gkiotsalitis and Alesiani, 2019; Gkiotsalitis, 2020a; Sadrani et al., 2022a).
- The maximum resource constraints for each vehicle type are specified by service providers based on depot inventories.
- We consider the scheduling of vehicles within a designated planning (simulation) period for a two-direction bus line.
- We distinguish between passengers' time valuations when waiting at stations and when riding inside vehicles.
- We distinguish between standing and sitting passengers' perceptions of crowding disutility (discomfort).

3.4.2.2 Optimization model for the advanced version of the mixed-fleet bus scheduling problem

The MFBS problem is formulated as follows:

$$\begin{aligned} Min\ Z = & \sum_{i\in V}\sum_{j\in S} \varphi^{w1} N_{i,j}^{w} \frac{T_{i,j}^{h}}{2} + \sum_{i\in V}\sum_{j\in S} \varphi^{v} T_{i,j}^{n} \left(\pi_{i,j}^{sit} N_{i,j}^{sit} + \pi_{i,j}^{\text{stand}} N_{i,j}^{\text{stand}}\right) \\ & + \sum_{i\in V}\sum_{j\in S} \varphi^{d} \left(T_{i,j}^{n} + T_{i,j}^{w}\right) + \sum_{i\in V}\sum_{j\in S} \varphi_{i}^{u} \left(T_{i,j}^{n} + T_{i,j}^{w}\right) \end{aligned} \tag{3-124}$$

Subject to:

$$\sum_{m \in M} x_{mi} = 1 \qquad \forall i \in V \tag{3-125}$$

$$\sum_{i \in V} x_{mi} = B_m \qquad \forall m \in M \tag{3-126}$$

$$C_i = \sum_{m \in M} x_{mi}\, c_m \qquad \forall i \in V \tag{3-127}$$

$$A_i^{\text{stand}} = \sum_{m \in M} x_{mi}\, a_m \qquad \forall i \in V \tag{3-128}$$

$$\varphi_i^u = \sum_{m \in M} x_{mi}\, \varphi_m^u \qquad \forall i \in V \tag{3-129}$$

$$h_{\min} \le T_{i,1}^d - T_{i-1,1}^d \le h_{\max} \qquad \forall i \in V - \{1\} \tag{3-130}$$

$$T_{i,j}^a = T_{i,j-1}^d + T_{i,j}^n \qquad \forall i \in V,\ j \in S - \{1\} \tag{3-131}$$

$$T_{i,j}^d = T_{i,j}^a + T_{i,j}^w \qquad \forall i \in V,\ j \in S - \{1\} \tag{3-132}$$

$$T_{i,j}^w = \tau + N_{i,j}^a\, \alpha_a + N_{i,j}^b\, \alpha_b \qquad \forall i \in V,\ j \in S \tag{3-133}$$

$$T_{i,j}^h = T_{i,j}^d - T_{i-1,j}^d \qquad \forall i \in V - \{1\},\ j \in S \tag{3-134}$$

$$N_{i,j,k}^w = \int_{T_{i-1,j}^d}^{T_{i,j}^d} \lambda_j[t].\, OD_{j,k}[t].\, dt \qquad \forall i \in V,\ j,k \in S \ \&\ k > j \tag{3-135}$$

$$N_{i,j}^w = \sum_{k \in S,\, k > j} N_{i,j,k}^w \qquad \forall i \in V,\ j \in S \tag{3-136}$$

$$N_{i,j}^v = C_i - N_{i,j}^{on} + N_{i,j}^a \qquad \forall i \in V,\ j \in S \tag{3-137}$$

$$N_{i,j}^b = N_{i,j}^w \le N_{i,j}^v \qquad \forall i \in V,\ j \in S \tag{3-138}$$

$$N_{i,j}^a = \sum_{\ell \in S,\, \ell < j} N_{i,\ell,j}^w \qquad \forall i \in V,\ j \in S \tag{3-139}$$

$$N_{i,j}^{on} = N_{i,j-1}^{on} - N_{i,j-1}^{a} + N_{i,j-1}^{b} \qquad \forall i \in V,\ j \in S \tag{3-140}$$

$$N_{i,j}^{sit} = \min\left\{N_{i,j}^{on}, G_i^{sit}\right\} \qquad \forall i \in V,\ j \in S \tag{3-141}$$

$$N_{i,j}^{\text{stand}} = \max\left\{N_{i,j}^{on} - G_i^{sit}, 0\right\} \qquad \forall i \in V,\ j \in S \tag{3-142}$$

$$D_{i,j}^{\text{stand}} = \frac{N_{r,j}^{\text{stand}}}{A_i^{\text{stand}}} \qquad \forall i \in V,\ j \in S \tag{3-143}$$

$$\pi_{i,j}^{sit}, \pi_{i,j}^{\text{stand}} = f(D_{i,j}^{\text{stand}}) \qquad \forall i \in V,\ j \in S \tag{3-144}$$

$$B_m \in \mathbb{Z},\ 0 \le B_m \le U_m \qquad \forall m \in M \tag{3-145}$$

$$T_{i,1}^{d} \ge 0 \qquad \forall i \in V \tag{3-146}$$

$$x_{mi} \in \{0,1\} \qquad \forall i \in V, m \in M \tag{3-147}$$

Our objective function is defined for the minimization of total costs, consisting of user costs and operating costs, as presented in Eq. (3-124). User costs are introduced in the first and second terms, which respectively reflect waiting time costs and crowding-sensitive in-vehicle time costs (as sensitive to on-board comfort levels for users). Operating costs are introduced in the third and fourth terms, which respectively represent human driver costs and size-sensitive vehicle running costs. Next, we discuss the functional form of the cost terms and problem constraints.

Commuters' waiting times are estimated in the first term of (3-124), formulated based on the random entering of commuters at stations. In this situation, the average waiting time is approximated as half of the headway (Dakic et al., 2021; Gkiotsalitis and Cats, 2018; Sadrani et al., 2022b, 2022a). Besides, parameter φ^{w1} is the value of waiting time savings, used to translate time values into cost values.

The second term calculates users' in-vehicle time costs, while accounting for users' trip comfort. It has been revealed that standing travelers are more impacted by the inconvenience of crowding than sitting travelers (Wardman and Whelan, 2011; Tirachini et al., 2017). Thus, we discern between standing and sitting passengers' perceptions of crowding discomfort by

means of crowding multipliers defined separately for standing and sitting cases (see Table 3-7). As a noteworthy aspect of our model, a microscopic tracking of alighting and boarding volumes at each station enables us to update the occupancy level of each service at each part of a route. This precise framework allows us to evaluate the impacts of crowding on passengers' comfort during their trips.

The third term accounts for human driving costs. The number of driving hours determines the drivers' earnings, regardless of the vehicle type being driven. By contrast, the fourth term calculates vehicle running costs (e.g., energy and upkeep expenses) depending on the size of each service (size-sensitive running costs) as operating larger vehicles (such as 18-m long buses) is more expensive than operating smaller ones (12-m long buses). However, larger vehicles offer the advantage of reducing passenger inconvenience caused by crowding. This aspect becomes crucial in optimizing vehicle assignment plans because, in addition to operators' costs, users' costs (such as waiting times and crowding costs) have a significant impact on supply decisions in public transport services when minimizing a total cost function (Mohring, 1972; Jara-Díaz and Gschwender, 2003; Tirachini et al., 2014). The proposed MFBS problem, containing a detailed definition of both user and operating costs, enables us to identify the most effective vehicle assignment solutions that produce a beneficial equilibrium between demand and supply.

In the following, we explain the model's constraints, presented in four categories: (i) vehicle assignment [Eqs. (3-125) and (3-126)], (ii) vehicle size-dependent characterization [Eqs. (3-127)-(3-129)], (iii) vehicle movement planning [Eqs. (3-130)-(3-134)], and (iv) user trip flows [Eqs. (3-135)-(3-144)].

In Eq. (3-125), we determine the vehicle type assigned to each bus service (i.e., to each vehicle dispatching). For example, suppose there are three different vehicle types (A, B, and C), if the 5th bus service is carried out by means of a type-A vehicle, then x_{A5} equals 1 (in this case, Eq. (3-125) will hold as $\underbrace{x_{A5}}_{1} + \underbrace{x_{B5}}_{0} + \underbrace{x_{C5}}_{0} = 1$). Eq. (3-126) indicates the number of vehicles of each type assigned for operations.

Eqs. (3-127)-(3-129) are specifically designed to handle size-sensitive parameters on a service-to-service resolution. This is crucial because the MFBS problem involves services with varying sizes, where size-sensitive attributes (such as on-board capacity) differ for each service based on its size characteristics. For instance, the capacity of service i (performed by means of a 12-m long vehicle) differs from that of service $i + 1$ (performed by means of an 18-m long

vehicle). Given the changing patterns of passenger flows over time and place, such modeling components allow for the introduction of best vehicle assignment and dispatching plans in the MFBS problem, resulting in a better adjustment of capacity to passenger demand.

Constraint (3-130) ensures that dispatching headways always remain within the permitted range established by policymakers. The dispatching times of services from the first terminal are defined as decision variables in our problem, allowing for the optimization of dispatching intervals between services according to temporal fluctuations in passenger requests. Besides, it is assumed that the dispatching of the first service is performed at the start of the planned period.

As presented in Eq. (3-131), to determine the entry time of a service at a station, the leaving time of that service from the earlier station would be added to the time spent riding between stations. Eq. (3-132) indicates that a service will leave a station after passengers' unloading and loading events at that station (dwelling time). As shown in Eq. (3-133), the dwell time is estimated in view of the time consumed for unloading and loading actions by passengers, as well as the time associated with the opening and closing of doors. In Eq. (3-134), the inter-departure headway is computed as the elapsed time between the leavings of two successive services from a designated station.

Considering time-varying arrival rates of travelers at stations, Eq. (3-135) computes the number of travelers (intending to carry out a journey from j to k by means of service i) who enter station j during the elapsed headway between service $i-1$ and service i. Given the notions of $N_{i,j,k}^{w}$ and $N_{i,j}^{w}$, Eq. (3-136) becomes apparent in our model, meaning that the aggregate of all travelers waiting at station j, whose journey destinations can differ from each other (journey from j to k, $k > j$), yields the total traveler volume waiting for service i at station j.

Eq. (3-137) updates the residual capacity inside each service, taking into account the passenger unloading process that occurs at each station. Constraint (3-138) ensures that the operational plans for service supply (including vehicle assignment and dispatching plans) are sufficient to satisfy passenger demands.

Eq. (3-139) calculates the unloading volume of travelers from service i at station j, considering the commuters who boarded service r at former stations in order to carry out a journey to station j. Considering passengers' unloading and loading events at each station, Eq. (3-140) is employed to update the passenger load (occupancy level) of each service in every

section of the route. Eqs. (3-141) and (3-142) are respectively used to compute the number of travelers sitting and standing inside service i during the journey between stations $j-1$ and j. Eq. (3-143) determines the density of standing passengers inside services, used as a proxy for representing the degree of crowding inside services (Tirachini et al., 2017). Accordingly, crowding multipliers for standing and sitting situations are determined as a function of the standing density, as stated in Eq. (3-144). In our dissertation, crowding multipliers are given in Table 3-7, taken from Tirachini et al. (2017). For instance, a multiplier of 1.93 means that, on average, travel time savings when standing with a density of 6 standees per square meter are valued almost doubled than travel time savings when sitting without any passenger standing. Ultimately, constraints (3-145)-(3-147) exhibit the scope of decision variables.

Table 3-7 Crowding multiplier values (source: Tirachini et al., 2017).

Standing density (pax/m^2)	Sitting multiplier	Standing multiplier
0	1.00	1.12
1	1.11	1.25
2	1.23	1.39
3	1.34	1.53
4	1.46	1.66
5	1.57	1.80
6	1.69	1.93

4 Solution algorithms

This chapter contains the solution algorithms developed to effectively address the computational complexities of the formulated models, encompassing various exact and metaheuristic approaches.

4.1 Solution approaches for automated bus planning

4.1.1 Full enumeration method

As discussed in the mathematical formulation, variables of service frequency and vehicle size, confined to the predetermined discrete sets of $\{f_{\min}, f_{\min}+1, \dots, f_{\max}-1, f_{\max}\}$ [veh/h] and {8,12,15,18} [meters] respectively, are considered as the decision variables in our model. As for vehicle sizes, our range goes from minibuses and standard 12-m long buses, to articulated 18-m long buses. Due to the combinatorial nature of the problem, there is a limited number of possible solutions that need to be evaluated in each scenario (with a full enumeration (exhaustive search) of the solution space) for exploring the whole solution space and finding the global optimal solution leading to the minimum total cost. For instance, for our experiments in Regensburg, $f_{\min}$ and $f_{\max}$ are set to be 5 and 40 respectively, i.e., the set of frequencies is regarded as {5, 6, 7, …, 38, 39, 40} [veh/h], containing a total of 36 elements. Thus, in the presence of 4 different bus sizes used as candidates, there are a total of 36×4=144 possible solutions for exploring the entire solution space using a Full Enumeration (FE) method. For the given bus route in Santiago, taken as the illustrative example of a corridor with a large volume of passengers [5764 pax/h], $f_{\min}$ and $f_{\max}$ are set to be 15 and 120 [veh/h] respectively. Hence, the total number of possible solutions that should be assessed would be 106×4=424.

It is worth noting that the FE method is a widely-used method in the relevant literature to solve bus scheduling design problems taking advantage of relatively small-scale instances in bus lines (e.g., Fu et al., 2003; Sun and Hickman, 2005; Gkiotsalitis and Cats, 2018; Gkiotsalitis, 2020b; Hatzenbühler et al., 2020; Sadrani et al., 2022a). Indeed, this exact method is able to return a globally optimal solution (within an acceptable time for relatively small instances), compared to metaheuristics that cannot guarantee the optimality of the solutions. In essence, the solution quality (e.g., finding the global optimal solution) is more important than the saving of computational time when solving such offline design problems (Lotfi et al., 2020; Sadrani et al., 2022a), where problems are generally solved once without a hard time pressure to prescribe medium or long-term decisions in the context of important financial investments

(Talbi, 2009; Sadrani et al., 2022a). That is, computational time saving is not the major issue for policymakers and practitioners in such design problems. Hence, if it is possible, the exact methods should be preferred rather than meta-heuristic algorithms that are not able to guarantee the global optimality.

To further describe the proposed FE method employed to solve our mathematical programming model in Eq. (3-2), the main steps of the FE method are described in Algorithm 4-1.

Algorithm 4-1 The main steps of the full enumeration method.

Step (1): Set the candidate values for vehicle size and frequency (as decision variables), which are respectively confined to the given discrete sets of {8,12,15,18} [meters] and $\{f_{\min}, f_{\min}+1, \dots, f_{\max}-1, f_{\max}\}$ [veh/h] in the proposed problem.

Step (2): In each deployment scenario, while vehicle size is fixed (for any given size) during the simulation time, set parameters **&** enumerate over all the frequency values to evaluate all the possible combinations of vehicle size and frequency (for a better view of this step, see Fig. 5-2), i.e., step (2) includes (2.1) **&** (2.2):

(2.1). Set input parameters. Note that the size-dependent parameters are set based on the vehicle size fixed.

(2.2). Evaluate the objective function value [in Eq. (3-1)] for each combination of vehicle size and frequency using Algorithm 4-2. In essence, to handle the uncertainty of stochastic travel times, each possible solution is evaluated over several replications through the Monte Carlo Simulation (MCS) method (see Algorithm 4-2 for more details).

Step (3): Return the best-found solution (among all the combinations of vehicle size and frequency) leading to the minimum total cost value.

4.1.2 Monte Carlo Simulation method

To manage travel time stochasticity in Stochastic travel times scenarios, we utilize a Monte Carlo Simulation (MCS) approach, allowing for the evaluation of each possible solution within multiple repetitions (Liu et al., 2013; Wu et al., 2017; Mou et al., 2020; Zhang et al., 2020; Gkiotsalitis and Van Berkum, 2020b; Sadrani et al., 2022a). In essence, the MCS is activated in the form of a subroutine in the proposed FE algorithm. That is, whenever the FE algorithm needs to do an evaluation process, this task is undertaken by the MCS method. In Algorithm 4-2, we describe the steps of the MCS method. The number of MCS runs is set to be 1000 in our research.

Algorithm 4-2 The main steps of the MCS method.

(i) **Set the MCS parameters:** Set the counter of simulations m and its initial value as 1; let $\bar{Z}^{(m)}$ denote the estimated objective function value in Eq. (3-1); set the maximum number of simulations as $M_{max} = 1000$.

(ii) **Perform travel time sampling:** The bus travel time between each two consecutive stops is a random variable with predetermined mean and standard deviation values. For each bus service, sample the travel time between stops $j-1$ and j (i.e., $T_{i,j}^{r}$) through Eq. (3-16) based on its log-normal distribution, where $i = 1, 2, \dots, N_v$ and $j = 2, 3, \dots, N_s$.

(iii) **Compute the variables:** Based on the sampled travel time value, update the relevant variables in the solution using Eqs. (3-13)–(3-32), including bus motion and passenger flow calculations: bus travel time, headways, dwell time, arrival/departure time at each stop, the number of passengers waiting, alighting and successfully boarding the vehicle, failing to board, sitting and standing inside the vehicle.

(iv) **Compute the objective function value:** Based on Eq. (3-1), compute and update the objective value $Z^{(m)}$, and the final output of objective value is determined through the average value of simulation samples:

$$\bar{Z}^{(m)} = \frac{Z^{(m)} + (m-1)\,.\,\bar{Z}^{(m-1)}}{m} \tag{4-1}$$

(v) **Check the stopping condition:** Increase the number of simulations by 1, i.e., $m = m + 1$. If $m < M_{max}$, return to step (ii); otherwise, stop and output the estimated objective function value $\bar{Z} = \bar{Z}^{(m)}$.

4.2 Solution approaches for electric bus planning

4.2.1 Full enumeration method

As outlined in the model formulation for EB planning (see Section 3.2) , our INLP model frames the EB planning problem as a combinatorial optimization problem, which aims to optimize vehicle type selection (e.g., choosing between a fleet of 12-m EBs or a fleet of 18-m EBs) and service frequencies (e.g., choosing from 56 feasible values, from a discrete set of values: $\{5, 6, 7, \dots, 59, 60\}$ [veh/h]). Due to the finite number of solutions, a Full Enumeration (FE) approach can be used to explore all possible solutions and identify the global optimum (see Algorithm 4-3 for the steps involved in the FE approach). In this tactical planning stage, where solution quality is paramount and computing time savings are less critical, exact methods like FE are preferred, as they can guarantee a globally optimal solution. Moreover, Fig. 4-1 provides a visual representation of our FE approach for 2 scenarios of vehicle type selection

and 56 feasible frequency values, resulting in a total of 112 solutions. This representation reflects the real-world conditions of our case study, and the FE method is able to solve our problem within 20 minutes, which is an acceptable processing time for this offline design problem.

Algorithm 4-3 The main steps of the full enumeration method.

Step (1): Enumerate binary decision variables (related to the vehicle type selection) by enumerating over possible scenarios of vehicle type selection. For example, given two common types of EBs (12-m standard and 18-m articulated buses), two possible scenarios[1] will appear:
(i) First scenario ($x_1 = 1$ and $x_2 = 0$): Operation with a fleet of 12-m long buses.
(ii) Second scenario ($x_1 = 0$ and $x_2 = 1$): Operation with a fleet of 18-m long buses.

Step (2): For each scenario identified in Step (1), enumerate over all possible frequency values (i.e., $\{f_{\min}, f_{\min}+1, \dots, f_{\max}-1, f_{\max}\}$) to find the best frequency.

Step (3): Return the best solution (with the lowest total cost value) among all possible solutions.

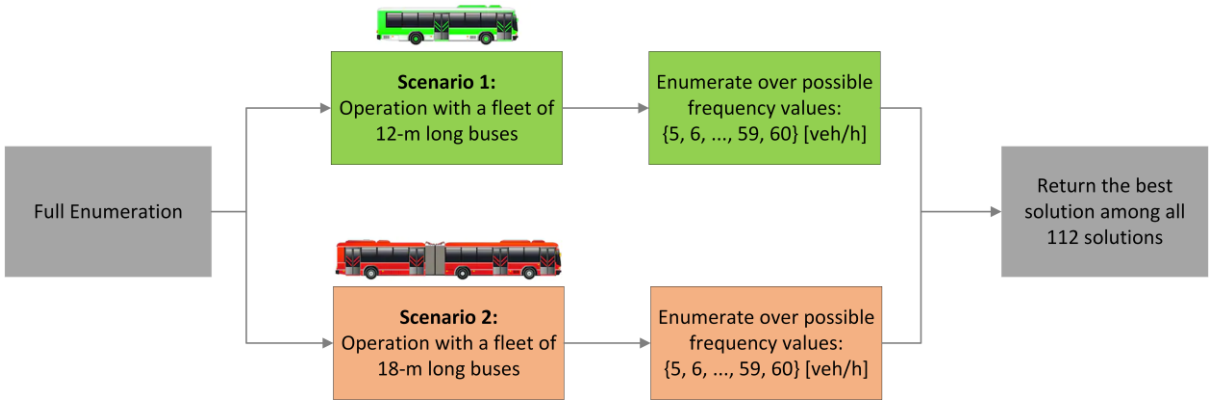

Figure 4-1 A visual representation of the FE approach for solving our real-life problem (with 2 possible scenarios of vehicle type selection and 56 frequency values).

[1] In the presence of buses of type 1 (12-m long buses) and type 2 (18-m long buses), binary variables x_m (for $m = 1, 2$) are treated as:
Binary variable x_1 that equals 1 if a fleet of 12-m long buses is operated, 0 otherwise,
Binary variable x_2 that equals 1 if a fleet of 18-m long buses is operated, 0 otherwise.
Also, the expression of $x_1 + x_2 = 1$ [in Eq. (3-52)] will always hold.

4.2.2 Genetic algorithm

To solve the EB fleet scheduling problem, we also implement a Genetic Algorithm (GA), which is a widely-used evolutionary algorithm that has demonstrated outstanding performance in solving complex combinatorial optimization problems (Karimi-Mamaghan et al., 2022). The GA draws inspiration from natural selection and genetics and operates on a population of chromosomes (individuals) to iteratively evolve solutions using the principles of selection, crossover, and mutation.

Solution representation, also known as encoding, is a crucial step in defining solutions for metaheuristic algorithms in a comprehensible way. With the GA, each solution is expressed in the form of a chromosome, with a set of genes characterizing the decision variables. As illustrated in Fig. 4-2, we adopt a two-section structure for the chromosome representation in our GA. The first section contains binary variables representing vehicle type selection, while the second section contains the frequency value expressed as an integer number.

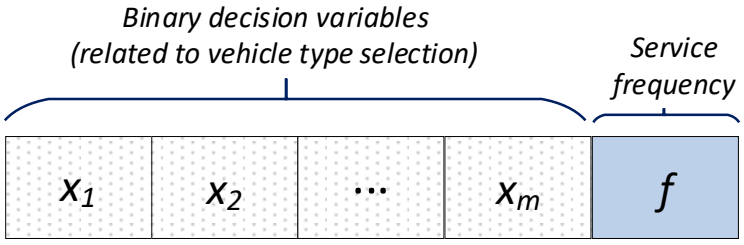

Figure 4-2 Chromosome encoding in the GA.

Initialize population size (N_{pop}), maximum number of iterations ($MaxIt$), crossover rate (P_c), and mutation rate (P_m)

Begin

Generate the initial population of chromosomes Y_i $(i = 1, 2, \dots, N_{pop})$

Evaluate the fitness of each chromosome in the population by Eq. (4-2)

Set iteration counter $t = 1$

while $(t < MaxIt)$

Select parents from the population using a selection method, e.g., roulette wheel selection

Perform crossover on the selected parents with a rate of P_c

Perform mutation on the offspring with a rate of P_m

Evaluate the fitness of the generated offspring by Eq. (4-2)

Merge the current population and offspring population (obtained from crossover and mutation), and sort the individuals based on their fitness

Select the best (top) N_{pop} individuals for the next generation

Increase the current iteration by 1, $t = t + 1$.

end

Return the chromosome with the best fitness value, Y_{best}, as the best solution

end

Figure 4-3 Pseudo code of the GA.

The GA employs three main operators - parent selection, crossover, and mutation - to generate new individuals (offspring) and enhance population diversity. The overall process of the GA is summarized in Fig. 4-3. In this research, we apply a single-point crossover (Fig. 4-4) and two different mutation operators to enhance population diversity. To mutate the first section of solutions, which involves binary variables for vehicle type selection, we use a swapping mutation operator. Specifically, we randomly select two elements and switch their positions (Fig. 4-5). For the second section of solutions, which involves frequency values, we apply a random mutation operator, where we replace the current frequency value with another feasible value selected at random.

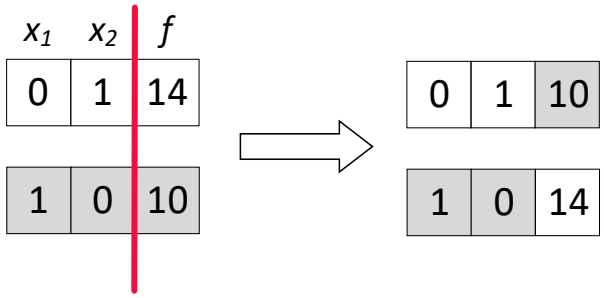

Figure 4-4 An example of single-point crossover.

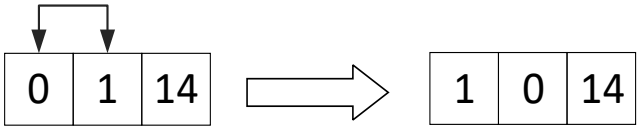

Figure 4-5 An example of swapping mutation.

In the parent selection stage, we adopt a roulette wheel selection method, which favors better solutions with higher fitness scores as parents (Katoch et al., 2021; Sadrani et al., 2022c). To evaluate the fitness (suitability) of solutions, we employ the fitness function expressed in Eq. (4-2):

$$F(x) = \frac{Z\max - Z(x)}{Z\max - Z\min} \tag{4-2}$$

where the scaled fitness score of individual x is represented by $F\ (x)$, and $Z\ (x)$ is the objective function value (OFV) of individual x. Besides, $Z_{\max}$ and $Z_{\min}$ represent the OFVs of the worst and best solutions in the present population, respectively. As this dissertation deals with a minimization problem, a higher fitness score corresponds to a lower cost value, according to Eq. (4-2).

Finally, the current population members and new offspring generated by crossover and mutation operators are combined to create the next generation. The individuals in the next generation are then sorted based on their fitness ratings, and the top N_{pop} individuals are selected for the upcoming generation.

4.3 Solution approaches for mixed-fleet bus scheduling

4.3.1 Solution approaches for the simple version of the mixed-fleet bus scheduling problem

The proposed heterogeneous fleet vehicle dispatching problem was formulated as a MINLP model, in which a number of constraints [e.g., constraints (3-118) and (3-120)] and the proposed objective function are nonlinear, thereby combining the difficulty of optimizing over integer variables with the handling of nonlinear functions.

For instance, in nonlinear constraint (3-120), all the terms (e.g., $N_{i,j}^{b}$ and $N_{i,j,k}^{w}$) are variables due to the presence of binary decision variables x_{mi} in the model. In essence, all the terms are dependent on the passenger-carrying capacity of bus services provided to users, and due to the possibility of dispatching services with varying capacities during a mixed-fleet operation [as presented in constraint (3-107)], those terms can change depending on the starting order of buses in a mixed-fleet operation. To be more precise, as explained for $N_{i,j}^{b}$ in Eq. (3-118), the actual number of passengers who can successfully board vehicle i at each stop depends on the capacity of vehicle i. Moreover, for $N_{i,j,k}^{w}$, as can be seen in Eq. (3-115), some of the passengers waiting for vehicle i at stop j are those passengers who were unsuccessful in boarding vehicle $i-1$ due to a shortage of capacity inside vehicle $i-1$, who have to wait for vehicle i. This indeed implies that $N_{i,j,k}^{w}$ can be dependent on the capacity of the preceding vehicle (vehicle $i-1$) during operations. In addition, $N_{i,j,k}^{w}$ is also affected by the dispatching times of vehicles (continuous decision variables in the model), as the number of new passengers arriving at stops is computed based on the headways between each two consecutive vehicles, as observed from Eq. (3-115).

As a further example in the objective function (3-105), according to part (ii) (i.e., the nonlinear expression of ($N_{i-1,j,k}^{f} \,.\, H_{i,j}$), in which all the terms are variables as well), the extra waiting times due to denied boarding can depend on both binary and continuous decision variables of the model (i.e., dispatching order and times). More precisely, the extra waiting time in the case of failing to board, which is equal to the entire headway (i.e., $H_{i,j}$), is directly influenced by the dispatching times of vehicles (continuous decision variables of the model, $T_{i,1}^{d}$). On the other hand, as discussed earlier, the actual number of passengers being left behind [i.e., $N_{i-1,j,k}^{f}$ obtained through Eq. (3-121)] can be strongly dependent on the capacity of bus services provided to travelers during a mixed-fleet operation, which essentially depends on the dispatching sequence of vehicles (binary decision variables of the model, x_{mi}). Such

arrangements further point to the difficulty of handling a mixed-fleet dispatching problem as long as the relevant binary variables on the dispatching order of vehicles are regarded as decision variables in our model. This aspect leads to the dependency of many passenger flow variables on the capacity of services, in such a detailed model that explicitly considers binding capacity constraints for any given bus size during a mixed-fleet operation.

Moreover, given the nature of the problem in terms of vehicle dispatching order (x_{mi}), constraint (3-108) (resource limitations on the buses of each size) transforms the situation into a permutation-based combinatorial optimization problem (permutations with repetition due to the existence of several identical buses in the given set of vehicles), and the computational complexity of the problem will grow with a factorial rule depending on the fleet size and on the number of buses of each size. Given a set of N_v vehicles, such that there are A identical buses of type 1, B identical buses of type 2, and C identical buses of type 3, there are a total of $\frac{N_v!}{A! \times B! \times C!}$ distinct sequences for dispatching buses in our mixed-fleet operations.

To illustrate the magnitude of the computational requirements, consider a scenario with a mixed fleet of 25 buses, including 10 buses of type A, 8 buses of type B, and 7 buses of type C for operations. The total number of unique dispatching orders from the first station can be calculated as $\frac{25!}{10! \times 8! \times 7!} = 21{,}034{,}470{,}600$. It is evident that exhaustively evaluating all potential solutions through FE becomes computationally infeasible for large instances. Such an approach is inefficient for addressing operational scheduling problems that require timely optimization of operational plans.

Overall, not only do MINLP problems amalgamate the two aspects of MILP and NLP problems, but also have some unique features. For example, although a strict convexity assumption can ensure the global uniqueness of an NLP solution, the same does not hold for MINLP problems (see Bonami et al., 2012 for further details on the scope and complex nature of MINLPs). Generally, MINLP problems turn out to be NP-hard by nature (Bonami et al., 2012; Burer and Letchford, 2012). Moreover, as it is obvious, typical combinatorial optimization problems with sequence-dependent setup are known to be strongly NP-hard (Bianco et al., 1987; Osman and Potts, 1989; Ruiz and Stützle, 2007; Alkaya and Duman, 2015; Lin et al., 2021). It would be practically challenging to find the best dispatching sequence of vehicles from a huge discrete set of possible sequences in real-life cases. Meta-heuristic algorithms are known as one of the most efficient and frequently used

search methods for solving such complex optimization problems, as they can find satisfactory suboptimal solutions within an acceptable computing time (Talbi, 2009).

In this research, we develop a SA algorithm with state-of-the-art features, taking the advantage of producing feasible neighboring solutions, to solve large real-world mixed-fleet vehicle dispatching problems within a reasonable computing time. Moreover, an additional complexity in our real-world problems is to deal with travel time stochasticity (due to the stochastic nature of the problem in terms of travel time uncertainty), which should be addressed when designing the solution algorithm. To tackle this issue, the SA algorithm is coupled with a MCS method, which evaluates candidate solutions over several replications. Further details on the MCS are provided in the next subsection.

To obtain certain insights about the quality of solutions suggested by the SA algorithm, we offer a full integer space enumeration method (in Section 4.3.1.2), whereby the master MINLP problem is decomposed into a particular number of continuous NLP subproblems through fixing integer variables, to provide a direction towards the optimal solutions for small and medium-sized dispatching problems, measuring later the difference to the best solution found by the SA. To efficiently deal with the difficulty of handling binary variables and constraint (3-108) in the proposed mixed-fleet dispatching problem, we extensively describe these aspects in the design of our solution approaches. For example, we discuss how the proposed SA and its operators are properly designed to produce feasible neighborhood solutions that can satisfy these constraints, thereby enhancing the capability of the algorithm for a better exploitation of the best solutions within the feasible search space.

4.3.1.1 Simulated annealing algorithm

Simulated Annealing (SA) is a metaheuristic algorithm known for its ability to avoid getting trapped into a local optimum by allowing for random neighborhood changes, which can be adapted to different optimization problems with discrete or continuous space states (Zhang et al., 2015). There has been a large amount of work where SA has been efficiently applied to various combinatorial optimization problems (Gomes and Oliveira, 2006; Karimi-Mamaghan et al., 2021). In essence, SA is a single-solution based[2] algorithm in which

[2] Single-solution based algorithms manipulate and improve a single solution during the search process. On the other hand, in population-based algorithms (e.g., particle swarm, and evolutionary algorithms), a population of solutions is evolved (Talbi, 2009).

the cooling process of molten metals is simulated (Askarzadeh et al., 2016). SA starts with a feasible initial solution and endeavors to ameliorate the current answer by generating a new solution in the vicinity of the current answer. Indeed, if the new solution leads to a lower objective function value, the current solution is replaced by the new solution; otherwise, SA rules decide whether the current solution is replaced by the new one or not. To be more precise, the algorithm starts with an initial positive temperature (T_0) and during the search, the temperature is steadily reduced. The probability of accepting a worse solution is also decreased as the temperature is reduced, i.e., although the algorithm might take a risk in accepting a worse solution in high temperatures, this risk-taking propensity will gradually decline with moving towards the end of the search process. In general, this strategy can help the algorithm to escape from local optimum solutions (Eglese, 1990; Meiri and Zahavi, 2006).

As discussed before, the proposed dispatching problem is a permutation-based problem in terms of vehicle dispatching order, i.e., a permutation of a given set of vehicles leads to a new ordering of those vehicles. As an illustrative example of adjusting vehicle dispatching order, Fig. 4-7 depicts a mixed-fleet dispatching problem with a given set of 8 vehicles: {12,12,12,15,15,15,18,18} that can be dispatched in $\mathrm{P}(8;3,3,2)=\frac{8!}{3!\times3!\times2!}=560$ different arrangements. In our SA algorithm, we employ efficient operators to produce diverse solutions in terms of dispatching sequence. In Algorithm 4-4, we describe the steps of the SA adopted to solve the proposed mixed-fleet vehicle dispatching problem.

Algorithm 4-4 The main steps of the proposed SA algorithm.

Step (1): Set T_0 and β. Let $t \leftarrow 0$.

Step (2): Generate a feasible initial solution y & evaluate the answer, i.e.,

(2.1). Generate a feasible initial solution y, in which the decision variables of the problem (dispatching orders and dispatching times) are randomly generated (the structure of one single solution is illustrated by Fig. 4-6, in which the first part of the figure is dedicated to the bus dispatching order and the second part indicates the dispatching times of buses from the first stop).

(2.2). Evaluate the value of the objective function for the initial solution, $f(y)$, through a Monte Carlo Simulation (MCS) method over several simulation-based trials to handle the uncertainty of stochastic travel times, drawn from a log-normal distribution (see Algorithm 4-2 for further information on the specific steps of the MCS method embedded into the SA). Let $y_{best} \leftarrow y$ and Go to Step 3.

Step (3): Create a neighboring solution y' using various operators & evaluate the answer, i.e.,

(3.1). Create a neighboring solution y', wherein *bus dispatching order* and *bus dispatching times* are randomly changed into a new arrangement, while taking the advantages of producing feasible solutions, i.e.,

Dispatching order schedule: To create a new bus dispatching order, as can be seen in Fig. 4-7, the dispatching order of vehicles in the former solution is changed into a new dispatching sequence through a random displacement by means of swapping or inversion operators. Such a permutation-based procedure in producing neighboring answers can ensure the new solutions will be feasible in terms of constraint (3-108), as the total fleet size and the number of buses of each size in the new solution will remain unchanged compared to the initial feasible solution, and merely the dispatching sequences of vehicles are updated in the new solutions.

Dispatching time schedule: To create a new departure time schedule, the departure times in the previous solution are changed for some vehicles using a normal distribution. First, based on a given rate, a number of vehicles in one solution are randomly selected (e.g., vehicles 2, 3, and 7 in Fig. 4-8). Then, for each vehicle selected in turn, its departure time is changed by means of a normal distribution while considering the departure times of preceding and subsequent vehicles as certain bounds, i.e., $nT_{i,1}^d \sim N\left(T_{i,1}^d, \sigma^2\right) \sim T_{i,1}^d + \sigma\, N(0,1)$, where the standard deviation σ is defined as $\sigma = \mu \times (T_{i+1,1}^d - T_{i-1,1}^d)$. Note that $T_{i,1}^d$ is the departure time of vehicle i in the previous solution and $nT_{i,1}^d$ is the new departure time generated for vehicle i. After performing several preliminary tests with different values, μ was set to be 0.1. In the meantime, the feasibility of the generated departure times is checked [to meet constraint (3-113)] and modified (regenerated), if needed.

(3.2). Evaluate the value of objective function for the generated neighboring solution, $f(y')$, through the MCS method in Algorithm 4-2.

Step (4): If $f(y') \le f(y)$ or $r \le P_{ac}$ then $y \leftarrow y'$. If $f(y') \le f(y_{best})$ then $y_{best} \leftarrow y'$.

Step (5): If the stopping criteria (I_{max}) is not met then $T_t = \beta \times T_{t-1}$, $t \leftarrow t+1$ and Go to Step 3; otherwise, stop and return y_{best}.

where:

$$P_{ac}(y, y', T_t) = \begin{cases} 1 & \text{if } f(y') \le f(y) \\ \exp\left(-\dfrac{f(y') - f(y)}{T_t}\right) & \text{Otherwise} \end{cases} \quad (4\text{-}3)$$

t	Iteration counter
I_{max}	Maximum number of iterations
T_0	Initial temperature
T_t	Temperature in iteration t
β	Cooling factor
y_{best}	Best found solution
$f(y)$	Objective function value for solution y
r	A uniform random number in [0, 1]
$P_{ac}(y, y', T_t)$	Probability function for accepting the non-improving solution y'

As can be seen in expression (4-3), the probability of accepting a non-improving solution will depend on the difference between the corresponding objective function values, and also on the temperature at the relevant iteration. As discussed in Step 3, for the dispatching order of vehicles, neighborhood solutions are created through two different operators that are randomly used, including swap and inversion operators. In the swapping operator, two vehicles are randomly selected to be swapped in the same solution [see Fig. 4-7 (a)]. In the inversion operator, a string of vehicles is randomly selected to be reversed in the same solution, as illustrated in Fig. 4-7 (b).

Binary decision variables on dispatching order (size assignment to each bus service)

x_{mi} $m = 1, 2, 3;\ \ i = 1, 2, \dots, N_v$

$m \setminus i$	$i = 1$	$i = 2$	...	$i = N_v - 1$	$i = N_v$
$m = 1$	x_{11}	x_{12}	...	$x_{1(N_v-1)}$	x_{1N_v}
$m = 2$	x_{21}	x_{22}	...	$x_{2(N_v-1)}$	x_{2N_v}
$m = 3$	x_{31}	x_{32}	...	$x_{3(N_v-1)}$	x_{3N_v}
	$T^d_{1,1}$	$T^d_{2,1}$	...	$T^d_{(N_v-1),1}$	$T^d_{N_v,1}$

Continuous decision variables on dispatching time

$T^d_{i,j}$ $i = 1, 2, \dots, N_v;\ \ j = 1$

Figure 4-6 Structure of one initial solution.

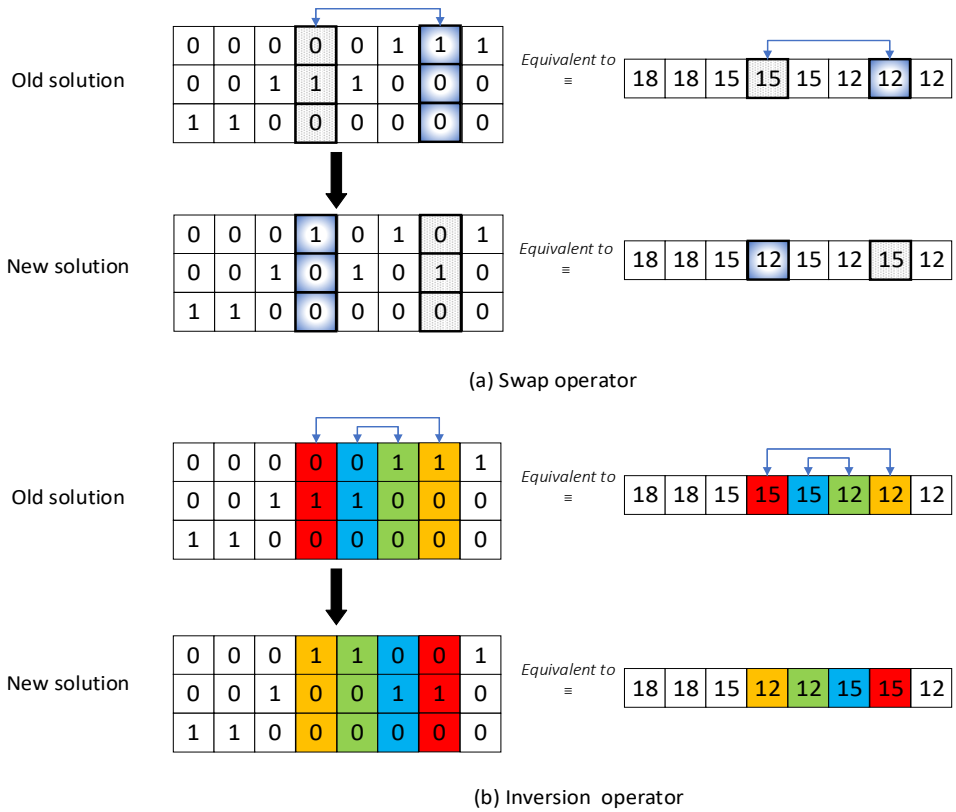

Figure 4-7 An illustrative example for creating new dispatching sequences using two operators: (a) swap operator; and (b) inversion operator.

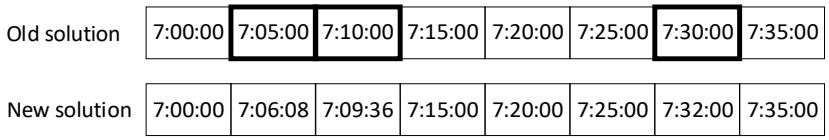

Figure 4-8 An illustrative example for changing the departure times of the selected buses.

To handle travel time uncertainty, each solution is repeatedly assessed over several simulation-based evaluations through a MCS method which is a well-established method among researchers to cope with the uncertainty in stochastic programming problems to estimate expected values (Marseguerra et al., 2002), particularly among transportation researchers to handle the uncertainty of stochastic travel times in urban bus operations (e.g., Liu et al., 2013; Chen et al., 2015; Wu et al., 2017; Mou et al., 2020; Zhang et al., 2020; Gkiotsalitis and Van Berkum, 2020b). For example, Liu et al. (2013) used a GA, combined with a MCS framework, to solve a stop-skipping service problem. In principle, the heuristic GA algorithm was employed to find the optimal stopping patterns, and the MCS method was employed to deal with travel time uncertainty in the process of solution evaluation. The same

procedure is also executed in the studies of Chen et al. (2015) and Mou et al. (2020). Likewise, the MCS method is embedded as a subroutine of the SA algorithm in our dissertation. Indeed, in Steps 2.2 and 3.2 of the SA algorithm, the evaluation of each solution is carried out by the MCS method over several replications due to the presence of stochastic travel times. The specific steps of the MCS scheme are summarized in Algorithm 4-2.

4.3.1.2 Decomposition based method

For the proposed mixed-fleet vehicle dispatching problem, we introduce a strategy to decompose the original MINLP problem into a certain series of continuous NLP subproblems with fixed binary variables for providing a direction towards the optimal solutions in the case of small and medium-sized instances. As discussed before, given the nature of the problem in terms of vehicle dispatching order, constraint (3-108) (resource limitations) transforms the proposed mixed-fleet dispatching problem into a permutation-based combinatorial optimization problem (permutations with repetition due to the existence of several identical buses in the given set of vehicles), and the complexity of the problem will grow based on a factorial function depending on the fleet size and on the number of buses of each size. In principle, there exists a total of $\frac{N_v!}{A! \times B! \times C!}$ possible ways (in terms of dispatching sequence) for dispatching vehicles in a mixed-fleet operation. Accordingly, by fixing the dispatching sequences in $\frac{N_v!}{A! \times B! \times C!}$ different ways, we decompose the master MINLP problem into a certain number (equivalent to $\frac{N_v!}{A! \times B! \times C!}$) of continuous NLP subproblems, in each of which the optimal dispatching times of vehicles should be determined.

Indeed, each possible dispatching sequence is reflected by one of those subproblems. In other words, binary variables (x_{mi}) have already been fixed in each NLP subproblem and we just need to find the optimal dispatching times of vehicles in each subproblem (note that dispatching times are continuous decision variables in our model). Obviously, since the number of buses of each size will remain unchanged after carrying out a permutation on a given set of buses and merely the dispatching order of those buses are renewed in each subproblem, constraint (3-108) has been spontaneously satisfied in all the resulted subproblems. Finally, each NLP subproblem (for optimizing vehicles' dispatching times in that subproblem) is solved using the GAMS/CONOPT package that can determine that the solution is globally optimal in the NLP case and it will return Modelstat = 1 (Optimal). After solving all the NLP subproblems

consecutively one after another, the best-found solution leading to the lowest passenger waiting time is identified. The specific steps of the proposed full integer space enumeration method are summarized in Algorithm 4-5. Indeed, the main aim of this method is to eliminate the difficulty of handling binary variables when solving small and medium dispatching instances. Hence, we will employ this procedure for solving a set of small and medium-sized test problems (in Section 5.4.1.1), measuring later the difference from the best solution found by the SA to obtain certain insights about the quality of the attained solutions by the SA. Note that Algorithm 4-5 is not designed to handle travel time uncertainty and our test problems are solved with deterministic running times between stops to avoid further complexity and growth of computing times.

In recent years, there has been a considerable progress within the field of MILP and NLP (Achterberg and Wunderling, 2013; Bazaraa et al., 2013), which also enriches the field of MINLP as decomposition techniques for MINLP problems rely often on solving these types of subproblems (Kronqvist et al., 2019). For example, there is a large number of different solvers available and the number is growing in the NLP case: solvers like CONOPT, SNOPT, Knitro, and Mosek are well-known commercial options, and IPOPT is a well-known opensource solver (see Kronqvist et al., 2019 for further details on the above-mentioned NLP solvers). Overall, there is a wide variety in the algorithms behind NLP solvers, e.g., CONOPT implements a generalized reduced gradient approach, whereas SNOPT employs a sequential quadratic programming method, and Knitro, Mosek, and IPOPT use an interior-point approach (see Biegler, 2010 for a comprehensive review of NLP).

Algorithm 4-5 The specific steps of the proposed full integer space enumeration method.

Step (1): Decompose the master MINLP problem into a certain number ($\frac{N_v!}{A! \times B! \times C!}$) of continuous NLP subproblems by fixing binary variables (vehicle dispatching order) in $\frac{N_v!}{A! \times B! \times C!}$ different ways, i.e., each subproblem is created based on one of those possible sequences, which can be prescribed for dispatching vehicles in a given mixed fleet.

Step (2): Solve the obtained NLP subproblems (with continuous decision variables of dispatching times) using the GAMS/CONOPT package for finding the optimal dispatching times of vehicles in each subproblem.

Step (3): Return the minimum-cost solution among the whole NLPs solved (return the obtained dispatching times together with the dispatching order already prescribed for that subproblem in Step 1).

4.3.2 Solution approaches for the advanced version of the mixed-fleet bus scheduling problem

As discussed earlier, the simplest forms of the MFBS problems have been demonstrated to be NP-hard, due to their combinatorial nature in dispatching sequence (Sadrani et al., 2022a). When modeling a more realistic and advanced version of the MFBS problem, which contains a comprehensive objective function (taking into account users' in-vehicle time, trip comfort, and operator costs) along with a broader set of real-world operational constraints and decision variables (especially integer decision variables related to resource allocation), the computational complexity of solving the MFBS problem increases significantly. This complexity arises from the inclusion of further recursive relationships, non-linear terms, and non-smooth elements in both the constraints and the objective function. Thus, a crucial need appears here to develop more advanced and reliable solution algorithms, specifically hybrid metaheuristics, to effectively address these challenges.

To explore efficient solution algorithms for the advance version of the MFBS problem, we utilize two established metaheuristics, the GA and the GWO. Additionally, we develop two new hybrid metaheuristic algorithms, GA-SA (a combination of GA and SA) and GWO-SA (a combination of GWO and SA), aiming to enhance the optimization capabilities and improve the quality of solutions for the MFBS problem.

4.3.2.1 Solution representation

Solution representation, also known as encoding, is a crucial step in the utilization of metaheuristics, as it enables the meaningful introduction of solutions into the algorithms. In our approach to the MFBS problem, we design a two-section structure for the solution box representation. This structure includes an integer-coded section (section a) and a continuous (real)-coded section (section b), as illustrated in Fig. 4-9.

In section a, the first encoding segment, we focus on characterizing vehicle assignment plans. This segment comprises two sublayers: a.1 represents the number of vehicles of each type assigned for operations, and a.2 denotes the dispatching sequence labels of the vehicles. Specifically, in sublayer a.1, non-negative integer values are randomly generated for each vehicle type, taking into account the maximum availability of each type. To assign a service priority label to each vehicle, a random permutation of integers from 1 to the total number of assigned vehicles is created in sublayer a.2. This permutation represents the dispatching sequence of the vehicles from the first terminal. Combining sublayers a.1 and a.2 results in

layer a.3, which presents the sorted dispatching sequence of the vehicles. In section b, the second encoding segment, we present the encoding of dispatching times using real-coded values.

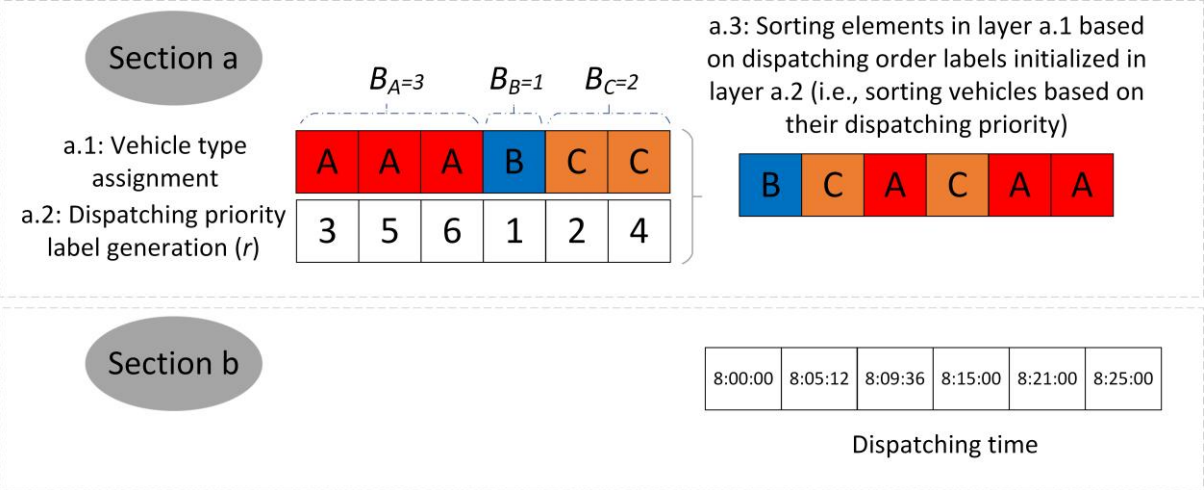

Figure 4-9 Solution encoding example.

4.3.2.2 Genetic algorithm

The GA search process was described in Section 4.2.2. Here, we describe the crossover and mutation operators specifically designed in the GA to solve the advanced MFBS problem. The crossover application leads to the exchange of genetic material between two parents. As shown in Fig. 4-10, we utilize a single-point crossover operator for the integer-coded sections of vehicle assignment solutions. However, for the vehicles' dispatching times in section b (Fig. 4-9), we employ an arithmetic crossover operator, which is a popular operator for increasing the diversity of real-coded values in the GA (Katoch et al., 2021; Mirjalili et al., 2020):

$$\begin{aligned} \text{Child1} &= m * \text{Parent1} + (1-m) * \text{Parent2} \\ \text{Child2} &= (1-m) * \text{Parent1} + m * \text{Parent2} \end{aligned} \tag{4-4}$$

where m is a random weighting vector generated for each crossover operation.

Notably, our crossover strategy allows for gene exchange between parents of different sizes (lengths) (Fig. 4-10), facilitating the exploration of a wider search space. This approach enhances the diversity of solutions in terms of both vehicle assignment (resource allocation)

and dispatching order in the MFBS problem. The length of a solution depends on the total number of vehicles assigned for operations. During the crossover process, the feasibility of the resulting offspring is checked regarding resource constraints, ensuring that the number of vehicles of each type assigned for operational activities does not exceed the available resources. If an offspring is found to be infeasible, a modification process is executed to correct it. In such cases, random corrections are made to the older parts of the offspring, while the genetic material moved through the crossover remains unchanged. Besides, Fig. 4-11 depicts an example of a swapping mutation, which involves randomly selecting two elements and interchanging their positions.

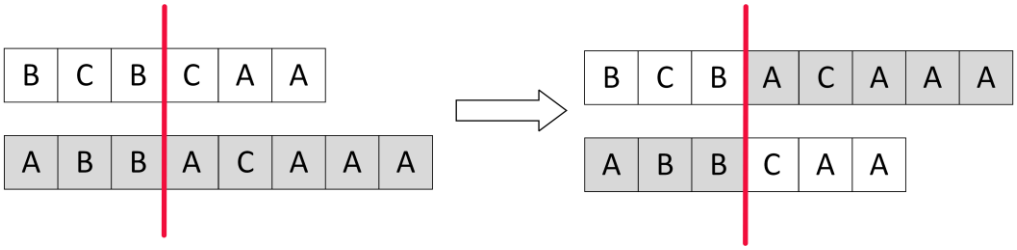

Figure 4-10 Example of single-point crossover.

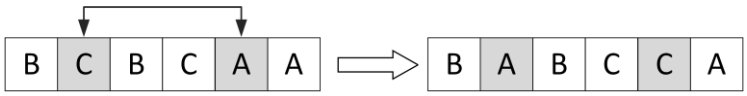

Figure 4-11 Example of swapping mutation operator.

4.3.2.3 Grey wolf optimizer

The Grey Wolf Optimizer (GWO), introduced by Mirjalili et al. (2014), is a nature-inspired swarm intelligence algorithm that mimics the social hierarchy and hunting behavior of grey wolves. It has demonstrated remarkable performance in solving various optimization problems, such as path planning, flow shop scheduling, and power dispatch (for an in-depth review of GWO applications, see Faris et al., 2018 and Sharma et al., 2022). One notable advantage of GWO is its low number of controlling parameters, which reduces the need for extensive parameter tuning (Faris et al., 2018; Wang et al., 2022). Despite its wide application in engineering optimization, there is a lack of research in the public transport literature utilizing GWO for bus/train planning problems (for recent review papers on public transport planning, see Liu et al., 2021 and Gkiotsalitis et al., 2022).

The search efforts of the GWO are described in the following. Overall, GWO considers four kinds of grey wolves for the simulation of leadership hierarchy: alpha, beta, delta, and omega. In essence, the alpha wolf (α) refers to the best (most important) individual in a grey wolf pack, known as the leader of the group. Besides, the second and third top individuals are known as beta (β) and delta wolves (δ) respectively. Other individuals are known as omega (ω) wolves, essentially steered by the α, β, and δ wolves during the search for prey. The hunting phase consists of three steps: encircling, hunting, and attacking steps.

In the encircling phase, the GWO simulates the motions of grey wolves encircling prey at the beginning of the hunting process. Mathematically speaking, such motions are modeled using the following equations:

$$\vec{D} = \left| \vec{C} . \vec{X}_p(t) - \vec{X}(t) \right| \tag{4-5}$$

$$\vec{X}(t+1) = \vec{X}_p(t) - \vec{A} . \vec{D} \tag{4-6}$$

$$\vec{A} = 2\vec{a} . \vec{r}_1 - \vec{a} \tag{4-7}$$

$$\vec{C} = 2 . \vec{r}_2 \tag{4-8}$$

where t refers to the current iteration, $\vec{X}_p$ refers to the location of the prey, and $\vec{X}$ refers to the location of a wolf. $\vec{A}$ and $\vec{C}$ are coefficient vectors allowing for the movement (relocation) of wolves at different positions around the prey. In essence, D reflects the distance between a wolf and a prey. Elements $\vec{a}$ will be reduced linearly from 2 to 0 as iteration progresses. Besides, $\vec{r}_1$ and $\vec{r}_2$ refer to random vectors within the range of [0, 1] (Mirjalili et al., 2014).

In the hunting phase, the locations of omega (ω) wolves will be updated based on the directions of the α, β, and δ wolves (which are the three best solutions identified so far). In essence, this idea stems from the fact that the three best search agents have a better overview (knowledge) about the location of the prey, and therefore other search agents (other solutions) should update their locations accordingly (see Fig. 4-12 for more details on the pseudo code of the GWO). Such a concept is mathematically modeled as follows:

$$\vec{D}_{\alpha}=\left|\vec{C}_1.\vec{X}_{\alpha}-\vec{X}\right|,\quad \vec{D}_{\beta}=\left|\vec{C}_2.\vec{X}_{\beta}-\vec{X}\right|,\quad \vec{D}_{\delta}=\left|\vec{C}_3.\vec{X}_{\delta}-\vec{X}\right| \tag{4-9}$$

$$\vec{X}_1=\vec{X}_{\alpha}-\vec{A}_1.\vec{D}_{\alpha},\quad \vec{X}_2=\vec{X}_{\beta}-\vec{A}_2.\vec{D}_{\beta},\quad \vec{X}_3=\vec{X}_{\delta}-\vec{A}_3.\vec{D}_{\delta} \tag{4-10}$$

$$\vec{X}(t+1)=\frac{\vec{X}_1+\vec{X}_2+\vec{X}_3}{3} \tag{4-11}$$

In the stage of attacking a prey, the GWO mimics the motions of grey wolves as they attempt to approach prey. This stage aims to create a better balance between the exploration and exploitation phases. Accordingly, when $\left|\vec{A}\right|>1$, search agents will diverge from each other to discover a better prey, thus enhancing the GWO's ability for exploration. By contrast, when $\left|\vec{A}\right|<1$, the grey wolves are directed to the prey, thus improving the GWO's ability for exploitation. It should be noted that $\vec{A}$ can vary within the range of [-2, 2], depending on parameter $\vec{a}$ reduced from 2 to 0.

Initialize the grey wolf population $X_i(i = 1, 2, \dots, n)$
Initialize a, A, and C
Evaluate the fitness of each search agent
X_α = the best search agent
X_β = the second best search agent
X_δ = the third best search agent
while $(t < MaxIt)$
  for each search agent
    Update the position of the current search agent by Eq. (4-11)
  end
  Update a, A, and C
  Evaluate the fitness of all search agents
  Update X_α, X_β, and X_δ
  $t = t + 1$
end
Return X_α

Figure 4-12 Pseudo code of the GWO algorithm (Mirjalili et al., 2014).

Given that the GWO is a continuous algorithm, an appropriate encoding procedure is required to encode solutions in a manner that adapts this algorithm to the discrete search region of the proposed MFBS problem. To address this, we utilize the Random-Key (RK) method as the chosen encoding scheme, which is widely recognized for its effectiveness in adapting continuous metaheuristics, such as GWO, to discrete search spaces (Mirjalili and Lewis, 2013; Beheshti, 2021; Goodarzian et al., 2021b; Nayeri et al., 2022). In particular, the RK method has been widely applied in permutation-based optimization problems, such as job shop scheduling and traveling salesman problems, demonstrating successful applications in these domains (Fathollahi-Fard et al., 2020a, 2020b; Yu et al., 2020; Goodarzian et al., 2021; Nayeri et al., 2022).

Our RK encoding scheme has two stages, as shown in Fig. 4-13. First, a vector with a length equal to the number of vehicles assigned for operations is created using a uniform distribution U [0, 1], i.e., each element in the vector represents a random number within the range [0, 1]. Then, the random numbers in the vector are arranged in ascending order to introduce the new sequence in which the vehicles will be dispatched. For instance, the encoded solution in Fig. 4-13 produces the dispatching sequence: C, A, A, C, A, B in a sequential manner. By utilizing the RK method, we adapt the discrete dispatching sequence into a

continuous representation that can be processed by the GWO, enabling the optimization process within the MFBS problem.

Vehicle ID	A	A	A	B	C	C
Random numbers *U [0, 1]*	0.36	0.22	0.72	0.91	0.14	0.59

⇩

Sorted dispatching sequence	C	A	A	C	A	B
Sorted numbers	0.14	0.22	0.36	0.59	0.72	0.91

Figure 4-13 Example of the RK encoding method.

4.3.2.4 Hybrid of genetic algorithm and simulated annealing

In this section, we develop a hybrid algorithm called GA-SA, which combines the GA and SA approaches. The GA-SA algorithm leverages the benefits of both algorithms by integrating SA into the GA's selection process for the next generation of individuals, allowing for the acceptance of non-improving solutions based on the SA strategy, rather than relying solely on a ranking-based selection of top individuals. Fig. 4-14 provides a visual representation of this integration. This hybridization enables an adaptive optimization process that balances exploration and exploitation, improving the algorithm's ability to escape local optima.

Fig. 4-15 illustrates the details of the GA-SA algorithm. The SA strategy adjusts the acceptance chance of non-improving solutions based on temperature and solution value differences at each iteration. Higher temperatures, occurring during the early search iterations, provide a greater chance for accepting non-improving solutions, promoting exploration-based search efforts. As the iterations progress, the temperatures decrease, leading to a gradual reduction in the acceptance chance of non-improving solutions and emphasizing exploitation-based search efforts.

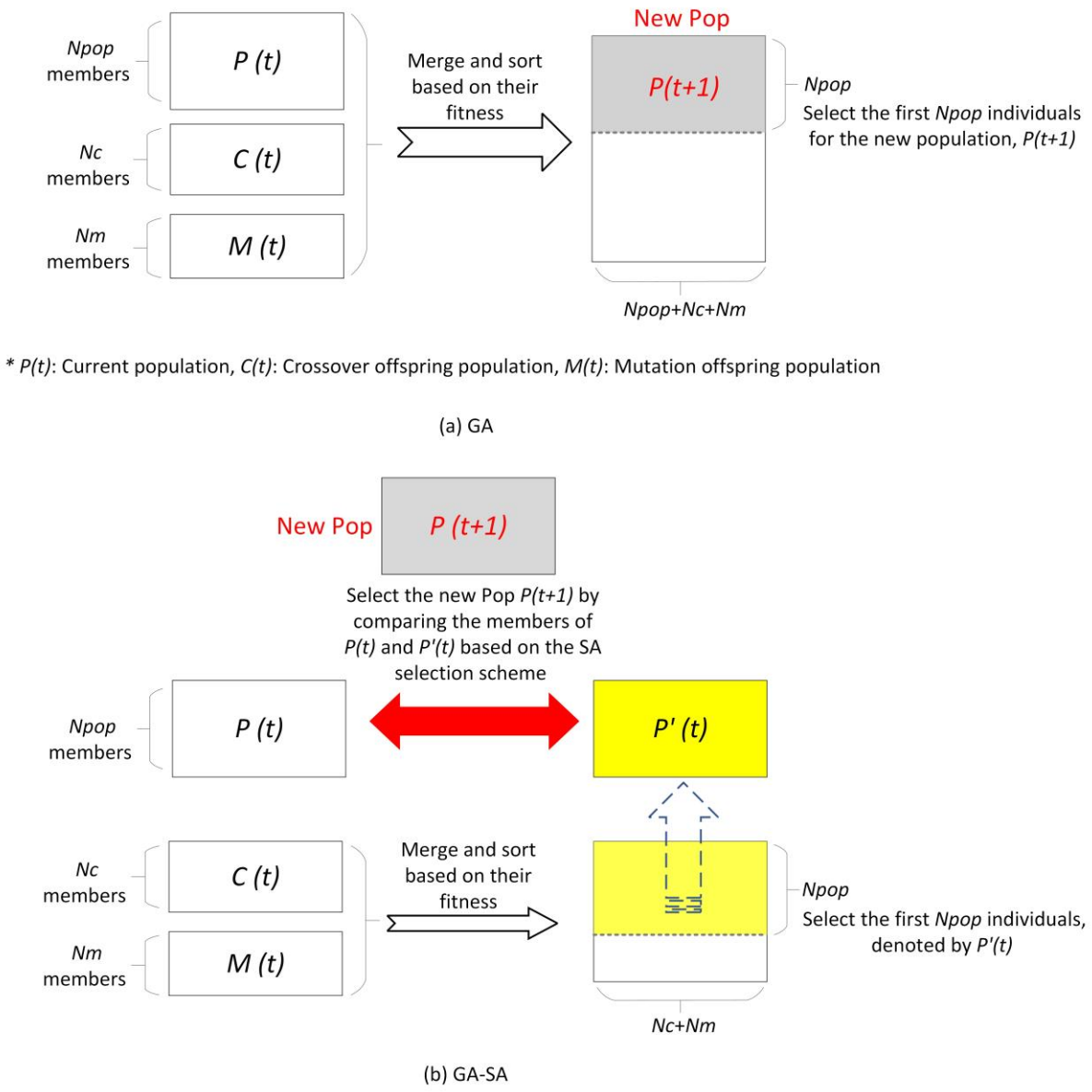

Figure 4-14 Selection of individuals for the next generation in the GA vs. GA-SA.

Initialize population size (N_{pop}), maximum number of iterations ($MaxIt$), maximum number of sub-iterations ($MaxsubIt$), crossover rate (P_c), mutation rate (P_m), initial temperature (T_0), cooling rate (α)

Generate the initial population of chromosomes Y_i $(i = 1, 2, \dots, N_{pop})$
Set iteration counter $t = 1$
Evaluate the fitness value of each chromosome

while $(t < MaxIt)$
while $(Cool\_iteration < MaxSubIt)$

Select parents and apply crossover and mutation phases (in the same manner as the GA)

Merge offspring created from crossover and mutation phases (offspring population)

Create the next generation by performing a random pairwise comparison between the members in the current population (y) and those in the offspring population (y') based on a SA strategy (see Fig. 4-14 for a better view of this step):

For each pairwise comparison using a SA strategy:

Compute $\Delta =$ Cost $(y') -$ Cost (y)
If $\Delta < 0$ **then**
$y = y'$
Else
Compute $P = e^{\frac{-\Delta}{T}}$
If $r =$ random $(0,1) \leq P$ **then**
$y = y'$
end
end
Update and store the cost of the best solution
$Cool\_iteration = Cool\_iteration + 1$
Reduce the temperature $T = T \times \alpha$
end
$t = t + 1$
end

Figure 4-15 Pseudo code of the GA-SA.

4.3.2.5 Hybrid of grey wolf optimizer and simulated annealing

In this section, we develop a hybrid GWO-SA algorithm that combines the convergence capabilities of GWO with the diversity-maintaining capabilities of SA. Specifically, the hybrid algorithm uses the acceptance probability function of SA to update the positions of the alpha, beta, and delta wolves by comparing them with the best three omega search agents identified in each iteration. For example, if an omega wolf exhibits better fitness than the current alpha

wolf, it replaces the alpha wolf; otherwise, the SA strategy determines whether the alpha wolf is replaced. The proposed GWO-SA algorithm's steps are illustrated in Fig. 4-16.

Initialize the grey wolf population $X_i (i = 1,2,...,n)$
Initialize $a, A,$ and C
Evaluate the fitness of each search agent
X_α = the best search agent
X_β = the second best search agent
X_δ = the third best search agent

while $(t < MaxIt)$
  while $(Cool\_iteration < MaxSubIt)$
    Update the position of each omega search agent by Eq. (4-11)
    Update $a, A,$ and C
    Evaluate the fitness of all omega search agents and select the three best ones in the omega population
    Update $X_\alpha, X_\beta,$ and X_δ based on a SA strategy, as described below:
    Comparing the current main members (alpha, beta, and delta) (denoted by y) with the three best agents identified in the omega population (denoted by y') based on a SA rule:
    For each random pairwise comparison by means of a SA strategy:
    Compute $\Delta =$ Cost $(y') -$ Cost (y)
      If $\Delta < 0$ **then**
        $y = y'$
      Else
        Compute $P = e^{\frac{-\Delta}{T}}$
        If $r =$ random $(0,1) \leq P$ **then**
          $y = y'$
        end
      end
    Update and store the best solution
    $Cool\_iteration = Cool\_iteration + 1$
      Reduce the temperature $T = T \times \alpha$
  end
  $t = t + 1$
end

Figure 4-16 Pseudo code of the GWO-SA.

4.4 Taguchi method for parameter tuning of metaheuristics

Metaheuristics' performance is known to be highly sensitive to the fine-tuning of their control parameters (Siarry, 2016; Mirjalili et al., 2020). To address this crucial aspect, we employ the Taguchi experimental design approach, which has been widely used in prior research (e.g., Ghannadpour and Zandiyeh, 2020; Goodarzian et al., 2021, 2020; Liu et al., 2020; Mokhtarzadeh et al., 2021; Nayeri et al., 2022; Tikani et al., 2021; Zandieh and Moradi, 2019). The Taguchi approach offers a systematic and efficient framework for the Design Of Experiments (DOE), allowing us to identify the most favorable parameter configurations with a reduced number of trials, minimizing the overall experimentation effort.

The Taguchi technique considers two groups of factors: controllable and noise (uncontrollable) factors. It aims to identify the optimal levels of controllable factors while minimizing the influence of noise factors, following the principle of robustness. To assess the variation in the response variable, Taguchi introduced the Signal-to-Noise (S/N) ratio. In essence, signal (S) and noise (N) represent the response variable (desirable value) and standard deviation (undesirable value) respectively, and therefore the objective is to maximize the S/N ratio (Ghannadpour and Zandiyeh, 2020; Nayeri et al., 2022):

$$\frac{S}{N} = -10 \times \log\left(\frac{1}{n}\sum_{i=1}^{n} y_i^2\right) \tag{4-12}$$

where n and y_i reflect the number of orthogonal arrays and the response in replication i respectively.

5 Results and discussion

This chapter presents the results obtained from applying the proposed models and solution algorithms in real-life case studies. It provides a thorough assessment of their practical applicability and discusses the implications of the findings.

5.1 Numerical experiments and application of automated bus planning model

5.1.1 Scenario setting and input data

To examine the applicability of the proposed mathematical model, an extensive range of scenarios are simulated for two real-world bus corridors in the cities of Regensburg in Germany and Santiago in Chile, averagely serving the total hourly demand of 638 [pax/h] and 5764 [pax/h] respectively during the morning rush hours. Regarding the analysis period, our simulations are conducted for a two-hour period extending from 7:00 to 9:00 AM. Time-dependent demand data related to the entire simulation period are presented in Appendix A (Table A4). The Regensburg case study is Bus Line 1 in the Konradsiedlung in Pommernstr, and the Santiago case study is Los Pajaritos corridor with bus passenger demand taken from Cortés et al. (2011). Both bus routes are bi-directional, containing a total number of 24 bus stops (12 stops in each direction) in Regensburg and 20 bus stops (10 stops in each direction) in Santiago.

Cost parameters for both Germany and Chile are based on EVs for both human-driven and automated public transport operations, and were estimated by Tirachini and Antoniou (2020) (see Appendix A). Moreover, for stochastic running times, a lognormal distribution is considered with the mean of 2.2 and 3.5 min and the standard deviations of 0.6 and 0.8 min for Regensburg and Santiago respectively. In the current programs of vehicle automation, the vast majority of studies in the literature have pointed out that automated buses might be operated at lower speeds than human-driven ones, owing to safety-related concerns considered more widely in the current phase of operation with automated vehicles in cities (e.g., Ainsalu et al., 2018; Pernestål et al., 2018; Kyriakidis et al., 2019; Zhang et al., 2019; Tirachini and Antoniou, 2020; Heikoop et al., 2020). Consistent with the available literature on automated buses, we also assume that automated bus systems are slower, operating with longer mean travel times by 10 percent.

It should be noted that we focus on a homogeneous fleet of buses (the fleet is composed of buses of the same size), and therefore size-dependent parameters (listed in Tables A2 and A3 for Regensburg and Santiago respectively) are not changed from one service to another, depending on the size of each service. In essence, such items are simply initialized (in the step of parameters' initialization) based on the (fixed) vehicle size assigned to our homogeneous fleet operation, and remain fixed during the entire simulation time for that fleet (note that the parameter initialization step was described further when presenting the main steps of the solution approach in subsection 4.1). Hence, we are not confronted with a particular difficulty in handling those parameters (e.g., in the objective function) during the simulation period. By contrast, this can be indeed a complicated issue in mixed/heterogeneous fleet problems (i.e., when buses of different sizes are operated). In this case, additional constraints and steps should be designed to handle the error and computational complexity of varying parameters, which can continuously vary from one service to another during operations.

Considering automated and human-driven vehicles, deterministic and stochastic travel times, and the presence or absence of in-vehicle crowding effects, a total of 8 different combinations of scenarios are simulated, as listed in Table 5-1. The optimal frequency and vehicle size are determined for any given scenario in both case studies of Regensburg and Santiago. Moreover, to comprehensively evaluate the possible effects of vehicle automation on the social costs of public transport services, several tests of sensitivity are performed on human driving cost savings with automation, travel time stochasticity, dwell time regularity, the time lost to open and close bus doors with automation, crowding multipliers, extra waiting time values, and user- and operator-oriented design cases.

Table 5-1 List of the simulated scenarios.

Scenarios	Vehicle technology		Travel time		In-vehicle crowding disutility effects	
	AV	HV	DT	ST	WOC	WC
AV, DT, WOC	✓		✓		✓	
AV, DT, WC	✓		✓			✓
AV, ST, WOC	✓			✓	✓	
AV, ST, WC	✓			✓		✓
HV, DT, WOC		✓	✓		✓	
HV, DT, WC		✓	✓			✓
HV, ST, WOC		✓		✓	✓	
HV, ST, WC		✓		✓		✓

AV: Automated vehicles.
HV: Human-driven vehicles.
DT: Deterministic travel times.
ST: Stochastic travel times.
WOC: Without in-vehicle crowding effects.
WC: With in-vehicle crowding effects.

Our model is coded in MATLAB R2019b, and all experiments are executed on a personal computer with Intel(R) Core(TM) i5-6500 CPU @ 3.20 GHz and 16.0 GB RAM. For Santiago encompassing more possible solutions to be evaluated compared to Regensburg, the enumeration method can averagely evaluate all the possible solutions within 3.32 minutes for scenarios assuming deterministic travel times. This is indeed an acceptable computing time for the enumeration of all solutions in an offline design problem. This average amount of time increases to 14.24 minutes for scenarios with stochastic travel times, due to the run of a MCS scheme for assessing each possible solution over several (1000) replications.

5.1.2 Optimal service frequency and vehicle size in base case scenarios

In the base case, we assume 50% human driving cost savings due to automation. Results on optimal frequencies and vehicle length are shown in Fig. 5-1 for Regensburg (5-1.a) and Santiago (5-1.b). Furthermore, Fig. 5-1 gives information on occupancy levels inside vehicles in terms of the average and maximum occupancy rates for any given scenario. Overall, we obtain that fleets of automated vehicles are dispatched with a higher optimal service frequency compared to conventional human-driven services, which is a known result for the case without crowding externalities and deterministic travel times (Fielbaum, 2019; Zhang et al., 2019; Hatzenbühler et al., 2020; Tirachini and Antoniou, 2020). Vehicles are dispatched at a higher

frequency in the case of Santiago, in which the total demand volume (5764 [pax/h]) is far larger than Regensburg with a total demand of 638 [pax/h].

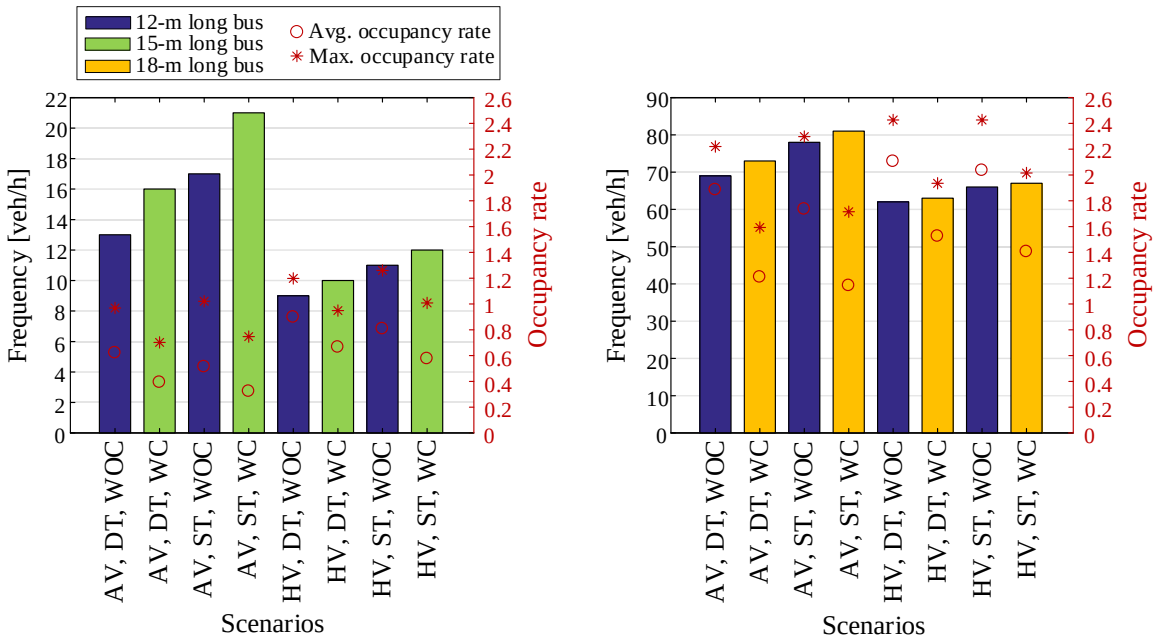

(a) Regensburg case study. (b) Santiago case study.

Figure 5-1 Optimal service frequency and vehicle size for different scenarios.

To alleviate in-vehicle crowding discomfort imposed on passengers when user cost is sensitive to on-board crowding levels, both vehicle size and service frequency are increased for both human-driven and automated vehicle fleet operations (see Fig. 5-1), i.e., the consideration of crowding discomfort externalities pushes solutions towards having larger and more frequent bus services. For instance, the results for Regensburg [see Fig. 5-1 (a)] show that vehicle sizes are increased at a similar rate in both human-driven and automated bus services, going from 12-m long buses for scenarios in which user cost is insensitive to on-board crowding levels to 15-m long buses for those scenarios in which on-board crowding is considered as a source of travel disutility when assessing user costs. However, service frequency is increased at a higher rate for automated vehicle fleet operations in the presence of on-board crowding effects. For example, service frequency increases by roughly 24%, going from 17 [veh/h] in the scenario of AV, ST, WOC to 21 [veh/h] in the scenario of AV, ST, WC, whereas it increases by 9%, going from 11 [veh/h] in the scenario of HV, ST, WOC to 12 [veh/h] in the scenario of HV, ST, WC. This result can be attributed to the fact that fleets of automated vehicles can reap much broader driving cost savings, thus opening up an opportunity

for bus agencies to provide more frequent bus services with lower operating costs in spite of the increase of capital costs due to the larger fleet size requirement, i.e., the higher capital costs are compensated by a marked reduction in operating costs at higher frequencies and allow the deployment of larger fleets (Hatzenbühler et al., 2020; Tirachini and Antoniou, 2020). Hence, vehicles can be operated with a higher optimal frequency to mitigate the user costs of crowding through the reduction of occupancy levels inside vehicles. As Fig. 5-1 (b) shows, the results have also the same pattern in the case of Santiago, however, vehicle sizes are increased from 12-m to 18-m long buses in the case of considering crowding as a source of dissatisfaction for users. This is because the given bus route in Santiago is known as an overcrowded corridor (5764 [pax/h]), in which vehicles operate at larger occupancy levels than Regensburg.

Overall, the deployment of automated bus services can significantly reduce occupancy levels inside vehicles, and thus in-vehicle crowding costs for on-board passengers, due to offering more frequent bus services with lower operating costs. In the case of Regensburg, assuming deterministic travel times, average occupancy goes down from 0.89 to 0.66 due to including crowding discomfort in the cost function for the case of human-driven vehicles, while the same figures are 0.62 and 0.39 for the case of automated vehicles, respectively. Therefore, the inclusion of crowding externalities in the model reduces average occupancy rates by 26% in the case of human-driven vehicles and 37% in the case of automated vehicles, a result that reinforces the relevance of automated vehicles in providing a higher standard of service for users under optimal operation conditions.

The assumption of stochastic travel times in dispatching scenarios (with the same standard deviation for human-driven and automated buses assumed in the base case) increases the optimal frequencies for both fleets of human-driven and automated buses, while vehicle sizes remain unchanged (e.g., see the scenarios of AV, DT, WOC and AV, ST, WOC in Fig. 5-1). Indeed, travel time stochasticity can lead to a further spread of irregularity among headways, thereby increasing passenger waiting times and reducing the reliability of a public transport system (Osuna and Newell, 1972). Hence, the setting of a higher service frequency can cope with the growth of passenger waiting times caused by travel time variability. As can be seen in Fig. 5-1 (a), the service frequency is increased at a higher rate for automated vehicle fleet operations, hovering around 30%, when travel times are assumed to be stochastic. This is because by deploying driverless vehicles, public transport operators can optimally provide more frequent services with lower operating costs to compensate for the growth of waiting times caused by travel time volatility in the scenarios with stochastic travel times. For example,

service frequency is increased from a value of 16 [veh/h] in the scenario of AV, DT, WC to a value of 21 [veh/h] in the scenario of AV, ST, WC, whereas it is increased by 20%, going from 10 [veh/h] in the scenario of HV, DT, WC to 12 [veh/h] in the scenario of HV, ST, WC.

To better understand the trade-offs established between the user and operator costs during the process of finding the optimal solution (optimal service frequency and vehicle size) for both fleets of human-driven and automated vehicles, we provide information on the average costs at different levels of frequency and bus sizes for any given scenario in the case of Regensburg (see Fig. 5-2). Indeed, in all scenarios, optimal and non-optimal deployment solutions can be easily compared to each other in terms of user and operator cost components, and therefore the total (social) costs. Overall, automated bus deployment scenarios lead to a lower social cost while operating at a higher optimal frequency.

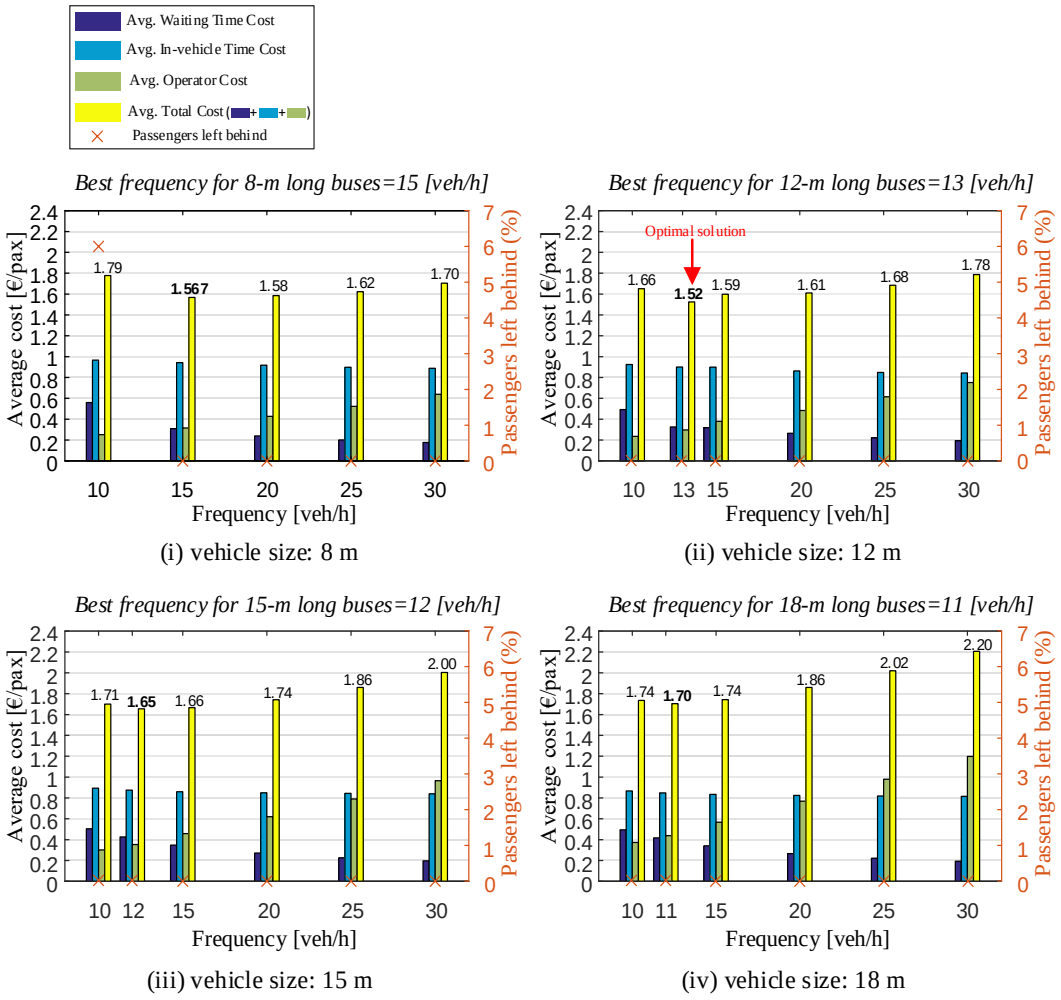

(i) vehicle size: 8 m

(ii) vehicle size: 12 m

(iii) vehicle size: 15 m

(iv) vehicle size: 18 m

(a) AV, DT, WOC

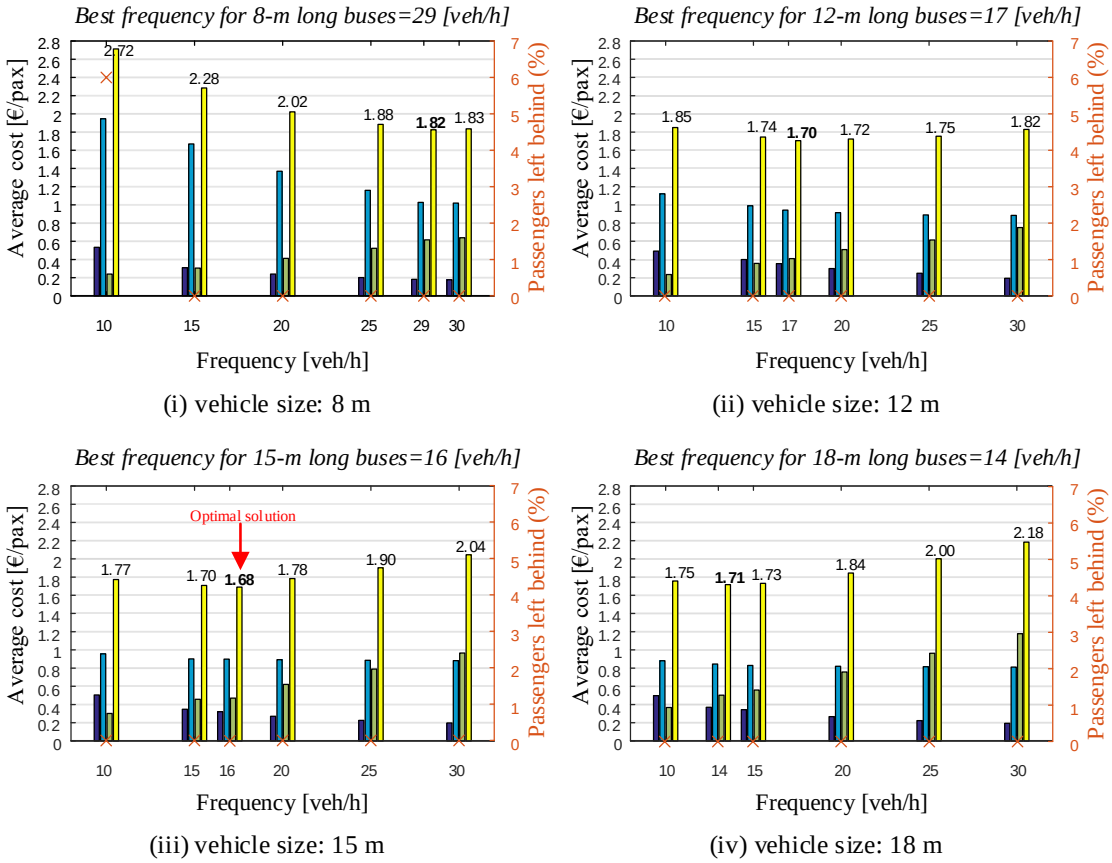

(i) vehicle size: 8 m

(ii) vehicle size: 12 m

(iii) vehicle size: 15 m

(iv) vehicle size: 18 m

(b) AV, DT, WC

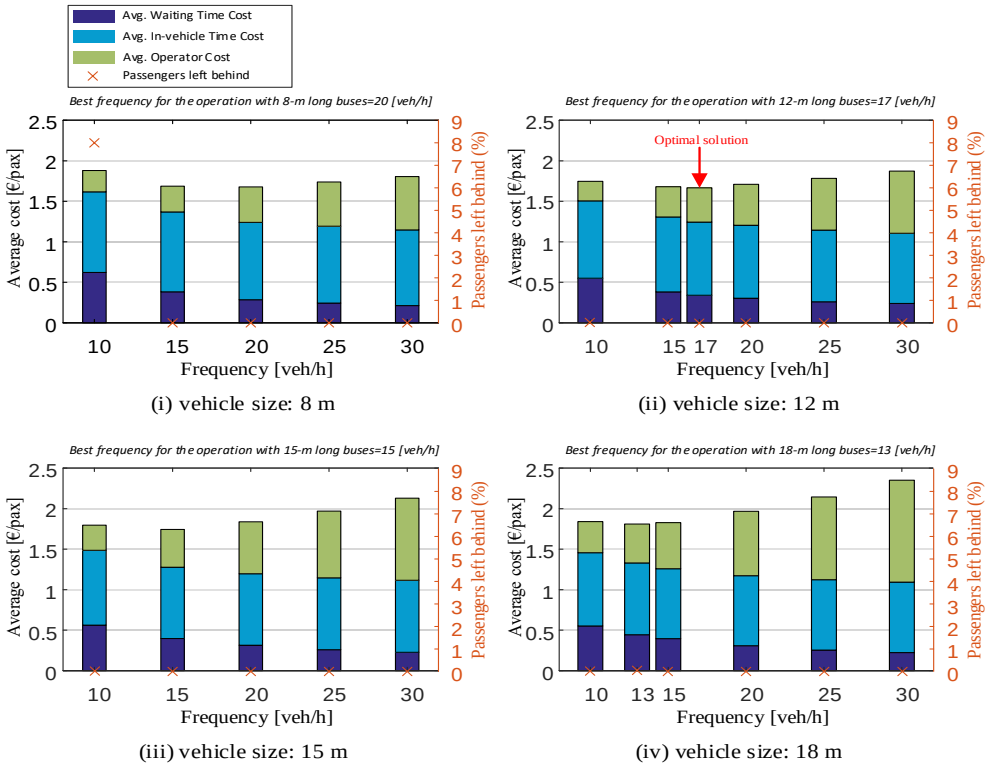

(i) vehicle size: 8 m

(ii) vehicle size: 12 m

(iii) vehicle size: 15 m

(iv) vehicle size: 18 m

Scenario: AV,ST,WOC

Optimal solution: bus size=12 m with frequency=17 [veh/h]

(c) AV,ST,WOC

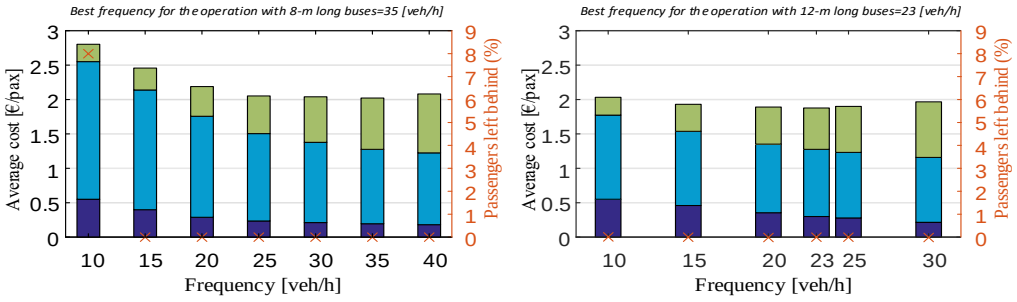

(i) vehicle size: 8 m

(ii) vehicle size: 12 m

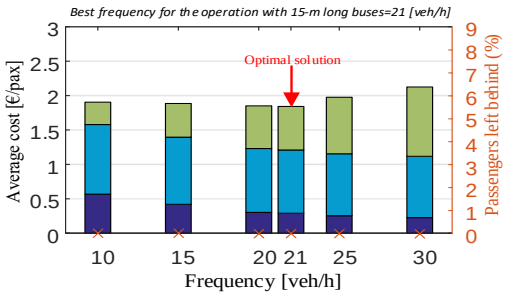

(iii) vehicle size: 15 m

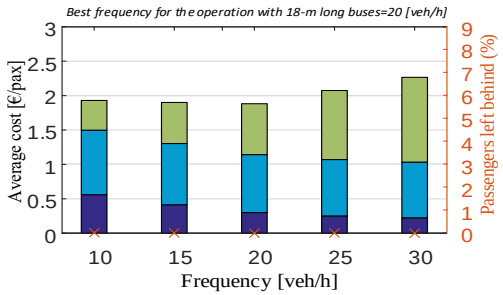

(iv) vehicle size: 18 m

Scenario: AV,ST,WC

Optimal solution: bus size=15 m with frequency=21 [veh/h]

(d) AV,ST,WC

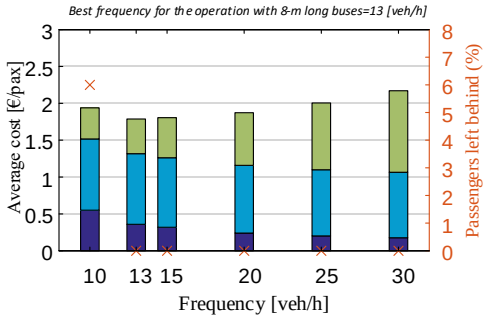

(i) vehicle size: 8 m

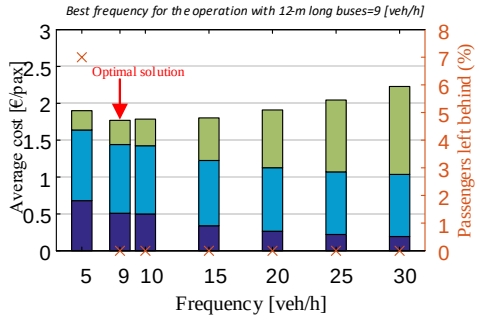

(ii) vehicle size: 12 m

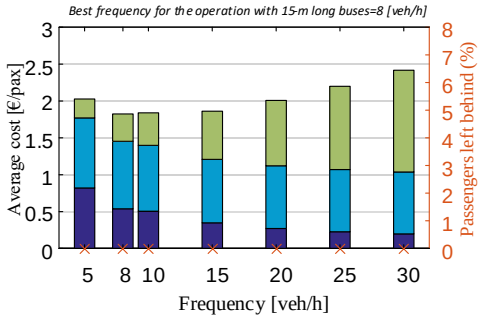

(iii) vehicle size: 15 m

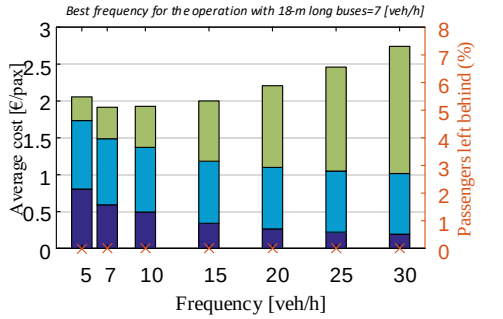

(iv) vehicle size: 18 m

Scenario: HV,DT,WOC

Optimal solution: bus size=12 m with frequency=9 [veh/h]

(e) HV,DT,WOC

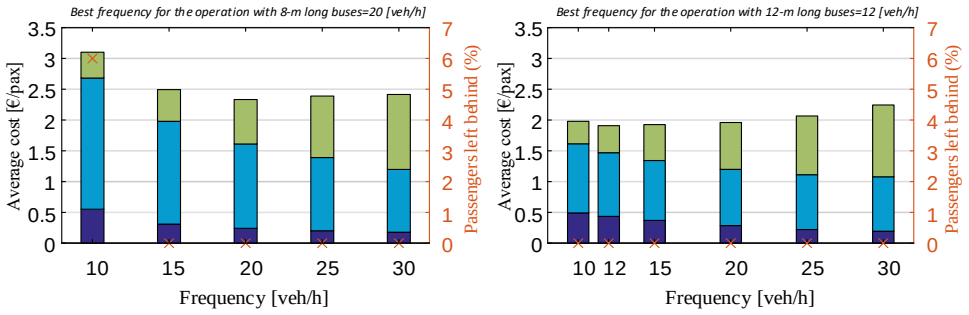

(i) vehicle size: 8 m (ii) vehicle size: 12 m

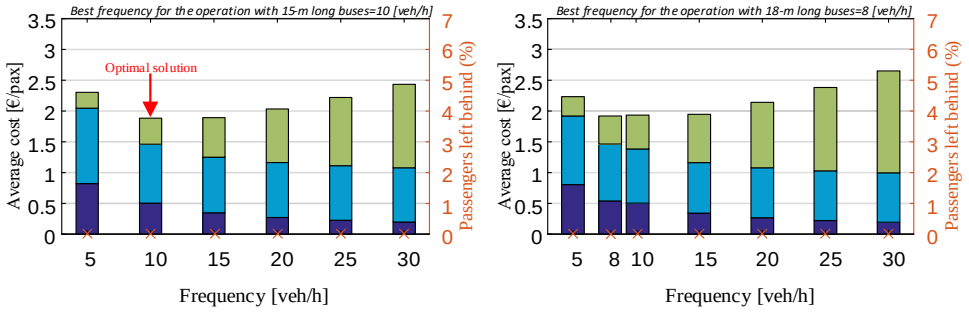

(iii) vehicle size: 15 m (iv) vehicle size: 18 m

Scenario: HV,DT,WC

Optimal solution: bus size=15 m with frequency=10 [veh/h]

(f) HV,DT,WC

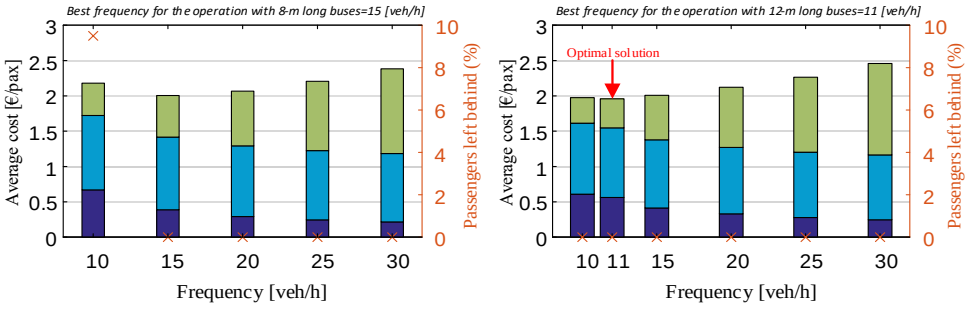

(i) vehicle size: 8 m (ii) vehicle size: 12 m

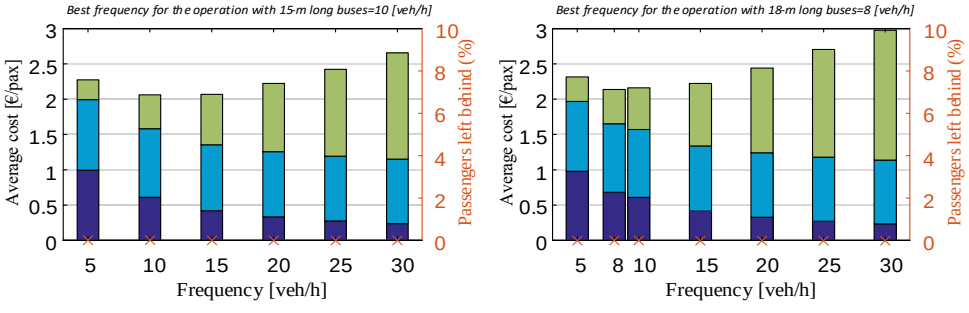

(iii) vehicle size: 15 m (iv) vehicle size: 18 m

Scenario: HV,ST,WOC

Optimal solution: bus size=12 m with frequency=11 [veh/h]

(g) HV,ST,WOC

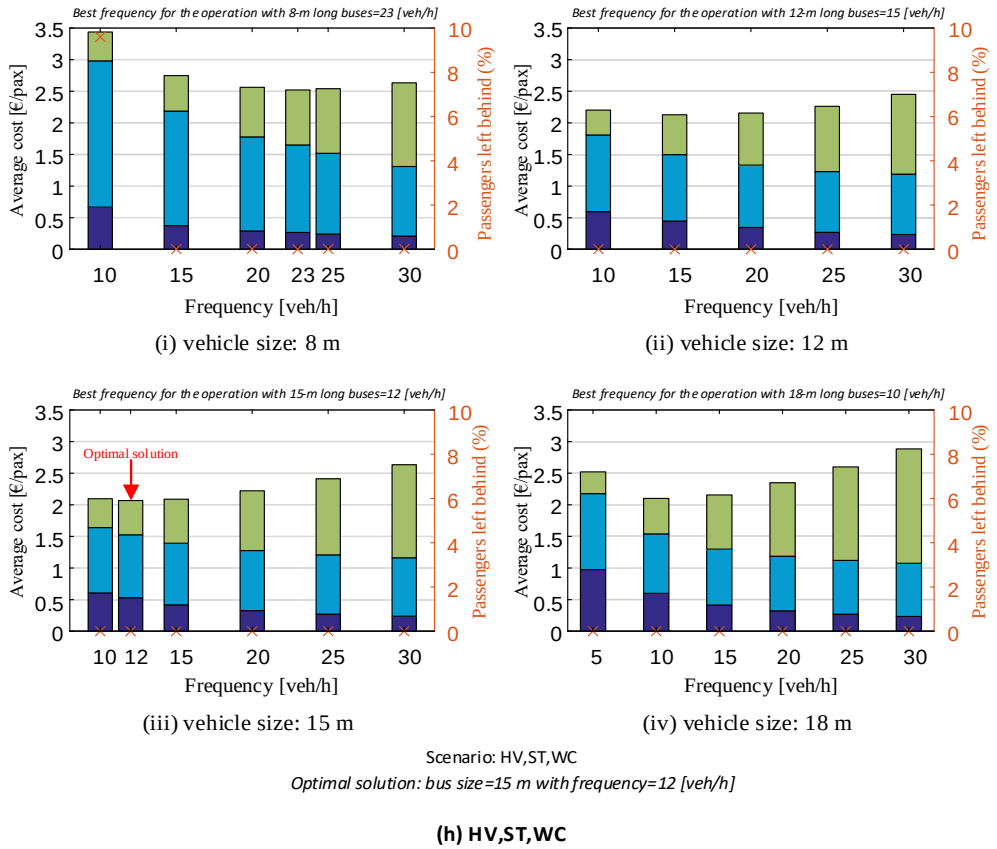

Figure 5-2 Comparison of cost elements for all scenarios with changes in frequencies and vehicle sizes (optimal vs. non-optimal deployment solutions), Regensburg case study.

5.1.3 The effects of automation on denied boarding

In this part, we examine the effects of automation on eliminating or reducing denied boardings. Given the high value of extra waiting time savings (Cats and Jenelius, 2018), the social costs of a public transportation service can climb dramatically if this problem is not effectively addressed, particularly on crowded bus corridors, such as the illustrative example of Santiago in our dissertation.

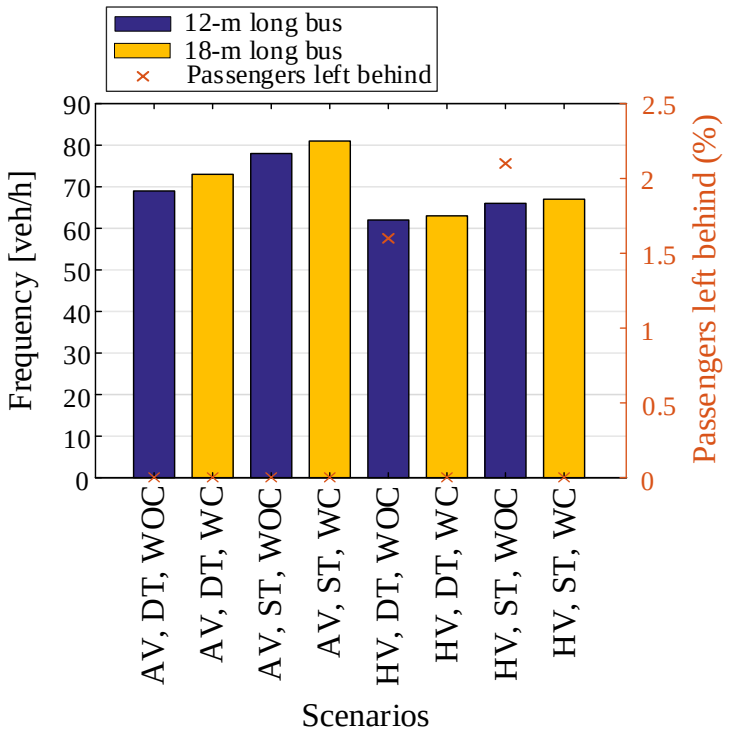

Figure 5-3 Denied boardings in different scenarios, Santiago case study.

For the case of Santiago, Fig. 5-3 shows the shares of passengers being left behind under the optimal solutions (optimal frequency and bus size). Buses are dispatched frequently enough under the optimal solutions, so that travelers are able to board the first arriving service. Nevertheless, the percentage of passengers failing to board is not zero in deployment scenarios of HV, DT, WOC (1.6% of denied boardings) and HV, ST, WOC (2.1% of denied boardings), both of which belong to human-driven vehicle fleet operations (HV), without consideration of crowding as increasing the value of travel time savings (WOC). In essence, in these two scenarios, the optimal frequency does not completely eliminate left-behind passengers, although the shares of passengers failing to board (1.6% and 2.1%) are relatively low. More precisely, in both scenarios, the user cost is insensitive to in-vehicle crowding levels, implying that the crowding cost component has no effect on pushing the optimal solution toward higher frequency levels in the favor of users. Besides, the human-driving cost plays a role against the increase of frequency. Overall, the high value of waiting time savings pushes the optimal deployment solutions toward the provision of sufficiently frequent services to properly meet passenger demand.

Enhancing service frequency is the most common way to mitigate rush-hour crowding effects (An et al., 2020). As indicated in Fig. 5-3, there are no passengers left behind in the

operations of automated bus services, explained by the fact that automated vehicles can be optimally operated at higher frequencies with lower operating costs, thereby providing an unprecedented opportunity for public transport operators to efficiently counteract crowding-related problems in high-demand corridors, in which the multiple manifestations of crowding externalities (denied boarding, seat availability, on-board passenger discomfort) are more prominent.

5.2 Numerical experiments and application of electric bus planning model

5.2.1 Case study characteristics

Our EB modeling framework is tested on a real bus route in Santiago, Chile, on bus route 506. This is a long bi-directional route that connects the east and west parts of the city (see the route map in Fig. 5-4), covering 84 bus stops per direction. This route exhibits a positive slope when moving from west to east in the upstream direction (when moving from terminal A to B), due to the proximity of the Andes Mountain Range, which is a natural barrier limiting the city's growth, close to terminal B in Fig. 5-4. Conversely, the opposite trend is observed when moving from terminal B to A. Besides, the distance between the depot and the original station A is short (1.8 km) and has a nearly flat gradient (+0.1%). We simulate several scenarios of operations on this route to illustrate the results and provide insights for management.

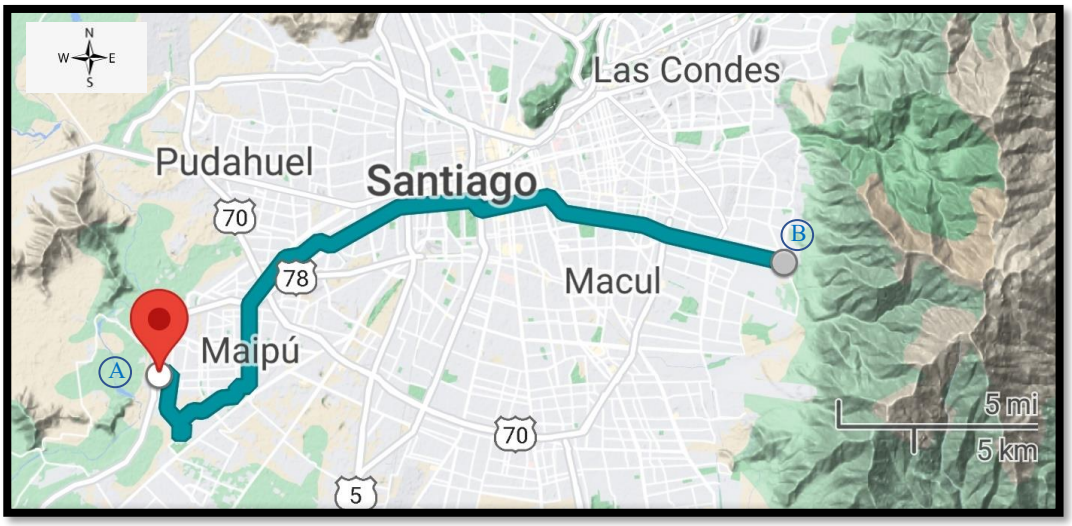

Figure 5-4 Test corridor, bus route 506 in Santiago.

Regarding the passenger demand, a total hourly demand of 3133 (pax/h) for route 506 is averagely served during the morning peak on normal weekdays in April 2019. This data is taken from smartcard transactions in Santiago's public transport service, which is accessed through the software ADATRAP, developed at Universidad de Chile in collaboration with Chile's Ministry of Transport. The observed frequency of service was 15 bus/h; 8 of these vehicles are articulated 18-m long buses and 7 vehicles are standard 12-m long buses.

In the base scenarios, our experiments are simulated and solved for a 3-h period, from 7:00 to 10:00 AM during the morning peak hours. Input parameters are given in Appendix A (Tables A1 and A3). The cost parameters have been calculated by Tirachini and Antoniou (2020) based on EB operations in Santiago.

5.2.2 Solution results

For the numerical applications of our model in Santiago, two common types of EBs are considered as candidates, including 12-m standard (rigid) and 18-m articulated buses, which are widely used EBs in real-world applications in large cities such as Santiago. Moreover, regarding the allowable frequency range, the lower and upper bounds ($f_{\min}$ and $f_{\max}$) are exogenously defined as 5 and 60 (veh/h) respectively (i.e., $f \in \{5, 6, 7, \dots, 59, 60\}$ [veh/h]).

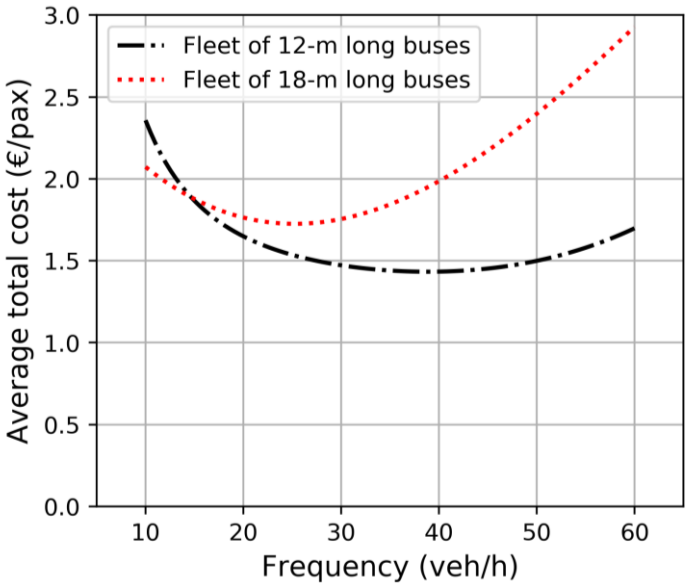

Figure 5-5 Results of the full enumeration approach.

As shown in Fig. 5-5, the FE approach yields the following results:

- In the first scenario, the optimal frequency level for a fleet of 12-m EBs is 38 [veh/h], which leads to the lowest average total cost of 1.44 (€/pax).
- In the second scenario, the optimal frequency level for a fleet of 18-m EBs is 27 [veh/h], which leads to the lowest average total cost of 1.69 (€/pax).

Thus, the global optimum solution is achieved by using a fleet of 12-m long buses with a frequency level of 38 (veh/h)[1]. To further analyze the economic aspects of the proposed solution, Section 5.2.3 presents a detailed analysis of the behavior of different cost elements and their impact on the overall cost.

All computations are performed on a PC with a Core i5, 3.20 GHz CPU, and 6 GB of RAM. The FE approach requires 9.66 and 9.14 (min) to explore the first and second scenarios, respectively, indicating that it can solve the problem in less than 20 minutes.

In addition, the GA suggests the same optimal solution as the FE approach: operating with a fleet of 12-m EBs at a frequency of 38 (veh/h). To assess the GA's performance, we run the GA 10 times, and it consistently identifies the same optimal solution in all 10 runs, demonstrating its stability. Additionally, the GA requires an average CPU time of 1.4 min.

5.2.3 Cost analysis

To gain a deeper understanding of the trade-offs involved in the proposed problem, we present the average cost values (per passenger) for different cost elements in Fig. 5-6, for the optimal bus size solution (12 meters). As expected, increasing the frequency of bus service reduces user costs, due to reductions in waiting times and bus dwell times at bus stops. Besides, an adequate level of frequency can reduce or eliminate the problem of being unable to board because of capacity limitations. However, as shown in Fig. 5-6, there is a considerable rise in user costs at low levels of frequency, primarily due to the extra waiting time experienced by passengers who fail to board due to overcrowding. For example, if vehicles are operated at a frequency of 10 (veh/h) on such a high-demand bus corridor, about 64% of passengers are confronted with capacity limitations in boarding the first coming service and will need to wait

[1] It is worth noting that our optimal solutions provide larger frequencies than the observed frequency (15 bus/h) in route 506, which is a common result when including user cost (waiting and in-vehicle time) in a total cost frequency setting problem, as shown by Jansson (1980) and Jara-Díaz and Gschwender (2003). In other words, the explicit consideration of the time of users in the total cost function to be minimized, leads to a more frequent service of smaller vehicles, mainly to reduce waiting times.

for the subsequent services. As discussed in Section 3.2.1, the monetary value of additional waiting time is more expensive than that of initial waiting time due to its more significant negative impact on user satisfaction. Thus, such additional waiting times can significantly increase the social costs and reduce the desirability of a public transport system.

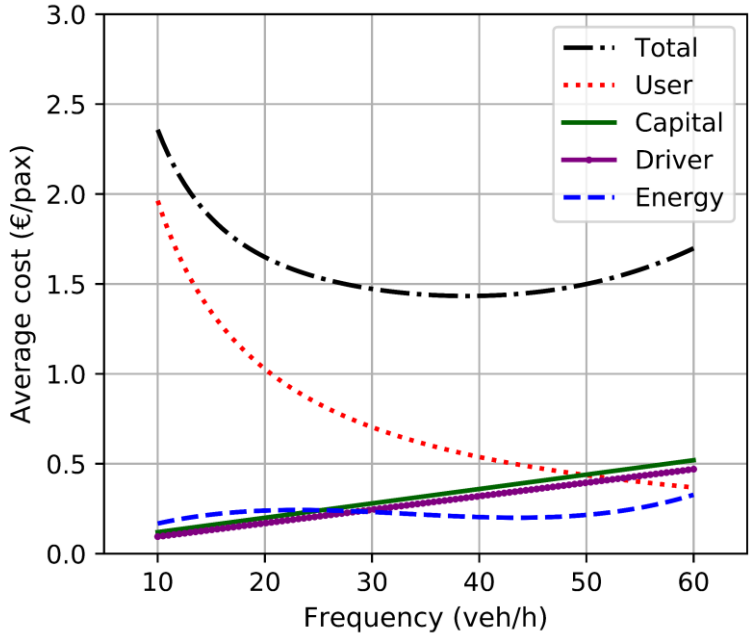

Figure 5-6 Cost element values at different levels of frequency.

As the frequency increases, the capital and driving costs increase due to the need for a larger fleet size with more vehicles and drivers. On the other hand, the energy cost exhibits a non-monotonic pattern, with two turning points where the trend changes from increasing to decreasing and vice versa. The first turning point is observed at around a frequency of 20, after which the average energy cost decreases until the second turning point where it increases again.

The initial ascending trend in the energy cost graph (before the first turning point) is attributed to the high payload carried by the vehicles when operating at full capacity. In such a busy bus corridor with a demand of 3133 (passengers/h), vehicles need to operate at maximum capacity if an insufficient frequency of 10 (veh/h) is implemented for operations. Consequently, vehicles carry the maximum passenger load (about 8 tons), resulting in higher energy consumption. Moreover, a significant percentage of passengers (about 60%) are left behind at this frequency level. To tackle this issue, increasing the frequency from 10 to 20 (veh/h) reduces the number of left-behind travelers but does not eliminate the problem

entirely, as the supply level (from the operator side) is not still sufficient to cover passenger flows. That is, vehicles continue to operate at near-full capacity (without a significant reduction in vehicles' passenger load). In addition, constant energy demand is consumed inside each vehicle for auxiliary facilities (such as air conditioners, heating, and in-vehicle displays). Hence, the average energy cost still increases until the frequency of 20 (veh/h).

After the first turning point, the energy cost experiences a decline mainly driven by the reduction in passenger load carried by vehicles during operations. Essentially, the crowding-related issues (due to full capacity operations) are reduced after that crucial point, where the balance of supply to demand is achieved. That is, vehicles do not have to run at crush capacity (occupancy rate of 100%) after that point. Thus, we find that such an equilibrium state between supply and demand is not only beneficial for users (e.g., by reducing passenger waiting times and reducing/eliminating denied boardings) but also for bus agencies due to EB energy savings. As shown after that point (in Fig. 5-6), the increase of service frequency will reduce user and energy costs, whereas capital and driving costs increase due to deploying a higher number of vehicles and drivers. Nonetheless, from a social welfare perspective, there is a greater potential for user and energy cost savings up to certain levels, which can counterbalance the total costs. Therefore, the minimum total cost is found around the frequency of 38 (veh/h)[2].

Finally, we see that the energy cost increases again after passing the second turning point (around the frequency of 43) towards the end of the graph. In other words, after a certain level, the addition of further vehicles can again lead to an increase in energy consumption. This can be attributed to multiple factors influencing energy consumption. For instance, a lasting part of the energy consumption is related to the power required for running auxiliary HVAC facilities and for propelling the constant curb weight of vehicles, leading to permanent tractive energy consumption during operating hours. Hence, at these non-optimal levels, a large number of vehicles are running along the route with occupancies far below capacities, while consuming energy for running auxiliary services. This outweighs the reduced crowding effect and increases the energy consumption per passenger.

In Fig. 5-7, we show the average costs for the optimal frequency as a function of demand. Previous studies have found the existence of economies of scale (i.e., average costs decreasing

[2] It should be noted that 38 (veh/h) is indeed a high level of frequency in reality, where special requirements are usually needed to control such crowded bus routes and avoid bus bunching issues. Typically, bus operators need to execute real-time bus control (regulation) strategies (such as holding strategies) to maintain and handle such short headways between vehicles, which is not the scope of this work (see Tirachini et al., 2022 for more information).

as a function of demand) for both operators and users, either with diesel buses (e.g., Allport, 1981) or with EBs under the assumption of a fixed energy consumption level per veh-km (Tirachini and Antoniou, 2020). Interestingly, we see that in our model average costs decrease as a function of demand, indicating the presence of economies of scale in any case, even though the energy consumption cost is not monotonic as a function of the service frequency (Fig. 5-6).

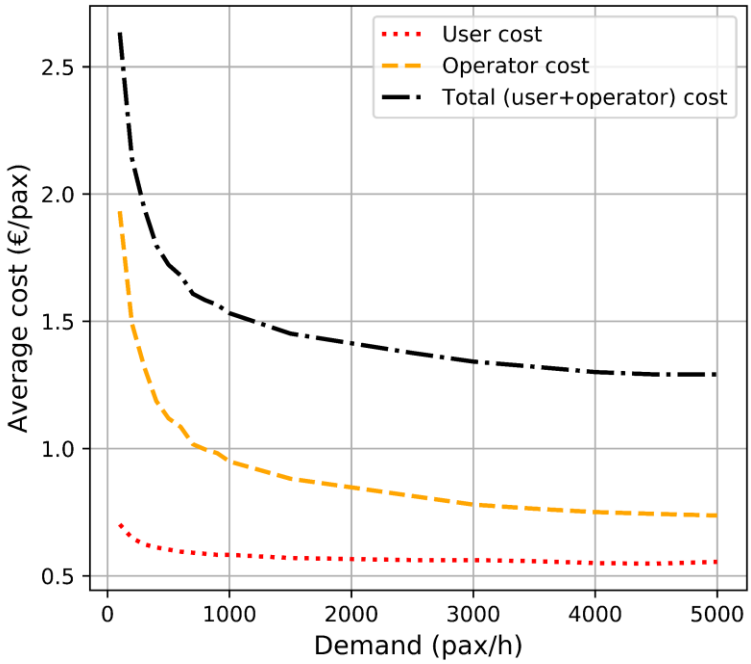

Figure 5-7 Average costs as a function of demand.

5.2.4 Variable vs. fixed energy consumption

As discussed in the literature review, previous studies on EB scheduling problems have mainly relied on a simplified fixed energy consumption rate per distance unit (kWh/km), while neglecting actual variations in driving and route conditions (such as variations in passenger loads and route gradients). In this dissertation, we compare the solutions obtained from fixed energy consumption rates to those obtained from our variable (microscopic) energy assessment framework. By doing so, we determine the loss of accuracy that arises from using a rough rate instead of a detailed modeling of energy consumption, and how this affects the total costs involved.

To carry out this comparison, we employ simplified fixed energy consumption rates calculated by Tirachini and Antoniou (2020) for different sizes of EBs, including 1.0 and 1.7 kWh/km for 12-m and 18-m EBs, respectively. As shown in Fig. 5-8, our results show that fixed energy consumption rates result in smaller optimal frequencies compared to detailed energy demand cases. For instance, for a fleet of 12-m long vehicles, the optimal frequency is underestimated by about 13% (33 vs. 38 veh/h) using fixed energy consumption rates.

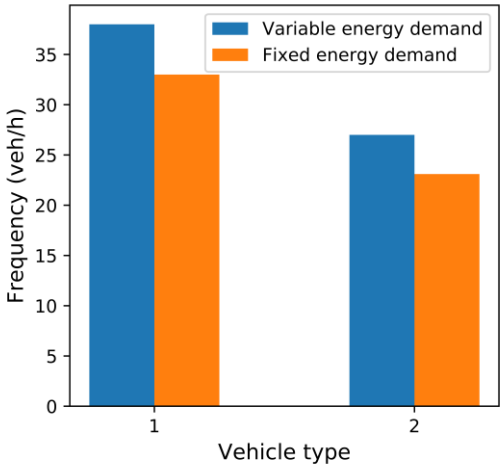

Figure 5-8 Optimal frequencies under the variable vs. fixed estimation of energy consumption[3].

5.2.5 Variations in energy consumption rates along the route

To better illustrate the variations in energy demand pattern, we estimate the average energy consumed by vehicles per kilometer (kWh/km) using our detailed energy model and show the results for different segments in Fig. 5-9. The total average energy demand over the entire route is estimated to be 1.34 (kWh/km), which is 34% higher than the simplified fixed energy rate of 1.00 (kWh/km) used in Tirachini and Antoniou (2020). We observe a significant increase in energy consumption at certain segments of the route, e.g., at segments 48-64 which are located near the central part of the city. This increase can be attributed to two main reasons: (i) a larger passenger demand is served at bus stops in that area, resulting in a higher passenger load carried by the vehicles; (ii) bus speed is reduced due to higher traffic congestion levels at those segments.

[3] The term 'Variable' refers to the scenarios in which our detailed energy consumption model, which considers the actual operating and route conditions, is used. The term 'Fixed' refers to the scenarios that consider fixed energy consumption rates (1.0 or 1.7 kWh/km) without considering the actual changes in operating and route conditions.

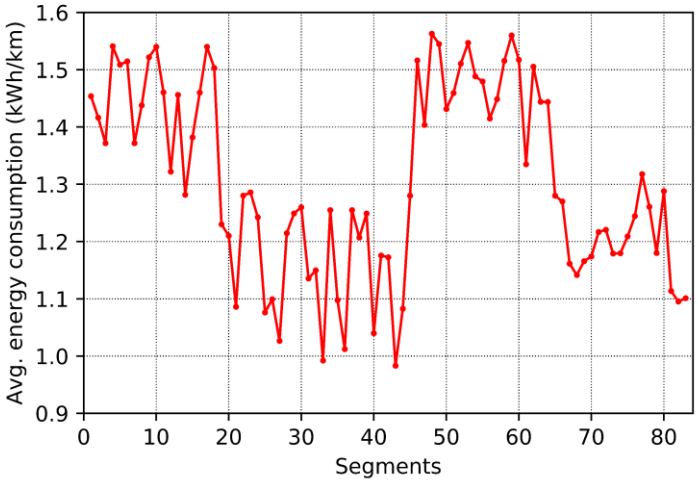

(a) Energy consumption at different segments of the route.

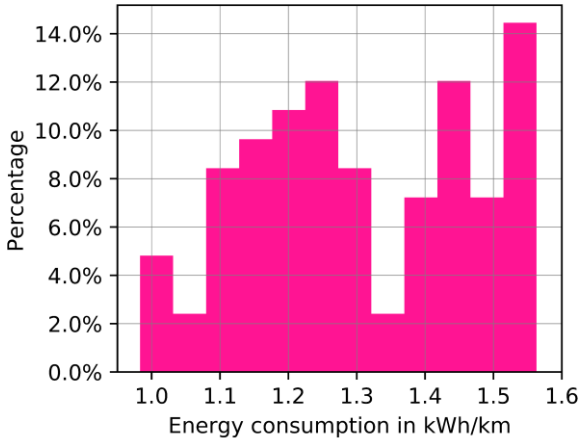

(b) Histogram of energy consumption range.

Figure 5-9 Energy consumption pattern.

5.2.6 Planning solutions with high-resolution average energy consumption rate

We compare planning solutions based on a high-resolution average energy consumption rate of 1.34 (kWh/km) with those obtained from our detailed variable energy estimation model, which allows for detailed tracking of energy usage. Interestingly, both scenarios yielded the same frequency answers, indicating that while precise energy estimations are necessary for accurate supply decisions, a high-resolution average energy consumption rate, 1.34 (kWh/km), could serve as a suitable alternative for planning purposes, rather than the simplified fixed value of 1.00 (kWh/km) used in literature, which lacks local slope and demand information. However, further network-level studies are needed to assess the applicability of such an approach to a group of routes with varying demand patterns and geometric properties.

Clustering routes based on their energy demand patterns could be a useful strategy to streamline the planning process and reduce computing efforts.

5.3 Results of decision making framework for electric bus charging strategy selection

5.3.1 Results of weighting criteria

Table 5-2 presents fuzzy weights and standard deviations for the five criteria at the main level. Besides, the number of times each criterion was chosen by experts as the best and worst criterion is indicated. The results indicate a strong consensus among experts about the best and worst criterion, with a clear preference for the economic aspect as the best criterion (by 8 experts), while the social aspect was selected as the worst criterion (by 10 experts). Besides, the consistency ratio of pairwise comparisons is displayed in the CR column.

Based on the experts' assessments, the economic aspect holds the highest significance, followed by the operational and environmental aspects. This can be related to the significant investments needed to electrify urban bus networks depending on the type of charging strategies deployed. The social criterion is identified as the least important criterion among the others. The fuzzy weight of each criterion is depicted in Fig. 5-10. The consistency ratio is very close to zero ($CR = 0.036$), indicating a very high consistency.

Table 5-2 Weights of the criteria in the first level.

Criteria	Fuzzy weight	Crisp weight	Standard deviation	Rank	Times of selection as the best criterion	Times of selection as the worst criterion	CR
Economic	(0.272,0.303,0.334)	0.303	0.032	1	8	0	0.036
Environmental	(0.177,0.209,0.249)	0.211	0.061	3	0	0	
Social	(0.088,0.093,0.102)	0.094	0.02	5	0	10	
Operation	(0.179,0.21,0.246)	0.211	0.062	2	2	0	
Quality of service	(0.153,0.181,0.216)	0.182	0.062	4	1	1	

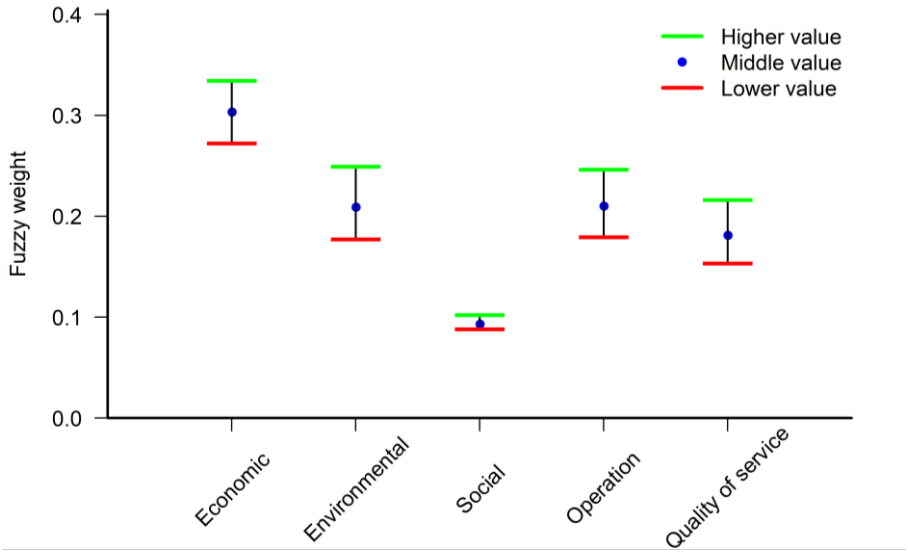

Figure 5-10 Fuzzy weights of the criteria in the first level.

5.3.2 Economic

As presented in Fig. 3-6, there are two levels, the second and third levels, for the economic sub-criteria. In the following, the weights obtained for the sub-criteria of each level are reported.

- **Second level of economic criteria**

The weights of the economic sub-criteria in the second level are shown in Table 5-3. According to the results, the experts consider the infrastructure cost criterion as the most significant factor within the economic category at the second level (see Table 5-3). This can be attributed to the high costs associated with deploying charging infrastructure and technology for EBs, including charging equipment and land acquisition, which can directly impact the overall costs and profitability of EB systems.

Table 5-3 Weights of the economic sub-criteria in the second level.

Criteria	Fuzzy weight	Crisp weight	Standard deviation	Rank	Times of selection as the best criterion	Times of selection as the worst criterion	CR
Battery cost	(0.296,0.333,0.394)	0.337	0.135	2	4	3	0.067
Infrastructure cost	(0.322,0.367,0.438)	0.371	0.105	1	5	0	
Operational cost	(0.272,0.29,0.318)	0.292	0.168	3	2	8	

- **Third level of economic criteria**

Table 5-4 shows the weights of the economic sub-criteria at the third level in relation to the infrastructure and operational components. As can be seen, the land acquisition cost and battery replacement cost were identified as the most important sub-criterion for infrastructure cost and operational cost, respectively.

Table 5-4 Weights of the economic sub-criteria in the third level.

Criteria	Sub-criteria	Fuzzy weight	Crisp weight	Standard deviation	Rank	Times of selection as the best criterion	Times of selection as the worst criterion	CR
Infrastructure cost	Charging equipment cost	(0.377,0.405,0.444)	0.407	0.161	2	2	9	0.022
	Land acquisition cost	(0.556,0.589,0.647)	0.593	0.162	1	9	2	
Operational cost	Labor cost	(0.19,0.224,0.262)	0.225	0.104	3	1	4	0.054
	Electricity tariff	(0.244,0.283,0.328)	0.284	0.109	2	5	2	
	Battery replacement cost	(0.262,0.297,0.339)	0.299	0.109	1	4	1	
	Maintenance cost	(0.162,0.191,0.23)	0.192	0.059	4	1	4	

5.3.3 Environmental

The weights of the sub-criteria in the second level of the environmental category are shown in Table 5-5. The experts identify the GHG emission as the most significant sub-criteria in the environmental category, followed by energy consumption and ecological environment impacts (see Table 5-5).

Table 5-5 Weights of the environmental sub-criteria in the second level.

Criteria	Fuzzy weight	Crisp weight	Standard deviation	Rank	Times of selection as the best criterion	Times of selection as the worst criterion	CR
GHG emission	(0.215,0.245,0.277)	0.245	0.061	1	5	0	0.036
Energy consumption	(0.185,0.211,0.239)	0.211	0.048	2	5	0	
Environmental pollution after demolition	(0.114,0.141,0.181)	0.143	0.032	4	0	1	
GHG emissions for battery production	(0.107,0.132,0.168)	0.134	0.033	5	0	0	
Water consumption in battery production	(0.08,0.089,0.105)	0.09	0.025	6	0	9	
Ecological environment impacts	(0.147,0.174,0.216)	0.176	0.066	3	1	1	

5.3.4 Social

The weights of the sub-criteria in the second level of the social category are shown in Table 5-6. Charging infrastructures' impacts on surrounding residential areas is selected as the most significant factor in this category. In addition, there is a slight difference between the job opportunity and the city landscape sub-criteria, recognized as the second and third most important sub-criteria.

Table 5-6 Weights of the social sub-criteria in the second level.

Criteria	Fuzzy weight	Crisp weight	Standard deviation	Rank	Times of selection as the best criterion	Times of selection as the worst criterion	CR
Job opportunity	(0.216,0.256,0.297)	0.256	0.097	2	2	2	0.030
Fire risk	(0.177,0.189,0.208)	0.19	0.142	4	2	7	
Charging infrastructures' impacts on surrounding residential areas	(0.257,0.296,0.341)	0.297	0.097	1	5	0	
City landscape	(0.217,0.255,0.297)	0.256	0.083	3	2	2	

5.3.5 Operation

Table 5-7 presents the weight values obtained for the sub-criteria in the operation category. According to the results, the driving range is identified as the most crucial sub-criteria in this category, followed by charging duration and energy monitoring (see Table 5-7).

Table 5-7 Weights of the operation sub-criteria in the second level.

Criteria	Fuzzy weight	Crisp weight	Standard deviation	Rank	Times of selection as the best criterion	Times of selection as the worst criterion	CR
Vehicle capacity	(0.119,0.134,0.157)	0.135	0.058	5	1	6	0.035
Energy monitoring	(0.132,0.157,0.192)	0.158	0.053	3	0	2	
Driving range	(0.253,0.287,0.323)	0.288	0.06	1	5	0	
Charging duration	(0.239,0.272,0.309)	0.272	0.068	2	4	0	
Scheduling complexity	(0.127,0.146,0.168)	0.146	0.055	4	1	3	

5.3.6 Quality of service

The weights of the sub-criteria in the quality-of-service category are presented in Table 5-8. Reliability is identified as the most influential sub-criteria in this category.

Table 5-8 Weights of the quality-of-service sub-criteria in the second level.

Criteria	Fuzzy weight	Crisp weight	Standard deviation	Rank	Times of selection as the best criterion	Times of selection as the worst criterion	CR
Crowding	(0.166,0.182,0.215)	0.185	0.06	3	0	8	0.019
Travel time	(0.33,0.37,0.423)	0.372	0.116	2	4	2	
Reliability	(0.405,0.441,0.487)	0.443	0.125	1	7	1	

5.3.7 Global ranking of criteria

The extracted criteria were organized into different levels, as shown in Fig. 3-6. The local weight for each level was determined through the methods described in previous sections. In this part, to compute the global weight of each sub-criterion in the final level of each category, its local weight is multiplied by the weight of the category it belongs to. Having determined the global weight of the criteria, the overall score of the alternatives can be computed. As indicated in Table 5-9, the experts consider battery cost to be the most important factor when evaluating charging strategy alternatives, followed by reliability, travel time, land acquisition cost, and driving range. Besides, Fig. 5-11 displays a bar chart of the crisp weights of the sub-criteria.

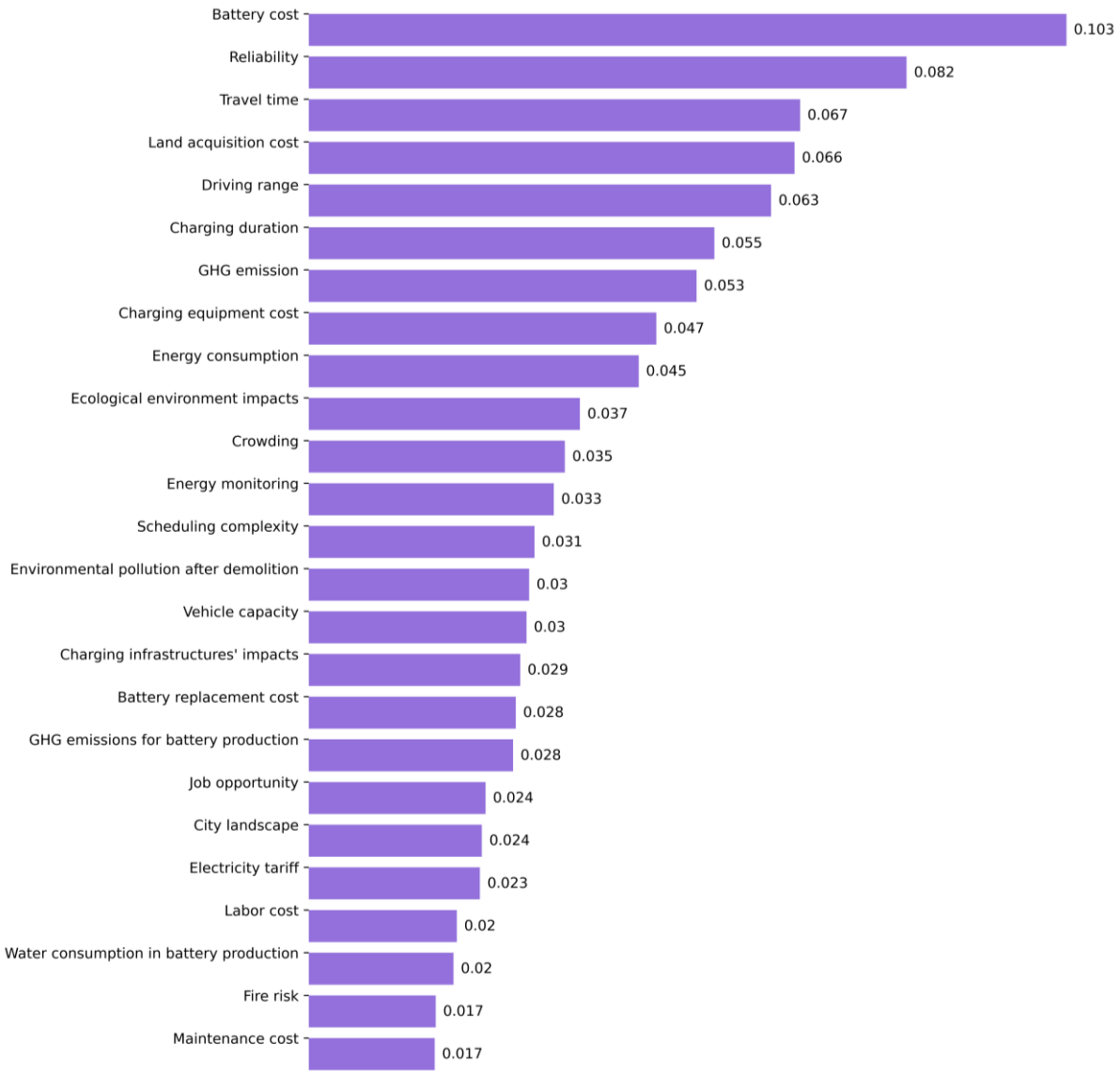

Figure 5-11 Crisp weights of the sub-criteria.

Table 5-9 Global weights of the sub-criteria.

Row	Criteria	Weight	Rank
1	Battery cost	(0.081,0.102,0.133)	1
2	Charging equipment cost	(0.033,0.046,0.067)	8
3	Land acquisition cost	(0.048,0.064,0.093)	4
4	Labor cost	(0.014,0.02,0.028)	22
5	Electricity tariff	(0.017,0.023,0.032)	21
6	Battery replacement cost	(0.022,0.028,0.037)	17
7	Maintenance cost	(0.012,0.017,0.024)	25
8	GHG emission	(0.039,0.052,0.07)	7
9	Energy consumption	(0.033,0.044,0.06)	9
10	Environmental pollution after demolition	(0.02,0.029,0.045)	15
11	GHG emissions for battery production	(0.018,0.027,0.041)	18
12	Water consumption in battery production	(0.014,0.019,0.027)	23
13	Ecological environment impacts	(0.025,0.036,0.054)	10
14	Job opportunity	(0.019,0.024,0.031)	19
15	Fire risk	(0.015,0.017,0.021)	24
16	Charging infrastructures' impacts on surrounding residential areas	(0.023,0.028,0.036)	16
17	City landscape	(0.019,0.023,0.03)	20
18	Vehicle capacity	(0.023,0.029,0.039)	14
19	Energy monitoring	(0.023,0.033,0.047)	12
20	Driving range	(0.047,0.062,0.082)	5
21	Charging duration	(0.04,0.054,0.074)	6
22	Scheduling complexity	(0.022,0.03,0.041)	13
23	Crowding	(0.026,0.034,0.048)	11
24	Travel time	(0.049,0.066,0.09)	3
25	Reliability	(0.062,0.08,0.106)	2

5.3.8 Results of ranking charging alternatives

5.3.8.1 Results of FRAFSI method

As mentioned before, the FRAFSI method is used to evaluate and rank alternative EB charging strategies for EB systems in Munich based on the defined criteria. The results of the expert evaluations indicate a preference for the overnight charging method over the opportunity charging method, as illustrated in Fig. 5-12. In addition, Fig. 5-13 highlights the relative superiority of each alternative in each criterion. The most prominent differences between the

two alternatives can be seen in terms of charging duration, battery cost, and reliability (see Table 5-10). However, minor differences can be seen in terms of vehicle capacity and charging infrastructures' impacts on surrounding residential areas.

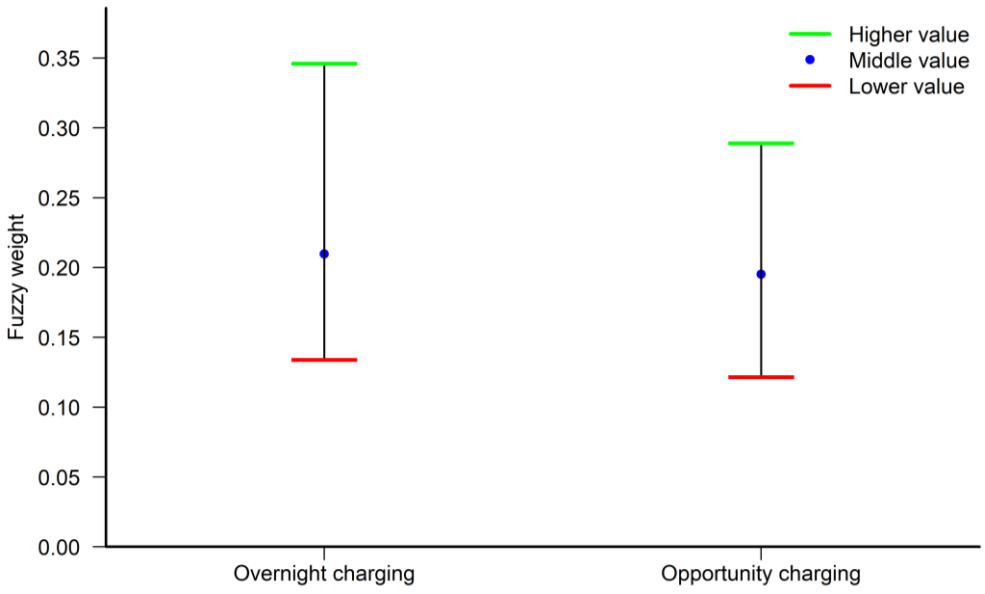

Figure 5-12 Fuzzy weights of alternatives.

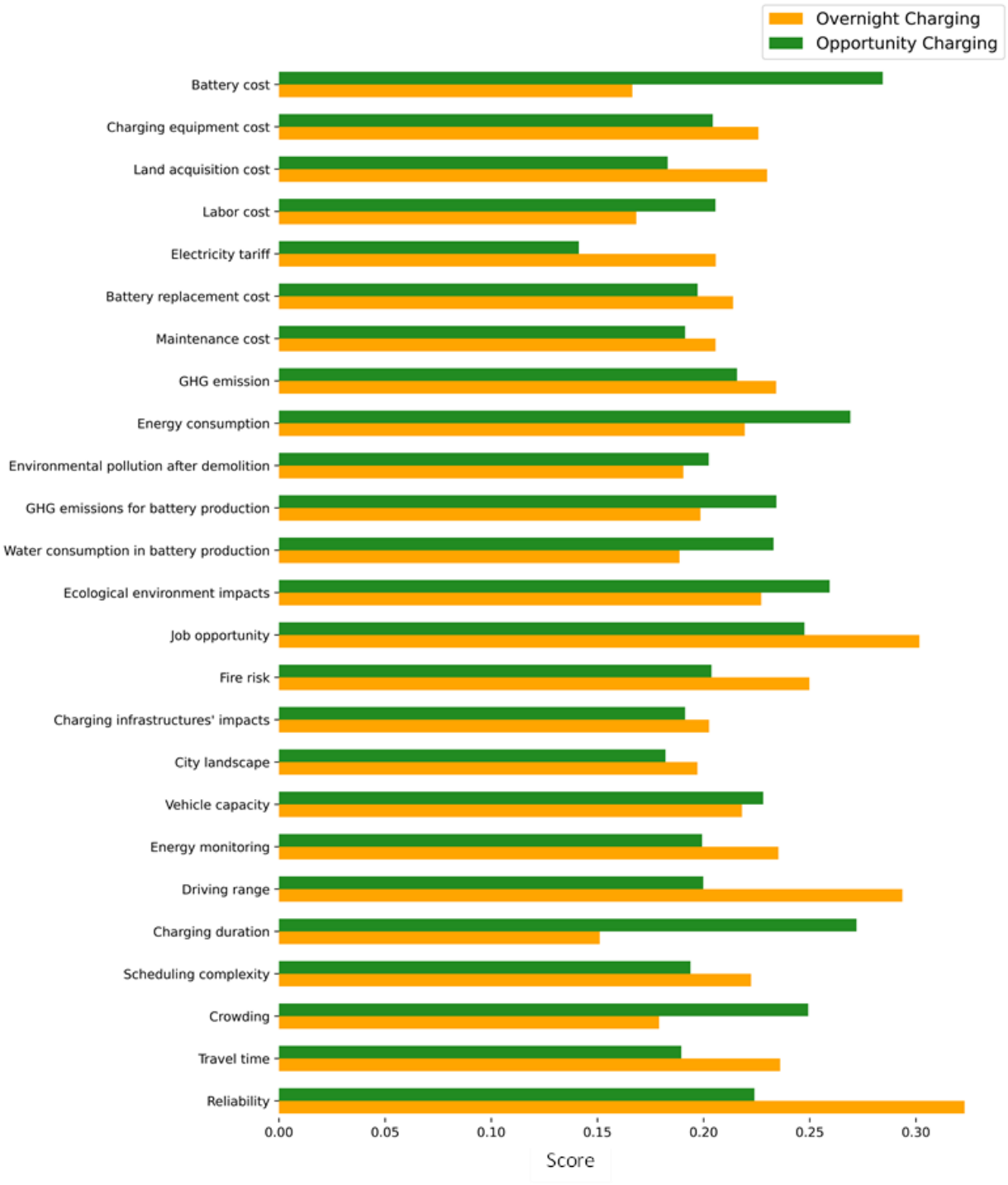

Figure 5-13 Comparing the scores of two alternatives in terms of each criterion.

Table 5-10 The scores of two alternatives in terms of each criterion.

Row	Criteria	Overnight Charging	Opportunity Charging	Difference	Rank
1	Battery cost	(0.146,0.165,0.192)	(0.209,0.285,0.358)	0.118	2
2	Charging equipment cost	(0.182,0.222,0.286)	(0.169,0.202,0.25)	0.022	18
3	Land acquisition cost	(0.192,0.227,0.28)	(0.152,0.181,0.223)	0.047	9
4	Labor cost	(0.144,0.167,0.198)	(0.167,0.203,0.256)	0.037	13
5	Electricity tariff	(0.17,0.203,0.252)	(0.124,0.14,0.162)	0.064	6
6	Battery replacement cost	(0.177,0.211,0.262)	(0.164,0.195,0.24)	0.017	20
7	Maintenance cost	(0.171,0.203,0.25)	(0.161,0.189,0.23)	0.014	22
8	GHG emission	(0.19,0.231,0.292)	(0.176,0.212,0.269)	0.018	19
9	Energy consumption	(0.185,0.221,0.248)	(0.207,0.263,0.357)	0.05	8
10	Environmental pollution after demolition	(0.169,0.189,0.217)	(0.174,0.198,0.248)	0.012	23
11	GHG emissions for battery production	(0.172,0.199,0.222)	(0.194,0.227,0.304)	0.036	14
12	Water consumption in battery production	(0.167,0.187,0.215)	(0.189,0.229,0.292)	0.044	12
13	Ecological environment impacts	(0.194,0.225,0.27)	(0.205,0.254,0.334)	0.032	16
14	Job opportunity	(0.259,0.302,0.344)	(0.204,0.248,0.291)	0.054	7
15	Fire risk	(0.203,0.246,0.312)	(0.169,0.201,0.25)	0.046	11
16	Charging infrastructures' impacts on surrounding residential areas	(0.168,0.2,0.248)	(0.16,0.189,0.231)	0.011	24
17	City landscape	(0.164,0.195,0.24)	(0.153,0.18,0.219)	0.015	21
18	Vehicle capacity	(0.174,0.218,0.261)	(0.186,0.228,0.27)	0.01	25
19	Energy monitoring	(0.187,0.23,0.303)	(0.166,0.197,0.242)	0.036	15
20	Driving range	(0.252,0.294,0.335)	(0.157,0.2,0.242)	0.094	4
21	Charging duration	(0.134,0.15,0.172)	(0.193,0.271,0.354)	0.121	1
22	Scheduling complexity	(0.18,0.218,0.28)	(0.162,0.192,0.234)	0.029	17
23	Crowding	(0.152,0.177,0.213)	(0.199,0.245,0.317)	0.07	5
24	Travel time	(0.192,0.232,0.297)	(0.156,0.187,0.232)	0.047	10
25	Reliability	(0.28,0.323,0.365)	(0.181,0.224,0.266)	0.099	3

5.3.8.2 Result comparison among different ranking methods

Table 5-11 compares the results from the FRAFSI method with those from two other methods, the fuzzy TOPSIS and fuzzy EDAS. It can be observed that the outcomes of all methods are consistent, with the overnight charging strategy receiving the first rank. The table also reports the number of times each alternative was selected as the best strategy by the experts.

Table 5-11 Comparing the results of different methods when ranking charging strategies.

	Fuzzy TOPSIS		**Fuzzy EDAS**		**FRAFSI**	
	Rank	**Frequency of experts selecting a strategy as the top-ranked**	**Rank**	**Frequency of experts selecting a strategy as the top-ranked**	**Rank**	**Frequency of experts selecting a strategy as the top-ranked**
Overnight charging	1	7	1	8	1	7
Opportunity charging	2	4	2	3	2	4

Fig. 5-14 provides information on the best EB charging strategy identified by each expert under different ranking methods.

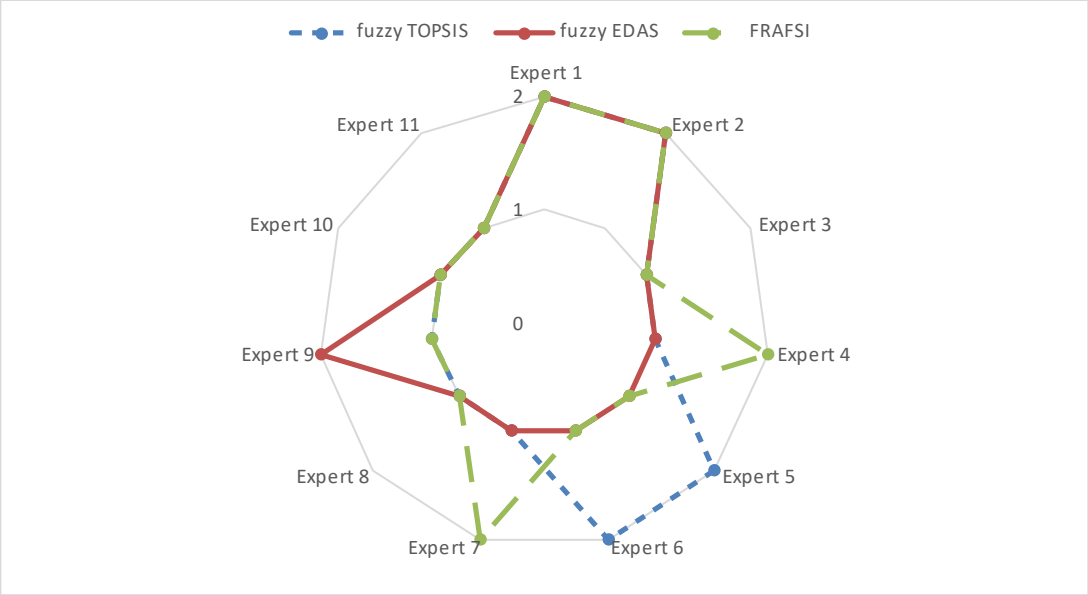

Figure 5-14 Comparing the judgment of experts about the best charging strategy under different ranking methods (numbers 1 and 2 indicate overnight and opportunity charging strategies, respectively).

5.4 Numerical experiments and application of mixed-fleet bus scheduling models

5.4.1 Numerical experiments and application of the simple version of the mixed-fleet bus scheduling model

5.4.1.1 Small and medium-sized test instances

To obtain certain insights about the quality of the solutions found by the SA algorithm, the performance of the SA is evaluated by comparing its results to the optimal solutions obtained through the GAMS software 24.7.1 in solving a set of test problems generated randomly. Indeed, 25 small and medium-sized test problems are randomly prepared with various sizes and features (see Table 5-12), including different number of vehicles (fleet size), buses of each size, and bus stops. The gaps between the best solutions found by the SA algorithm and the optimal solutions obtained by GAMS are computed using Eq. (5-1).

$$GAP=\frac{(SA_{answer}-GAMS_{answer})}{GAMS_{answer}} \times 100 \qquad (5\text{-}1)$$

All the computational experiments are performed on a personal computer with Intel(R) Core(TM) i5-6500 CPU @ 3.20 GHz and 16.0 GB RAM. As can be seen in Table 5-12, the SA has found the optimal solutions in most of the test problems. Furthermore, the maximum gap (0.83%) is observed in instance #21 and is less than 1 percent. Note that the average passenger waiting time (i.e., objective function value) is measured in minutes and the results of the SA and GAMS are compared to each other with two decimals (i.e., 0.01 minute which is less than one second). Indeed, a neglectable gap of 0.83% (between the average waiting times of 1.21 and 1.22 minutes) is even less than one second and passengers do not notice from a practical viewpoint; nonetheless, we have merely provided such results with 2 decimals for research purposes. The computing time required by the SA is always less than 0.5 minutes even for medium test instances. By contrast, the computing times are much more expensive in the case of GAMS, where computation times will increase markedly with a growth of the fleet size. This is due to the fact that the total number of continuous NLP subproblems that needed to be solved using GAMS (in Algorithm 4-5) is increased substantially as a function of $\frac{N_v!}{A! \times B! \times C!}$ that indeed represents the number of possible sequences to dispatch buses in a mixed-fleet dispatching problem (e.g., in instance #25, 560 NLP subproblems are solved consecutively one after another without interruption, due to the existence of 560 possible sequences for dispatching vehicles). This is indeed a great challenge in solving real-life instances, in which a tremendous number of dispatching sequences can be prescribed for a

mixed-fleet operation, e.g., there exist 400,400 possible arrangements for dispatching buses in our real-world example (with $N_v = 16$, $A = 9$, $B = 4$, $C = 3$) presented in the next section. This challenging issue further highlights the importance and application of heuristic optimization algorithms that enable practitioners to discover good suboptimal solutions within a rational computing time for such a complex problem, coping with the difficulty of handling binary variables in large practical instances.

It should be noted that, in all the test problems, the dispatching orders found by the SA are exactly the same as those obtained in the optimal solutions. Indeed, the only difference that leads to such an insignificant gap (0.83% in instance #21) is attributed to a very slight difference (about seconds) in some dispatching times suggested by the SA compared to the optimal results of GAMS. This shows that the capability of SA's operators with their special neighborhood search mechanisms is quite promising, as the designed swapping and inversion operators (in Fig. 4-7) can fruitfully generate a new feasible dispatching order of vehicles through a random displacement of vehicles within the same fleet, thereby enabling the algorithm for a better exploitation of the best solutions in the feasible search space. This prominent feature would be of paramount importance in finding a suitable dispatching arrangement for real-life instances, in which bus operators are practically confronted with numerous dispatching arrangements.

Table 5-12 Computational results of the SA vs. GAMS in solving small and medium instances.

Class	Instance number	Instance features						Objective value			Comp. time (sec)	
		N_s	N_v	A	B	C	NLP*	GAMS	SA	GAP (%)	GAMS	SA
Small	#1	6	3	1	1	1	6	0.24	0.24	0.00	270	7
	#2	6	4	2	1	1	12	0.32	0.32	0.00	1450	14
	#3	6	4	1	2	1	12	0.30	0.30	0.00	1461	13
	#4	6	4	1	1	2	12	0.29	0.29	0.00	1455	14
	#5	8	5	1	1	3	20	0.36	0.36	0.00	3020	16
	#6	8	5	2	2	1	30	0.40	0.40	0.00	3002	15
	#7	8	5	2	1	2	30	0.39	0.39	0.00	3014	15
	#8	10	6	1	4	1	30	0.55	0.55	0.00	4681	17
	#9	10	6	1	1	4	30	0.49	0.49	0.00	4570	15
	#10	10	6	1	3	2	60	0.53	0.53	0.00	9365	17
	#11	10	6	1	2	3	60	0.51	0.51	0.00	9359	16
	#12	10	6	2	2	2	90	0.55	0.55	0.00	14256	17
Medium	#13	12	7	5	1	1	42	0.94	0.94	0.00	7560	21
	#14	12	7	1	1	5	42	0.77	0.77	0.00	7551	19
	#15	12	7	4	2	1	105	0.92	0.92	0.00	18910	20
	#16	12	7	4	1	2	105	0.88	0.88	0.00	19215	21
	#17	12	7	1	3	3	140	0.82	0.82	0.00	25536	22
	#18	12	7	2	2	3	210	0.85	0.85	0.00	38316	20
	#19	14	8	6	1	1	56	1.56	1.56	0.00	13448	25
	#20	14	8	1	1	6	56	1.13	1.13	0.00	13372	22
	#21	14	8	1	2	5	168	1.21	1.22	0.83	40328	25
	#22	14	8	2	4	2	420	1.41	1.41	0.00	>86400	26
	#23	14	8	2	2	4	420	1.29	1.29	0.00	>86400	24
	#24	14	8	3	3	2	560	1.45	1.46	0.69	>86400	25
	#25	14	8	2	3	3	560	1.35	1.35	0.00	>86400	24
Max. gap %										**0.83**		

* No. of continuous NLP subproblems (i.e., $\frac{N_v!}{A! \times B! \times C!}$) solved by GAMS.

The performance of the SA can be sensitive to the user-defined parameters, including initial temperature T_0, and cooling factor β. Hence, several preliminary runs are carried out with different values of parameters to select the most suitable parameter values from a set of candidate values (the range of each parameter is given). Indeed, our initial experiments are performed under different combinations of parameters, including changes in T_0 (from 6 to 12 with a step value of 1) and in β (from 0.85 to 0.99 with a step value of 0.01), and the results are evaluated for each parameter combination through a maximum number of 100 iterations for each run. This is indeed a commonly-used procedure in the literature for tuning the parameters of metaheuristics, such as the SA algorithm (e.g., Pishvaee et al., 2010; f and Kamalabadi, 2016). Moreover, since the performance of metaheuristics can vary when solving instances with different sizes, the SA's parameters are separately adjusted for small, medium, and large-scale problems. Finally, the preferred values were set as $T_0 = 9$ and $\beta = 0.95$ for small instances, $T_0 = 9$ and $\beta = 0.99$ for medium ones, as well as $T_0 = 10$ and $\beta = 0.99$ for large real-life instances presented in the next section.

5.4.1.2 Application area and real-life case study (large-scale instance)

To assess the effectiveness and efficiency of the proposed optimization model and the solution approach, several numerical experiments are carried out based on data from a bi-directional bus route, Military Road in North Sydney, Australia, which consists of a total of $N_s = 24$ stops (12 stops in each direction) (see Tirachini et al. (2014) for more details of the bus route). We consider the planning horizon from 7:00 am to 8:30 am. In the base case scenario, it is assumed that the bus route is served by a given mixed fleet of 16 buses: {12, 12, 12, 12, 12, 12, 12, 12, 12, 15, 15, 15, 15, 18, 18, 18}. For example, under the assumption of even dispatching headways of 6 minutes (service frequency of 10 bus/h) and in a situation of constant passenger arrival rates at bus stops, regular bus headways and no passengers left behind (i.e., if buses never run at full capacity), the average waiting time would be 3 minutes.

The parameters used in this dissertation are taken from Tirachini et al. (2014) and Tirachini (2014). For the sake of brevity, detailed information on demand rates is presented in Appendix A. In order to determine how the solution is sensitive to different degrees of demand availability, we compare the cases of low and high-resolution passenger arrival rates. As can be seen in Table A6 and Fig. 5-15, in the high-resolution demand case, the passenger arrival rates ($\lambda_j[t]$) are assumed to be constant during each 15-minute time interval, and they basically follow a bell-shaped pattern during the simulation time, peaking roughly at 7:45 am. In the low-resolution demand case; however, the passenger arrival rates remain constant during each one-hour period (see Table A7), as commonly assumed in several bus supply optimization models (e.g., Hadas et al., 2010; Tirachini et al., 2014; Niu et al., 2015).

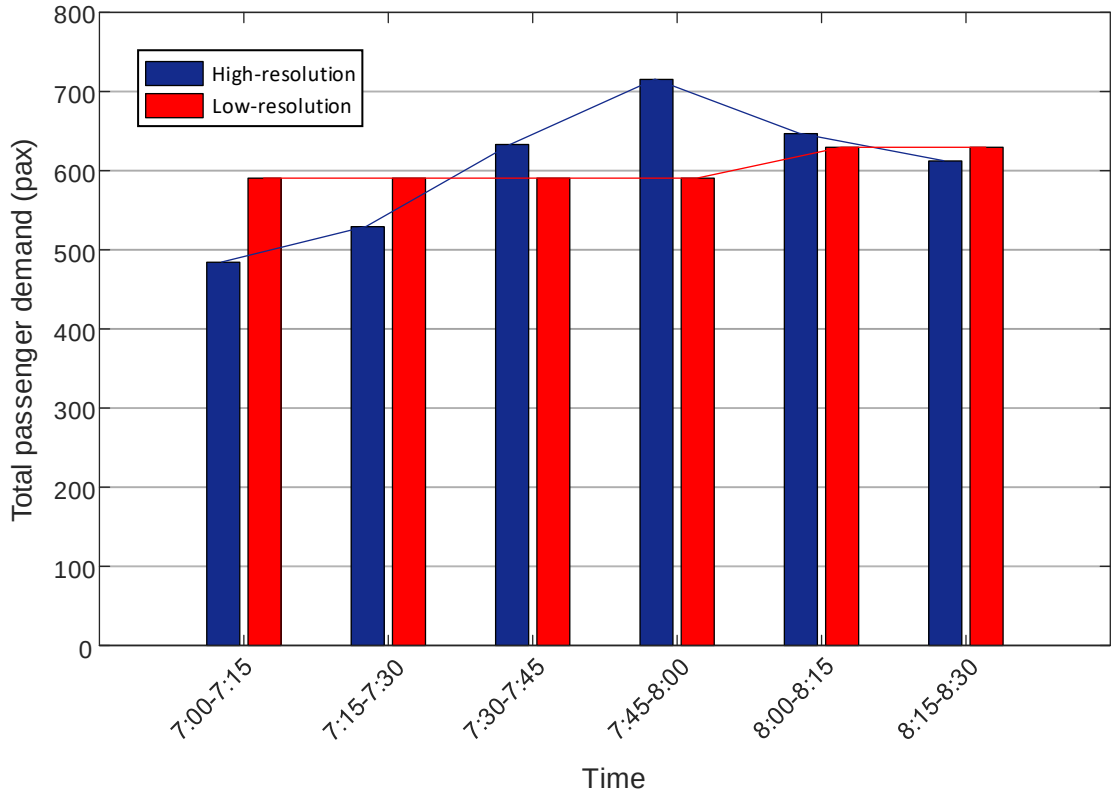

Figure 5-15 The total number of passengers arriving in the bus corridor during each 15-minute time interval.

Regarding travel times between stops, we assume that they are stochastic and the relevant travel time distribution parameters are given here. As introduced in Section 3.4.1, we assume a lognormal distribution of bus travel times between stops $j-1$ and j with mean and standard deviation of r_j and σ_j respectively.

$r_2 = 1.36$ (min); $r_3 = 1.35$; $r_4 = 1.37$; $r_5 = 0.95$; $r_6 = 1.25$; $r_7 = 1.59$; $r_8 = 0.79$; $r_9 = 0.77$; $r_{10} = 0.91$; $r_{11} = 1.09$; $r_{12} = 1.36$; $r_{14} = 1.49$; $r_{15} = 1.50$; $r_{16} = 1.48$; $r_{17} = 1.08$; $r_{18} = 1.38$; $r_{19} = 1.74$; $r_{20} = 0.92$; $r_{21} = 0.90$; $r_{22} = 1.03$; $r_{23} = 1.21$; $r_{24} = 1.49$.

$\sigma_2 = 0.11$ (min); $\sigma_3 = 0.11$; $\sigma_4 = 0.12$; $\sigma_5 = 0.06$; $\sigma_6 = 0.09$; $\sigma_7 = 0.15$; $\sigma_8 = 0.05$; $\sigma_9 = 0.04$; $\sigma_{10} = 0.06$; $\sigma_{11} = 0.08$; $\sigma_{12} = 0.11$; $\sigma_{14} = 0.14$; $\sigma_{15} = 0.15$; $\sigma_{16} = 0.14$; $\sigma_{17} = 0.08$; $\sigma_{18} = 0.13$; $\sigma_{19} = 0.19$; $\sigma_{20} = 0.06$; $\sigma_{21} = 0.06$; $\sigma_{22} = 0.08$; $\sigma_{23} = 0.10$; $\sigma_{24} = 0.14$.

The proposed SA is coupled with a MCS method to handle travel time uncertainty. Accordingly, the number of MCSs is set to be 1000.

5.4.1.3 Optimal dispatching policy under high-resolution demand volumes

Fig. 5-16 shows the convergence trend of the SA algorithm. As can be seen, the SA experiences a sharp decline in average waiting time, from 3.84 to 3.55 (min/pax) in the first twenty-four iterations before tailing off, i.e., the SA reached a plateau after 24 iterations within 5.8 minutes. Note that each candidate solution is being evaluated over several (1000) replications, due to the implementation of the MCS method incorporated as a subroutine into the SA to accomplish the evaluation process. Obviously, the computing time would be much shorter if a bus motion model ignores real-life operating conditions, such as stochastic travel times between stops, for the sake of simplicity.

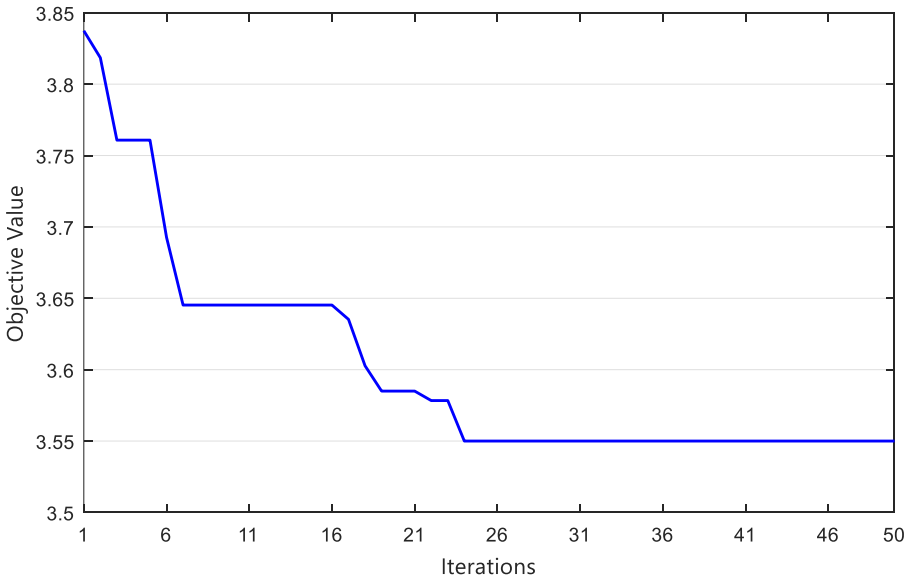

Figure 5-16 Convergence trend of the SA algorithm in the large-scale problem.

Fig. 6-13 (a) gives information about the optimal dispatching headways and the optimal bus dispatching order found by the SA under the high-resolution demand case (15-minute-dependent demand volumes), by showing the bus dispatching order in a time scale. Passengers experience an average waiting time of 3.55 (min/pax) under this optimal dispatching strategy. In total, 9.9% of passengers are left behind and need to wait for a second

bus to board, which explains that the average waiting time is larger than 3 minutes. Importantly, with the proposed strategy, buses of one size are not necessarily dispatched consecutively one after the other, because not doing so allows us to have a more precise adjustment of supply (vehicle capacity) to demand in accordance with time-dependent passenger demand, thereby leading to a better utilization of vehicles' capacity in a given fleet of heterogeneous buses. Indeed, due to the provision of services with varying passenger-carrying capacities under a mixed-fleet operation, vehicles' capacity should be supplied to public transport users in line with temporal changes in demand. Otherwise, if buses are not dispatched in an optimal sequence together with considering the passengers' demand that may fluctuate within the planning horizon (i.e., spatial and temporal demand unbalances), the capacity of vehicles might not be used in due course (non-optimal utilization of resources), thus increasing the average passenger waiting time due to an increase in the number of passengers left behind owing to capacity constraints. For example, 18-m long buses, having more capacity to accommodate passenger volumes at the maximum loading sections, are mostly dispatched to cover the 7:45 am spike in passenger volumes. Moreover, as it is clear from Fig. 6-13 (a), larger buses are dispatched with a larger headway between vehicles compared to smaller buses. Indeed, when different sizes of buses are dispatched to serve a single route, due to their different capacities, the headway between them should be different, otherwise more passengers would be left behind by the smaller buses, resulting in greater delays. This aspect is further discussed in the next subsection. The values of mean, standard deviation, and coefficient of variation for dispatching headway are respectively equal to 5.96 min, 1.85 min, and 0.31 in the optimal solution.

5.4.2 Numerical experiments and application of the advanced version of the mixed-fleet bus scheduling model

In this section, we use a Taguchi approach as a means to fine-tune the parameters of the metaheuristics. We also conduct a computational experiment using random test instances of various sizes (small, medium, and large-scale) to provide a comprehensive assessment of the metaheuristics' capabilities based on two crucial metrics: solution quality and CPU time. Additionally, a comparison is made between the metaheuristics' results and the exact solutions derived from GAMS software for small and medium examples.

5.4.2.1 Taguchi results in the calibration of metaheuristics' parameters

Table 5-13 presents the parameters for each algorithm, with three levels considered for each parameter. To analyze the experiments, we utilize Minitab 17 software and adopt a three-level Taguchi scheme. For example, for the GA with 4 parameters at 3 levels, the L9 orthogonal array is utilized to design the experiments, resulting in a total of 9 trials. Table 5-14 provides detailed information on the L9 orthogonal array, showcasing the parameter combinations in each trial. The findings are depicted in Fig. 5-17, where the highest mean of the Signal-to-Noise (S/N) ratio indicates the best level for each parameter.

Table 5-13 Parameter calibration of the proposed algorithms.

Algorithm	Parameter	Level			Best level
		1	2	3	
GA	Maximum iterations ($MaxIt$)	100	150	200	1
	Population size (N_{pop})	30	50	70	3
	Crossover rate (P_c)	0.6	0.7	0.8	3
	Mutation rate (P_m)	0.1	0.2	0.3	3
GWO	Maximum iterations ($MaxIt$)	100	150	200	1
	Grey wolf pack size (N_{pop})	30	60	90	3
GA-SA	Maximum iterations ($MaxIt$)	100	150	200	2
	Population size (N_{pop})	30	50	70	2
	Crossover rate (P_c)	0.6	0.7	0.8	3
	Mutation rate (P_m)	0.1	0.2	0.3	2
	Cooling rate ($Alpha$)	0.90	0.95	0.99	1
	Initial temperature (T_0)	10	15	20	3
GWO-SA	Maximum iterations ($MaxIt$)	100	150	200	1
	Grey wolf pack size (N_{pop})	30	60	90	3
	Cooling rate ($Alpha$)	0.90	0.95	0.99	3
	Initial temperature (T_0)	10	15	20	3

Table 5-14 Taguchi orthogonal array L9 (3^4) (4 factors (A, B, C, and D) at 3 levels).

Trial	A	B	C	D
1	1	1	1	1
2	1	2	2	2
3	1	3	3	3
4	2	1	2	3
5	2	2	3	1
6	2	3	1	2
7	3	1	3	2
8	3	2	1	3
9	3	3	2	1

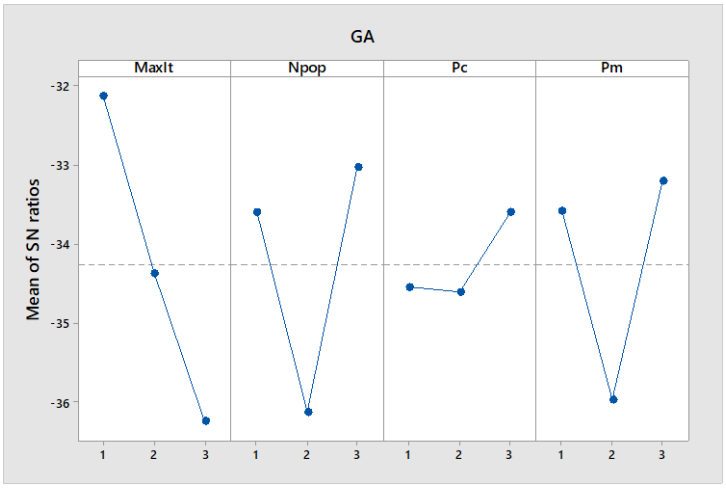

(a) GA

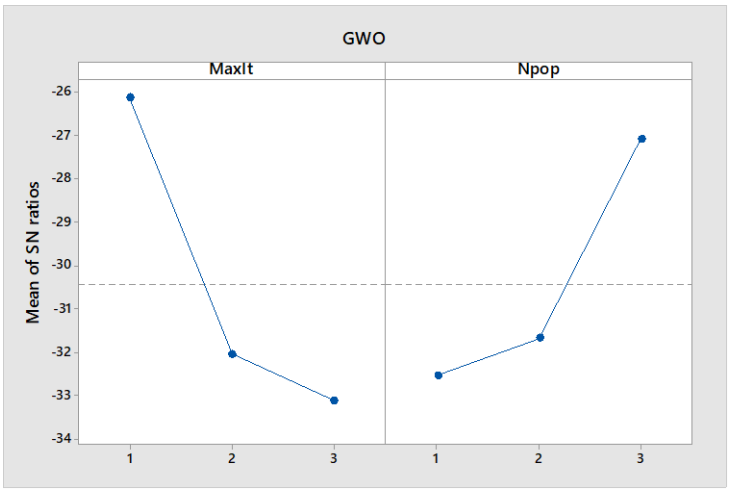

(b) GWO

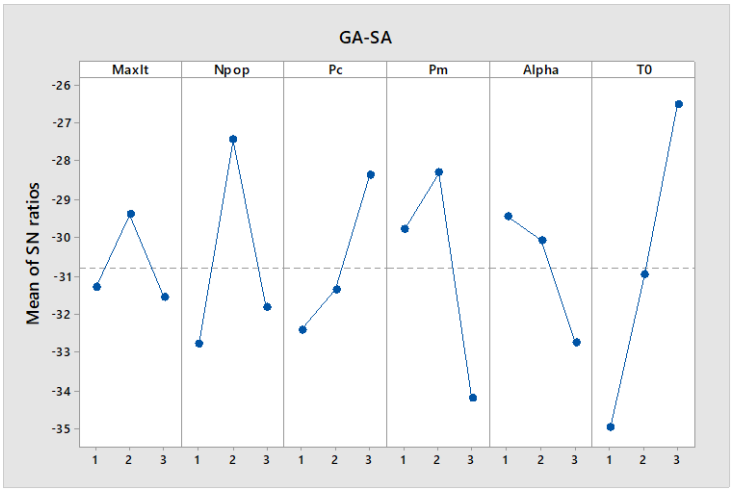

(c) GA-SA

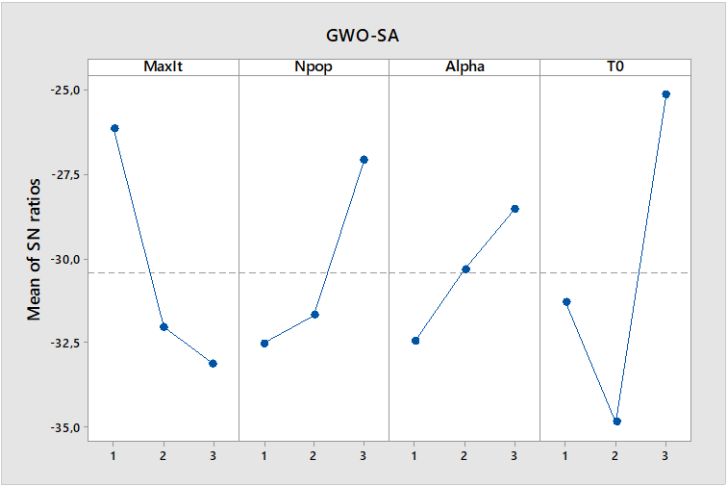

(d) GWO-SA

Figure 5-17 Results of the Taguchi method for adjusting metaheuristics' parameters.

5.4.2.2 Test problems for the assessment of metaheuristics

This section presents a computational experiment that employs random test instances of varying sizes to examine the validity and efficiency of the proposed metaheuristics. To this end, 30 randomly-generated test problems are designed, containing small, medium, and large-sized samples (the characteristics of the test samples are given in Appendix A).

For small- and medium-scale instances, which can be solved by GAMS software optimally, we compare the results of the four metaheuristics (GA, GWO, GA-SA, and GWO-SA) with optimal results achieved by GAMS software using the BARON optimization solver. Besides, all computational programs have been conducted on a PC with an Intel(R) Core(TM) i5-6500 CPU operating at 3.20 GHz and 16.0 GB of RAM. To assess the solution quality of the proposed metaheuristics, we measure the gap as follows:

$$GAP = \frac{Heur_{sol} - GAMS_{sol}}{GAMS_{sol}} \times 100 \qquad (5\text{-}2)$$

where $GAMS_{sol}$ is the optimal solution achieved by GAMS, and $Heur_{sol}$ is the solution found by the selected metaheuristic. Each metaheuristic algorithm is executed 10 times to solve each test instance. The results, including the average and standard deviation of the objective function values (OFVs) across all runs, as well as the average CPU times for each test problem, are presented in Table 5-15. Additionally, the gap values are computed based on the average results. As depicted in Table 5-15 and Fig. 5-19, the GAMS's CPU times are notably high

(even for small-scale cases), making it inefficient for addressing operational scheduling problems, where timely optimization of operational plans is crucial. In contrast, the proposed metaheuristics offer the advantage of providing practically good solutions within significantly shorter (rational) CPU times.

Since GAMS software is unable to address large-scale test instances, we only employ the proposed metaheuristics to solve those instances (see Table 5-16). In this case, we utilize the relative percentage deviation (RPD) metric with the findings of the best-performing metaheuristic as our benchmark to compare the effectiveness of the methods:

$$RPD = \frac{Heur_{sol} - Min_{sol}}{Min_{sol}} \times 100 \qquad (5\text{-}3)$$

where $Heur_{sol}$ is the solution produced by the selected metaheuristic, and Min_{sol} is the best solution found among all the metaheuristics.

Table 5-15 Small (S) and medium (M) test instance results.

Instance ID	GAMS		GA			GWO			GA-SA			GWO-SA			GAP (%) relative to GAMS			
	OFV	CPUT*	Avg. OFV	SD. OFV	CPUT	Avg. OFV	SD. OFV	CPUT	Avg. OFV	SD. OFV	CPUT	Avg. OFV	SD. OFV	CPUT	GA	GWO	GA-SA	GWO-SA
S1	270.69	532.06	270.69	0.00	21.24	270.69	0.00	20.63	270.69	0.00	28.87	270.69	0.00	26.48	0.00	0.00	0.00	0.00
S2	276.52	607.33	276.52	0.00	29.70	276.52	0.00	26.58	276.52	0.00	29.57	276.52	0.00	27.34	0.00	0.00	0.00	0.00
S3	356.64	1516.65	357.66	0.42	32.31	356.64	0.00	26.64	356.64	0.00	38.75	356.64	0.00	35.78	0.28	0.00	0.00	0.00
S4	370.90	1676.98	370.90	0.00	33.54	370.90	0.00	30.50	370.90	0.00	42.20	370.9	0.00	39.03	0.00	0.00	0.00	0.00
S5	405.94	3619.97	414.18	3.25	38.91	410.87	0.91	36.54	409.39	0.47	47.52	405.94	0.00	44.03	2.02	1.21	0.84	0.00
S6	424.80	4073.96	433.18	3.53	46.05	430.20	0.68	41.82	427.85	0.63	52.10	424.8	0.00	48.09	1.97	1.27	0.71	0.00
S7	440.27	5159.58	450.43	4.01	54.62	446.56	0.67	42.36	444.20	0.45	61.94	440.27	0.00	56.87	2.30	1.42	0.89	0.00
S8	468.42	6241.24	479.90	4.14	53.96	475.02	0.72	40.45	473.13	0.54	62.59	468.42	0.00	57.43	2.45	1.40	1.00	0.00
S9	484.99	7358.86	496.32	3.85	57.68	491.52	0.91	46.33	489.05	0.27	66.96	484.99	0.00	61.16	2.33	1.34	0.83	0.00
S10	518.98	8006.62	530.62	3.22	66.40	526.38	0.86	46.83	522.13	0.19	77.27	518.98	0.00	70.47	2.24	1.42	0.60	0.00
M1	539.40	9088.34	550.12	4.06	68.16	539.40	0.00	54.52	539.40	0.00	84.77	539.40	0.00	77.36	1.98	0.00	0.00	0.00
M2	561.97	10338.05	584.31	4.48	70.46	572.54	3.31	56.05	567.12	3.17	85.43	564.26	0.70	77.97	3.97	1.88	0.91	0.40
M3	590.05	-**	610.10	3.61	68.54	599.22	2.19	59.13	596.61	2.63	86.14	590.05	0.00	78.65	3.39	1.55	1.11	0.00
M4	619.57	-	639.24	3.67	73.21	629.19	0.00	60.95	619.57	3.28	88.28	619.57	0.00	80.97	3.17	1.55	0.00	0.00
M5	621.60	-	640.14	4.00	86.56	632.35	2.45	65.90	628.10	2.50	100.91	623.43	0.45	92.41	2.98	1.72	1.04	0.29
M6	660.51	-	680.41	3.46	88.41	670.20	2.34	69.75	668.22	2.07	104.09	662.12	0.73	95.26	3.01	1.46	1.16	0.24
M7	765.85	-	787.11	2.67	92.18	779.41	3.06	67.81	774.14	2.47	104.97	768.20	0.71	96.06	2.77	1.77	1.08	0.30
M8	755.14	-	774.26	2.81	100.10	763.34	3.14	79.27	763.52	1.87	119.46	758.26	0.87	109.01	2.53	1.08	1.10	0.41
M9	769.95	-	789.15	3.01	105.13	778.61	2.06	88.91	777.15	1.27	130.89	771.43	0.40	119.51	2.49	1.12	0.93	0.19
M10	788.07	-	808.30	2.71	118.27	798.10	2.31	89.87	796.56	2.54	137.46	790.37	0.51	125.32	2.56	1.27	1.07	0.29

* The acronym CPUT corresponds to CPU time, measured in seconds.

** A hyphen is used to indicate instances where GAMS's CPU times exceed 3 hours (10800 seconds).

Table 5-16 Large (L) test instance results.

Instance ID	GA			GWO			GA-SA			GWO-SA			RPD (%) relative to the best metaheuristic			
	Avg. OFV	SD. OFV	CPUT	Avg. OFV	SD. OFV	CPUT	Avg. OFV	SD. OFV	CPUT	Avg. OFV	SD. OFV	CPUT	GA	GWO	GA-SA	GWO-SA
L1	917.33	9.34	122.81	907.52	7.42	92.73	902.84	3.67	144.02	879.59	0.00	131.13	4.29	3.17	1.61	0.00
L2	1016.21	7.62	123.17	997.04	5.69	95.74	994.09	3.44	149.08	972.49	0.00	135.55	4.50	2.44	2.13	0.00
L3	1203.86	9.18	138.90	1167.15	7.71	109.19	1162.69	4.32	166.19	1145.40	4.11	151.12	5.10	2.02	1.62	0.00
L4	1372.64	7.83	143.75	1332.11	6.63	113.59	1326.60	3.85	170.83	1311.75	3.74	155.36	4.64	1.86	1.32	0.00
L5	1908.32	7.58	154.35	1837.92	6.17	124.21	1829.11	4.14	184.02	1773.56	3.23	168.07	7.60	3.49	2.94	0.00
L6	2182.44	8.69	171.28	2105.04	7.23	132.12	2093.28	4.47	202.87	2038.12	3.84	185.44	7.05	3.24	2.62	0.00
L7	2815.78	8.26	187.02	2718.95	6.94	147.02	2699.58	3.63	223.05	2651.88	3.11	204.19	6.13	2.44	1.82	0.00
L8	2605.44	8.15	193.77	2516.83	6.86	150.78	2503.97	3.84	230.92	2463.72	3.76	211.60	5.69	2.13	1.85	0.00
L9	2840.85	8.74	210.32	2745.61	7.19	167.96	2721.60	5.11	250.07	2658.29	3.96	228.77	6.88	3.11	1.97	0.00
L10	3127.48	7.91	225.67	3037.18	6.33	178.52	2975.76	4.92	262.14	2903.93	3.87	247.57	7.69	4.59	2.44	0.00

To facilitate a comprehensive comparison, we present a boxplot in Fig. 5-18 (a) showing the solution gaps of the metaheuristics relative to the GAMS's solutions in small and medium-scale samples. Additionally, Fig. 5-18 (b) displays the RPDs among the metaheuristics in large-scale samples. Our analysis demonstrates the GWO-SA algorithm's ability to provide superior solutions. In small and medium-scale test samples, the GWO-SA algorithm consistently achieves zero or negligible solution gaps compared to the GAMS's solutions. This trend carries over to large-scale samples, where the GWO-SA algorithm maintains its position as the top-performing algorithm. Significantly, no other algorithm outperforms the GWO-SA algorithm across large-scale instances, leading to the RPD values of zero. The ranking of the other algorithms, in descending order, is as follows: GA-SA, GWO, and GA. We also evaluated the stability of the metaheuristics by examining the standard deviation of their answers across multiple runs (Tables 5-15 and 5-16). The GWO-SA algorithm demonstrates superior stability with fewer variations, ensuring a higher level of confidence in the obtained solutions.

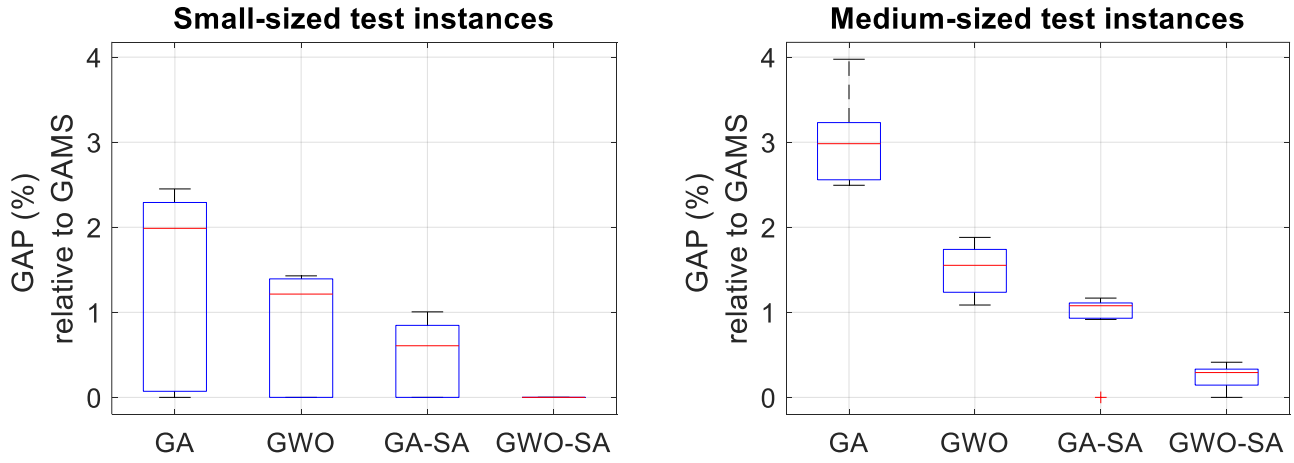

(a) Comparison of solution gaps in small and medium-sized samples: Relative to the GAMS's solutions.

(b) Comparison of solution gaps in large-sized samples: Relative to the best-found solution among all the metaheuristics.

Figure 5-18 Comparing the solution gaps of the metaheuristics.

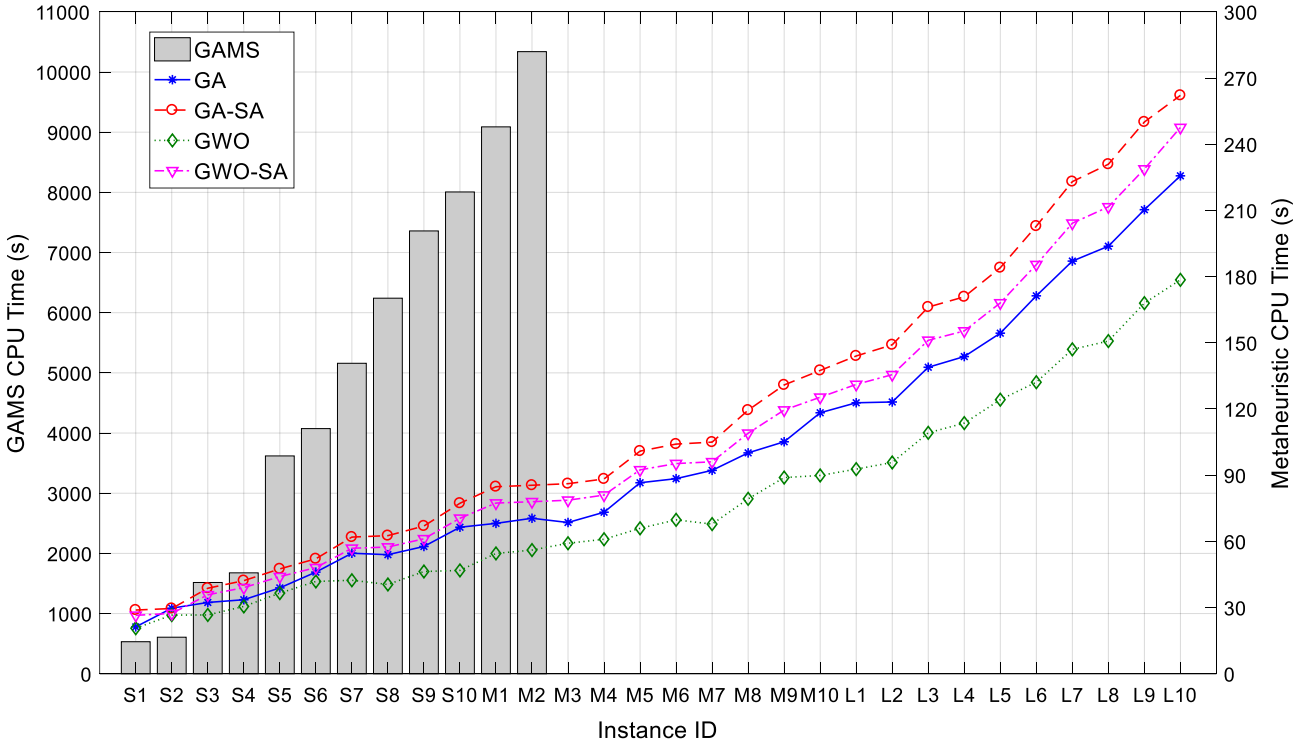

Figure 5-19 Comparison of the solution methods in terms of CPU time.

In Fig. 5-19, the CPU times of the algorithms are presented, with the GWO algorithm showing the shortest times. However, the difference in CPU times between GWO-SA and

GWO, around 1 minute in large-scale problems like L10, is not considered significant in the MFBS context, while the GWO-SA algorithm delivers superior solutions. Besides, in Fig. 5-20, the convergence behavior of the algorithms for different-sized examples (M1 and L10) is depicted. The GWO-SA algorithm witnesses a faster convergence compared to the other algorithms, and this trend is consistent across all examples. Overall, our findings affirm the superiority of the GWO-SA algorithm and position it as a favorable choice for solving the MFBS problem.

To assess whether there is a significant difference between the solutions generated by the metaheuristics, we conduct a nonparametric Wilcoxon signed rank test at a significance level of 0.05. The corresponding *p*-values, obtained from pairwise comparisons of the metaheuristics, are presented in Table 5-17, indicating statistically significant differences among the solutions (*p*-value $\leq$ 0.05). Overall, based on the Wilcoxon test results and the reported solution values, it is confirmed that the GWO-SA outperforms the other metaheuristics. Furthermore, the superiority of the GA-SA over the GWO and GA, as well as the superiority of the GWO over the GA, are validated.

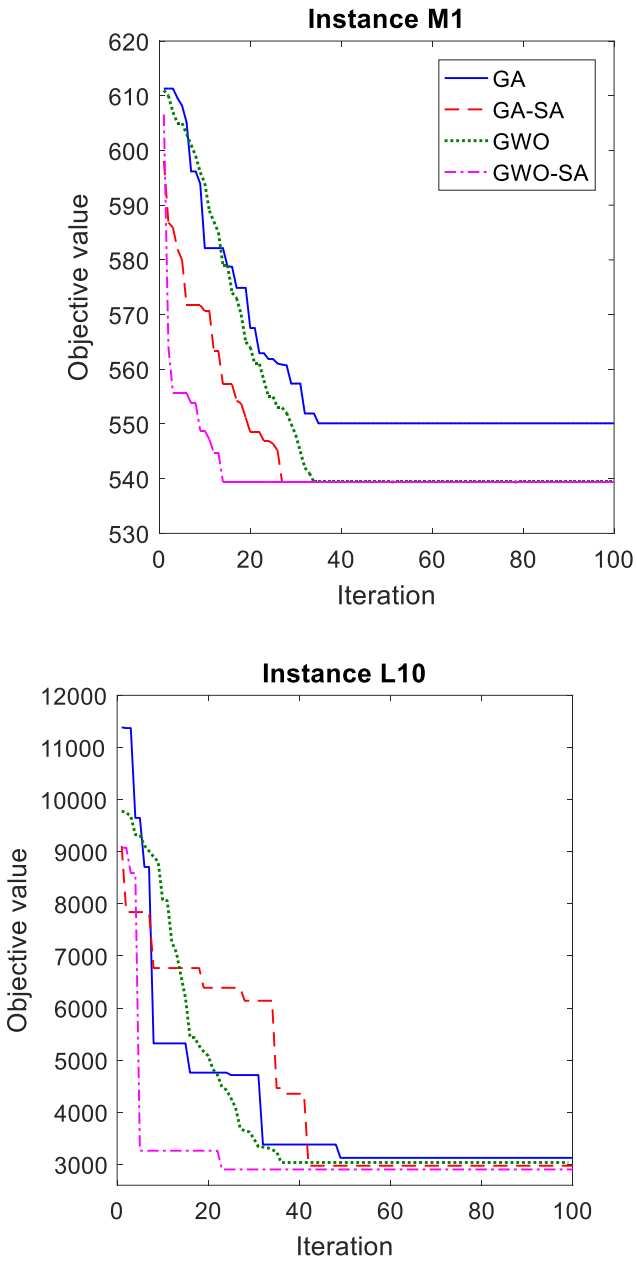

Figure 5-20 Convergence curves of the proposed metaheuristics.

Table 5-17 Results of Wilcoxon test on the proposed metaheuristics.

Algorithms	*p*-values
GWO-SA vs. GA	0.000
GWO-SA vs. GWO	0.000
GWO-SA vs. GA-SA	0.000
GA-SA vs. GA	0.000
GA-SA vs. GWO	0.000
GWO vs. GA	0.000

5.4.2.3 Real-world application

In this section, we examine the practicality of the model through a series of computational tests conducted on a real case study, the Los Pajaritos bus corridor in Santiago, Chile. This bidirectional corridor consists of 20 stations, with 10 stations in each direction, spanning from the south-west of the city towards the center. Our analysis utilizes the demand data sourced from Sadrani et al. (2022b). During the morning peak period, the corridor experiences a high passenger volume, averaging 4500 passengers per hour, resulting in significant crowding. The primary objective for planners is to optimize operational plans to enhance the quality of service for travelers, by reducing waiting times and improving trip comfort, while minimizing operating expenses. For the simulation of our numerical programs, we take into account the crucial morning peak period from 7:00 AM to 10:00 AM, with the demand profile displayed in Fig. 5-21. To operate the designated bus corridor, we assume a maximum availability of 25 type A buses (12-m long), 10 type B buses (15-m long), and 16 type C buses (18-m long).

Fig. 5-22 illustrates the best vehicle dispatching plans for the first hour of the simulations. As can be seen, the algorithms propose different resource allocation solutions. Fig. 5-23 presents a comparison of the cost and average occupancy levels (measured as the ratio of the number of passengers to the capacity of the vehicles) among the solutions obtained by each metaheuristic. The GWO-SA algorithm suggests the most cost-effective solution, with a fleet configuration of 39 buses, including 19 type-A, 7 type-B, and 13 type-C buses. Besides, the GWO-SA's solution exhibits the lowest occupancy levels, indicating its effectiveness in optimizing resource utilization and minimizing crowding.

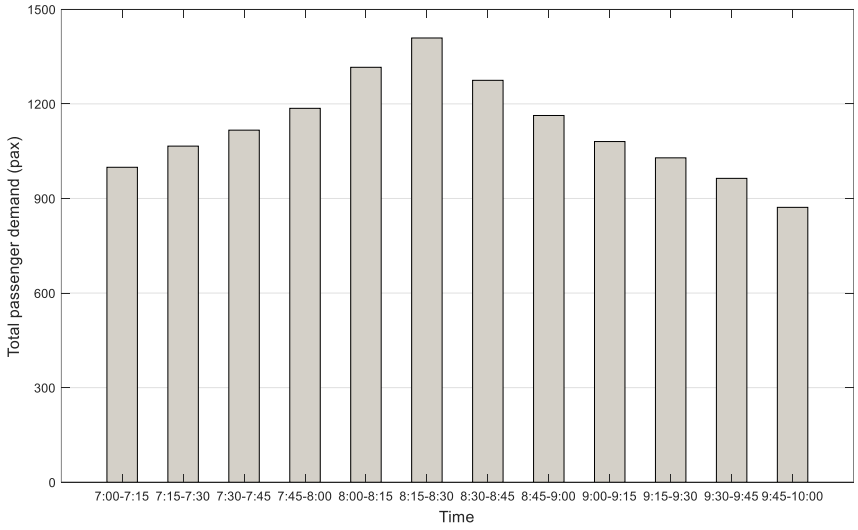

Figure 5-21 Passenger arrival volumes on the route at various periods.

Figure 5-22 Best vehicle dispatching solutions suggested by each metaheuristic.

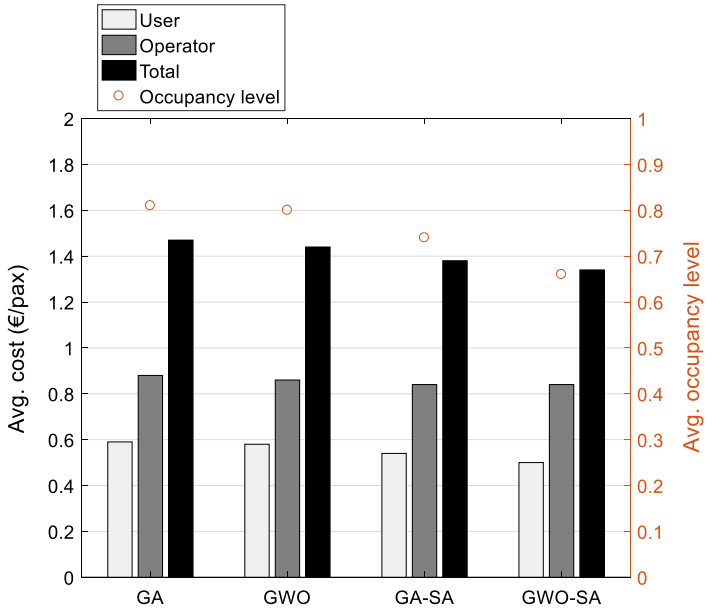

Figure 5-23 Comparison of cost and occupancy levels in the best solutions found by each metaheuristic.

Furthermore, while both GWO-SA and GA-SA suggest the same fleet composition, they offer different dispatching plans regarding sequence and timing, as illustrated in Fig. 5-22. Notably, the dispatching plan generated by the GWO-SA demonstrates superior efficiency compared to the GA-SA, resulting in a 7.4% decrease in user costs, and consequently, a 2.9%

decrease in overall costs. Additionally, the average occupancy level inside buses decreases by 10.8% (from 0.74 to 0.66). Overall, during periods of high demand, it is common practice to deploy larger vehicles and reduce dispatching headways compared to periods of lower demand, aligning with the temporal variations in demand illustrated in Fig. 5-21. By implementing these optimized programs, users experience improved trip comfort due to reduced vehicle loads, and their waiting times are reduced due to shorter dispatching headways during periods of high demand. Only a framework that explicitly accounts for crowding externalities is able to correctly measure the advantage of using GWO-SA, in terms of increased service quality, in this type of busy transport corridor.

Interestingly, the GA and GWO algorithms propose larger fleet sizes of 41 and 40 buses, respectively, compared to the GA-SA and GWO-SA algorithms recommending a fleet size of 39 buses. However, the optimal dispatching plans derived from the GA-SA and GWO-SA algorithms result in lower user costs and vehicle occupancy levels, despite their smaller fleet sizes. This emphasizes the crucial role of efficient and precise dispatching plans obtained from these advanced algorithms in achieving cost savings and improving the overall performance of the transportation system.

6 Sensitivity analysis

This chapter explores sensitivity analysis, examining how variations in model parameters impact the outcomes. It provides a deeper understanding of the models' robustness and sensitivity to different factors.

6.1 Sensitivity analysis for automated bus planning model

6.1.1 Sensitivity to human driving cost savings due to automation

In the base case scenarios, we assumed 50% savings in human driving costs with automated vehicles. Now, we test cases in which human driving costs are fully (100%) saved with automation. As Fig. 6-1 shows, if automation capabilities can completely save human-related driven costs, automated bus scenarios are optimally pushed toward providing services with higher frequencies than the cases of 50% driving cost savings, and hence waiting and crowding costs are further reduced for users. Note that optimal vehicle sizes remain unchanged, which are similar to those obtained in the base case scenarios.

It is normally expected that, with full human driving cost savings, frequencies are increased at a higher degree for Regensburg than for Santiago, since the level of drivers' wages is larger in Germany than in Chile. Accordingly, when the user cost is insensitive to in-vehicle crowding levels, we see that frequencies are increased at a higher rate in the case of Regensburg (22%) than Santiago (12%). This is also in line with the findings of Tirachini and Antoniou (2020), who did not take crowding effects into account. However, in the presence of in-vehicle crowding effects, we interestingly see that there is not a salient difference between the increased rates, which are at 34% and 30% in Regensburg and Santiago respectively. This is because the crowding phenomenon is far more serious in the case of Santiago than Regensburg, which can persuade public transport providers (in light of full human driving cost savings) to boost optimal frequencies up to 30% in order to offset crowding discomfort costs exerted upon travelers in such a crowded bus corridor. Only a model, in which the value of travel time savings is sensitive to in-vehicle crowding levels, would be able to catch this effect. This result explicitly accentuates the importance of taking crowding discomfort externalities and their implications into account when assessing the actual benefits of automated public transport systems, especially for overcrowded bus corridors.

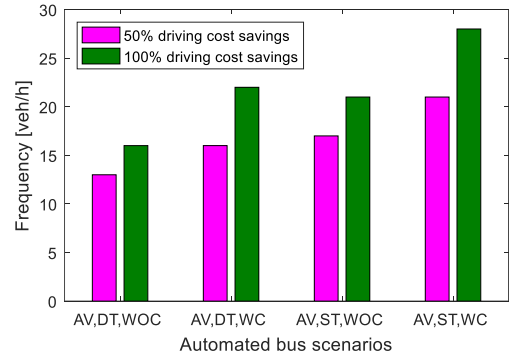

(a) Regensburg case study

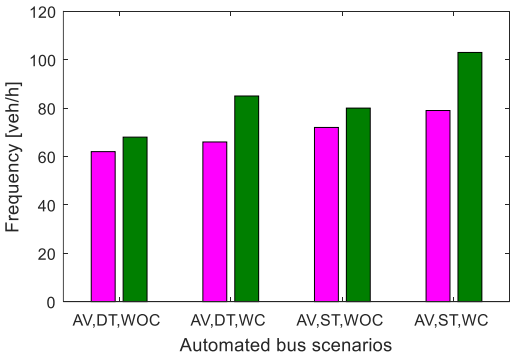

(b) Santiago case study

Figure 6-1 Sensitivity to human driving cost savings due to automation.

6.1.2 Sensitivity to travel time uncertainty

In the base case scenarios, we assumed that driving times between consecutive stops are stochastic (in ST scenarios), but at the same level of variability for both human-driven and automated bus services. In this part, we carry out a series of sensitivity analyses, in which travel time uncertainty is improved/degraded with automation through a reduction/rise in the standard deviation of travel times (values of σ_j in Eq. (3-16), used to model stochastic running times). We numerically investigate how an automated public transport system can yield larger/smaller savings in waiting time costs if the standard deviations of travel times are reduced/increased by $\pm$10, $\pm$20, $\pm$30, $\pm$40, and $\pm$50% due to automation (see Fig. 6-2).

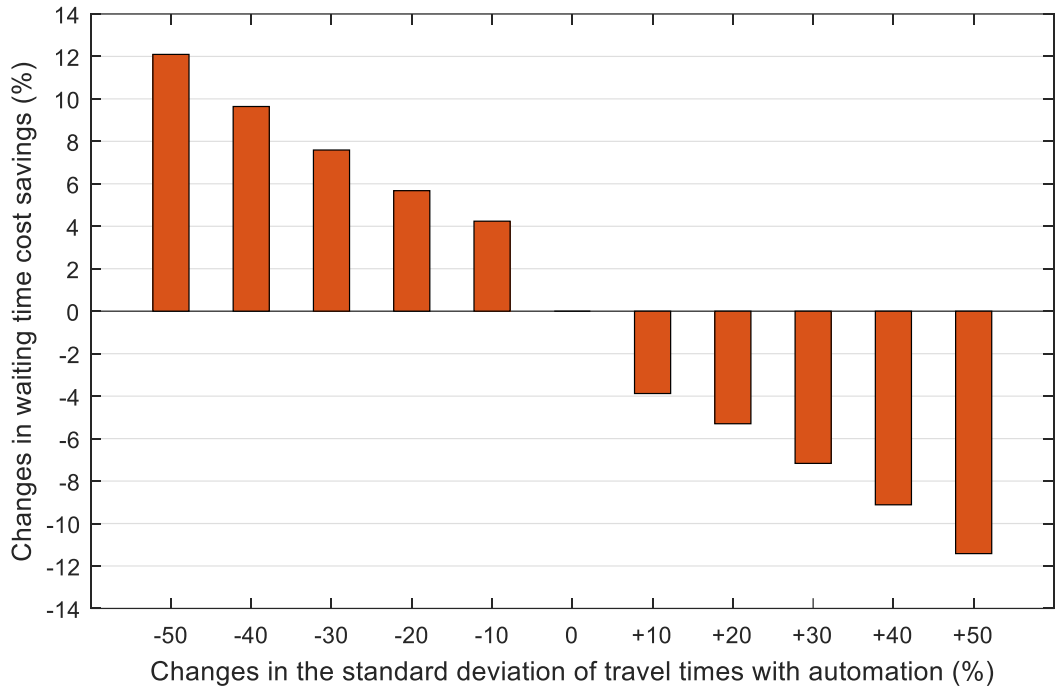

Figure 6-2 Sensitivity to travel time variability due to automation.

As indicated in Fig. 6-2, our numerical results in Regensburg show that passenger waiting time costs could be saved by 12.1% if the technology of automation improved the reliability of public transport services through a reduction of travel time volatility by 50%. While waiting time is related to overall customer satisfaction (Tyrinopoulos and Antoniou, 2008; Dell'Olio et al., 2011), waiting time due to unreliability (e.g., travel time uncertainty) can have deeper negative consequences and be burdensome to public transport commuters (Rietveld et al., 2001; Van Lierop et al., 2018). The diversity in human driving habits can considerably aggravate travel time stochasticity in reality (Wang and Sun, 2020). Nonetheless, such differences in driving functions can be much less pronounced in the case of automated driving systems, due to the elimination of human interventions (Azad et al., 2019). Hence, public transport providers could potentially improve passengers' perceptions of reliability through the mitigation of unexpected waiting delays associated with unreliable services if automated public transport systems can offer a more reliable operation (more stable travel times) through leveraging full automation capabilities.

6.1.3 Effects of automation and travel time stochasticity on dwell time regularity

Dwell time variability can negatively affect bus operations and users' satisfaction, due to negative effects on the reliability of systems and predictability of trip times (Sun et al., 2014). Given the stochastic nature of public transport operations, the influences of driving time variations on the irregularity of dwell times at stations have been already investigated in the literature of travel time reliability for human-driven bus services (e.g., van Oort, 2014; van Oort, 2016; Schmidt et al., 2016). Overall, driving time volatility between stops can lead to a further spread of irregularity among vehicle dwell times due to poor service reliability, early or late services (van Oort, 2014). This is because travel time variations have adverse effects on load distributions, i.e., with a further growth of uncertainty in driving times between stops, passenger loads (the demand for getting on and off) will be irregularly distributed between buses on the same line, thus aggravating dwell time variability (Muñoz et al., 2020). An extra benefit of more regular operations is having more balanced passenger loads between vehicles.

To account for realistic operating conditions in the formulation of dwell time, we modeled flow-dependent dwell times which can vary at each station given alighting and boarding demands at that station. For example, a small delay due to driving time fluctuations provokes a rise in the number of travelers waiting at the next stop. This in turn leads to a rise in the dwell time, and consequently the bus delay and the risk of service unreliability are further exacerbated due to a positive feedback loop between the number of travelers waiting at stops, dwell times, and travel times between successive bus stops (Moreira-Matias et al., 2016).

Here, we numerically investigate how the deployment of an automated public transport system can lead to more regular/irregular dwell times at stops if the reliability of driving times between stops is improved/declined during operations with automation. To evaluate the dispersion in vehicles' dwell times affected by driving time variation levels, we measure the standard deviation of dwell times for automated vehicles, while changing the standard deviation of driving times between stops by $\pm$10, $\pm$20, $\pm$30, $\pm$40, and $\pm$50%. Results are shown in Fig. 6-3 for the case of Regensburg at a given frequency of 20 [veh/h]. Note that the average length of dwell time is similarly 0.8 min in each case, as the total number of passengers alighting and boarding during the entire simulation time is the same for all the cases. As can be seen, the irregularity of dwell times is reduced if automated vehicles can provide a more stable operation with lower driving time variations. For instance, if the standard deviation of

driving times between stops is reduced by 50% with automation, the standard deviation of dwell times at stops is decreased by 34%, dropping from 0.29 min to 0.19 min.

Besides, using a boxplot in Fig. 6-4, we illustrate the level of disparity in the dwell times of vehicles at each stop along the upstream direction. It is clearly observed that the dwell times of automated vehicles follow a more regular pattern with a reduction of 50% in travel time volatility compared to the base case (with no changes, 0%, in travel time variations).

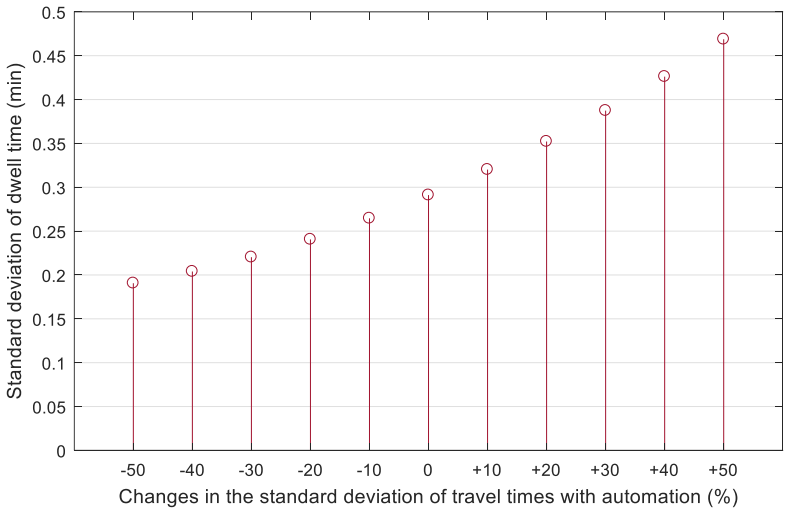

Figure 6-3 Standard deviation of dwell times under different levels of change in travel time variability between stops with automation.

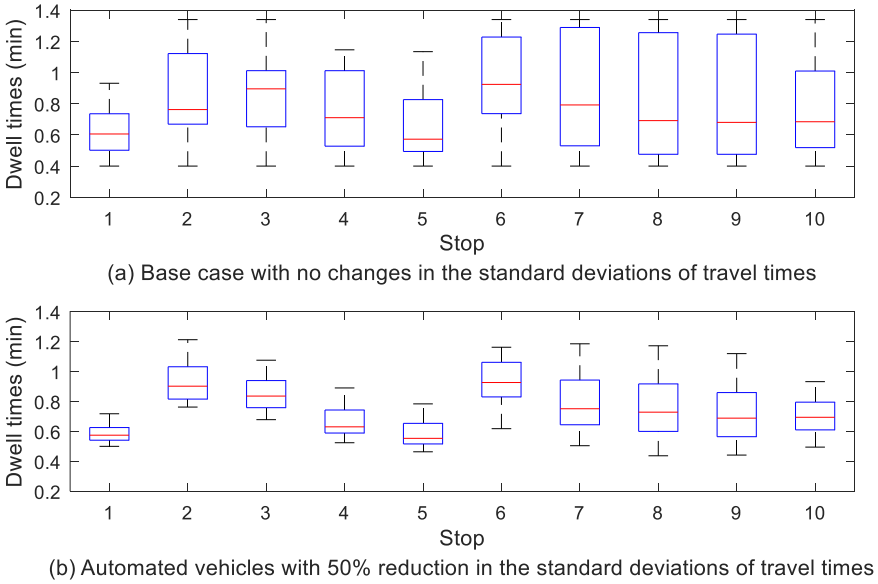

Figure 6-4 Display of dispersion between dwell times of vehicles at each station.

6.1.4 Sensitivity to time spent opening and closing bus doors with automation

As described in Eq. (3-18), a part of the dwell time is related to the dead time needed for opening and closing bus doors, affecting bus stop delays. In the base case scenarios, we assumed that this time is the same for both human-driven and automated buses. Although this time might be larger or shorter with automation in reality, there appears to be no conclusive scientific evidence on this aspect yet.

On the one hand, this time might be increased with automation due to the inclusion of marginal safety factors when opening and closing doors without a human driver directly inspecting this procedure. Overall, the current programs of autonomous mobility services underline the need for operating automated vehicles with broader safety standards, due to security and safety reasons, i.e., given the operational obstacles and unknown aspects that might become apparent in practical terms, there is still a propensity toward the run of automated bus systems with a higher margin of safety in the current phase of deployment (Nemoto et al., 2020). Hence, due to the elimination of human checks formerly carried out by drivers inside human-driven buses, this dead time might be considered a bit longer for automated vehicles.

On the other hand, the technology of automation might be able to mitigate bus stop delays, associated with drivers' behavior and reaction times, through the elimination of human interventions. Moreover, for larger buses with more doors, drivers may need more time to check whether all doors are clear of passengers before activating the process of closing doors to leave stops (Tirachini et al., 2014). Automated vehicles, equipped with several advanced internal/external sensors and versatile monitoring technologies, can accurately detect the moment at which each door is clear of passengers. Hence, a shorter time might be needed for closing doors installed at different parts of a bus (e.g., front, middle, and back doors in a bus).

To assess the possible effects of vehicle automation on the process of opening and closing bus doors, we perform a series of sensitivity analysis tests, in which the relevant dead time is enlarged and reduced by ±10, ±20, ±30, ±40, and ±50% with automation (see Fig. 6-5). For instance, passengers' in-vehicle time costs are saved by 4.4% if such a time is reduced by 50% with automation.

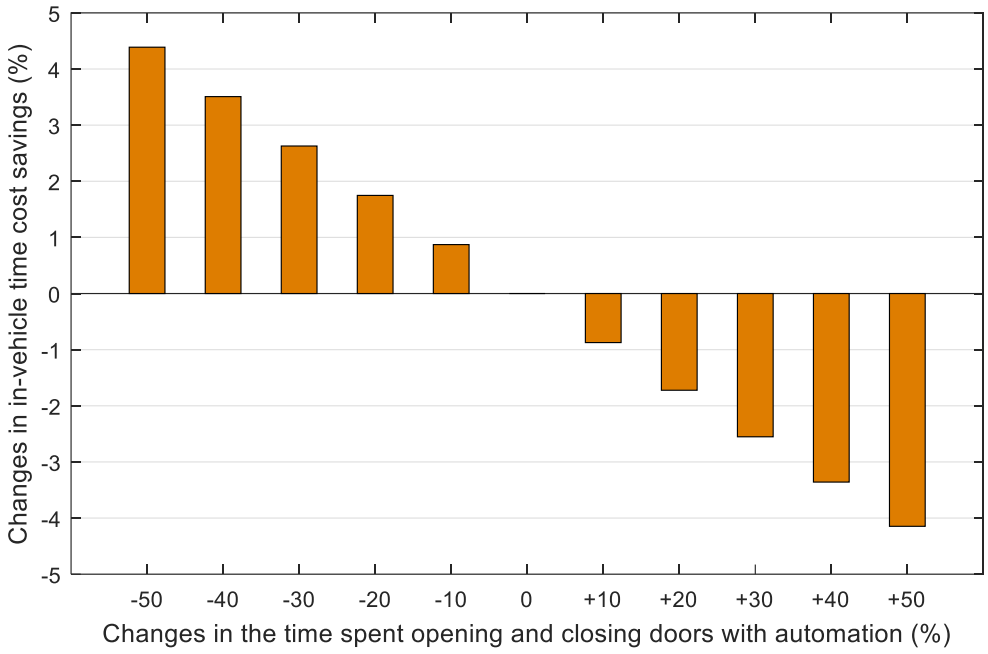

Figure 6-5 Sensitivity to the time required for opening and closing doors with automation.

6.1.5 Sensitivity to demand fluctuation

In this part, we aim to investigate the sensitivity of solutions to the demand fluctuation. Our base-case experiments were performed under 15-minute-dependent demand flows witnessing fluctuations during the simulation time (see Table A4 in Appendix A and Fig. 6-6). Now, we consider another demand case, under which passenger arrival rates remain fixed (without fluctuation) during the whole simulation period (7:00-9:00 AM), while the total demand is the same for both demand cases (see Table A5).

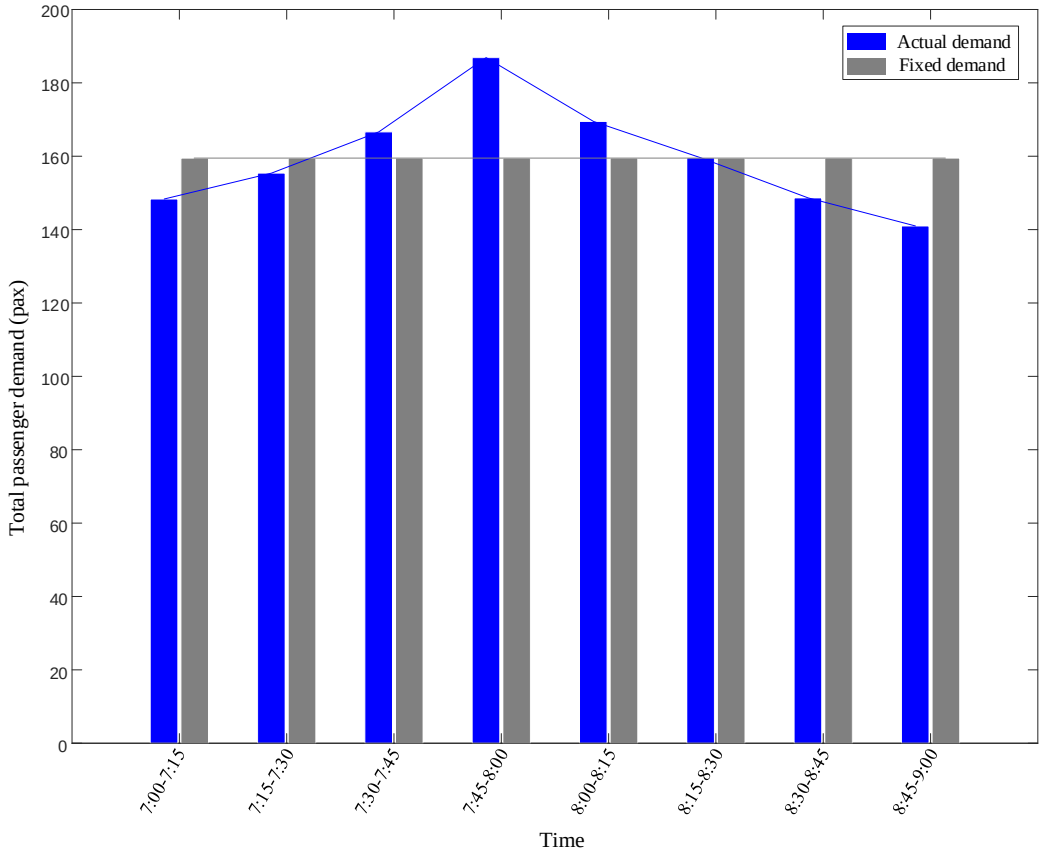

Figure 6-6 Total passenger demand entering the bus route during each interval of 15 minutes, as listed in Tables A4 and A5.

The optimal vehicle size and service frequency in the Regensburg case study are determined under this new case of passenger arrival rates. We see that the optimal vehicle size does not change. Nevertheless, as shown in Fig. 6-7, the optimal service frequency is reduced compared to the case of 15-minute-dependent arrival rates, tested in our base-case scenarios. For example, the optimal service frequency is reduced by about 8% and 5% in the deployment scenarios of HV, ST, WC and AV, ST, WC respectively. This is because although the total demand is the same for both actual (with fluctuation) and fixed (without fluctuation) demand cases, the passenger flow experiences a larger peak demand (i.e., peak inside the peak) in the actual demand case, observed around 7:45-8:00 AM (see Fig. 6-6). Hence, the crowding-related problems (e.g., occupancy levels inside vehicles) can be increased at such maximum-load points, and therefore a higher level of frequency is optimally suggested to avoid the growth of crowding levels. Note that such effects are well captured in our crowding-sensitive model. This result accentuates the importance of considering demand

volatility in the determination of service supply items, particularly at critical loading points (demand spikes) that can further exacerbate crowding-related issues.

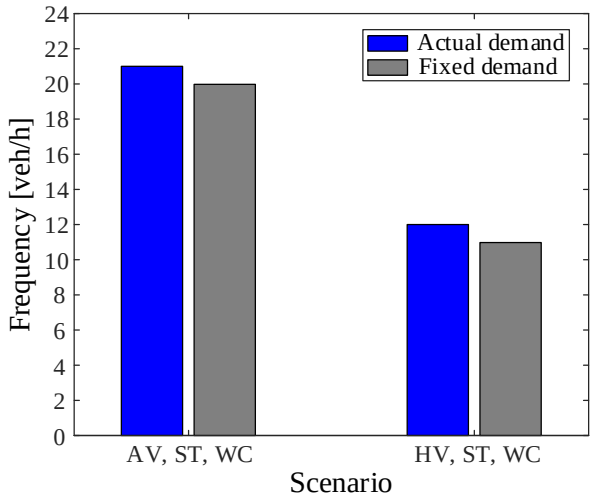

Figure 6-7 Sensitivity to demand fluctuation.

6.1.6 Sensitivity to crowding multipliers

We assess the sensitivity of solutions to changes in crowding cost parameters. In particular, lower levels of crowding multipliers have been reported in studies using revealed preference data in this context (Yap et al., 2020). Thus, we evaluate cases in which crowding multipliers (associated with load factors $>$ 100% in Table 3-2) are reduced by 20%, 40%, and 60%. It should be noted that to avoid reaching multipliers that are smaller than 1, for an old multiplier α, the reduction is applied on (α-1), then it is summed by 1 to introduce the new multiplier. For example, for an old multiplier of 2.10 in the case of 50% reduction, the new multiplier would be 1.55.

In Table 6-1, the results are given for the main scenarios (HV, ST, WC vs. AV, ST, WC) in the case of Santiago. Overall, automated bus solutions witness a slower reduction in frequencies as crowding multipliers are reduced. For example, with a reduction of 60% in crowding multipliers, frequencies reduce by 7% (from 81 to 75[veh/h]) in the AV, ST, WC scenario, while they reduce by 13% (from 67 to 58 [veh/h]) in the HV, ST, WC scenario. In essence, since operating costs are more noticeable in human-driven bus operations, frequencies decline at a faster trend (in the favor of operators) when travelers are less sensitive to the

crowding disutility. It should be noted that the optimal vehicle size is obtained as 18-m long buses in all cases.

Table 6-1 Sensitivity to crowding multipliers.

Reduction in crowding multipliers (%)	Scenario	Frequency (veh/h)
0	AV, ST, WC	81
	HV, ST, WC	67
20	AV, ST, WC	79
	HV, ST, WC	64
40	AV, ST, WC	77
	HV, ST, WC	61
60	AV, ST, WC	75
	HV, ST, WC	58

6.1.7 Sensitivity to extra waiting time values

In this part, we investigate the sensitivity of solutions to the value of extra waiting time savings caused by denied boarding. Particularly, compared to the value suggested by Cats et al. (2016) (as 3.5 times higher than the initial waiting time), lower values have been reported by recent studies employing revealed preference data in this context (Yap and Cats, 2021). Hence, we consider cases in which the value of extra waiting time savings is reduced by 20%, 40%, and 60%.

As shown in Table 6-2 for the case of Santiago, frequency solutions and the share of left-behind travelers are reported for the scenarios of HV, ST, WC and AV, ST, WC. Overall, vehicle automation still leads to the elimination of denied boardings. In essence, in such scenarios, to compensate for crowding discomfort and initial waiting time that has a high value of time savings, operating cost savings allow automated bus scenarios to still suggest high levels of frequency in the favor of users, and therefore optimal operations will not even become close to the critical denied boarding situations. Therefore, automated bus fleets can avoid denied boardings with higher degrees of robustness than human-driven fleets. Besides, our results show that the individual consideration of crowding discomfort in the planning of automated bus systems can even play a preventive role against denied boardings.

Table 6-2 Sensitivity to the extra waiting time value.

Reduction in extra waiting time value (%)	Scenario	Frequency (veh/h)	Left-behind travelers (%)
0	AV, ST, WC	81	0
	HV, ST, WC	67	0
20	AV, ST, WC	81	0
	HV, ST, WC	67	0
40	AV, ST, WC	81	0
	HV, ST, WC	65	0.1
60	AV, ST, WC	81	0
	HV, ST, WC	61	2.1

6.1.8 Sensitivity to user- and operator-oriented designs

In this part, we investigate the sensitivity of results to user- and operator-oriented design cases. For this purpose, we define two multipliers, as η and ℓ, to increase the value of user and operator cost savings respectively (i.e., the total cost in the objective function (3-1) can be expressed as $Z = \eta Z_p + \ell Z_o$, considering the fact that such multipliers were considered as 1 in the base-case experiments). For example, $\eta = 1.2$ and $\ell = 1.0$ imply that the current time valuations are increased by 20% for users, while the value of operator cost savings will remain unchanged the same as base-case valuations.

We test two scenarios: (i) $\eta = 1.2$ and $\ell = 1.0$, and (ii) $\eta = 1.0$ and $\ell = 1.2$ to represent user- and operator-oriented design cases respectively. Obviously, in line with the preference of users and operators, service frequency will increase and decrease in user- and operator-oriented design solutions respectively. However, cost savings achieved by vehicle automation deserve further analysis in such design conditions. Hence, comparing automated and human-driven bus scenarios, average cost savings with automation are reported for the case of Regensburg in Table 6-3. Overall, the results show that the savings of total costs with automation are roughly similar in both design cases, however, the benefits of automation are slightly more pronounced in the operator-oriented design case.

Table 6-3 Sensitivity to user- and operator-oriented designs.

Cost multipliers	UCS with automation (%)	OCS with automation (%)
$\eta = 1.0, \ell = 1.0$	19.8	15.8
$\eta = 1.2, \ell = 1.0$	20.3	15.1
$\eta = 1.0, \ell = 1.2$	19.1	16.4

UCS stands for user cost savings.
OCS stands for operator cost savings.

6.2 Sensitivity analysis for electric bus planning model

6.2.1 Sensitivity to demand level

We define a Demand Multiplier (DM) used to reduce/increase the basic demand level. For instance, a DM of 0.75 would reduce the base demand level by 25%. Fig. 6-8 illustrates the optimal frequencies obtained at various demand levels under two scenarios: fixed energy consumption rate (1.00 kWh/km) and variable energy demand. We find that the accuracy loss in supply decisions becomes larger as the DM increases. For instance, when DM is 1.50, the optimal frequency using the variable energy consumption model is 59 (veh/h), whereas the simplified fixed energy consumption rate yields 49 (veh/h), resulting in a loss of accuracy of 17%, compared to 13% when DM is 1.00.

Overall, our analysis indicates that the sensitivity of solutions to the energy estimation method is more pronounced at higher demand levels, emphasizing the need for incorporating a detailed energy consumption model in the scheduling of EB fleets, particularly for public transport operators serving busy bus corridors. Moreover, our variable energy demand model estimates the following average energy consumption rates for EBs across five different demand levels respectively: 1.12, 1.22, 1.34, 1.44, and 1.56 kWh/km.

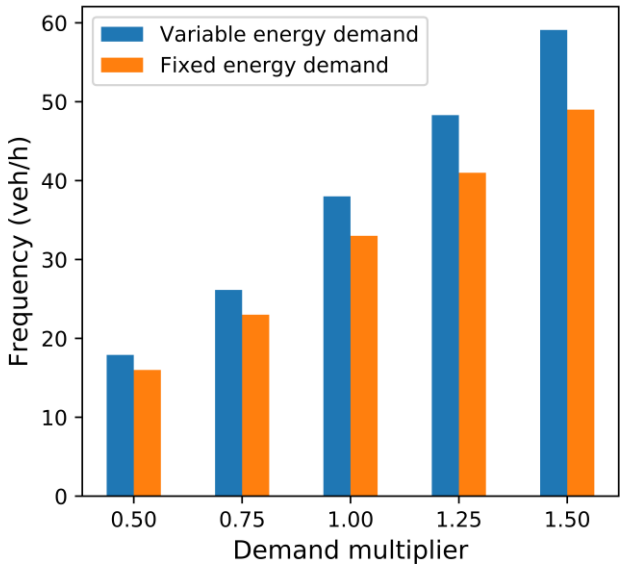

Figure 6-8 Comparing solutions under different demand levels based on the variable vs. fixed energy consumption model.

6.2.2 Sensitivity to route gradients

Optimal bus frequencies are influenced by changes in route gradients. Fig. 6-9 shows the gradient profile for the west-to-east direction of the route, where around 50% of the route is relatively flat, while the rest mostly has a positive slope ranging from +2% to +6%. We assume a symmetric bi-directional bus route, meaning that uphill sections in one direction are perceived as downhill sections in the other direction, although the absolute slope is the same in both directions.

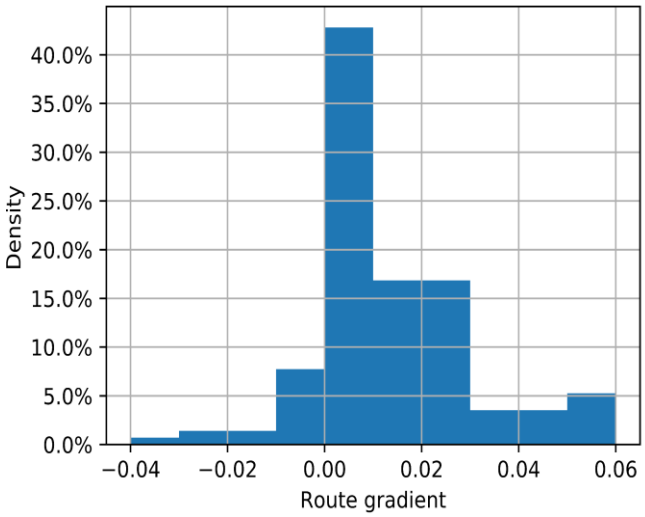

Figure 6-9 Histogram of route gradients (west-to-east direction).

The energy consumed by vehicles to overcome grade resistance is significant on uphill sections, and the mass of vehicles affects this resistance. We examine two cases with and without considering route gradients under different demand levels, as illustrated in Fig. 6-10. The solutions are more sensitive to slope variations at larger demand levels, and ignoring route gradients leads to an underestimation of the optimal frequency level by about 7% under DM=1.00 and 10% under DM=1.50. This discrepancy is particularly pronounced at higher demand levels, where grade resistance is amplified.

The average energy consumption rate is 1.46 (kWh/km) in the west-to-east direction, mostly containing positive gradients, and 1.22 (kWh/km) in the opposite direction, mostly containing negative gradients. Besides, since the passenger demand is higher in the west-to-east direction, vehicles are operated with an average occupancy rate of 79% in that direction, whereas this value is 71% in the east-to-west direction.

Our results highlight the importance of incorporating route characteristics into energy estimation models to capture load- and slope-sensitive effects concurrently. This is particularly relevant for public transportation agencies that need to deploy EB fleets on highly crowded and inclined bus corridors, such as our case study in Santiago, Chile.

It should be noted that the user cost element always seeks to improve its equilibrium state in favor of users. Therefore, the energy cost element's efforts to increase frequency (to reduce the passenger load per bus) are also supported by the user cost element, which seeks to further improve its own situation. Table 6-4 shows that the reduction in energy and user costs is stronger than the increase in operator costs caused by the need for more buses.

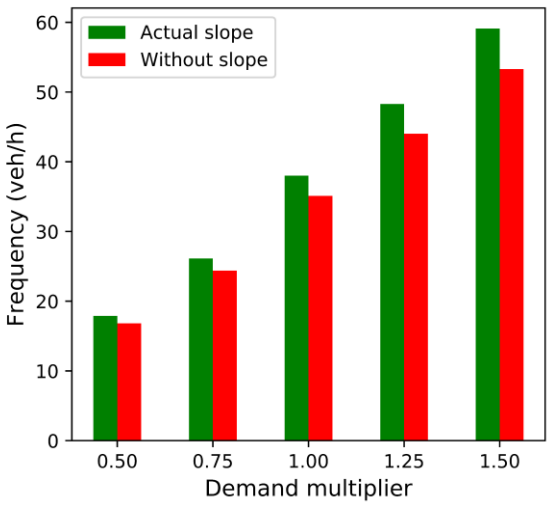

Figure 6-10 Sensitivity of solutions to route slope under different demand levels.

Table 6-4 Cost element comparison: Optimal vs. non-optimal frequencies with and without slope consideration.

Demand level	Solution	Avg. cost (€/pax)				
		User	Capital	Driver	Energy	Total
0.5	OP	0.60	0.42	0.38	0.27	1.67
	NOP[1]	0.61	0.41	0.37	0.29	1.68
0.75	OP	0.58	0.38	0.33	0.24	1.53
	NOP	0.60	0.36	0.32	0.27	1.55
1.00	OP	0.56	0.35	0.31	0.22	1.44
	NOP	0.60	0.32	0.29	0.26	1.47
1.25	OP	0.54	0.32	0.29	0.20	1.35
	NOP	0.58	0.29	0.26	0.24	1.38
1.50	OP	0.53	0.31	0.28	0.19	1.31
	NOP	0.59	0.27	0.25	0.24	1.35

6.2.3 Sensitivity energy regeneration capabilities

We conduct simulations to examine how different levels of the regeneration factor[2] can affect energy demand and planning decisions, considering both energy consumption and regeneration phases. In our case study, uphill energy consumption mainly occurs when traveling from west to east, while downhill energy regeneration occurs in the opposite direction.

Table 6-5 provides details on optimal frequency solutions, corresponding total costs, and average energy demand observed in different driving cycles under varying regeneration factor levels. Our findings demonstrate that regenerative technology can significantly reduce total costs and optimal frequencies, with a 100% regeneration factor reducing costs by about 9.5% compared to a regeneration factor of 20%. These results demonstrate the potential benefits of leveraging maximum regenerative braking capabilities in future EVs.

[1] In NOP, cost elements are estimated if a non-optimal (NOP) frequency solution, which is obtained without considering slope (red answers in Fig. 6-10), is applied for real-life operations while accounting for detailed energy demand requirements with slope. Note that, in OP, cost elements are presented in the operation with optimal solutions (green answers in Fig. 6-10).

[2] While several studies have explored the efficiency of regenerative braking systems for electric cars, there is limited evidence for heavy-duty vehicles, such as EBs. However, a few studies assume a regeneration factor of 60% for EBs (e.g., Gallet et al., 2018; Ma et al., 2021).

Table 6-5 Sensitivity to regenerative braking capability.

Regeneration factor (%)	Optimal frequency (veh/h)	Avg. energy demand (kWh/km)	Avg. total cost (€/pax)
20	38	1.31	1.47
30	38	1.28	1.46
40	37	1.25	1.44
50	37	1.22	1.43
60	36	1.19	1.40
70	36	1.16	1.39
80	35	1.12	1.36
90	34	1.09	1.34
100	34	1.05	1.33

6.2.4 Sensitivity to vehicle energy consumption in depot trips

We conduct a sensitivity analysis on the distance between the depot and the first station of the line to understand how it can affect frequency planning solutions. It should be noted that even if we run the base-case trials in our case study without considering the energy consumption of vehicles in depot trips, the same frequency planning solutions are obtained as in cases where this energy is taken into account. This is because the depot distance is relatively short (1.8 km) and the trip is almost flat in our case study[3]. Besides, vehicles are empty of passengers during depot trips (i.e., passenger load is zero), as well as vehicles do not need to cover any stations during the depot path, which saves energy consumption required for deceleration/acceleration activities when entering and exiting bus stations. Therefore, the energy required for depot trips is reasonably less pronounced than en-route energy consumption.

To further explore the impact of depot distance, we study the sensitivity of frequency determination by increasing the depot distance by 100%, 150%, and 200% (Table 6-6). Our results show that optimal frequencies are slightly reduced as the operator's energy cost increases with the bus depot being further away from the bus line. These findings emphasize

[3] It should be noted that in our peak analysis period (7-10 AM), the trips of all vehicles [based on the optimal peak frequency of 38 (veh/h)] are considered from the depot to the first station at the beginning of the planning period (7 AM). However, regarding the return trips to the depot after 10 AM, we assume some vehicles (34% of the whole fleet), still needed to continue the off-peak operations based on the frequency of 13 (veh/h), will remain in the line and other vehicles (66% of the fleet) will return to the depot (i.e., we do not consider the scenario of returning all vehicles to the depot).

the significance of depot distance in determining frequency plans when the distance traveled by vehicles between the depot and the bus line is significant.

Table 6-6 Sensitivity of frequency solutions to the depot distance.

Increase in the depot trip distance (%)	Frequency (veh/h)	Frequency reduction (%)
0	38	0
100	37	2.6
150	36	5.2
200	35	7.9

6.3 Sensitivity analysis for electric bus charging strategy selection

In this section, we examine the sensitivity of the charging alternatives' rankings to changes in the calculated weights for charging duration and battery cost. Assuming $W = (W^l, W^s, W^u)$ as the calculated weight for the relevant criterion, a changing interval is established by decreasing and increasing W by 50%, i.e., $[0.5W, 1.5W]$. This interval is then divided into 50 equal parts, resulting in the formation of 50 new criterion weight vectors. The impact of these weight changes on the alternatives' criterion functions is analyzed in Figs. 6-11 and 6-12. The results show that the ranking of the alternatives is impacted by changes in the criteria weights. For example, a 13% increase in the weight of the charging duration criterion leads to a shift in ranking, as seen in scenario 31. Besides, a 24% increase in the battery cost criterion weight leads to a shift in ranking in scenario 37. This highlights the sensitivity of the model to changes in the criteria weights, and suggests that variations in the weight assignment could result in the selection of the opportunity charging strategy as the optimal alternative.

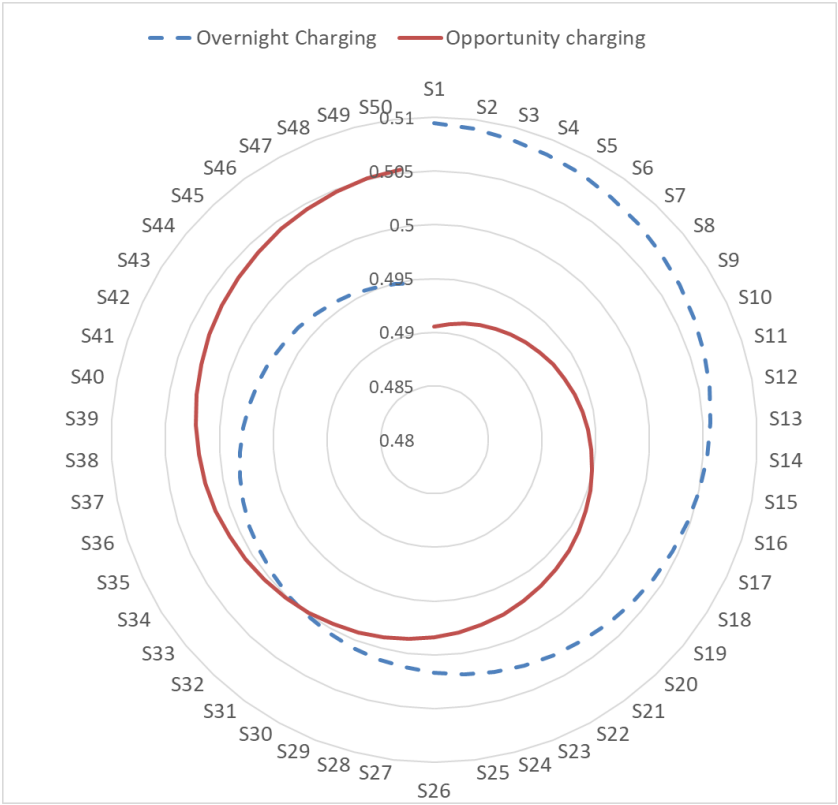

Figure 6-11 Sensitivity analysis on charging duration weight.

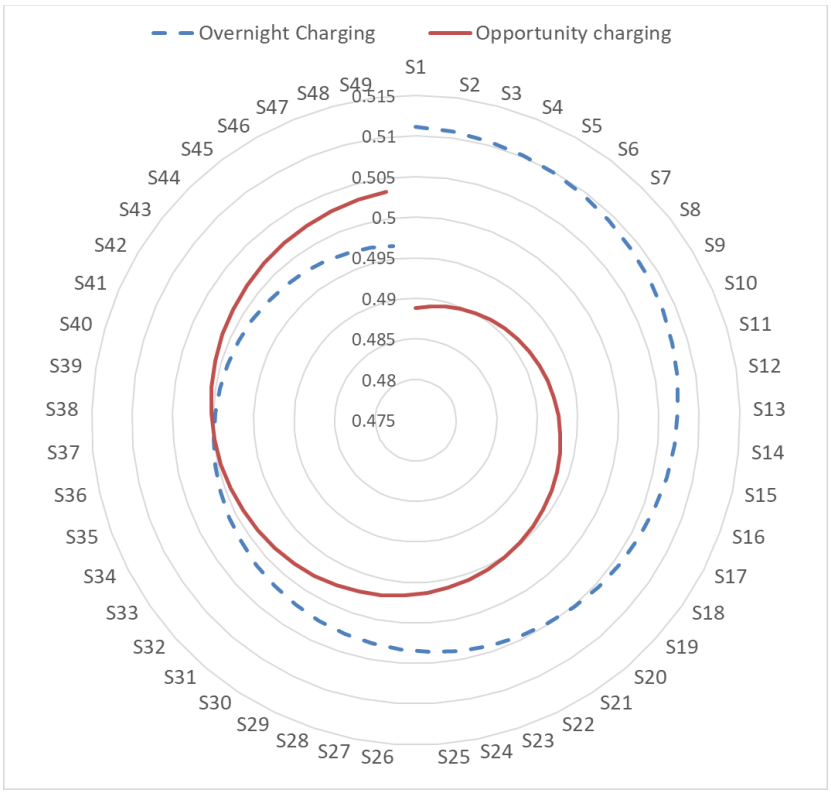

Figure 6-12 Sensitivity analysis on battery cost weight.

6.4 Sensitivity analysis for mixed-fleet bus scheduling models

6.4.1 Sensitivity analysis for the simple version of the mixed-fleet bus scheduling model

6.4.1.1 Sensitivity to dispatching headways (even and uneven headways)

We compare the optimal solution from Section 5.4.1.3 to the case in which buses are dispatched at a uniform headway of 6 minutes. As has been shown, as long as vehicle capacity constraints are not binding and passenger arrival rates at bus stops are uniform, an even headway minimizes waiting time (Osuna and Newell, 1972). We develop two even-headway dispatching scenarios:

(i) Same dispatching order as in Fig. 6-13 (a), under the constraint of a fixed 6-minute dispatching headway [see Fig. 6-13 (b)].

(ii) Optimal dispatching order, under the constraint of a fixed 6-minute dispatching headway [see Fig. 6-13 (c)].

In case (i), we see that the number of passengers left behind, and consequently the average passenger waiting time increase by 55% and 11.5%, going from 309 to 480 (pax) and from 3.55 to 3.96 (min/pax) respectively, if buses in the optimal solution are dispatched at an even headway of 6 minutes, while maintaining their dispatching order. In case (ii), we assume that vehicles are operated with a fixed 6-minute dispatching headway and only the dispatching order of each vehicle is optimized in this situation. We see that the percentage of passengers left behind is 14% and passenger waiting time increases by 9%, reaching 3.87 (min/pax). This shows the benefits of dispatching buses at uneven headways in a situation with different bus sizes and binding vehicle capacity constraints.

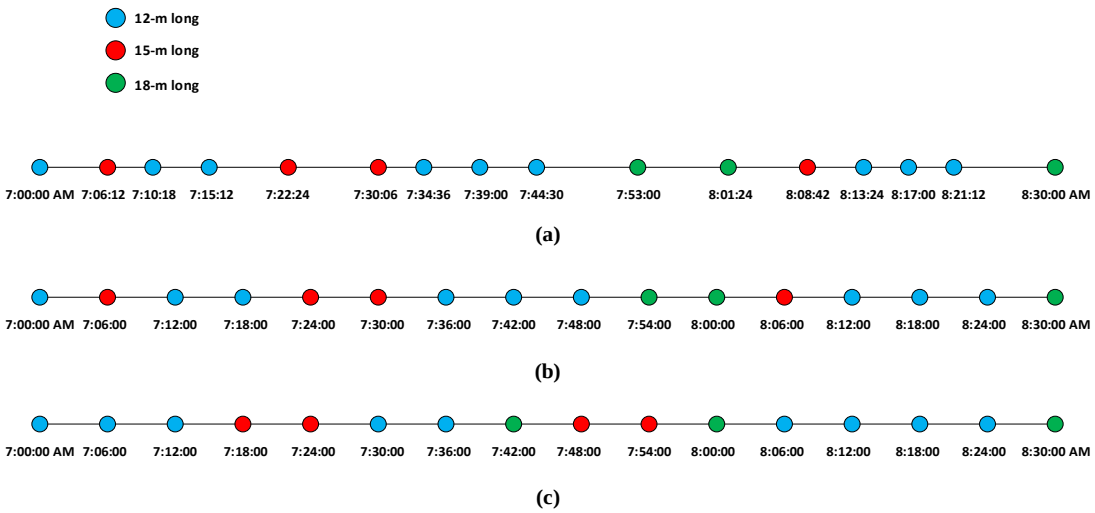

Figure 6-13 Dispatching patterns under high-resolution demand data: (a) optimal dispatching pattern; (b) same dispatching order in (a) with the constraint of a fixed 6-minute dispatching headway; and (c) optimal dispatching order with the constraint of a fixed 6-minute dispatching headway.

6.4.1.2 Comparing the optimal dispatching order with other predefined orders

In this section, we conduct further comparisons between the optimal solution and alternative dispatching schemes. Here we test the case of different patterns in which buses of the same size are dispatched consecutively. We test six different dispatching scenarios: $D_{12\text{-}15\text{-}18}$, $D_{12\text{-}18\text{-}15}$, $D_{15\text{-}12\text{-}18}$, $D_{15\text{-}18\text{-}12}$, $D_{18\text{-}12\text{-}15}$, $D_{18\text{-}15\text{-}12}$, in which buses are dispatched with a predetermined order and only the dispatching time of each bus is optimized. For example, in scenario $D_{12\text{-}15\text{-}18}$, 12 meters long buses are firstly dispatched, then 15 meters long buses, and finally 18 meters long buses are dispatched. The results are compared with the optimal scenario (see Table 6-7). Overall, the average passenger waiting time increases broadly in line with the percentage of passengers left behind. In the optimal scenario, the average passenger waiting time is 3.55 (min/pax), followed by a value of 4.04 (min/pax) in scenario $D_{15\text{-}12\text{-}18}$. Indeed, by comparing these two dispatching scenarios, we see that the optimal scenario leads to a decrease of 12.1% in the average passenger waiting, mainly caused by a further reduction in the percentage of passengers left behind, declining from 15.9% to 9.9%. Furthermore, using the optimal dispatching pattern instead of scenarios $D_{18\text{-}12\text{-}15}$, $D_{12\text{-}15\text{-}18}$, $D_{15\text{-}18\text{-}12}$, $D_{18\text{-}15\text{-}12}$, and $D_{12\text{-}18\text{-}15}$ can produce savings in the average passenger waiting time by 25.7, 20.2, 19.7, 16.8, and 14.3 percent, respectively. Therefore, in a mixed-fleet operation, it is relevant that bus agencies not only set bus dispatching headways, but also correctly assign vehicles of specific

sizes at the right time, in order to minimize the unwanted effects of large peak demands that temporally use all the available vehicle capacities.

Table 6-7 Comparing the optimal dispatching order with other predefined orders.

Scenario	The average passenger waiting time (min/pax)	Percentage of passengers left behind (%)
SA solution	3.55	9.9
$D_{12\text{-}15\text{-}18}$	4.45	20.6
$D_{12\text{-}18\text{-}15}$	4.14	17.1
$D_{15\text{-}12\text{-}18}$	4.04	15.9
$D_{15\text{-}18\text{-}12}$	4.42	19.9
$D_{18\text{-}12\text{-}15}$	4.78	23.6
$D_{18\text{-}15\text{-}12}$	4.24	18.2

As can be seen in Fig. 6-13 (a), 18-meter long buses are not dispatched early in the optimal scenario, showing that if larger buses (which have more room to carry passenger volumes at the maximum-load point of a route) are dispatched in an appropriate time to improve capacity utilization, they can reduce the number of passengers left behind; otherwise, it is probable that bus capacity is not used efficiently due to temporal and spatial differences in passenger volumes, thereby increasing passenger waiting times.

Fig. 6-14 gives information regarding the number of passengers left behind by each bus during the simulation time (a) in scenario $D_{15\text{-}12\text{-}18}$, and (b) in the optimal scenario. Looking firstly at Fig. 6-14 (a), we see that the number of passengers who fail to board increases steadily when 12-m long buses are dispatched sequentially. Indeed, these buses have no enough room to accommodate passengers who missed the previous buses due to a shortage of capacity, and consequently this situation will continue to deteriorate when they are dispatched sequentially. As Fig. 6-14 (b) shows, to optimize the capacity utilization of vehicles under the optimal scenario, buses of different capacities can be properly dispatched at specific times in accordance with demand conditions, and therefore the total number of passengers left behind by 12-m long buses reduces dramatically, dropping from 514 to 295 (pax).

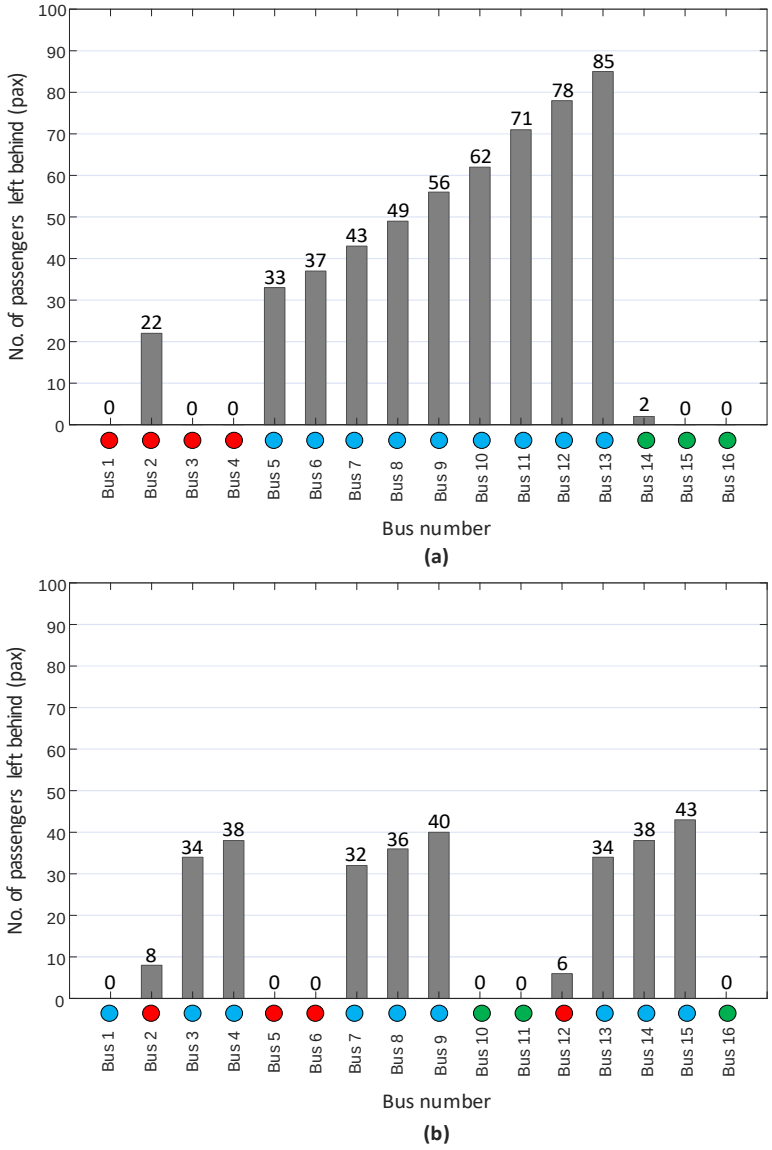

Figure 6-14 Total number of passengers left behind by each bus during the entire analysis period: (a) in scenario D15-12-18; and (b) in the optimal scenario.

6.4.1.3 Sensitivity to demand data resolution

To understand how having high-resolution demand data instead of low-resolution demand information (one-hour-dependent demand volumes) can affect the optimal solution, a comparison between these two demand cases is made in this section. The relevance of this comparison rests on the fact that demand fixed on an hourly basis is common in most public transport frequency or dispatching setting models, e.g., Hadas et al. (2010), Tirachini et al. (2014), and Niu et al. (2015).

If the optimal solution (the optimal dispatching headways and the optimal bus dispatching order) found with low-resolution demand (see Fig. 6-15) is applied to

high-resolution demand volumes, the average passenger waiting time increases by 15.5%, going from 3.55 to 4.10 (min/pax), due to an increase of 80% in the number of passengers left behind, going from 309 to 556 (pax). This result explicitly accentuates the advantage of having detailed demand information, especially when passenger arrival rates follow a bell-shaped pattern as time progresses. The peak inside the peak should be properly accounted for when designing dispatching schemes, which points to the relevance on investing to have detailed demand information for public transportation agencies, which includes the use of, e.g., smartcards and mobile phone data.

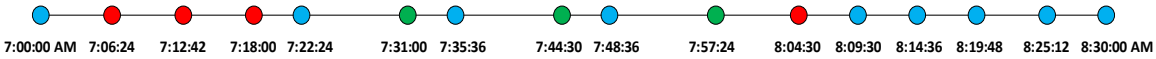

Figure 6-15 Optimal dispatching pattern under low-resolution demand data.

6.4.1.4 Uniform fleet

Next, we analyze the case in which a fleet with uniform bus sizes is available and only the dispatching time of each bus is optimized under high-resolution demand. The optimal dispatching solution with uniform fleets is presented in Fig. 10. In uniform fleets with 12, 15, and 18-meter long buses, the average passenger waiting time reaches the values of 5.96, 3.21, and 2.93 (min/pax) respectively, while the percentage of passengers left behind is equal to 34.2%, 5.6%, and 0% respectively in these three cases, showing that passengers are not confronted with a lack of capacity when an 18-meter fleet is used.

Regarding the optimal dispatching headways, as it is clear from Fig. 6-16, buses are not dispatched at quite even headways in order to deal with passenger demand fluctuation during the time operation, if capacity constraints are binding. This is clear for the case of 12-meter and 15-meter long buses, in which it is optimal to dispatch vehicles at uneven headways; in these cases the coefficient of variation of dispatching headways are 0.14 and 0.13, respectively. On the other hand, for 18-meter long buses, the dispatching headways are almost uniform, with a coefficient of variation of only 0.03. In any case, these coefficients of variation are much lower than that of the optimal solution with a mixed fleet in the base case (coefficient of variation 0.31). Therefore, we can conclude that the optimality of uneven dispatching headways stems from two elements: having a mixed fleet and having localized peaks on demand that make buses run full.

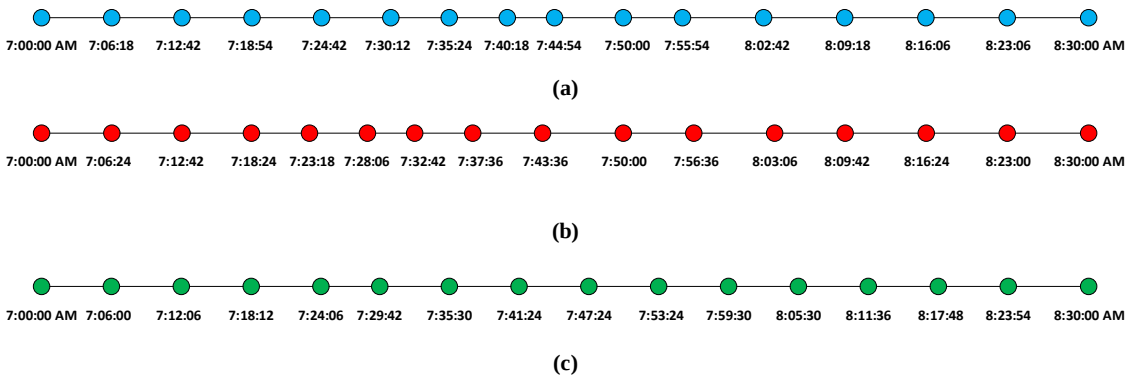

Figure 6-16 Optimal dispatching headway for uniform fleets: (a) 12-meter fleet; (b) 15-meter fleet; and (c) 18-meter fleet.

6.4.2 Sensitivity analysis for the advanced version of the mixed-fleet bus scheduling model

6.4.2.1 Sensitivity to demand

In this section, we analyze the sensitivity of solutions to variations in the demand level. To accomplish this, we introduce a Demand Multiplier (DM) to adjust the demand accordingly. Given that the base demand level is already high in this busy corridor (4500 pax/h), our analysis includes the application of various DMs to simulate decreased demand levels, such as DM=0.8 representing a 20% reduction from the base case demand.

For each demand level, Fig. 6-17 displays the fleet configurations recommended by each metaheuristic. In addition, Fig. 6-18 provides a comparative analysis of the cost and occupancy levels among the different metaheuristics. Based on our findings, utilizing more accurate and advanced solution algorithms, such as GWO-SA and GA-SA, proves to be more relevant for the optimal scheduling of mixed fleets in highly crowded situations that require a larger fleet size. The diversity of potential solutions for assigning different types of vehicles becomes increasingly intricate in such scenarios. However, as the demand decreases, the performance differences among the algorithms become less significant, and the use of simpler algorithms is enough to produce satisfactory results. For example, when comparing the solutions of the GA and GWO-SA at DM=0.8 (Fig. 6-18), the GWO-SA's solution leads to an 8.1% reduction in total cost (from 1.48 to 1.36 €/pax) and an 18.2% reduction in occupancy level (from 0.77 to 0.63). However, at lower demand levels, there are no significant differences in the solutions provided by the algorithms. The occupancy levels depicted in Fig. 6-20 highlight the superiority of the GWO-SA algorithm in highly crowded situations, whereas the performance differences between the algorithms diminish as the demand decreases.

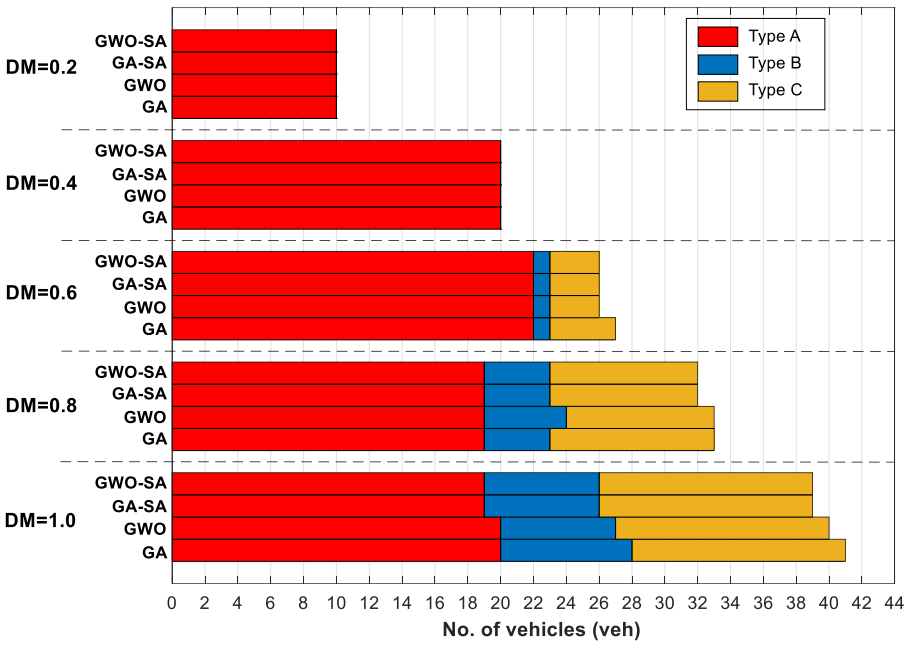

Figure 6-17 Fleet composition (vehicle assignment solutions) proposed by each metaheuristic for different demand levels (DM stands for demand multiplier, e.g., DM=0.8 represents a 20% reduction in the base case demand).

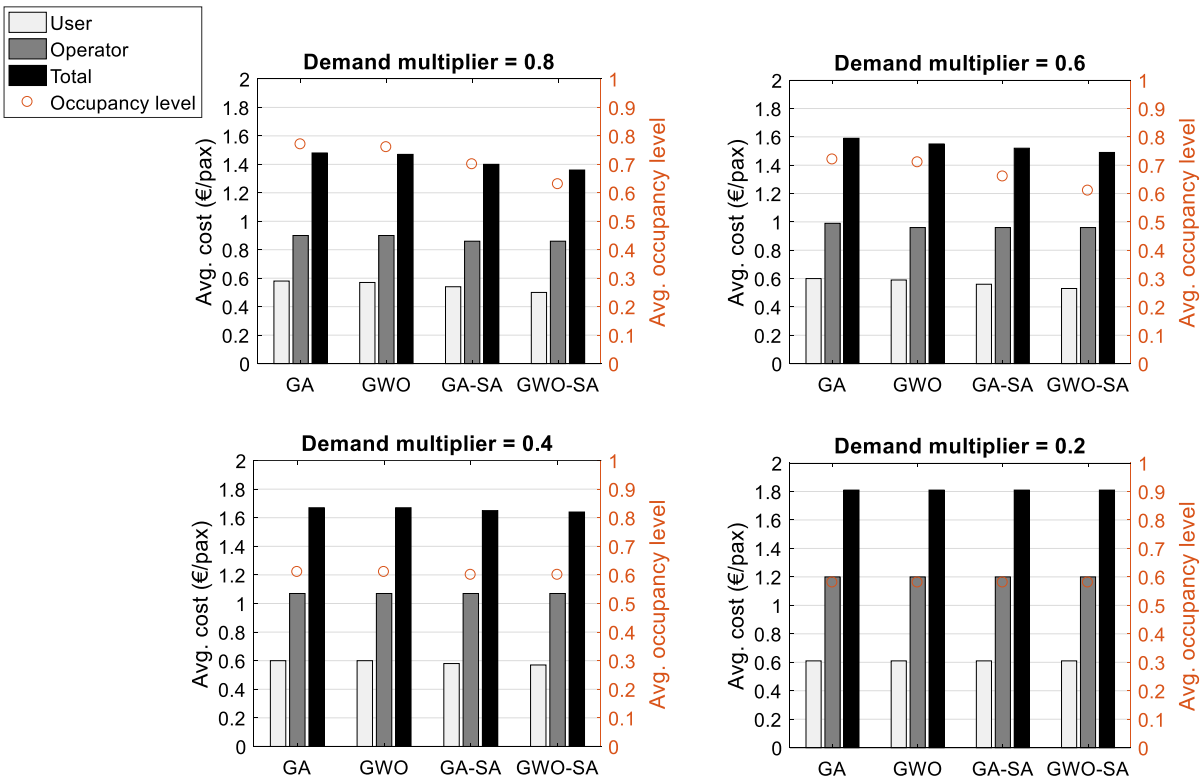

Figure 6-18 Comparison of cost and occupancy levels obtained by each metaheuristic at different demand levels.

Fig. 6-19 showcases the dispatching plans for heterogeneous fleet operations at DM=0.8 and DM=0.6. Although all three algorithms (GWO, GA-SA, and GWO-SA) propose the same fleet composition of 26 vehicles at DM=0.6, the dispatching scheme generated by GWO-SA proves to be more effective, resulting in greater reductions in cost and occupancy levels.

Figure 6-19 Dispatching schemes offered by each metaheuristic for different demand levels.

As the demand declines in the scheduling of heterogeneous fleets, the overall size of the allocated fleet, particularly the proportion of larger vehicles, decreases. For instance, when the

demand is reduced using a DM of 0.6 (Fig. 6-17), the fleet size of 39 vehicles (including 19 type-A, 7 type-B, and 13 type-C buses) decreases to a fleet size of 26 vehicles (including 22 type-A, 1 type-B, and 3 type-C buses) in the GWO-SA algorithm. This indicates that the number of smaller (type A) vehicles increases while the number of larger vehicles decreases, resulting in a more cost-effective operation.

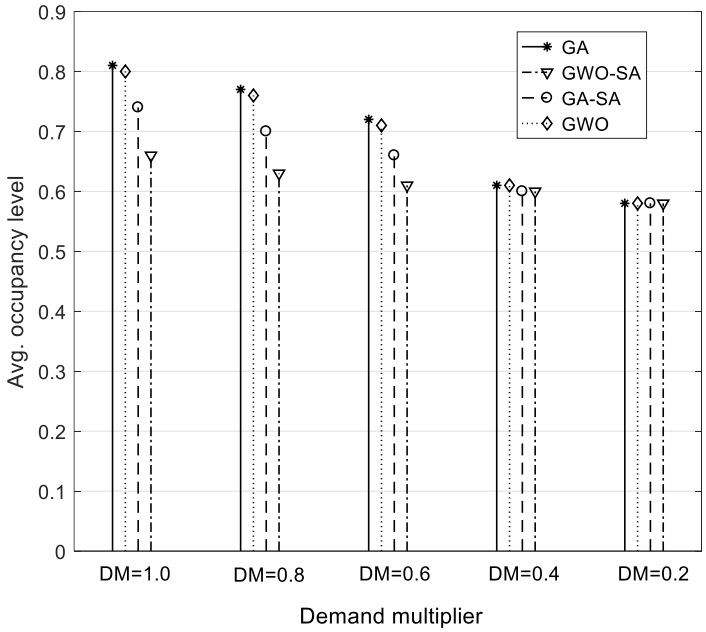

Figure 6-20 Occupancy levels of vehicles in the best solutions proposed by each metaheuristic for different demand levels.

6.4.2.2 Sensitivity to crowding discomfort valuations

We conduct a sensitivity analysis on the solutions generated by the GWO-SA algorithm to assess their sensitivity to variations in user cost savings from crowding. We change the crowding multiplier values by ±10%, ±20%, and ±30% to evaluate the algorithm's response. The higher crowding multipliers represent scenarios comparable to the COVID-19 situation, where the fear or possibility of infection can increase passenger discomfort inside vehicles, as demonstrated by studies such as Basnak et al. (2022) estimating crowding multipliers during the COVID-19 pandemic. The results of the sensitivity analysis provide valuable managerial insights for fleet operational planning in pandemic-related circumstances, as shown in Fig. 6-21. For example, when user dissatisfaction from crowding increases by 30%, we observe a corresponding 18% increase in the fleet size. Notably, the number of larger vehicles (type B

and type C) shows a higher rate of increase by 42.8% and 15.4%, respectively. In contrast, the number of type-A vehicles shows a more modest increase of 10.5%.

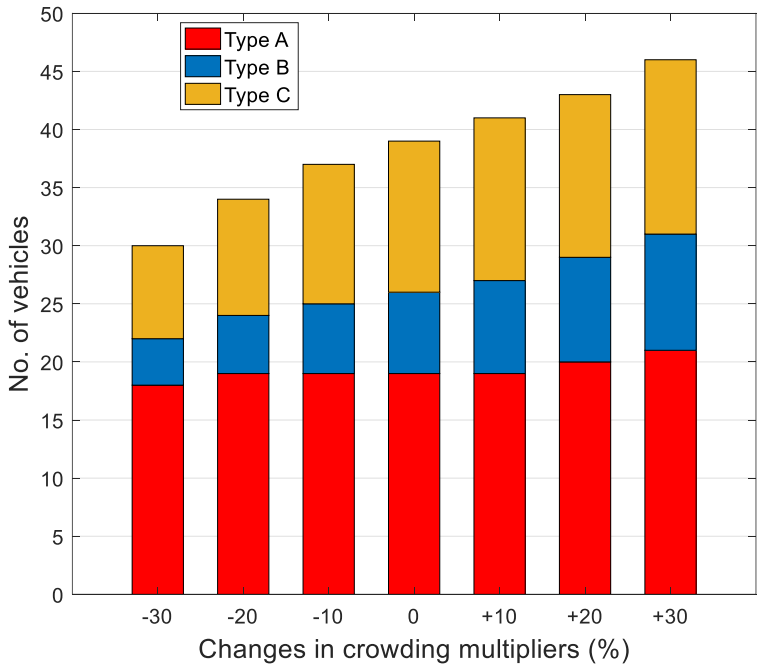

Figure 6-21 Sensitivity to crowding discomfort.

6.4.2.3 Sensitivity to uncertain driving times

We investigate the impact of uncertain travel times on vehicle assignment strategies in the MFBS problem. External factors such as road congestion, driver performance, and weather can introduce variability in the driving times of vehicles (Sadrani et al., 2022b). In this part, instead of using deterministic driving times, we incorporate random driving times derived from a log-normal distribution[4].

In the stochastic setting, each service may encounter a different driving time for the same segment, introducing uncertainty in travel times. To handle this uncertainty, we deploy an independent MCS program during the evaluation phase of the metaheuristics, enabling us to conduct enough evaluation runs (1000) to determine the OFV of each solution (Zhang et al., 2021, Sadrani et al., 2022a), as opposed to a single run that is suitable for

[4] Asymmetrical distributions such as the lognormal, loglogistic and gamma are usually found to provide good fits to the observed distributions of travel times by cars and buses, given that travel times are skewed with long right tails due to congestion (Duran-Hormazábal and Tirachini, 2016), while in some cases normal distributions have also been proposed (for a full review of travel time distributions in public transport see Büchel and Corman 2020).

deterministic cases. Essentially, the MCS program functions as a subroutine and is triggered specifically during the evaluation phase.

In Table 6-8, we report the sensitivity of the GWO-SA algorithm's solutions when uncertain travel times are incorporated. The results show an increase in the number of operational services, specifically a 13.6% rise in the number of type-A vehicles (from 19 to 22). This adjustment compensates for unfavorable waiting times experienced by users due to the unpredictability of driving times.

Table 6-8 Sensitivity to driving time uncertainty.

Travel time scenario	No. of vehicles (veh)		
	Type A	Type B	Type C
Deterministic	19	7	13
Uncertain	22	7	13

7 Conclusions

This dissertation explores the evolving landscape of urban bus systems, primarily focusing on developing mathematical optimization models and solution algorithms to address the aspects and complexities associated with the planning of automated, electric, and mixed-sized vehicle fleets. Furthermore, it introduces novel findings and insights, substantially enriching our scientific understanding of the optimal design and planning of these emerging bus fleets compared to traditional ones.

First, we develop a mathematical modeling framework to optimize service frequency and vehicle size for automated bus services, with stochastic travel times, time-dependent demand volumes, crowding externalities for both sitting and standing passengers, and the possibility of denied boarding due to capacity constraints. The model is able to estimate in-vehicle crowding discomfort at a microscopic level, bus by bus. Considering both passengers' and operators' costs, the model aims to find the optimal service frequency and vehicle size with minimal total costs of a public transport service. Extensive experiments are performed under different scenarios to achieve a detailed assessment of the service and cost implications of the deployment of automated bus systems.

To evaluate the applicability of the proposed model, several deployment scenarios are simulated through the combination of different cases: (i) vehicle technology (human-driven or automated vehicles), (ii) travel time between stops (deterministic or stochastic travel times), and (iii) crowding discomfort externalities (considering or ignoring in-vehicle crowding costs). Our experiments are executed for two real-world case studies in Regensburg, Germany, and Santiago, Chile. Besides, to further assess the possible effects of automation on the social costs of a public transportation service, an extensive range of sensitivity analysis tests are carried out on human driving cost savings with automation, travel time uncertainty, dwell time regularity, the time lost to open and close doors with automation, crowding multipliers, denied boarding saving values, and user- and operator-oriented design solutions.

The main findings are summarized as follows:

- When considering passenger comfort, both human-driven and automated bus fleets increase vehicle size. However, automated fleets increase service frequency at a higher rate.
- The deployment of automated bus services can significantly alleviate crowding-related capacity shortages as well, through a reduction or elimination

of denied boarding problems. Indeed, the actual benefits of automation might be underestimated if crowding effects are not considered in the design of an automated bus system.

- The consideration of stochastic travel times between stops in the deployment scenarios results in optimal frequencies that are increased for both fleets of human-driven and automated driving buses; however, frequencies are increased at a higher rate for automated bus fleets.
- Automation can have significant impacts on the reliability of public transport operations. Improved reliability in automated bus services can reduce passenger waiting time costs by enhancing the predictability of travel times.
- Interestingly, even though the potential of vehicle automation on reducing waiting times through increased frequencies is larger in high-income countries (Tirachini and Antoniou, 2020), we find that the final outcome is counterbalanced by the actual demand level in crowding-sensitive environments. In our case, the relative increase in optimal frequency was roughly similar in the Santiago and Regensburg case studies with the adoption of automated vehicles, because even though there is a greater potential of cost reduction in Regensburg due to larger driver cost savings, passenger demand in the Santiago case study was significantly larger, and therefore the crowding discomfort effect on pushing optimal frequencies up was stronger in Santiago than in Regensburg. Only a model, in which the value of travel time savings is sensitive to passenger occupancy levels, would be able to catch this effect.

Second, we propose an Electric Bus (EB) fleet planning problem in the form of an Integer Nonlinear Programming (INLP) model, which integrates a variable energy consumption model into the planning process. Our contributions include optimizing vehicle type selection and service frequencies with EBs, developing a comprehensive cost model, considering size-varying factors affecting the economic aspects of EB operations, time-dependent passenger demand modeling, and formulation of the EB planning problem as a combinatorial optimization model. From a policy point of view, this model would be useful specially in the early stages of an electric bus project, when making decisions on the type of bus and the number of vehicles to acquire. We apply our model to a bus route in Santiago de Chile and conducted several sensitivity tests to analyze the results. Our model yields several relevant findings:

- We demonstrate that using a fixed energy rate instead of a variable (detailed) energy estimation model can significantly reduce the accuracy of planning outcomes in terms of optimal supply levels.
- We quantify the accuracy loss in supply decisions and find that as the demand level rises, the sensitivity of solutions to the energy estimation method and to slope variations becomes increasingly important.
- We find that the energy consumption cost function is not monotonic as a function of service frequency. Only an EB planning problem with a variable energy consumption model (which measures load- and slope-sensitive effects) was able to identify this effect.
- We find that the average operator costs decrease as a function of demand, indicating the existence of economies of scale on a service with electric buses, even though the energy consumption cost function is not monotonic.
- We show that despite the increased capital and labor costs associated with higher EB frequency, cost savings from decreased user and energy costs are more noticeable up to certain levels, which can balance overall costs.
- We indicate the importance of depot distance in determining frequency plans when the distance traveled by vehicles between the depot and the bus line is significant.
- We explore the potential effects of regenerative braking systems on the EB planning and show that frequencies and total costs can be optimally reduced due to the role of regenerative technology in electric bus energy savings.

Third, we also develop a Multi-Criteria Decision-Making (MCDM) approach for selecting the best EB charging strategy, considering a comprehensive range of criteria, including economic, environmental, social, operational, and quality-of-service criteria. We consider two common charging strategies - overnight (slow) charging and opportunity (fast) charging - each with its advantages and disadvantages. A thorough literature review and a survey of EB experts are conducted to identify key decision-making factors in this area. A Fuzzy Best-Worst Method (FBWM) is designed to determine the weight of criteria, and a Fuzzy Ranking of Alternatives through Functional mapping of criterion subintervals into a Single Interval (FRAFSI) method is designed to rank available charging strategies for EB

systems in Munich, Germany. Other alternative-ranking methods are also tested for comparison, including fuzzy TOPSIS and fuzzy EDAS methods.

The research yields insightful findings that can serve as a valuable resource for transport agencies, decision makers, and future EB research:

- The most crucial aspect, affecting policymakers' decisions in selecting charging strategies, is found to be the economic one, followed by the operational and environmental aspects. The social aspect is considered the least important criterion.
- The infrastructure cost is identified as the most important factor in the economic category, followed by the battery cost and operational cost.
- In the global ranking of criteria, the battery cost is found to be the most important factor, followed by reliability, travel time, land acquisition cost, and driving range.
- The experts' assessments indicate a preference for overnight charging over opportunity charging. Besides, the results of the FRAFSI are in line with other methods (fuzzy TOPSIS and fuzzy EDAS).
- Analyzing the relative superiority of each alternative, the most significant differences between the two charging methods are evident in the charging duration, battery cost, and reliability. However, minor differences are found in terms of vehicle capacity and charging infrastructures' impacts on surrounding residential areas.
- The ranking of alternatives is shown to be sensitive to changes in the calculated weights for charging duration and battery cost.

Finally, we develop two novel Mixed-Integer Nonlinear Programming (MINLP) models to address Mixed-Fleet Bus Scheduling (MFBS) problems in simple and advanced versions, as combinational optimization problems.

In the simpler version of the MFBS problem, we formulate a MINLP model to optimize dispatching schemes (dispatching orders and times) when a given set of buses of different sizes are available to serve demand along a route. The objective is to minimize the average passenger waiting time under time-dependent demand volumes. Stochastic travel times between stops and vehicle capacity constraints (denied boarding situations) are explicitly modeled. A

Simulated Annealing (SA) algorithm coupled with a Monte Carlo Simulation (MCS) framework is developed to solve large real-world instances in the presence of stochastic travel times. The SA's results are also compared with the optimal answers achieved by GAMS in small- and medium-sized problems. To highlight the value of having fine-grained demand information (every 15 minutes instead of every 60 minutes) when designing a dispatching scheme, the experiments are also tested with low-resolution demand volumes (one-hour-dependent demand volumes). Overall, results show that:

- In addition to dispatching headway, bus dispatching sequence can strongly affect waiting times under a mixed-fleet operation.
- With an optimal dispatching sequence, a more accurate adjustment of supply to demand is possible in accordance with time-dependent demand conditions, and the total savings in waiting time are mainly driven by a further reduction in the number of passengers left behind.
- The optimality of uneven dispatching headways stems from two elements: having a mixed fleet and having localized peaks on demand that make buses run full.
- In heavy-demand bus corridors in which passenger arrival rates follow a bell-shaped pattern, not taking the detailed (high-resolution) demand information into account can lead to an unrealistic estimation of the passenger waiting time.

Then, we progress to the development of a more comprehensive MFBS model, expanding significantly on the simpler version. This advanced model incorporates a more comprehensive set of real-world operational constraints. These constraints include resource availability, sitting and standing space limitations, and various objective functions. Unlike the simpler MFBS model, this advanced version considers operator costs and user costs, which encompass in-vehicle trip times and trip comfort. Additionally, it introduces new integer decision variables for optimizing vehicle assignment programs. Consequently, this advanced problem goes beyond simply optimizing vehicle dispatching plans, and also determining the optimal number and types of vehicles required for mixed-fleet operations.

To tackle the complexity of this version of the MFBS problem and ensure practical viability, we employ two well-established metaheuristics: Genetic Algorithm (GA) and Grey Wolf Optimizer (GWO). We also developed two hybrid metaheuristic algorithms, GA-SA (a combination of GA and SA) and GWO-SA (a combination of GWO and SA), demonstrating promising performance in improving solution quality and optimization capabilities. A Taguchi

approach is utilized to calibrate the parameters of these metaheuristics, ensuring their robustness in solving the MFBS problem.

The performance of the proposed metaheuristics is evaluated on various test samples, including small, medium, and large-scale samples, considering CPU times and solution quality. We also compare the solutions of the metaheuristics with the optimal solutions acquired by GAMS software in small and medium-scale samples. By applying our model to a real bus corridor in Santiago, Chile, we optimize the operational plans and improve the quality of service for travelers. Overall, the main results are listed here:

- The GWO-SA outperforms the other metaheuristics. It also exhibits superior stability with fewer variations across multiple runs.
- The GA-SA demonstrates superior solution quality compared to both GA and GWO.
- Although GA and GWO algorithms propose larger fleet sizes, GA-SA and GWO-SA algorithms with smaller fleet sizes achieve lower user costs and vehicle occupancy levels. This underscores the importance of generating precise dispatching plans through advanced algorithms for cost savings and improved performance.
- Utilizing more advanced algorithms makes a difference in terms of service quality and optimal fleet size in crowded scenarios, whereas the choice of solution algorithm becomes less significant as demand decreases.

- **Work limitations and future research ideas**

This dissertation has some limitations normally. In future investigations regarding the design of automated bus systems, it is possible to incorporate additional decision variables into our models. For example, one could determine the optimal number of seats for different sizes of automated buses, along with the optimal internal layout and space allocated to seating and standing areas. Future studies may also explore a network modeling framework for the optimal deployment of automated bus services on multiple lines within a bus network, taking into account crowding externalities.

To extend our EB planning models, it could be interesting to incorporate uncertainties in energy consumption due to factors such as temperature and travel times. Developing solution algorithms that can handle these uncertainties would be a valuable avenue for future research. Additionally, considering the effects of in-vehicle occupancy levels on HVAC energy

consumption is worth exploring, as increasing passenger occupancy can impact HVAC energy consumption.

Regarding the charging strategy selection research, the number of experts involved in our BWM surveys was limited. Future research with a more diverse panel of experts could enhance the reliability of our findings. Additionally, it is useful to recognize that the criteria used in our work may not account for all relevant factors, and there could be potential biases in human judgments. Future studies could also build upon this research by considering the integration of renewable energy sources in the charging process and exploring the impact of advancements in battery technology on the charging strategy selection process.

In the realm of mixed-fleet operations, although we considered stochastic riding times in our models, another possible extension is considering dwell times at bus stops to be stochastic. Future research can expand the models to include other vehicle technologies, such as automated buses, and explore the combined case of human-driven and automated vehicles for public transport services. These avenues for future research provide opportunities to build upon the contributions made in this dissertation.

Appendix A. Data description.

Table A1 Parameter values for model applications.

Parameter	Unit	Regensburg	Santiago
Total demand	pax/h	638	5764
Route length	km	6.3	9
Acceleration time	s	6	6
Deceleration time	s	6	6
Time for opening and closing bus doors	s	6	6
Average alighting time per passenger	s/pax	1.5	1.5
Average boarding time per passenger	s/pax	2.5	2.5
Monetary value of in-vehicle time*	€/h	5.2	2.9
Monetary value of initial waiting time*	€/h	11.4	3.5
Monetary value of extra waiting time due to denied boarding**	€/h	39.9	12.3
Driver cost*	€/veh-h	15.3	6.2
Electric energy tariff	€/kWh	0.31	0.14
Average weight of one passenger	kg	75	75
Reduced human driving cost automation (base case scenarios)	%	50	50
Reduced running cost automation	%	10	10

* Source: Tirachini and Antoniou (2020).

** The monetary value of extra waiting time due to denied boarding is 3.5 times higher than that of initial waiting time (Cats et al., 2016).

Size-dependent parameters are presented in Tables A2 and A3, taken from the work of Tirachini and Antoniou (2020) for both Germany and Chile.

Table A2 Size-dependent parameters, Regensburg (Source: Tirachini and Antoniou, 2020).

Parameter	Unit	Mini bus	Standard bus	Rigid bus	Articulated bus
Vehicle length	m	8	12	15	18
Vehicle capacity	pax/veh	44	70	90	110
No. of seats	-	25	40	50	60
No. of doors	-	1	2	3	4
PA=PB*	%	100	60	43	30
Vehicle running cost	€/veh-km	0.7	1.1	1.3	1.6
Vehicle capital cost	€/veh-h	7.7	11.5	14.7	17.2
Increased capital cost automation	%	37	25	25	24

* PA and PB are the proportions of passengers getting off and on through the busiest door respectively.

Table A3 Size-dependent parameters, Santiago (Source: Tirachini and Antoniou, 2020).

Parameter	Unit	Mini bus	Standard bus	Rigid bus	Articulated bus
Vehicle length	m	8	12	15	18
Vehicle capacity[1]	pax/veh	50	90	115	145
No. of seats	-	25	40	50	60
No. of doors	-	1	2	3	4
PA=PB*	%	100	60	43	30
Vehicle running cost	€/veh-km	0.4	0.7	0.9	1.1
Vehicle capital cost	€/veh-h	5.2	7.7	9.5	11.6
Increased capital cost automation	%	37	25	25	24

- **Demand data for the application of automated bus planning model**

In Table A4, time-dependent passenger arrival rates are listed for the bus corridor in Regensburg during a planning period extending from 7:00 to 9:00 AM. As can be seen, we provide a 15-minute-dependent passenger demand (remaining fixed during each interval of 15 minutes). Moreover, in Table A5, we provide a fixed demand case used for performing a

[1] It should be noted that the bus capacity is commonly assumed to be larger in Santiago, due to a higher density of standees normally accepted among public transport users in Santiago compared to Germany (Tirachini and Antoniou, 2020).

sensitivity analysis test in Section 6.1.5. The values in Table A5 are derived from averaging arrival flow rates within the corresponding 15-minute intervals, given in Table A4.

Table A4 15-minute-dependent passenger arrival rates (unit: pax/min).

Stop	7:00-7:15	7:15-7:30	7:30-7:45	7:45-8:00	8:00-8:15	8:15-8:30	8:30-8:45	8:45-9:00
1	0.80	0.86	0.95	1.16	1.10	1.00	0.95	0.85
2	0.25	0.27	0.27	0.33	0.29	0.27	0.25	0.23
3	0.20	0.21	0.21	0.26	0.25	0.23	0.21	0.20
4	0.32	0.34	0.34	0.36	0.35	0.30	0.27	0.25
5	0.26	0.28	0.31	0.38	0.36	0.35	0.29	0.27
6	0.50	0.52	0.65	0.75	0.60	0.71	0.65	0.61
7	0.21	0.23	0.24	0.30	0.26	0.25	0.22	0.20
8	0.86	0.91	0.79	0.93	0.95	0.81	0.77	0.71
9	0.46	0.49	0.56	0.68	0.65	0.62	0.55	0.51
10	0.64	0.69	0.7	0.83	0.82	0.78	0.71	0.66
11	0.23	0.25	0.27	0.30	0.29	0.27	0.23	0.21
12	0.00	0.00	0.00	0.00	0.00	0.00	0.00	0.00
13	0.81	0.76	1.00	1.15	1.10	0.95	1.00	0.95
14	0.33	0.35	0.34	0.28	0.37	0.20	0.19	0.18
15	0.14	0.14	0.21	0.26	0.22	0.30	0.14	0.13
16	0.42	0.44	0.39	0.45	0.26	0.28	0.29	0.28
17	0.31	0.33	0.30	0.44	0.36	0.33	0.38	0.35
18	0.45	0.47	0.76	0.64	0.63	0.78	0.58	0.54
19	0.25	0.26	0.24	0.19	0.20	0.21	0.25	0.23
20	0.91	0.95	0.74	0.88	0.76	0.49	0.53	0.65
21	0.56	0.59	0.67	0.88	0.59	0.78	0.50	0.46
22	0.71	0.74	0.83	0.83	0.54	0.50	0.77	0.72
23	0.27	0.28	0.34	0.18	0.35	0.23	0.18	0.21
24	0.00	0.00	0.00	0.00	0.00	0.00	0.00	0.00

Table A5 Fixed passenger arrival rates (unit: pax/min).

Stop	7:00-9:00
1	0.96
2	0.27
3	0.22
4	0.32
5	0.31
6	0.62
7	0.24
8	0.84
9	0.57
10	0.73
11	0.26
12	0
13	0.95
14	0.28
15	0.19
16	0.35
17	0.35
18	0.61
19	0.23
20	0.74
21	0.63
22	0.71
23	0.26
24	0

- **Demand data for the application of simple mixed-fleet bus scheduling model**

For the bus corridor in Sydney, Tables A6 and A7 list the time-dependent passenger arrival rate ($\lambda_j[t]$) at each stop during the considered time horizon for every 15 minutes (high-resolution demand) vs. every 60 minutes (low-resolution demand). Indeed, in the high-resolution demand case, the passenger arrival rates are assumed to be constant during each 15-minute time interval; however, in the low-resolution demand case, the passenger arrival rates remain constant during each one-hour period. The unit of arrival rate is passengers/min, i.e., the number of passengers arriving at a stop per minute.

Table A6 High-resolution passenger arrival rates (unit: pax/min).

Stop	7:00-7:15	7:15-7:30	7:30-7:45	7:45-8:00	8:00-8:15	8:15-8:30
1	2.56	3.22	3.94	4.42	4.21	3.81
2	0.85	0.89	1.01	1.27	1.13	1.06
3	0.67	0.77	0.82	0.99	0.97	0.89
4	1.08	0.96	1.31	1.38	1.35	1.15
5	0.88	1.05	1.21	1.47	1.37	1.33
6	1.66	2.32	2.32	2.88	2.29	2.72
7	0.72	0.79	0.93	1.15	1.02	0.96
8	2.87	2.72	3.02	3.56	3.64	3.11
9	1.55	1.95	2.15	2.59	2.49	2.39
10	2.14	2.52	2.66	3.17	3.15	2.98
11	0.79	0.83	1.06	1.17	1.11	1.04
12	0	0	0	0	0	0
13	2.04	3.54	3.96	4.34	4.04	3.62
14	1.11	0.71	1.31	1.07	1.41	0.79
15	0.47	0.51	0.82	0.99	0.87	1.16
16	1.40	1.06	1.51	1.73	1.01	1.09
17	1.05	1.36	1.15	1.69	1.37	1.26
18	1.49	2.08	2.90	2.45	2.40	2.99
19	0.83	0.91	0.93	0.75	0.76	0.81
20	3.01	1.91	2.11	3.38	2.91	1.87
21	1.86	1.76	2.58	3.37	2.24	2.98
22	2.35	2.77	3.19	3.17	2.05	1.93
23	0.91	0.66	1.32	0.70	1.33	0.88
24	0	0	0	0	0	0

Table A7 Low-resolution passenger arrival rates[2] (unit: pax/min).

Stop	7:00-8:00	8:00-8:30
1	3.54	4.01
2	1.01	1.09
3	0.81	0.93
4	1.18	1.25
5	1.15	1.35
6	2.29	2.51
7	0.89	0.99
8	3.04	3.37
9	2.06	2.44
10	2.62	3.06
11	0.96	1.07
12	0	0
13	3.47	3.83
14	1.05	1.10
15	0.69	1.02
16	1.43	1.05
17	1.31	1.32
18	2.23	2.69
19	0.86	0.78
20	2.60	2.39
21	2.39	2.61
22	2.87	1.99
23	0.89	1.11
24	0	0

- **Generated data for testing advanced mixed-fleet bus scheduling model**

Table A8 lists the characteristics of fleet composition (resource availability), demand level, and bus route for the simulation of test instances, solved to validate the performance of the metaheuristics.

[2] The values in Table A7 are obtained through the average of passenger arrival rates during the relevant 15-minute time intervals presented in Table A6.

Table A8 Characteristics of test instances.

Class	Instance ID	Max No. of available vehicles for operations	U_A	U_B	U_C	No. of stations	Demand level (pax/h)
Small	S1	4	2	1	1	6	300
	S2	4	1	1	2	6	310
	S3	5	2	2	1	6	400
	S4	5	2	1	2	6	420
	S5	6	2	2	2	8	450
	S6	6	1	3	2	8	480
	S7	6	1	2	3	8	500
	S8	7	3	3	1	8	520
	S9	7	2	3	2	8	550
	S10	7	1	3	3	8	590
Medium	M1	8	4	2	2	10	600
	M2	8	3	3	2	10	635
	M3	8	2	3	3	10	670
	M4	9	4	3	2	12	700
	M5	9	3	3	3	12	700
	M6	9	2	3	4	12	750
	M7	10	4	4	2	14	850
	M8	10	4	3	3	14	850
	M9	10	2	4	4	14	870
	M10	11	3	4	4	14	950
Large	L1	12	5	4	3	16	1000
	L2	15	7	4	4	16	1100
	L3	18	9	5	4	16	1300
	L4	22	12	5	5	16	1500
	L5	26	13	7	6	18	2000
	L6	30	15	8	7	18	2300
	L7	33	16	9	8	18	2800
	L8	33	12	11	10	18	2800
	L9	38	22	8	8	20	3000
	L10	40	20	10	10	20	3300

U_A, U_B, and U_C stand for the maximum resource availability on type A (12-m long), type B (15-m long), and type C (18-m long) vehicles, respectively.

Bibliography

Abdelaty, H., Al-Obaidi, A., Mohamed, M., Farag, H.E.Z., 2021. Machine learning prediction models for battery-electric bus energy consumption in transit. Transp. Res. Part D Transp. Environ. 96, 102868.

Abdelaty, H., Mohamed, M., 2022. A framework for BEB energy prediction using low-resolution open-source data-driven model. Transp. Res. Part D Transp. Environ. 103, 103170.

Abe, R., 2019. Introducing autonomous buses and taxis: Quantifying the potential benefits in Japanese transportation systems. Transp. Res. Part A Policy Pract. 126, 94–113.

Adheesh, S.R., Vasisht, M.S., Ramasesha, S.K., 2016. Air-pollution and economics: diesel bus versus electric bus. Curr. Sci. 858–862.

Agrawal, K., Suman, H.K., Bolia, N.B., 2020. Frequency optimization models for reducing overcrowding discomfort. Transp. Res. Rec. 2674, 160–171.

Ainsalu, J., Arffman, V., Bellone, M., Ellner, M., Haapamäki, T., Haavisto, N., Josefson, E., Ismailogullari, A., Lee, B., Madland, O., 2018. State of the art of automated buses. Sustainability 10, 3118.

Akbari, M., Rashidi, H., Alizadeh, S.H., 2017. An enhanced genetic algorithm with new operators for task scheduling in heterogeneous computing systems. Eng Appl Artif Intell 61, 35–46.

Alessandrini, A., Holguin, C., Parent, M., 2011. Advanced transport systems showcased in La Rochelle, in: 2011 14th International IEEE Conference on Intelligent Transportation Systems (ITSC). IEEE, pp. 896–900.

Allport, R.J., 1981. The costing of bus, light rail transit and metro public transport systems. Traffic Engineering and Control, 22, 633–639.

Al-Ogaili, A.S., Ramasamy, A., Hashim, T.J.T., Al-Masri, A.N., Hoon, Y., Jebur, M.N., Verayiah, R., Marsadek, M., 2020. Estimation of the energy consumption of battery driven electric buses by integrating digital elevation and longitudinal dynamic models: Malaysia as a case study. Appl. Energy 280, 115873.

Alwesabi, Y., Wang, Y., Avalos, R., Liu, Z., 2020. Electric bus scheduling under single depot dynamic wireless charging infrastructure planning. Energy 213, 118855.

Amiri, M. P. 2010. Project selection for oil-fields development by using the AHP and fuzzy TOPSIS methods. Expert Systems with Applications, 37(9), 6218-6224.

An, Q., Fu, X., Huang, D., Cheng, Q., Liu, Z., 2020. Analysis of adding-runs strategy for peak-hour regular bus services. Transp. Res. Part E Logist. Transp. Rev. 143, 102100.

Azad, M., Hoseinzadeh, N., Brakewood, C., Cherry, C.R., Han, L.D., 2019. Fully autonomous buses: A literature review and future research directions. J. Adv. Transp. 2019.

Badia, H., Jenelius, E., 2021. Design and operation of feeder systems in the era of automated and electric buses. Transp. Res. Part A Policy Pract. 152, 146–172.

Bansal, P., Kockelman, K.M., 2017. Forecasting Americans' long-term adoption of connected and autonomous vehicle technologies. Transp. Res. Part A Policy Pract. 95, 49–63.

Bartholdi III, J.J., Eisenstein, D.D., 2012. A self-coördinating bus route to resist bus bunching. Transp. Res. Part B Methodol. 46, 481–491.

Basma, H., Haddad, M., Mansour, C., Nemer, M., and Stabat, P. 2022a. Evaluation of the techno-economic performance of battery electric buses: Case study of a bus line in paris. Research in Transportation Economics, 95, 101207. doi:https://doi.org/10.1016/j.retrec.2022.101207

Basma, H., Mansour, C., Haddad, M., Nemer, M., and Stabat, P. 2020. Comprehensive energy modeling methodology for battery electric buses. Energy, 207, 118241. doi:https://doi.org/10.1016/j.energy.2020.118241

Basma, H., Mansour, C., Haddad, M., Nemer, M., and Stabat, P. 2022b. Energy consumption and battery sizing for different types of electric bus service. Energy, 239, 122454. doi:https://doi.org/10.1016/j.energy.2021.122454

Basnak, P., Giesen, R., Muñoz, J.C., 2022. Estimation of crowding factors for public transport during the COVID-19 pandemic in Santiago, Chile. Transp Res Part A Policy Pract 159, 140–156.

Basso, R., Kulcsár, B., Egardt, B., Lindroth, P., Sanchez-Diaz, I., 2019. Energy consumption estimation integrated into the electric vehicle routing problem. Transp. Res. Part D Transp. Environ. 69, 141–167.

Batarce, M., Muñoz, J.C., de Dios Ortúzar, J., 2016. Valuing crowding in public transport: Implications for cost-benefit analysis. Transp. Res. Part A Policy Pract. 91, 358–378.

Beheshti, Z., 2021. A novel x-shaped binary particle swarm optimization. Soft comput 25, 3013–3042.

Behzad, M., Hashemkhani Zolfani, S., Pamucar, D., and Behzad, M. 2020. A comparative assessment of solid waste management performance in the Nordic countries based on BWM-EDAS. Journal of Cleaner Production, 266, 122008. doi:https://doi.org/10.1016/j.jclepro.2020.122008

Benoliel, P., Jenn, A., and Tal, G. 2021. Examining energy uncertainty in battery bus deployments for transit agencies in California. Transportation Research Part D: Transport and Environment, 98, 102963. doi:https://doi.org/10.1016/j.trd.2021.102963

Berrebi, S.J., Watkins, K.E., Laval, J.A., 2015. A real-time bus dispatching policy to minimize passenger wait on a high frequency route. Transportation Research Part B: Methodological 81, 377–389.

Bi, Z., De Kleine, R., Keoleian, G.A., 2017. Integrated Life Cycle Assessment and Life Cycle Cost Model for Comparing Plug-in versus Wireless Charging for an Electric Bus System. J. Ind. Ecol. 21, 344–355.

Boden, T.A., Andres, R.J., Marland, G., 2017. Global, regional, and national fossil-fuel co2 emissions (1751-2014)(v. 2017). Environmental System Science Data Infrastructure for a Virtual Ecosystem.

Boré, A., Cui, J., Huang, Z., Huang, Q., Fellner, J., and Ma, W. 2022. Monitored air pollutants from waste-to-energy facilities in China: Human health risk, and buffer distance assessment. Atmospheric Pollution Research, 13(7), 101484. doi:https://doi.org/10.1016/j.apr.2022.101484

Bösch, P.M., Becker, F., Becker, H., Axhausen, K.W., 2018. Cost-based analysis of autonomous mobility services. Transp. Policy 64, 76–91.

Boussaïd, I., Lepagnot, J., Siarry, P., 2013. A survey on optimization metaheuristics. Inf Sci (N Y) 237, 82–117.

Brinckerhoff, P., 2013. Group, K.; Texas, A.: Transit capacity and quality of service manual. Transit Cooperative Highway Research Program (TCRP) Report 165. Transp. Res. Board Washington, DC.

Büchel, B., & Corman, F. (2020). Review on statistical modeling of travel time variability for road-based public transport. Frontiers in Built Environment, 6, 70.

Campos, M., Mensión, J., and Estrada, M. 2021. Charging operations in battery electric bus systems at the depot. Transportation Research Procedia, 58, 103-110. doi:https://doi.org/10.1016/j.trpro.2021.11.015

Cao, Z., Ceder, A.A., 2019. Autonomous shuttle bus service timetabling and vehicle scheduling using skip-stop tactic. Transp. Res. Part C Emerg. Technol. 102, 370–395.

Cao, Z., Ceder, A.A., Zhang, S., 2019. Real-time schedule adjustments for autonomous public transport vehicles. Transp. Res. Part C Emerg. Technol. 109, 60–78.
Cats, O., Glück, S., 2019. Frequency and vehicle capacity determination using a dynamic transit assignment model. Transp. Res. Rec. 2673, 574–585.
Cats, O., Jenelius, E., 2018. Beyond a complete failure: the impact of partial capacity degradation on public transport network vulnerability. Transp. B Transp. Dyn. 6, 77–96.
Cats, O., Larijani, A.N., Koutsopoulos, H.N., Burghout, W., 2011. Impacts of Holding Control Strategies on Transit Performance: Bus Simulation Model Analysis. Transp. Res. Rec. 2216, 51–58. https://doi.org/10.3141/2216-06
Cats, O., West, J., Eliasson, J., 2016. A dynamic stochastic model for evaluating congestion and crowding effects in transit systems. Transp. Res. Part B Methodol. 89, 43–57. https://doi.org/https://doi.org/10.1016/j.trb.2016.04.001
Ceder, A.A., 2021. Syncing sustainable urban mobility with public transit policy trends based on global data analysis. Sci. Rep. 11, 1–13.
Ceder, A.A., Hassold, S., Dano, B., 2013. Approaching even-load and even-headway transit timetables using different bus sizes. Public transport 5, 193–217.
Chao, Z., Xiaohong, C., 2013. Optimizing battery electric bus transit vehicle scheduling with battery exchanging: Model and case study. Procedia-Social Behav. Sci. 96, 2725–2736.
Chen, C.-T. 2000. Extensions of the TOPSIS for group decision-making under fuzzy environment. Fuzzy Sets and Systems, 114(1), 1-9. doi:https://doi.org/10.1016/S0165-0114(97)00377-1
Chen, J., Liu, Z., Zhu, S., Wang, W., 2015. Design of limited-stop bus service with capacity constraint and stochastic travel time. Transp Res E Logist Transp Rev 83, 1–15.
Chen, X., Zhang, H., Xu, Z., Nielsen, C. P., McElroy, M. B., and Lv, J. 2018. Impacts of fleet types and charging modes for electric vehicles on emissions under different penetrations of wind power. Nature Energy, 3(5), 413-421. doi:10.1038/s41560-018-0133-0
Chen, Y., Zhang, Y., Sun, R., 2021. Data-driven estimation of energy consumption for electric bus under real-world driving conditions. Transp. Res. Part D Transp. Environ. 98, 102969.
Chiraphadhanakul, V., Barnhart, C., 2013. Incremental bus service design: combining limited-stop and local bus services. Public Transp. 5, 53–78.
Chu, T.-C., and Lin, Y.-C. 2003. A fuzzy TOPSIS method for robot selection. The International Journal of Advanced Manufacturing Technology, 21, 284-290.
Cortés, C.E., Jara-Díaz, S., Tirachini, A., 2011. Integrating short turning and deadheading in the optimization of transit services. Transp. Res. Part A Policy Pract. 45, 419–434.
Dai, Z., Liu, X.C., Chen, X., Ma, X., 2020. Joint optimization of scheduling and capacity for mixed traffic with autonomous and human-driven buses: A dynamic programming approach. Transp. Res. Part C Emerg. Technol. 114, 598–619.
Dai, Z., Ma, X., Chen, X., 2019. Bus travel time modelling using GPS probe and smart card data: A probabilistic approach considering link travel time and station dwell time. J. Intell. Transp. Syst. 23, 175–190.
Dakic, I., Yang, K., Menendez, M., Chow, J.Y.J., 2021. On the design of an optimal flexible bus dispatching system with modular bus units: Using the three-dimensional macroscopic fundamental diagram. Transportation Research Part B: Methodological 148, 38–59. https://doi.org/https://doi.org/10.1016/j.trb.2021.04.005
De Palma, A., Kilani, M., Proost, S., 2015. Discomfort in mass transit and its implication for scheduling and pricing. Transp. Res. Part B Methodol. 71, 1–18.

Delgado, F., Munoz, J.C., Giesen, R., 2012. How much can holding and/or limiting boarding improve transit performance? Transp. Res. Part B Methodol. 46, 1202–1217. https://doi.org/https://doi.org/10.1016/j.trb.2012.04.005

Dell'Olio, L., Ibeas, A., Cecin, P., 2011. The quality of service desired by public transport users. Transp. Policy 18, 217–227.

Demirtas, O., Derindag, O. F., Zarali, F., Ocal, O., and Aslan, A. 2021. Which renewable energy consumption is more efficient by fuzzy EDAS method based on PESTLE dimensions? Environmental Science and Pollution Research, 28(27), 36274-36287.

Deveci, M., and Torkayesh, A. E. 2021. Charging Type Selection for Electric Buses Using Interval-Valued Neutrosophic Decision Support Model. IEEE Transactions on Engineering Management, 1-14. doi:10.1109/TEM.2021.3108062

Deveci, M., Gokasar, I., Pamucar, D., Chen, Y., and Coffman, D. M. 2023. Sustainable E-scooter parking operation in urban areas using fuzzy Dombi based RAFSI model. Sustainable Cities and Society, 91, 104426. doi:https://doi.org/10.1016/j.scs.2023.104426

Deveci, M., Özcan, E., John, R., Pamucar, D., and Karaman, H. 2021. Offshore wind farm site selection using interval rough numbers based Best-Worst Method and MARCOS. Applied soft computing, 109, 107532. doi:https://doi.org/10.1016/j.asoc.2021.107532

Deveci, M., Pamucar, D., and Oguz, E. 2022a. Floating photovoltaic site selection using fuzzy rough numbers based LAAW and RAFSI model. Applied Energy, 324, 119597. doi:https://doi.org/10.1016/j.apenergy.2022.119597

Deveci, M., Pamucar, D., Gokasar, I., Köppen, M., and Gupta, B. B. 2022b. Personal mobility in metaverse with autonomous vehicles using Q-rung orthopair fuzzy sets based OPA-RAFSI model. IEEE Transactions on Intelligent Transportation Systems.

Distler, V., Lallemand, C., Bellet, T., 2018. Acceptability and acceptance of autonomous mobility on demand: The impact of an immersive experience, in: Proceedings of the 2018 CHI Conference on Human Factors in Computing Systems. pp. 1–10.

Dong, X., DiScenna, M., Guerra, E., 2019. Transit user perceptions of driverless buses. Transportation (Amst). 46, 35–50.

Drabicki, A., Cats, O., Kucharski, R., Fonzone, A., Szarata, A., 2023. Should I stay or should I board? Willingness to wait with real-time crowding information in urban public transport. Research in Transportation Business & Management, 47, 100963. https://doi.org/10.1016/j.rtbm.2023.100963

Drabicki, A., Kucharski, R., Cats, O., Szarata, A., 2020. Modelling the effects of real-time crowding information in urban public transport systems. Transp. A Transp. Sci. 1–39.

Durán-Hormazábal, E., Tirachini, A., 2016. Estimation of travel time variability for cars, buses, metro and door-to-door public transport trips in Santiago, Chile. Res. Transp. Econ. 59, 26–39.

Duran-Micco, J., Vermeir, E., Vansteenwegen, P., 2020. Considering emissions in the transit network design and frequency setting problem with a heterogeneous fleet. Eur J Oper Res 282, 580–592.

Ecer, F. 2021. A consolidated MCDM framework for performance assessment of battery electric vehicles based on ranking strategies. Renewable and Sustainable Energy Reviews, 143, 110916. doi:https://doi.org/10.1016/j.rser.2021.110916

Ecer, F., and Pamucar, D. 2020. Sustainable supplier selection: A novel integrated fuzzy best worst method (F-BWM) and fuzzy CoCoSo with Bonferroni (CoCoSo'B) multi-criteria model. Journal of Cleaner Production, 266, 121981. doi:https://doi.org/10.1016/j.jclepro.2020.121981

Eden, G., Nanchen, B., Ramseyer, R., Evéquoz, F., 2017. Expectation and experience: Passenger acceptance of autonomous public transportation vehicles, in: IFIP Conference on Human-Computer Interaction. Springer, pp. 360–363.
Ertuğrul, İ., and Karakaşoğlu, N. 2008. Comparison of fuzzy AHP and fuzzy TOPSIS methods for facility location selection. The International Journal of Advanced Manufacturing Technology, 39, 783-795.
Faris, H., Aljarah, I., Al-Betar, M.A., Mirjalili, S., 2018. Grey wolf optimizer: a review of recent variants and applications. Neural Comput Appl 30, 413–435.
Fathollahi-Fard, A.M., Ahmadi, A., Goodarzian, F., Cheikhrouhou, N., 2020a. A bi-objective home healthcare routing and scheduling problem considering patients' satisfaction in a fuzzy environment. Appl Soft Comput 93, 106385.
Fathollahi-Fard, A.M., Hajiaghaei-Keshteli, M., Tavakkoli-Moghaddam, R., 2020b. Red deer algorithm (RDA): a new nature-inspired meta-heuristic. Soft comput 24, 14637–14665.
Fielbaum, A., 2019. Strategic public transport design using autonomous vehicles and other new technologies. Int. J. Intell. Transp. Syst. Res. 1–9.
Fiori, C., Montanino, M., Nielsen, S., Seredynski, M., Viti, F., 2021. Microscopic energy consumption modelling of electric buses: model development, calibration, and validation. Transp. Res. Part D Transp. Environ. 98, 102978.
Franca, A., 2018. Electricity consumption and battery lifespan estimation for transit electric buses: drivetrain simulations and electrochemical modelling.
Fu, L., Liu, Q., Calamai, P., 2003. Real-time optimization model for dynamic scheduling of transit operations. Transp. Res. Rec. 1857, 48–55.
Furth, P.G., Wilson, N.H.M., 1981. Setting frequencies on bus routes: Theory and practice. Transp. Res. Rec. 818, 1–7.
Gallet, M., Massier, T., and Hamacher, T. 2018. Estimation of the energy demand of electric buses based on real-world data for large-scale public transport networks. Applied Energy, 230, 344-356. doi:https://doi.org/10.1016/j.apenergy.2018.08.086
Gao, Y., Kroon, L., Schmidt, M., Yang, L., 2016. Rescheduling a metro line in an over-crowded situation after disruptions. Transp. Res. Part B Methodol. 93, 425–449. https://doi.org/https://doi.org/10.1016/j.trb.2016.08.011
Gao, Z., Lin, Z., LaClair, T.J., Liu, C., Li, J.-M., Birky, A.K., Ward, J., 2017. Battery capacity and recharging needs for electric buses in city transit service. Energy 122, 588–600.
Ge, L., Voß, S., Xie, L., 2022. Robustness and disturbances in public transport. Public Transport 1–71.
Ghannadpour, S.F., Zandiyeh, F., 2020. An adapted multi-objective genetic algorithm for solving the cash in transit vehicle routing problem with vulnerability estimation for risk quantification. Eng Appl Artif Intell 96, 103964.
Gkiotsalitis, K., 2020a. A model for the periodic optimization of bus dispatching times. Appl Math Model 82, 785–801.
Gkiotsalitis, K., 2020b. Stop-skipping in rolling horizons. Transp. A Transp. Sci. 1–29.
Gkiotsalitis, K., 2022. Coordinating feeder and collector public transit lines for efficient MaaS services. EURO Journal on Transportation and Logistics 11, 100057.
Gkiotsalitis, K., Alesiani, F., 2019. Robust timetable optimization for bus lines subject to resource and regulatory constraints. Transp. Res. Part E Logist. Transp Rev 128, 30–51.
Gkiotsalitis, K., Cats, O., 2018. Reliable frequency determination: Incorporating information on service uncertainty when setting dispatching headways. Transp. Res. Part C Emerg. Technol. 88, 187–207.
Gkiotsalitis, K., Cats, O., 2021. At-stop control measures in public transport: Literature review and research agenda. Transp Res E Logist Transp Rev 145, 102176.

Gkiotsalitis, K., Cats, O., Liu, T., 2022a. A review of public transport transfer synchronisation at the real-time control phase. Transp Rev 1–20.
Gkiotsalitis, K., Liu, T., 2022. Periodic Optimization of Bus Dispatching Times and Vehicle Schedules Considering the COVID-19 Capacity Limits: A Dutch Case Study. Transp Res Rec 03611981221114119.
Gkiotsalitis, K., Schmidt, M., van der Hurk, E., 2022b. Subline frequency setting for autonomous minibusses under demand uncertainty. Transp. Res. Part C Emerg. Technol. 135, 103492.
Gkiotsalitis, K., Van Berkum, E.C., 2020a. An exact method for the bus dispatching problem in rolling horizons. Transp. Res. Part C Emerg. Technol. 110, 143–165.
Gkiotsalitis, K., Van Berkum, E.C., 2020b. An analytic solution for real-time bus holding subject to vehicle capacity limits. Transp. Res. Part C Emerg. Technol. 121, 102815.
Glotz-Richter, M., and Koch, H. 2016. Electrification of Public Transport in Cities (Horizon 2020 ELIPTIC Project). Transportation Research Procedia, 14, 2614-2619. doi:https://doi.org/10.1016/j.trpro.2016.05.416
Goeke, D., Schneider, M., 2015. Routing a mixed fleet of electric and conventional vehicles. Eur. J. Oper. Res. 245, 81–99.
Göhlich, D., Fay, T.-A., Jefferies, D., Lauth, E., Kunith, A., Zhang, X., 2018. Design of urban electric bus systems. Des. Sci. 4.
Goodarzian, F., Hosseini-Nasab, H., Muñuzuri, J., Fakhrzad, M.-B., 2020. A multi-objective pharmaceutical supply chain network based on a robust fuzzy model: A comparison of meta-heuristics. Appl Soft Comput 92, 106331.
Goodarzian, F., Kumar, V., Abraham, A., 2021a. Hybrid meta-heuristic algorithms for a supply chain network considering different carbon emission regulations using big data characteristics. Soft comput 25, 7527–7557.
Goodarzian, F., Taleizadeh, A.A., Ghasemi, P., Abraham, A., 2021b. An integrated sustainable medical supply chain network during COVID-19. Eng Appl Artif Intell 100, 104188.
Guo, S., and Zhao, H. 2015. Optimal site selection of electric vehicle charging station by using fuzzy TOPSIS based on sustainability perspective. Applied Energy, 158, 390-402. doi:https://doi.org/10.1016/j.apenergy.2015.08.082
Guo, S., and Zhao, H. 2017. Fuzzy best-worst multi-criteria decision-making method and its applications. Knowledge-Based Systems, 121, 23-31.
Häll, C.H., Ceder, A., Ekström, J., Quttineh, N.-H., 2019. Adjustments of public transit operations planning process for the use of electric buses. J. Intell. Transp. Syst. 23, 216–230.
Hamdouch, Y., Ho, H.W., Sumalee, A., Wang, G., 2011. Schedule-based transit assignment model with vehicle capacity and seat availability. Transp. Res. Part B Methodol. 45, 1805–1830.
Harris, A., Soban, D., Smyth, B.M., Best, R., 2020. A probabilistic fleet analysis for energy consumption, life cycle cost and greenhouse gas emissions modelling of bus technologies. Appl. Energy 261, 114422.
Hatzenbühler, J., Cats, O., Jenelius, E., 2020. Transitioning towards the deployment of line-based autonomous buses: Consequences for service frequency and vehicle capacity. Transp. Res. Part A Policy Pract. 138, 491–507.
Hatzenbühler, J., Cats, O., Jenelius, E., 2021. Network design for line-based autonomous bus services. Transportation (Amst). 1–36.
He, Y., Song, Z., Liu, Z., 2019. Fast-charging station deployment for battery electric bus systems considering electricity demand charges. Sustain. Cities Soc. 48, 101530.

Heikoop, D.D., Velasco, J.P.N., Boersma, R., Bjørnskau, T., Hagenzieker, M.P., 2020. Automated bus systems in Europe: A systematic review of passenger experience and road user interaction.
Hickman, M.D., 2001. An analytic stochastic model for the transit vehicle holding problem. Transp. Sci. 35, 215–237.
Hiermann, G., Puchinger, J., Ropke, S., Hartl, R.F., 2016. The electric fleet size and mix vehicle routing problem with time windows and recharging stations. Eur. J. Oper. Res. 252, 995–1018.
Hjelkrem, O.A., Lervåg, K.Y., Babri, S., Lu, C., Södersten, C.-J., 2021. A battery electric bus energy consumption model for strategic purposes: Validation of a proposed model structure with data from bus fleets in China and Norway. Transp. Res. Part D Transp. Environ. 94, 102804.
Hörcher, D., De Borger, B., Seifu, W., Graham, D.J., 2020. Public transport provision under agglomeration economies. Reg. Sci. Urban Econ. 81, 103503.
Hörcher, D., Graham, D.J., 2018. Demand imbalances and multi-period public transport supply. Transp. Res. Part B Methodol. 108, 106–126.
Hörcher, D., Graham, D.J., Anderson, R.J., 2017. Crowding cost estimation with large scale smart card and vehicle location data. Transportation Research Part B: Methodological 95, 105–125.
Hörcher, D., Graham, D.J., Anderson, R.J., 2018. The economics of seat provision in public transport. Transp. Res. Part E Logist. Transp. Rev. 109, 277–292.
Hörcher, D., Tirachini, A., 2021. A review of public transport economics. Econ. Transp. 25, 100196.
Houbbadi, A., Trigui, R., Pelissier, S., Redondo-Iglesias, E., Bouton, T., 2019. Optimal scheduling to manage an electric bus fleet overnight charging. Energies 12, 2727.
Ibarra-Rojas, O.J., Delgado, F., Giesen, R., Muñoz, J.C., 2015. Planning, operation, and control of bus transport systems: A literature review. Transp. Res. Part B Methodol. 77, 38–75.
Jaguemont, J., Boulon, L., and Dubé, Y. 2016. A comprehensive review of lithium-ion batteries used in hybrid and electric vehicles at cold temperatures. Applied Energy, 164, 99-114. doi:https://doi.org/10.1016/j.apenergy.2015.11.034
Jansson, J.O., 1980. A simple bus line model for optimisation of service frequency and bus size. J. Transport Econ. Pol. 53–80.
Jara-Díaz, S., Gschwender, A., 2003. Towards a general microeconomic model for the operation of public transport. Transp. Rev. 23, 453–469.
Jefferies, D., Göhlich, D., 2018. Integrated TCO Assessment of Bus Network Electrification Considering Rescheduling and Delays: Modelling Framework and Case Study, in: EVS31 International Electric Vehicle Symposium & Exhibition, Kobe, Japan.
Jenelius, E., 2018. Public transport experienced service reliability: Integrating travel time and travel conditions. Transp. Res. Part A Policy Pract. 117, 275–291.
Jenelius, E., 2020. Personalized predictive public transport crowding information with automated data sources. Transp. Res. Part C Emerg. Technol. 117, 102647.
Jiang, X., Guo, X., Ran, B., 2014. Optimization model for headway of a suburban bus route. Math. Probl. Eng. 2014.
Junior, F. R. L., Osiro, L., and Carpinetti, L. C. R. 2014. A comparison between Fuzzy AHP and Fuzzy TOPSIS methods to supplier selection. Applied soft computing, 21, 194-209.
Kahraman, C., Keshavarz Ghorabaee, M., Zavadskas, E. K., Cevik Onar, S., Yazdani, M., and Oztaysi, B. 2017. Intuitionistic fuzzy EDAS method: an application to solid waste disposal site selection. Journal of Environmental Engineering and Landscape Management, 25(1), 1-12.

Karimi-Mamaghan, M., Mohammadi, M., Meyer, P., Karimi-Mamaghan, A.M., Talbi, E.-G., 2022. Machine learning at the service of meta-heuristics for solving combinatorial optimization problems: A state-of-the-art. Eur J Oper Res 296, 393–422.

Katoch, S., Chauhan, S.S., Kumar, V., 2021. A review on genetic algorithm: past, present, and future. Multimed Tools Appl 80, 8091–8126.

Kaya, S. K., Pamucar, D., and Aycin, E. 2022. A New Hybrid Fuzzy Multi-Criteria Decision Methodology for Prioritizing the Antivirus Mask Over COVID-19 Pandemic. Informatica, 33(3), 545-572. doi:10.15388/22-INFOR475

Ke, B.-R., Chung, C.-Y., Chen, Y.-C., 2016. Minimizing the costs of constructing an all plug-in electric bus transportation system: A case study in Penghu. Appl. Energy 177, 649–660.

Kelly, J. C., Wang, M., Dai, Q., and Winjobi, O. 2021. Energy, greenhouse gas, and water life cycle analysis of lithium carbonate and lithium hydroxide monohydrate from brine and ore resources and their use in lithium ion battery cathodes and lithium ion batteries. Resources, Conservation and Recycling, 174, 105762. doi:https://doi.org/10.1016/j.resconrec.2021.105762

Keshavarz-Ghorabaee, M., Zavadskas, E., Amiri, M., and Turskis, Z. 2016. Extended EDAS Method for Fuzzy Multi-criteria Decision-making: An Application to Supplier Selection. International journal of computers communications & control, 11, 358-371. doi:10.15837/ijccc.2016.3.2557

Keskin, M., Çatay, B., 2016. Partial recharge strategies for the electric vehicle routing problem with time windows. Transp. Res. Part C Emerg. Technol. 65, 111–127.

Kivekäs, K., VepsäläInen, J., Tammi, K., 2018. Stochastic driving cycle synthesis for analyzing the energy consumption of a battery electric bus. IEEE Access 6, 55586–55598.

Klumpenhouwer, W., Wirasinghe, S.C., 2016. Cost-of-crowding model for light rail train and platform length. Public Transp. 8, 85–101.

Koirala, K., Tamang, M., and Shabbiruddin. 2022. Planning and establishment of battery swapping station - A support for faster electric vehicle adoption. Journal of Energy Storage, 51, 104351. doi:https://doi.org/10.1016/j.est.2022.104351

Kraft, W., Stahl, V., and Vetter, P. 2020. Thermal Storage Using Metallic Phase Change Materials for Bus Heating—State of the Art of Electric Buses and Requirements for the Storage System. Energies, 13(11), 3023. Retrieved from https://www.mdpi.com/1996-1073/13/11/3023

Kunith, A., Mendelevitch, R., and Goehlich, D. 2017. Electrification of a city bus network—An optimization model for cost-effective placing of charging infrastructure and battery sizing of fast-charging electric bus systems. International Journal of Sustainable Transportation, 11(10), 707-720. doi:10.1080/15568318.2017.1310962

Kutlu Gündoğdu, F., Kahraman, C., and Civan, H. N. 2018. A novel hesitant fuzzy EDAS method and its application to hospital selection. Journal of Intelligent & Fuzzy Systems, 35(6), 6353-6365.

Kyriakidis, M., de Winter, J.C.F., Stanton, N., Bellet, T., van Arem, B., Brookhuis, K., Martens, M.H., Bengler, K., Andersson, J., Merat, N., 2019. A human factors perspective on automated driving. Theor. Issues Ergon. Sci. 20, 223–249.

Lai, X., Chen, Q., Tang, X., Zhou, Y., Gao, F., Guo, Y., Bhagat, R., and Zheng, Y. 2022. Critical review of life cycle assessment of lithium-ion batteries for electric vehicles: A lifespan perspective. eTransportation, 12, 100169. doi:https://doi.org/10.1016/j.etran.2022.100169

Lajunen, A., and Lipman, T. 2016. Lifecycle cost assessment and carbon dioxide emissions of diesel, natural gas, hybrid electric, fuel cell hybrid and electric transit buses. Energy, 106, 329-342. doi:https://doi.org/10.1016/j.energy.2016.03.075

Lazarus, J., Shaheen, S., Young, S.E., Fagnant, D., Voege, T., Baumgardner, W., Fishelson, J., Lott, J.S., 2018. Shared automated mobility and public transport, in: Road Vehicle Automation 4. Springer, pp. 141–161.
Li, J., Klee Barillas, J., Guenther, C., and Danzer, M. A. 2013. A comparative study of state of charge estimation algorithms for LiFePO4 batteries used in electric vehicles. Journal of Power Sources, 230, 244-250. doi:https://doi.org/10.1016/j.jpowsour.2012.12.057
Li, J., Wang, F., He, Y., 2020. Electric Vehicle Routing Problem with Battery Swapping Considering Energy Consumption and Carbon Emissions. Sustainability 12, 10537.
Li, L., Lo, H.K., Xiao, F., 2019. Mixed bus fleet scheduling under range and refueling constraints. Transp. Res. Part C Emerg. Technol. 104, 443–462.
Lin, J., Zhou, W., Wolfson, O., 2016. Electric Vehicle Routing Problem. Transp. Res. Procedia 12, 508–521. https://doi.org/https://doi.org/10.1016/j.trpro.2016.02.007
Liu, K., Yamamoto, T., Morikawa, T., 2017. Impact of road gradient on energy consumption of electric vehicles. Transp. Res. Part D Transp. Environ. 54, 74–81.
Liu, T., Cats, O., Gkiotsalitis, K., 2021. A review of public transport transfer coordination at the tactical planning phase. Transp Res Part C Emerg Technol 133, 103450.
Liu, X., Qu, X., Ma, X., 2021. Optimizing electric bus charging infrastructure considering power matching and seasonality. Transp. Res. Part D Transp. Environ. 100, 103057.
Liu, Y., Dehghani, E., Jabalameli, M.S., Diabat, A., Lu, C.-C., 2020. A coordinated location-inventory problem with supply disruptions: A two-phase queuing theory–optimization model approach. Comput Ind Eng 142, 106326.
Liu, Z., Yan, Y., Qu, X., Zhang, Y., 2013. Bus stop-skipping scheme with random travel time. Transp. Res. Part C Emerg. Technol. 35, 46–56.
Logan, K. G., Nelson, J. D., and Hastings, A. 2020. Electric and hydrogen buses: Shifting from conventionally fuelled cars in the UK. Transportation Research Part D: Transport and Environment, 85, 102350. doi:https://doi.org/10.1016/j.trd.2020.102350
Loganathan, M. K., Mishra, B., Tan, C. M., Kongsvik, T., and Rai, R. N. 2021. Multi-criteria decision making (MCDM) for the selection of Li-ion batteries used in electric vehicles (EVs). Materials Today: Proceedings, 41, 1073-1077. doi:https://doi.org/10.1016/j.matpr.2020.07.179
Longo, M., Leone, C., Lorenz, L., Strada, A., and Yaici, W. 2021. Electrification of a Bus Line in Savona Considering Depot and Opportunity Charging. Advances in Science, Technology and Engineering Systems Journal, 6(5), 213-221. doi:10.25046/aj060523
Lopez de Briñas Gorosabel, O., Xylia, M., and Silveira, S. 2022. A framework for the assessment of electric bus charging station construction: A case study for Stockholm's inner city. Sustainable Cities and Society, 78, 103610. doi:https://doi.org/10.1016/j.scs.2021.103610
Lu, H., Burge, P., Heywood, C., Sheldon, R., Lee, P., Barber, K., Phillips, A., 2018. The impact of real-time information on passengers' value of bus waiting time. Transp. Res. Procedia 31, 18–34.
Luo, X., Liu, Y., Yu, Y., Tang, J., Li, W., 2019. Dynamic bus dispatching using multiple types of real-time information. Transportmetrica B: Transport Dynamics 7, 519–545.
Luo, Y., Tan, Y.-P., Li, L.-F., 2020. Study on saving energy for electric auxiliary systems of electric bus. Energy Sources, Part A Recover. Util. Environ. Eff. 1–13.
Lutin, J.M., 2018. Not If, but when: autonomous driving and the future of transit. J. Public Transp. 21, 10.
Ma, X., Miao, R., Wu, X., Liu, X., 2021. Examining influential factors on the energy consumption of electric and diesel buses: A data-driven analysis of large-scale public transit network in Beijing. Energy 216, 119196.

Mahmoud, M., Garnett, R., Ferguson, M., and Kanaroglou, P. 2016. Electric buses: A review of alternative powertrains. Renewable and Sustainable Energy Reviews, 62, 673-684. doi:https://doi.org/10.1016/j.rser.2016.05.019

Manzolli, J. A., Trovão, J. P., and Antunes, C. H. 2022. A review of electric bus vehicles research topics – Methods and trends. Renewable and Sustainable Energy Reviews, 159, 112211. doi:https://doi.org/10.1016/j.rser.2022.112211

Mirjalili, S., Dong, J.S., Lewis, A., 2020. Nature-inspired optimizers. Cham, Switzerland: Springer 69–85.

Mirjalili, S., Lewis, A., 2013. S-shaped versus V-shaped transfer functions for binary particle swarm optimization. Swarm Evol Comput 9, 1–14.

Mirjalili, S., Mirjalili, S.M., Lewis, A., 2014. Grey wolf optimizer. Advances in engineering software 69, 46–61.

Mohring, H., 1972. Optimization and scale economies in urban bus transportation. Am. Econ. Rev. 62 (4), 591–604.

Mokhtarzadeh, M., Tavakkoli-Moghaddam, R., Triki, C., Rahimi, Y., 2021. A hybrid of clustering and meta-heuristic algorithms to solve a p-mobile hub location–allocation problem with the depreciation cost of hub facilities. Eng Appl Artif Intell 98, 104121.

Moreira-Matias, L., Cats, O., Gama, J., Mendes-Moreira, J., De Sousa, J.F., 2016. An online learning approach to eliminate Bus Bunching in real-time. Appl. Soft Comput. 47, 460–482.

Mosquet, X., Dauner, T., Lang, N., Russmann, M., Mei-Pochtler, A., Agrawal, R., Schmieg, F., 2015. Revolution in the Driver's Seat: The Road to Autonomous Vehicles. Bcg. perspectives, Boston Consulting Group, April 21, 2015.

Mostafaeipour, A., Alvandimanesh, M., Najafi, F., and Issakhov, A. 2021. Identifying challenges and barriers for development of solar energy by using fuzzy best-worst method: A case study. Energy, 226, 120355. doi:https://doi.org/10.1016/j.energy.2021.120355

Mou, Z., Zhang, H., Liang, S., 2020. Reliability Optimization Model of Stop-Skipping Bus Operation with Capacity Constraints. J. Adv. Transp. 2020.

Muñoz, J.C., Soza-Parra, J., Raveau, S., 2020. A comprehensive perspective of unreliable public transport services' costs. Transp. A Transp. Sci. 16, 734–748.

Nair, G.S., Bhat, C.R., 2021. Sharing the road with autonomous vehicles: Perceived safety and regulatory preferences. Transp. Res. Part C Emerg. Technol. 122, 102885. https://doi.org/https://doi.org/10.1016/j.trc.2020.102885

Nayeri, S., Tavakkoli-Moghaddam, R., Sazvar, Z., Heydari, J., 2022. A heuristic-based simulated annealing algorithm for the scheduling of relief teams in natural disasters. Soft comput 26, 1825–1843.

Nazim, M., Mohammad, C. W., and Sadiq, M. 2022. A comparison between fuzzy AHP and fuzzy TOPSIS methods to software requirements selection. Alexandria Engineering Journal, 61(12), 10851-10870.

Nemoto, E.H., Jaroudi, I., Fournier, G., 2020. Introducing Automated Shuttles in the Public Transport of European Cities: The Case of the AVENUE Project, in: Conference on Sustainable Urban Mobility. Springer, pp. 272–285.

Nichoals, M., Hall, D. 2018. Lessons Learned on Early Electric Vehicle Fast-charging Deployments, White Paper for the International Council on Clean Transportation.

OECD/ITF, 2014. Valuing convenience in public transport. ITF Round Tables, No. 156. OECD Publishing, F., n.d. France. France.

Omrani, H., Alizadeh, A., and Emrouznejad, A. 2018. Finding the optimal combination of power plants alternatives: A multi response Taguchi-neural network using TOPSIS and fuzzy best-worst method. Journal of Cleaner Production, 203, 210-223. doi:https://doi.org/10.1016/j.jclepro.2018.08.238

Osuna, E.E., Newell, G.F., 1972. Control strategies for an idealized public transportation system. Transp. Sci. 6, 52–72.

Pathak, P., Agrawal, K., Suman, H.K., Bolia, N.B., 2020. Frequency optimization-based approach for reducing crowding discomfort in Delhi bus system. Procedia Comput. Sci. 170, 265–272.

Paul, T., Yamada, H., 2014. Operation and charging scheduling of electric buses in a city bus route network, in: 17th International IEEE Conference on Intelligent Transportation Systems (ITSC). IEEE, pp. 2780–2786.

Pelletier, S., Jabali, O., Laporte, G., 2019a. The electric vehicle routing problem with energy consumption uncertainty. Transp. Res. Part B Methodol. 126, 225–255.

Pelletier, S., Jabali, O., Mendoza, J. E., and Laporte, G. 2019b. The electric bus fleet transition problem. Transportation Research Part C: Emerging Technologies, 109, 174-193. doi:https://doi.org/10.1016/j.trc.2019.10.012

Pernestål, A., Darwish, R., Susilo, Y., Nen, E.C.P., Jenelius, E., Hatzenbühler, J., Hafmar, P., 2018. SARA1 Results Report Shared Automated Vehicles-Research & Assessment in a 1st Pilot. ITRL-Integrated Transp. Res. Lab. KTH Roya l Inst. Technol. Sweden.

Perumal, S. S. G., Lusby, R. M., and Larsen, J. 2022. Electric bus planning & scheduling: A review of related problems and methodologies. European Journal of Operational Research, 301(2), 395-413. doi:https://doi.org/10.1016/j.ejor.2021.10.058

Pfeffer, K. 2003. Integrating spatio-temporal environmental models for planning ski runs. Nederlandse Geografische Studies.

Qin, F., 2014. Investigating the in-vehicle crowding cost functions for public transit modes. Math. Probl. Eng. 2014.

Rahman, M., Oni, A. O., Gemechu, E. D., and Kumar, A. 2020. Assessment of energy storage technologies: A review. Energy Conversion and Management, 223, 113295.

Rezaei, J. 2015. Best-worst multi-criteria decision-making method. Omega, 53, 49-57.

Rietveld, P., Bruinsma, F.R., Van Vuuren, D.J., 2001. Coping with unreliability in public transport chains: A case study for Netherlands. Transp. Res. Part A Policy Pract. 35, 539–559.

Rogge, M., van der Hurk, E., Larsen, A., Sauer, D.U., 2018. Electric bus fleet size and mix problem with optimization of charging infrastructure. Appl. Energy 211, 282–295.

Rupp, M., Rieke, C., Handschuh, N., and Kuperjans, I. 2020. Economic and ecological optimization of electric bus charging considering variable electricity prices and CO2eq intensities. Transportation Research Part D: Transport and Environment, 81, 102293. doi:https://doi.org/10.1016/j.trd.2020.102293

Saadon Al-Ogaili, A., Ramasamy, A., Juhana Tengku Hashim, T., Al-Masri, A. N., Hoon, Y., Neamah Jebur, M., Verayiah, R., and Marsadek, M. 2020. Estimation of the energy consumption of battery driven electric buses by integrating digital elevation and longitudinal dynamic models: Malaysia as a case study. Applied Energy, 280, 115873. doi:https://doi.org/10.1016/j.apenergy.2020.115873.

Sadrani, M., Tirachini, A., and Antoniou, C. 2022a. Vehicle dispatching plan for minimizing passenger waiting time in a corridor with buses of different sizes: Model formulation and solution approaches. European Journal of Operational Research, 299(1), 263-282. doi:https://doi.org/10.1016/j.ejor.2021.07.054.

Sadrani, M., Tirachini, A., and Antoniou, C. 2022b. Optimization of service frequency and vehicle size for automated bus systems with crowding externalities and travel time stochasticity. Transportation Research Part C: Emerging Technologies, 143, 103793. doi:https://doi.org/10.1016/j.trc.2022.103793.

Sadrani, M., A. Tirachini, and Antoniou, C. 2023a. Bus scheduling with heterogeneous fleets: A proposal and analysis of computational intelligence algorithms. Under review.

Sadrani, M., A. Tirachini, and Antoniou, C. 2023b. Electric bus line planning with a detailed energy consumption model. Under review.

Sadrani, M., Jafarian-Moghaddam, A.R., Esfahani, M.A., Rahimi, A.M., 2022c. Designing limited-stop bus services for minimizing operator and user costs under crowding conditions. Public Transport 1–32.

Sadrani, M., Najafi, A., Mirqasemi, R., and Antoniou, C. 2023c. Charging strategy selection for electric bus systems: A multi-criteria decision-making approach. Applied Energy, 347, 121415. doi:https://doi.org/10.1016/j.apenergy.2023.121415.

SAE, 2018. Taxonomy and definitions for terms related to driving automation systems for on-road motor vehicles. SAE Int. Warrendale, PA, USA.

Salonen, A.O., 2018. Passenger's subjective traffic safety, in-vehicle security and emergency management in the driverless shuttle bus in Finland. Transp. policy 61, 106–110.

Sánchez-Martínez, G.E., Koutsopoulos, H.N., Wilson, N.H.M., 2016. Real-time holding control for high-frequency transit with dynamics. Transp. Res. Part B Methodol. 83, 1–19. https://doi.org/https://doi.org/10.1016/j.trb.2015.11.013

Sang, X., Yu, X., Chang, C.-T., and Liu, X. 2022. Electric bus charging station site selection based on the combined DEMATEL and PROMETHEE-PT framework. Computers & Industrial Engineering, 168, 108116. doi:https://doi.org/10.1016/j.cie.2022.108116

Schmidt, A., Muñoz, J.C., Bucknell, C., Navarro, M., Simonetti, C., 2016. Increasing the Speed: Case Study from Santiago, Chile. Transp. Res. Rec. 2539, 65–71.

Schneider, M., Stenger, A., Goeke, D., 2014. The electric vehicle-routing problem with time windows and recharging stations. Transp. Sci. 48, 500–520.

Sebastiani, M.T., Lüders, R., Fonseca, K.V.O., 2016. Evaluating electric bus operation for a real-world BRT public transportation using simulation optimization. IEEE Trans. Intell. Transp. Syst. 17, 2777–2786.

Şengül, Ü., Eren, M., Shiraz, S. E., Gezder, V., and Şengül, A. B. 2015. Fuzzy TOPSIS method for ranking renewable energy supply systems in Turkey. Renewable energy, 75, 617-625.

Seyfi-Shishavan, S. A., Gündoğdu, F. K., and Farrokhizadeh, E. 2021. An assessment of the banking industry performance based on Intuitionistic fuzzy Best-Worst Method and fuzzy inference system. Applied soft computing, 113, 107990. doi:https://doi.org/10.1016/j.asoc.2021.107990

Shang, H.-Y., Huang, H.-J., Wu, W.-X., 2019. Bus timetabling considering passenger satisfaction: An empirical study in Beijing. Comput. Ind. Eng. 135, 1155–1166.

Sharma, I., Kumar, V., Sharma, S., 2022. A comprehensive survey on grey wolf optimization. Recent Advances in Computer Science and Communications (Formerly: Recent Patents on Computer Science) 15, 323–333.

Shekhar, A., Prasanth, V., Bauer, P., Bolech, M., 2016. Economic viability study of an on-road wireless charging system with a generic driving range estimation method. Energies 9, 76.

Shen, Z.-J.M., Feng, B., Mao, C., Ran, L., 2019. Optimization models for electric vehicle service operations: A literature review. Transp. Res. Part B Methodol. 128, 462–477.

Siarry, P., 2016. Metaheuristics. Springer.

Soner, O., Celik, E., and Akyuz, E. 2022. A fuzzy best–worst method (BWM) to assess the potential environmental impacts of the process of ship recycling. Maritime Policy & Management, 49(3), 396-409. doi:10.1080/03088839.2021.1889066

Soza-Parra, J., Raveau, S., Muñoz, J.C., Cats, O., 2019. The underlying effect of public transport reliability on users' satisfaction. Transp. Res. Part A Policy Pract. 126, 83–93.

Stević, Ž., Vasiljević, M., Zavadskas, E. K., Sremac, S., and Turskis, Z. 2018. Selection of carpenter manufacturer using fuzzy EDAS method. Engineering Economics, 29(3), 281-290.

Suman, H.K., Bolia, N.B., 2019. Mitigation of overcrowding in buses through bus planning. Public Transp. 11, 159–187.

Sun, A., Hickman, M., 2005. The real–time stop–skipping problem. J. Intell. Transp. Syst. 9, 91–109.

Sun, C.-C., and Lin, G. T. 2009. Using fuzzy TOPSIS method for evaluating the competitive advantages of shopping websites. Expert Systems with Applications, 36(9), 11764-11771.

Sun, L., Tirachini, A., Axhausen, K.W., Erath, A., Lee, D.-H., 2014. Models of bus boarding and alighting dynamics. Transp. Res. Part A Policy Pract. 69, 447–460. https://doi.org/https://doi.org/10.1016/j.tra.2014.09.007

Sun, P., Bisschop, R., Niu, H., and Huang, X. 2020. A Review of Battery Fires in Electric Vehicles. Fire Technology, 56(4), 1361-1410. doi:10.1007/s10694-019-00944-3

Talbi, E.-G., 2009. Metaheuristics: from design to implementation. John Wiley & Sons.

Tang, R., de Donato, L., Besinović, N., Flammini, F., Goverde, R.M.P., Lin, Z., Liu, R., Tang, T., Vittorini, V., Wang, Z., 2022. A literature review of Artificial Intelligence applications in railway systems. Transp Res Part C Emerg Technol 140, 103679.

Tang, X., Lin, X., He, F., 2019. Robust scheduling strategies of electric buses under stochastic traffic conditions. Transp. Res. Part C Emerg. Technol. 105, 163–182.

Teichert, O., Chang, F., Ongel, A., and Lienkamp, M. 2019. Joint Optimization of Vehicle Battery Pack Capacity and Charging Infrastructure for Electrified Public Bus Systems. IEEE Transactions on Transportation Electrification, 5(3), 672-682. doi:10.1109/TTE.2019.2932700

Tian, Q., Lin, Y.H., Wang, D.Z.W., 2020. Autonomous and conventional bus fleet optimization for fixed-route operations considering demand uncertainty. Transportation (Amst). 1–29.

Tikani, H., Ramezanian, R., Setak, M., van Woensel, T., 2021. Hybrid evolutionary algorithms and Lagrangian relaxation for multi-period star hub median problem considering financial and service quality issues. Eng Appl Artif Intell 97, 104056.

Tirachini, A., 2014. The economics and engineering of bus stops: Spacing, design and congestion. Transp. Res. Part A Policy Pract. 59, 37–57. https://doi.org/https://doi.org/10.1016/j.tra.2013.10.010

Tirachini, A., Antoniou, C., 2020. The economics of automated public transport: Effects on operator cost, travel time, fare and subsidy. Econ. Transp. 21, 100151.

Tirachini, A., Godachevich, J., Cats, O., Muñoz, J.C. and Soza-Parra, J., 2022. Headway variability in public transport: a review of metrics, determinants, effects for quality of service and control strategies. Transport Reviews, 42(3), pp.337-361.

Tirachini, A., Hensher, D.A., Rose, J.M., 2013. Crowding in public transport systems: effects on users, operation and implications for the estimation of demand. Transp. Res. part A policy Pract. 53, 36–52.

Tirachini, A., Hensher, D.A., Rose, J.M., 2014. Multimodal pricing and optimal design of urban public transport : The interplay between traffic congestion and bus crowding. Transp. Res. PART B 61, 33–54. https://doi.org/10.1016/j.trb.2014.01.003

Tirachini, A., Hurtubia, R., Dekker, T., Daziano, R.A., 2017. Estimation of crowding discomfort in public transport: Results from Santiago de Chile. Transp. Res. Part A Policy Pract. 103, 311–326. https://doi.org/https://doi.org/10.1016/j.tra.2017.06.008

Tirachini, A., Sun, L., Erath, A., Chakirov, A., 2016. Valuation of sitting and standing in metro trains using revealed preferences. Transp. Policy 47, 94–104.

Torkayesh, A. E., Hashemkhani Zolfani, S., Kahvand, M., and Khazaelpour, P. 2021a. Landfill location selection for healthcare waste of urban areas using hybrid BWM-grey MARCOS model based on GIS. Sustainable Cities and Society, 67, 102712. doi:https://doi.org/10.1016/j.scs.2021.102712

Torkayesh, A. E., Pamucar, D., Ecer, F., and Chatterjee, P. 2021b. An integrated BWM-LBWA-CoCoSo framework for evaluation of healthcare sectors in Eastern Europe. Socio-Economic Planning Sciences, 78, 101052. doi:https://doi.org/10.1016/j.seps.2021.101052

Torkayesh, A. E., Yazdani, M., and Ribeiro-Soriano, D. 2022. Analysis of industry 4.0 implementation in mobility sector: An integrated approach based on QFD, BWM, and stratified combined compromise solution under fuzzy environment. Journal of Industrial Information Integration, 30, 100406. doi:https://doi.org/10.1016/j.jii.2022.100406

Türk, S., Deveci, M., Özcan, E., Canıtez, F., and John, R. 2021. Interval type-2 fuzzy sets improved by Simulated Annealing for locating the electric charging stations. Information Sciences, 547, 641-666. doi:https://doi.org/10.1016/j.ins.2020.08.076

Tyrinopoulos, Y., Antoniou, C., 2008. Public transit user satisfaction: Variability and policy implications. Transp. Policy 15, 260–272.

Uslu, T., Kaya, O., 2021. Location and capacity decisions for electric bus charging stations considering waiting times. Transp. Res. Part D Transp. Environ. 90, 102645.

Van Lierop, D., Badami, M.G., El-Geneidy, A.M., 2018. What influences satisfaction and loyalty in public transport? A review of the literature. Transp. Rev. 38, 52–72.

van Oort, N., 2014. Incorporating service reliability in public transport design and performance requirements: International survey results and recommendations. Res. Transp. Econ. 48, 92–100.

van Oort, N., 2016. Incorporating enhanced service reliability of public transport in cost-benefit analyses. Public Transp. 8, 143–160.

Vepsäläinen, J., Otto, K., Lajunen, A., Tammi, K., 2019. Computationally efficient model for energy demand prediction of electric city bus in varying operating conditions. Energy 169, 433–443.

Vilppo, O., and Markkula, J. 2015. Feasibility of Electric Buses in Public Transport. World Electric Vehicle Journal, 7(3), 357-365. doi:10.3390/wevj7030357

Vuchic, V.R., 2017. Urban transit: operations, planning, and economics. John Wiley & Sons.

Wadud, Z., 2017. Fully automated vehicles: A cost of ownership analysis to inform early adoption. Transp. Res. Part A Policy Pract. 101, 163–176.

Wang, J., Lin, D., Zhang, Y., Huang, S., 2022. An adaptively balanced grey wolf optimization algorithm for feature selection on high-dimensional classification. Eng Appl Artif Intell 114, 105088.

Wang, J., Sun, L., 2020. Dynamic holding control to avoid bus bunching: A multi-agent deep reinforcement learning framework. Transp. Res. Part C Emerg. Technol. 116, 102661.

Wang, M., Wang, L., Xu, X., Qin, Y., Qin, L., 2019. Genetic algorithm-based particle swarm optimization approach to reschedule high-speed railway timetables: a case study in China. J Adv Transp 2019.

Wang, Y., Huang, Y., Xu, J., Barclay, N., 2017. Optimal recharging scheduling for urban electric buses: A case study in Davis. Transp. Res. Part E Logist. Transp. Rev. 100, 115–132.

Wang, Y., Tang, T., Ning, B., van den Boom, T.J.J., De Schutter, B., 2015. Passenger-demands-oriented train scheduling for an urban rail transit network. Transp. Res. Part C Emerg. Technol. 60, 1–23. https://doi.org/https://doi.org/10.1016/j.trc.2015.07.012

Wanke, P., Azad, M. A. K., Barros, C. P., and Hassan, M. K. 2016. Predicting efficiency in Islamic banks: An integrated multicriteria decision making (MCDM) approach. Journal of International Financial Markets, Institutions and Money, 45, 126-141. doi:https://doi.org/10.1016/j.intfin.2016.07.004

Wardman, M., 2004. Public transport values of time. Transp. Policy 11, 363–377. https://doi.org/https://doi.org/10.1016/j.tranpol.2004.05.001

Wardman, M., Whelan, G., 2011. Twenty years of rail crowding valuation studies: evidence and lessons from British experience. Transp. Rev. 31, 379–398.

Whelan, G., Crockett, J., 2009. An investigation of the willingness to pay to reduce rail overcrowding, in: Proceedings of the First International Conference on Choice Modelling, Harrogate, England. Citeseer.

Wołek, M., Jagiełło, A., and Wolański, M. 2021. Multi-Criteria Analysis in the Decision-Making Process on the Electrification of Public Transport in Cities in Poland: A Case Study Analysis. Energies, 14(19), 6391. Retrieved from https://www.mdpi.com/1996-1073/14/19/6391

Wu, H., Hu, Y., Yu, Y., Huang, K., and Wang, L. 2021. The environmental footprint of electric vehicle battery packs during the production and use phases with different functional units. The International Journal of Life Cycle Assessment, 26(1), 97-113. doi:10.1007/s11367-020-01836-3

Wu, W., Liu, R., Jin, W., 2017. Modelling bus bunching and holding control with vehicle overtaking and distributed passenger boarding behaviour. Transp. Res. Part B Methodol. 104, 175–197.

x, Akyurt, Z., Pamucar, D., Deveci, M., Kalan, O., and Kuvvetli, Y. 2021. A Flight Base Selection for Flight Academy Using a Rough MACBETH and RAFSI Based Decision-Making Analysis. IEEE Transactions on Engineering Management, 1-16. doi:10.1109/TEM.2021.3119659

Xu, W., Zhao, P., Ning, L., 2018. Last train delay management in urban rail transit network: bi-objective MIP model and genetic algorithm. KSCE Journal of Civil Engineering 22, 1436–1445.

Xylia, M., and Silveira, S. 2018. The role of charging technologies in upscaling the use of electric buses in public transport: Experiences from demonstration projects. Transportation Research Part A: Policy and Practice, 118, 399-415. doi:https://doi.org/10.1016/j.tra.2018.09.011

Xylia, M., Leduc, S., Patrizio, P., Kraxner, F., Silveira, S., 2017. Locating charging infrastructure for electric buses in Stockholm. Transp. Res. Part C Emerg. Technol. 78, 183–200.

Yamagishi, K., Gantalao, C., Tiu, A. M., Tanaid, R. A., Medalla, M. E., Abellana, D. P., Selerio, E., and Ocampo, L. 2022. Evaluating the destination management performance of small islands with the fuzzy best-worst method and fuzzy simple additive weighting. Current Issues in Tourism, 1-30. doi:10.1080/13683500.2022.2054404

Yao, E., Liu, T., Lu, T., Yang, Y., 2020. Optimization of electric vehicle scheduling with multiple vehicle types in public transport. Sustain. Cities Soc. 52, 101862.

Yap, M., Cats, O., 2021. Taking the path less travelled: Valuation of denied boarding in crowded public transport systems. Transp. Res. Part A Policy Pract. 147, 1–13.

Yap, M., Cats, O., van Arem, B., 2020. Crowding valuation in urban tram and bus transportation based on smart card data. Transp. A Transp. Sci. 16, 23–42.
Yu, D. 2013. Intuitionistic fuzzy geometric Heronian mean aggregation operators. Applied soft computing, 13(2), 1235-1246. doi:https://doi.org/10.1016/j.asoc.2012.09.021
Yu, D., Li, Y., Zhang, S., Dong, H., Han, G., and Xian, X. (2019, 18-20 Oct. 2019). Fire Extinguishing Test of Lithium-Ion Battery Case in Electric Bus. Paper presented at the 2019 9th International Conference on Fire Science and Fire Protection Engineering (ICFSFPE).
Yu, H., Gao, Y., Wang, L., Meng, J., 2020. A hybrid particle swarm optimization algorithm enhanced with nonlinear inertial weight and Gaussian mutation for job shop scheduling problems. Mathematics 8, 1355.
Zandieh, M., Moradi, H., 2019. An imperialist competitive algorithm in mixed-model assembly line sequencing problem to minimise unfinished works. International Journal of Systems Science: Operations & Logistics 6, 179–192.
Zaneti, L. A. L., Arias, N. B., de Almeida, M. C., and Rider, M. J. 2022. Sustainable charging schedule of electric buses in a University Campus: A rolling horizon approach. Renewable and Sustainable Energy Reviews, 161, 112276. doi:https://doi.org/10.1016/j.rser.2022.112276
Zhang, F., Liu, W., 2019. Responsive bus dispatching strategy in a multi-modal and multi-directional transportation system: A doubly dynamical approach. Transportation Research Procedia 38, 119–138.
Zhang, J., Yang, H., Lindsey, R., Li, X., 2020. Modeling and managing congested transit service with heterogeneous users under monopoly. Transp. Res. Part B Methodol. 132, 249–266.
Zhang, L., Huang, J., Liu, Z., Vu, H.L., 2020. An agent-based model for real-time bus stop-skipping and holding schemes. Transp. A Transp. Sci. 1–33.
Zhang, S., Gajpal, Y., Appadoo, S.S., Abdulkader, M.M.S., 2018. Electric vehicle routing problem with recharging stations for minimizing energy consumption. Int. J. Prod. Econ. 203, 404–413.
Zhang, S., Wei, G., Gao, H., Wei, C., and Wei, Y. 2019. EDAS method for multiple criteria group decision making with picture fuzzy information and its application to green suppliers selections. Technological and Economic Development of Economy, 25(6), 1123-1138.
Zhang, T., Li, D., Qiao, Y., 2018. Comprehensive optimization of urban rail transit timetable by minimizing total travel times under time-dependent passenger demand and congested conditions. Appl Math Model 58, 421–446.
Zhang, W., Jenelius, E., Badia, H., 2019. Efficiency of semi-autonomous and fully autonomous bus services in trunk-and-branches networks. J. Adv. Transp. 2019.
Zhao, J., Bukkapatnam, S., Dessouky, M.M., 2003. Distributed architecture for real-time coordination of bus holding in transit networks. IEEE Trans. Intell. Transp. Syst. 4, 43–51. https://doi.org/10.1109/TITS.2003.809769
Zhou, Boya, Wu, Y., Zhou, Bin, Wang, R., Ke, W., Zhang, S., Hao, J., 2016. Real-world performance of battery electric buses and their life-cycle benefits with respect to energy consumption and carbon dioxide emissions. Energy 96, 603–613.
Zhou, Y., Meng, Q., & Ong, G. P. 2022. Electric bus charging scheduling for a single public transport route considering nonlinear charging profile and battery degradation effect. Transportation Research Part B: Methodological, 159, 49–75.
Žižović, M., Pamučar, D., Albijanić, M., Chatterjee, P., and Pribićević, I. 2020. Eliminating Rank Reversal Problem Using a New Multi-Attribute Model—The RAFSI Method. Mathematics, 8(6). doi:10.3390/math8061015

Zolfani, S. H., and Chatterjee, P. 2019. Comparative Evaluation of Sustainable Design Based on Step-Wise Weight Assessment Ratio Analysis (SWARA) and Best Worst Method (BWM) Methods: A Perspective on Household Furnishing Materials. Symmetry, 11(1). doi:10.3390/sym11010074

Zolfani, S., Chatterjee, P., and Yazdani, M. 2019. A structured framework for sustainable supplier selection using a combined BWM-CoCoSo model.